Direct Monitoring of Speciation for Minor Actinide Separations

Wanda T. Stuber

Somerville College

University of Oxford

A thesis submitted for the degree of

Doctor of Philosophy

Trinity 2017

Declaration of Authorship

The work presented in this thesis has been conducted in the Chemistry Research Laboratory of the University of Oxford, under the supervision of Prof. Stephen Faulkner. I declare that all of the work presented is my own, except where stated otherwise, and has not been submitted for any other degree at this or any other university.

Table of Contents

Abstract

"Direct Monitoring of Speciation for Minor Actinide Separations"

Wanda Tanja Stuber, Somerville College, University of Oxford.

DPhil. Thesis, Trinity Term 2017.

One of the major challenges in the development of future generations of nuclear reprocessing procedures is the separation of the minor actinides from the chemically similar trivalent lanthanide ions.

In this thesis, the potential of two purely N-donor ligands for minor actinide separations is evaluated and behaviour in aqueous and extraction conditions investigated. Of two chosen ligands, 12N4Py4 and 9N3Py3, only the larger 12N4Py4 was found to be able to complex lanthanide ions; however, both bind readily to divalent calcium ions. In comparison to earlier published properties of Ln(III)-12N4Py4 complexes, the cerium complex was found to show differences based on greater d-orbital mixing.

Conjugated acid dissociation constants and metal binding constants were determined using newly developed fitting functions in several conditions and found to be comparable to those of other extractants. As the investigation was performed in aqueous conditions, side reactions such as hydroxide formation and precipitation had to be considered and included into fitting procedures. Studies on U(IV) and Am(III) were conducted, but due to unfavourable conditions complexation by 12N4Py4 could not be verified beyond reasonable doubt.

Extraction of ligand species and metal complexes was studied in various conditions and in the presence of various anions. Beside the main target cations, Ln(III) and An(III), 12N4Py4 is also capable of complexing and extracting protonated ligand

species and Na^+ with considerably higher partition coefficients than those observed for species with higher charge. Low solubilities of potassium, sodium and protonated species involving 12N4Py4 in presence of lipophilic anions such as pertechnetate, perrhenate and triiodide lead to precipitation. Formation of solids is of considerable concern in minor actinide separations, but could also offer novel pathways for iodine trapping.

Acknowledgement

This project and thesis would not have been possible without the constant support of a number of people and organisations, all of whom I owe my thanks.

I would like to thank Prof. Stephen Faulkner, who has supervised and guided me through the last 3.5 years and helped me navigate around and over scientific and administrative obstacles and never lost his patience. He has been a great mentor.

I am truly grateful to the University of Oxford and Somerville College for this opportunity to spend the last years in this amazing research environment and the EPSRC for providing me with the neccessary funds for this project.

My thanks go to members of the Faulkner research group past and present, for insightful discussions and great entertainment, with special mentioning of Dr. Rebecca Hüting, Dr. Manuel Tropiano, Dr. Octavia Blackburn, Dr. Gearóid Ó Máille, Dr. Michael Jones, Leila Hill and Laura Mason.

Dr. Tamara Griffiths and Dr. Sean Woodall have spent a lot of time with and for me in the laboratory conducting the americium experiments.

The collaboration with the University of Zürich allowed investigations into the behaviour of technetium in extractions that proved vital to the understanding of the system. I would like to thank Prof. Roger Alberto for allowing me to work in his laboratory and Henrik Braband for supporting me throughout my work and for always being happy to help and answer all of my questions. Work in Zürich would not have been the same without the help and entertainment of Mathias Mosberger and Sara Jordi. I miss you all!

Research and analyses vital to my project would not have been possible without the constant support of the staff of the Department of Chemistry and the Chemistry Research Laboratory. Special thanks go to Dr. Nick Rees for support and services

connected to NMR measurements, Dr. Amber Thompson for solving and refining my crystal structures, Dr. James Wicken for fast services connected to mass spectrometry and Stephen Boyer in London who provided the elemental analyses.

I also would like to thank Mark Bradley and Gillian for the support during the set up of the uranium laboratory.

I will never forget the lunch breaks, pub nights and biscuit baking sessions with "the Germans", who have kept me motivated and provided me with many insightful scientific discussions, thank you Dr. Mirjam O'Duill, Dr. Michael Schedler, Dr. Lukas Pfeier, Dr. Emeline Rideau and Gregor Cremosnik. It was also Dr. Lukas Pfeifer to whom I owe my crystal structures and who had to measure more iodine containing crystals than he probably had expected to see in his scientific career.

My biggest thanks however have to go to Gregor Cremosnik, who has kept me focused and motivated, absorbed my frustrations and shared my successes, read and corrected all of my thesis and been my emotional support for the last six years.

Abbreviations

12N4Py4	1,4,7,10-tetrapicolyl-1,4,7,10-tetraazacyclododecane
2λ artefact	artefact caused by the excitation irradiation observed at double the wavelength
9N3Py3	1,4,7-tripicolyl-1,4,7-triazacyclononane
Å	Ångstrom(s)
An	Actinide
cyclen	1,4,7,10-tetraazacyclododecane
d	day(s)
DCM	dichloromethane
eq.	equivalent(s)
g	gram(s)
GWd/t	gigawatt day per ton
h	hour(s)
[Hb]	concentration of protons bound by species other than water
IR	infra-red
J	Joule
K_w	autoprotolysis constant of water
L	ligand
λ	wavelength
Ln	Lanthanide
L_{tot}	total amount of ligand
M	mol per litre
[M]	metal
MeCN	acetonitrile
MeOD	deuterated methanol
MeOH	methanol
mg	milligram(s)
ml	millilitre(s)
mmol	millimol
M_{tot}	total amount of metal
nH_b	average number of protons bound by a species other than water

nm	nanometers
NMR	nuclear magnetic resonance
pH	negative logarithm of concentration of [H3O+]
pK_a	negative logarithm of general acid dissociation constant
pm	picometer(s)
pM	negative logarithm of metal concentration
RT	room temperature
T	temperature
TACN	1,4,7-triazacyclononane
UV-Vis	Ultraviolet and visible spectroscopy
Z_{eff}	effective nuclear charge

Chapter 1: General Introduction

1.1 f-Elements

1.1.1 Lanthanides

The lanthanides (Ln) are a group of elements with very similar chemical behaviour, which is shaped by the gradual filling of the 4f orbitals. Their atomic electron configuration roughly follows the scheme $6s^2$ $5d^1$ $4f^n$, where the 6s and 5d electrons are relatively easily removed to form stable 3+ cations, the natural oxidation state of the lanthanides.[1] The remaining 4f electrons are only slightly more stable, but are located much closer to the core and shielded from interaction with the chemical environment by the 5s/p and even partially by the 4s/p/d orbitals (Figure 1.1).[1–4] Therefore even partially filled 4f orbitals are very unreactive, while giving rise to a variety of interesting physical behaviour, such as magnetism and long lived luminescence.[1]

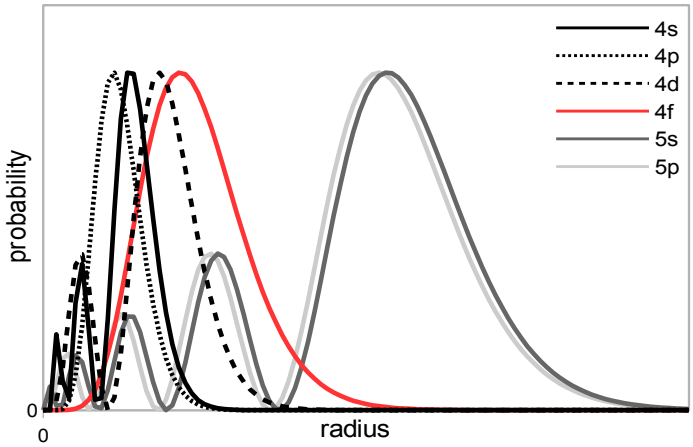

Figure 1.1: Normalised radial distribution function of orbitals in Nd(III) [1–4]

Oxidation states other than Ln(III) (e.g. Ln(II) and Ln(IV)) are known, but relatively rare and generally not stable in aqueous conditions, owing to the large difference between the 3rd and the 4th ionisation energy. The probably best known exception is cerium, whose 4f and 5d orbitals energetically lie very close together. Its 4f electron can therefore be removed easily to form Ce(IV). Ce(IV) salts

such as ceric ammonium nitrate (CAN) are exploited in organic chemistry as oxidative agents.[5]

In terms of their coordination chemistry the Ln(III) ions behave much like the transition metals Sc(III) and Y(III), as their valence electrons are core-like and cannot easily interact with their environment.[1] They also show similarities with alkali and earth alkali metals (as will be shown in chapter 4).

Ln(III) salts are generally moderately soluble in water and polar solvents or completely insoluble. and act as hard Lewis acids. Good ligands to complex them are usually polydentate molecules with hard donor atoms and negatively charged binding sites (e.g. carboxylic acids) like DOTA (Figure 1.2).[6] Common coordination numbers are 8 - 12, reflecting the large size of Ln(III) ions.[1]

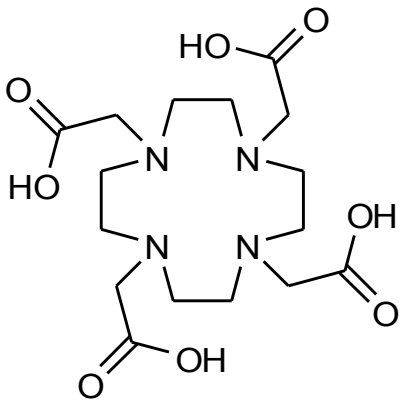

Figure 1.2: 1,4,7,10-Tetraazacyclododecane-1,4,7,10-tetraacetic acid (DOTA)

Throughout the series of the lanthanides, the ions gradually get smaller due to the lanthanide contraction as a consequence of increasing Z_{eff}, while the hydration enthalpy increases due to the increased charge density.[1]

Lanthanides have been and still are extensively studied for their luminescent properties. Due to the core-like nature of the f orbitals the emission bands are very narrow and make it possible to identify lanthanide ions by their emission spectrum (Figure 1.3). The relative intensities of the observed bands of one element is a response to the symmetry of electron density around the f-orbitals, indicating the coordination environment of the ion.[7]

f-f transitions are generally parity forbidden, but become partially allowed in certain

chemical environments due f-d hybridisation if the symmetry becomes non-centrosymmetric. However, the low core like nature of the f-orbitals, combined with the weak crystal field effects associated with lanthanide ions, mean that the relaxation of selection rules is much less than would commonly be seen with open shell d-block complexes.

The transitions remain very long lived, but also make for low quantum yields.[8] Therefore most lanthanide luminescence applications use a separate chromophore

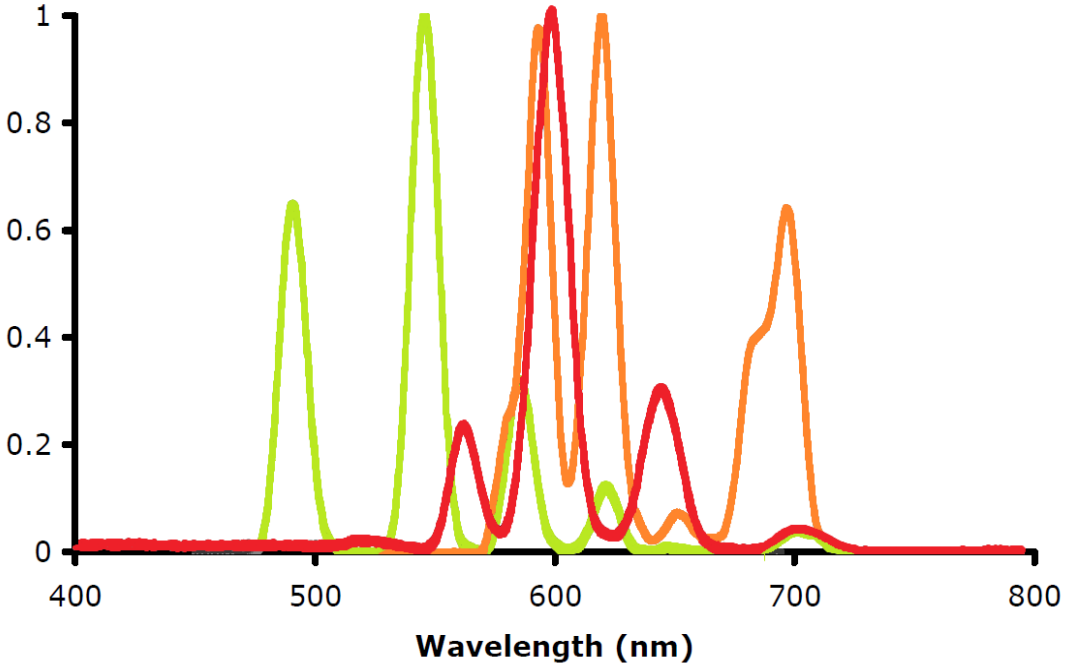

Figure 1.3: Emission spectra of tetrapicolyl-cyclen (see Chapter 2) and lanthanides. Tb (green, in D_2O), Sm (red, in MeOD) and Eu (orange, in D_2O), excitation at 260 nm. Modified from literature[30]

and excite the lanthanide indirectly. In molecular applications this is often referred to as the antenna effect and underlies several conditions such as distance and overlap of the excited states. Quenching can occur from gases, ions or solvent molecules.[9]

The subtle differences between the elements can be used to investigate chemical systems in great detail, however also make it very difficult to separate mixtures of them, a problem often encountered in lanthanide mining.[10]

1.1.2 Actinides

The second set of elements with incompletely filled 5f orbitals are the actinides (An). Their f-orbitals are well shielded against the environment, but in terms of energy the 5f orbitals lie much closer to the 7s and 6d orbitals and can therefore be removed more easily. Figure 1.4 shows a slightly greater overlap of 5f and the 6s/6p orbitals, however does not account for relativistic effects and spatial expansion of the orbitals that further shift the 5f orbitals towards the surface of the atom.

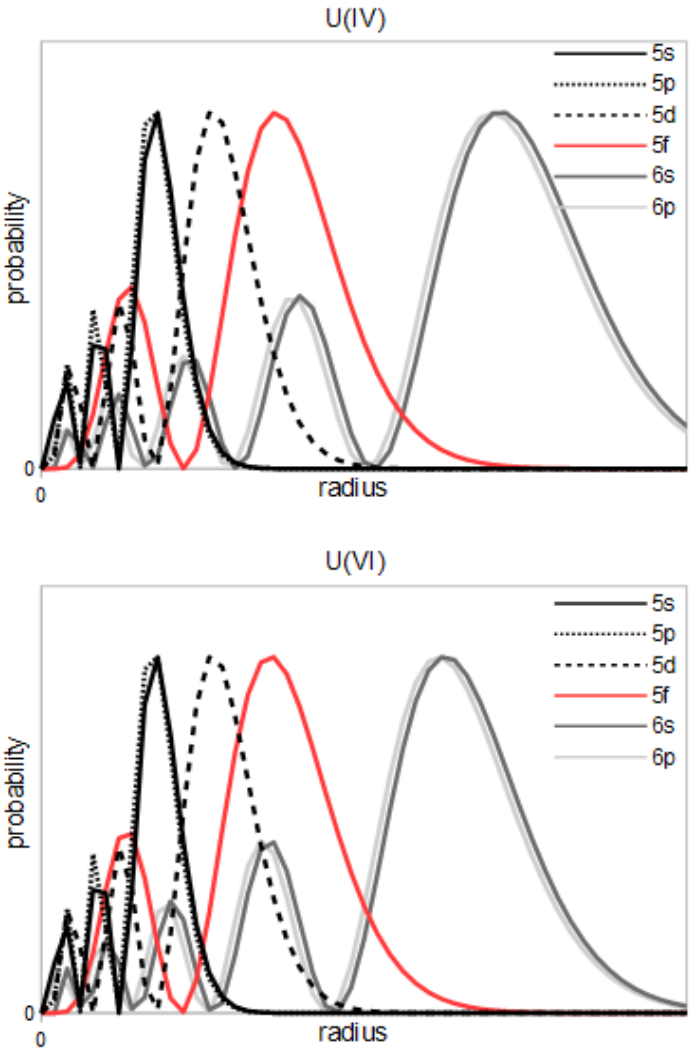

Figure 1.4: Normalised radial distribution function of orbitals in U(IV) and U(VI) [1–4]

The decrease in shielding gives rise to a very varied redox chemistry of the actinides which ranges from +2 to +7, although interestingly many later actinides do prefer the 3+ oxidation state, much like the lanthanides, as a consequence of the 5f orbitals becoming more shielded.[11] The combination of shielding and redox chemistry gives rise to complex behaviour in luminescence, magnetism and synthesis.[1]

The shielding of the 5f orbitals is somewhat less effective than that of the 4f orbitals,

allowing more covalent interactions with other atoms.[1] Distinct molecular species like uranyl ions (UO_2^{2+}) are more common.

The unique combination of a strong Lewis acidity, high coordination numbers, facile change of oxidation states and slightly covalent binding to ligands and substrates in early actinides allows for unusual binding modes and reactions. Uranium catalysis exploits this to activate small molecules like N_2 or CO as well as hydrocarbons.[12] Also polymerisation reactions and hydrogen production have been investigated.[13,14]

All the actinides are radioactive due to the large mass of their nuclei, as the attractive strong force is no longer sufficient to balance the repulsive Coulombic forces between the protons. Most of them do not occur naturally except for trace amounts.[11] However some isotopes of uranium and thorium have exceptionally long half-lives, so significant quantities are left from the formation of the planet.[15] Decay of uranium/thorium and natural fission events in uranium ores earlier in earth's history also supplied some smaller amounts of actinium, proactinium, neptunium and plutonium.[11,15] The later transuranic actinides only occur as synthetic elements, for example forming through neutron bombardment of uranium in nuclear power plants.[11]

Many actinide ions are highly coloured by comparison to the lanthanides, the wavelength range is often highly characteristic of the oxidation state of the respective element.[1] Luminescence occurs in ways similar to the lanthanides, but the emission is usually less sharp and more responsive to the chemical environment.[1] Mixing of states also causes 5f-5f transitions to be more allowed than 4f-4f transitions, resulting in broader emission bands and shorter lifetimes.

1.2 The Nuclear Fuel Cycle

One of the most talked about topics in today's society is the future of energy production. Among the "traditional" methods is the fission of actinides to produce heat in nuclear power plants. Even though it can be considered to be a renewable energy source as it does not produce carbon dioxide emissions, problems with waste disposal and dangers to the public in case of accidents have made large scale nuclear power generation a controversial issue. Advances are continuously made to change how fuel and waste is managed and processes have become more secure. In this part of the introduction the basics of nuclear power production, recycling of fuel and waste disposal are presented.

1.2.1 Fission of Actinides in Nuclear Power Plants

The radioactivity of the actinides is based on their core being too heavy to be held together by the nuclear force. The most common route of decay is the emission of alpha particles. Some of the actinides however can also undergo fission, a process where the core breaks apart into two smaller ones, often combined with the emission of neutrons, protons, alpha particles and a lot of energy. Some isotopes undergo spontaneous fission, many other only do so by induced fission, where the capture of a neutron by the nucleus triggers the nuclear reaction.[11]

Fissile material with a sufficient output of neutrons can uphold nuclear chain reactions. If the amount of a fissile nuclide surpasses a certain concentration, related to the critical mass, this chain reaction speeds up and causes violent reactions with production of large amounts of energy and radiation. Supercriticality is exploited in

nuclear weapons. Below criticality, the chain reaction slows down or cannot be upheld at all, depending on the neutron flux. Through mediation and control, some chain reactions can be upheld at a relatively constant level, giving a constant output of heat. This is exploited in nuclear power plant for electricity production.[11]

Fuel for nuclear reactors is based on uranium. It has one naturally occurring fissile isotope, U-235. Its abundance in natural uranium (0.7%) is rather low.

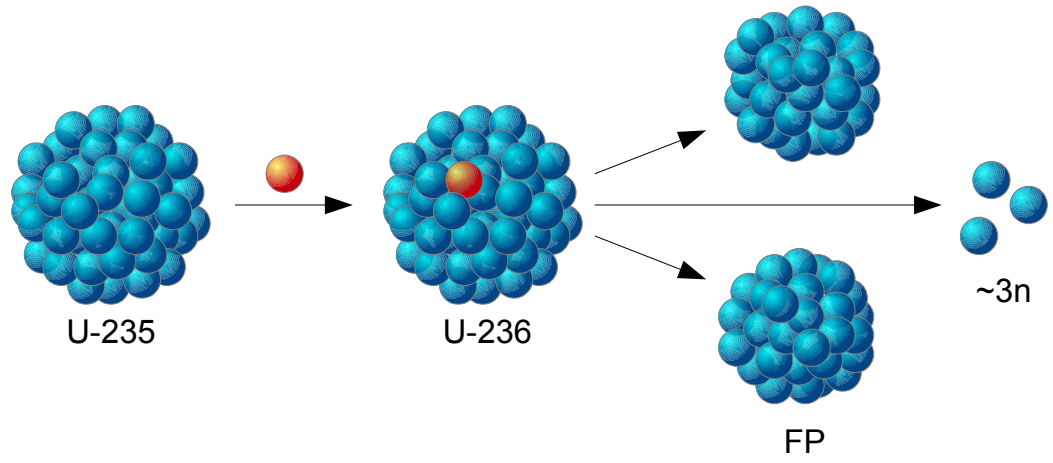

Figure 1.5: Schematic fission process of U-235 with thermal neutrons[11]

Uranium is mined in many places around the globe and chemically purified. By forming gaseous uranium hexafluoride, a material enriched in U-235 can be produced by gas centrifugation. For reactors, U-235 percentages of 3-4% are commonly produced. The remaining mass is mostly the non-fissile U-238.[11]

In the fission process a thermal or a fast neutron collides with and is taken up by the U-235 nucleus, causing it then to fall apart into two smaller nuclei, while releasing on average another 3 neutrons that drive the chain reaction (Figure 1.5). The resulting fission products show a characteristic distribution pattern with one heavier and one lighter fragment, as shown in Figure 1.6.[11]

In nuclear power plants the uranium fuel produces large amounts of heat. To regulate the heat output, control rods can be inserted into the reactor core. They are made

from material that absorbs neutrons well but cannot undergo fission itself, like boron or cadmium, removing neutrons from the fission chain. If the reactor employs the fission by thermal neutrons, additional moderators are used to slow down fast neutrons. This very often is the cooling water.[11]

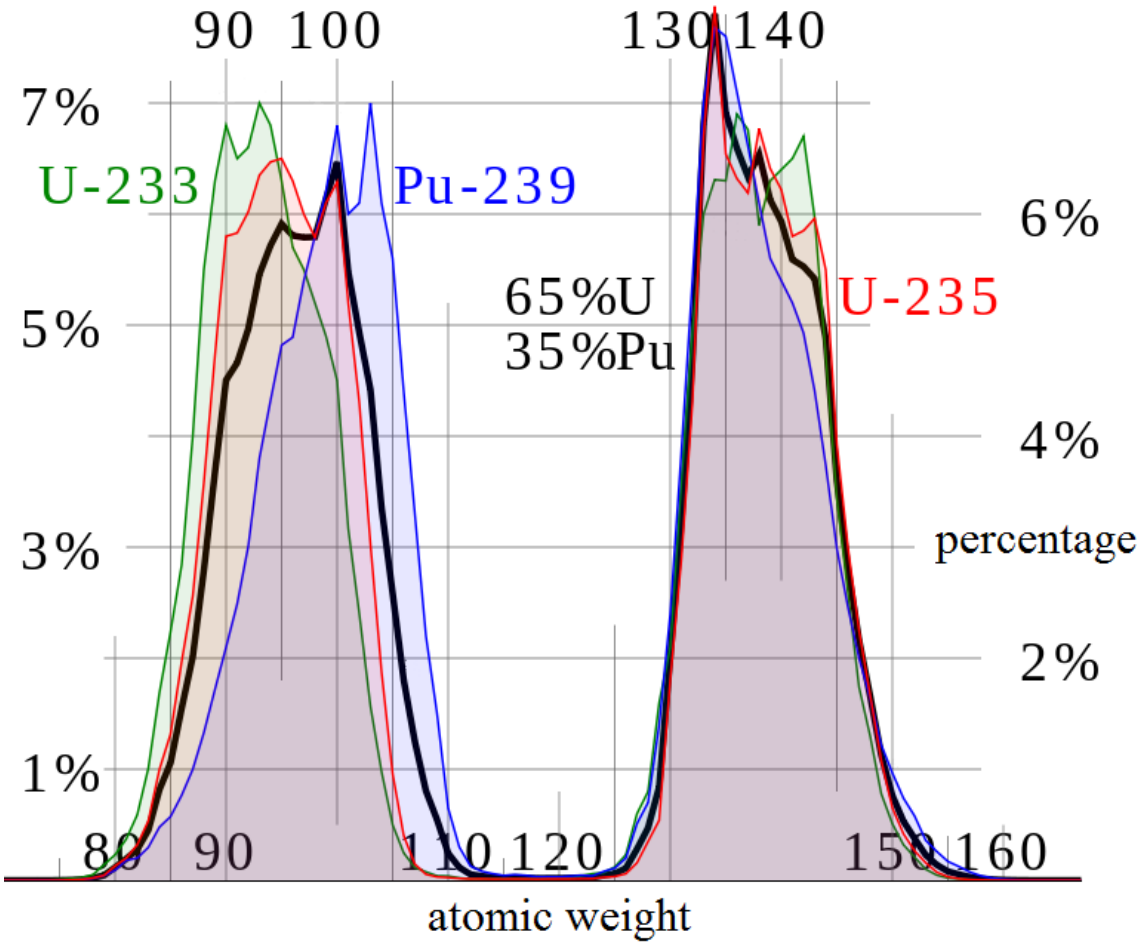

Figure 1.6: Fission product distribution from U and Pu. Modified from Wikipedia.[31]

A liquid medium, such as (pressurised) water or sodium, transports the generated heat away from the central nuclear element (core). The heat contained in this medium is used to generate electricity, for example with steam turbines. In order to avoid contamination of the turbines, the heat transportation is usually divided into two isolated systems with a heat exchange between the two.[11] A simplified plan of such a plant is shown in Figure 1.7.

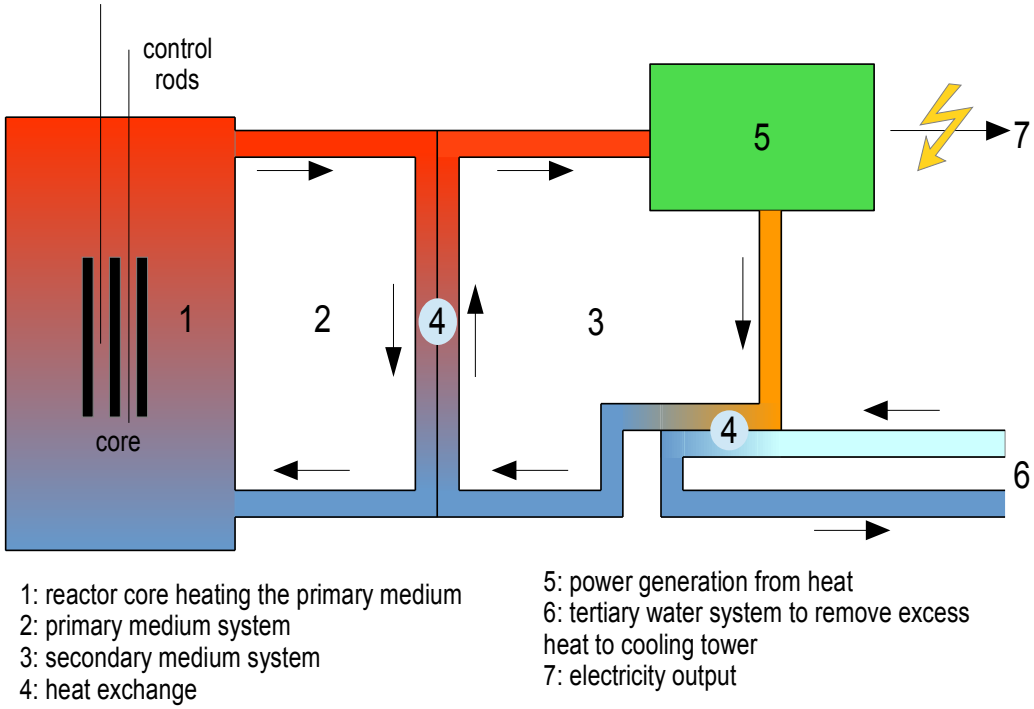

Figure 1.7: Basic layout of a nuclear power plant[11]

1.2.2 Nuclear Waste

During prolonged irradiation of uranium fuel the fission products start to accumulate. Some of them, like gadolinium, are good neutron capturers, but are not fissionable themselves.[11] This removes neutrons necessary to uphold the chain reaction, causing it to slow down. After a few years, the fuel needs to be removed from the reactor and replaced by fresh material.[11] Even though it is not enough to continue to produce enough heat for energy production, short-lived radioactive decay still heats up the fuel elements considerably and they need to be stored in water tanks for several years before they can be further processed.[11]

Spent nuclear fuel contains a whole range of fission products. Many of the isotopes formed are radioactive themselves and will decay into further elements. Neutron capture and subsequent β-decay also cause the formation of transuranic actinides.

Figure 1.8 shows an overview of the elements that are commonly present.

A typical nuclear power plant produces between 20 and 140 tons of spent fuel per year and GWe (gigawatt electrical) production.[16] Most countries are left with nuclear

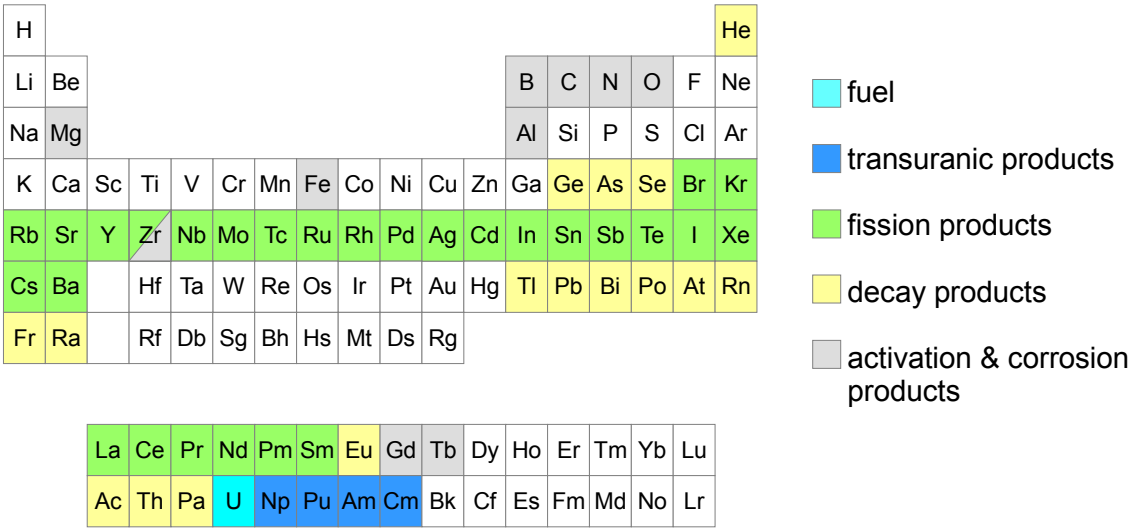

Figure 1.8: Elements of importance for nuclear reprocessing[11]

inventories of several thousand tons of nuclear material. In the early days of nuclear power production, the spent nuclear fuel was commonly stored dry or as aqueous solutions in storage tanks, often above ground or shallowly buried.[11] Slow degradation of the (single walled) tanks led to leaks, the most prominent case happening at the Hanford site, a plant that was built as part of the Manhattan Project.[11] Their storage tanks were designed to last for 20 years, but they have now been in operations for 31-74 years. Of the 177 tanks containing a total volume of over 210 million litres of waste 67 tanks have leaked more than 3.7 million litres of radioactive material.[17]

Great efforts have been made to find better solutions for storage of nuclear fuel on a geological time scale to cope with highly radioactive material with half-life times of several thousands to millions of years. For this, deep underground space in robust rock must be found, with a minimal risk of flooding and geological disturbance.[11] The

identification of such places is not simple and political discussion and public unease further complicate the process.[18–20]

Scientific advances gave rise to novel ways of creating safer waste forms. More robust tanks and especially the development of advanced vitrification techniques lower the risk of degradation and leakage over time.[21]

There is one more very important step to give a long term solution to the nuclear waste problem: waste separation. A large proportion of spent nuclear fuel could be used in the production of new nuclear fuel or other radioactive applications. Stable fission products, decay products and cladding material need decontamination before reuse or disposal in normal deposits. Short lived nuclides require limited special storage before they can be considered completely decayed, which is significantly easier to manage. Long term storage is only necessary for high-level waste containing nuclides with intermediate to long half-life times and a large amount of radiation output. If this type of waste is separated from the remaining material, only a fraction of the space would be required to store nuclear waste. The separation of waste and reintroduction of fissile material as new fuel is generally referred to as "closing the fuel cycle".

1.2.3 Composition of spent nuclear waste

The composition of spent nuclear fuel is strongly influenced by the initial enrichment, burn up time, reactor type and cooling time after removal from the reactor.[11] General trends however can easily be made out. The following numbers are used as an example, based on data from 1 ton of initial uranium with an output of 33 GWd/t and a cooling period of 3 years.[22] A graphical representation is shown in Figure 1.9.

The vast majority of the waste mass, 95.6%, remains as uranium. Of this, about 1% is U-235, so technically this is still considered enriched uranium. It could be used to produce fresh fuel and burned up further.

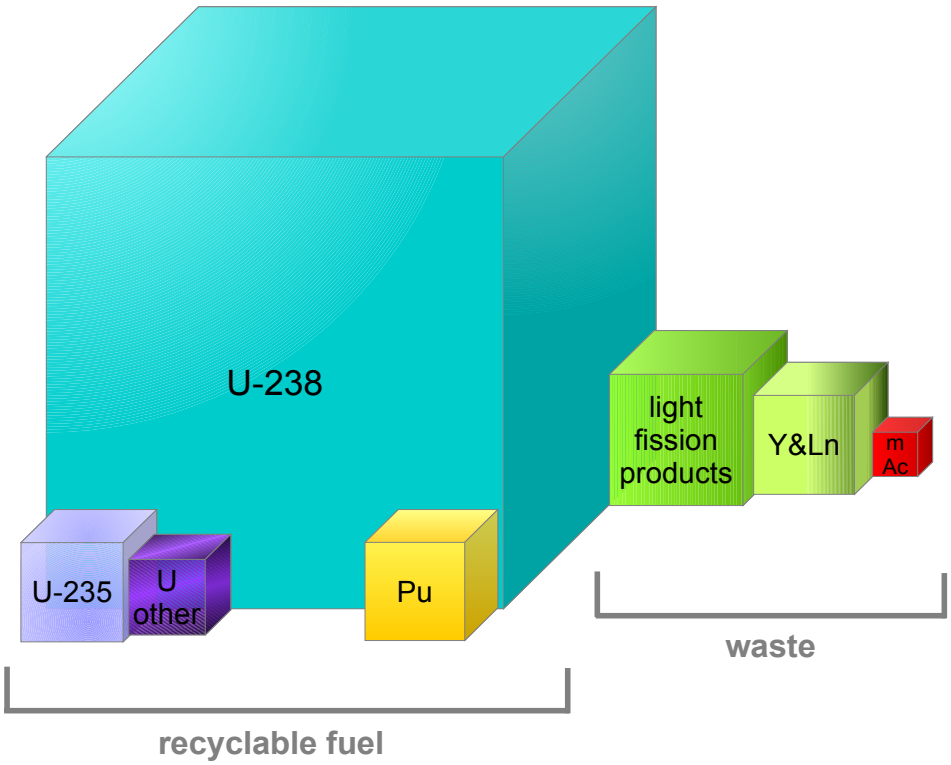

Figure 1.9: Volumetric representation of the mass of components of nuclear waste.[16]

If U-238 absorbs a neutron from the U-235 chain reaction it becomes U-239, which rapidly decays by two consecutive β-emissions to Pu-239. This nuclide is fissile itself and contributes to heat production in the reactor core.[11] Together with other plutonium isotopes it makes up around 0.9% of the spent fuel. Beside its use for nuclear weapons and specialised applications, it could be incorporated into mixed oxide fuel (MOX) alongside uranium and reintroduced into the nuclear fuel cycle. By mixing uranium and plutonium and thereby avoiding production of pure plutonium the possibility of weapon proliferation can be minimised.[15] At the same time, more energy is extracted from the initial uranium fuel.

Other transuranic elements, namely neptunium, americium and curium are represented by 0.09%. Some of these actinides have applications such as americium in smoke detectors. As the minor actinides show high levels of radioactivity and have long half life times, they are the main reason storage on a geological time scale is necessary. However if they are separated from the shorter lived fission and decay products, they require a lot less storage space than the original fuel waste.

The remaining 3.4% of the fuel goes to the fission products. Many of these are stable or show short to intermediate half-life times. Their storage is considerably easier to manage.[11] The early lanthanides, together with yttrium, make up for a good 30% of the fission products.

Traces of activation products can also be found. They are produced by the reaction of stray neutrons with any material present, e.g. the cladding material. Activation products in structural material add to the total amount of waste produced by nuclear power plants and the variety of elements present in reprocessing.

1.2.4 Reprocessing of Spent Nuclear Fuel

Efforts to separate nuclear waste have been made from the very start of nuclear energy production.[11,15] The desire for plutonium to produce atomic bombs created the first form of waste separation, ending in the best known process in nuclear recycling: the PUREX process. PUREX stands for Plutonium-Uranium Recovery by EXtraction. The solid fuel rods are dissolved in concentrated nitric acid and extracted with tri-n-butyl phosphate (TBP, Figure 1.10) in an organic solvent. TBP binds uranium and plutonium species and forms extractable lipophilic complexes. Reducing the plutonium selectively to Pu(III) returns them into a hydrophilic state, it is then

separated from the uranium by back extraction into water.[11,15] Several different species are involved in the extraction processes, though detailed equilibria and speciation are still subject to investigations.[23,24]

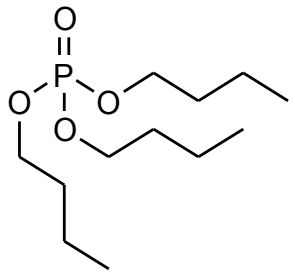

Figure 1.10: Tri-n-butyl phosphate (TBP)

With the current decommissioning of nuclear weapons, the need for pure plutonium has strongly decreased. The danger of proliferation of weapon grade material now requires a novel approach to PUREX.

Reintegration of plutonium into the nuclear fuel cycle as MOX or other mixed fuels is currently the preferred option in the UK.[15] Several other procedures have been developed since. Some can be seen as alternatives to PUREX, but others are meant to be combined with PUREX or other separation methods and take on the difficult task of separating the (minor) actinides from the lanthanides. They rely on different extractants, separation sequences and combinations thereof. So far, no standardised procedure has been established and many countries and companies prefer the one they developed.

One possible combination of separation is shown in Figure 1.11. Following the original PUREX separation and purification of uranium/plutonium, the remaining f-elements are extracted together in a DIAMEX (DIAMide EXtraction) step. The lanthanides are back extracted into a water phase using SANEX (Selective ActiNide EXtraction) while the minor actinides are held back in the organic phase. The fission products stay in the water phase during the DIAMEX separation and could possibly be further separated and/or disposed of as soon as the shorter lived isotopes have decayed.

Several other procedures have been developed that differ in sequence and/or conditions used.[11,15,22]

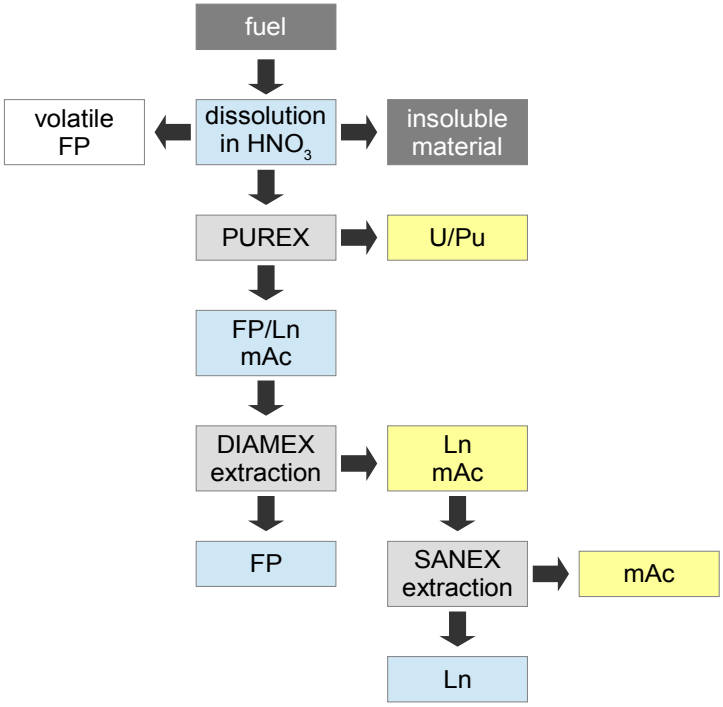

Figure 1.11: Potential flowsheet for nuclear fuel separation

During cutting and dissolving the spent fuel, some fission products already separate from the waste stream: volatile or gaseous elements and compounds are released from the solid fuel and need to be captured. These compounds contain isotopes of iodine, krypton, xenon, bromine, hydrogen and some technetium, alongside gases like CO_2.[11] Other elements, especially transition metals, can form insoluble alloys that precipitate from solution and need to be treated separately. The exact composition of these alloys however strongly depends on reactors, fuel type and reprocessing methods.[15]

A few fission products are of special interest due to their low occurrence in nature and high demands in industry and modern technology, such as rhodium and palladium. Possible means to recover them from the waste stream are currently being explored[25], although industrial application of these techniques will not be commercially viable for quite some time.

For the minor actinides, several options exist once they have been separated from

the waste stream. Disposal in long term storage is one option, and elaborate methods of incorporating them in chemically inert glasses (vitrification) are widely used or planned.[11,15,21] Disposal into space was discussed, but at the moment the consequences of accidents while launching would be disastrous.[11] Another way would be to expose them to transmutation. This involves the nuclei being treated with neutrons or other radiation to "transmute" them into different elements/isotopes that decay more rapidly. Some of the newly formed nuclides can undergo fission and their "parent" nuclide is then considered fertile.[11] Transmutation can be achieved in reactors using fast neutrons (in contrast to the thermal neutrons in most reactors) or breeder reactors. For some nuclides, including long lived fission products, transmutation in special transmutation reactors would be preferable to control the process and minimise the production of other long lived products. Transmutation would further decrease the amount of high-level waste and reduce the radioactive legacy of our generation.[11]

1.2.5 Common problems in fuel recycling

Many of the procedures used in fuel processing are several decades old and have shown flaws in their design.[15] Since their development, new requirements have been set up dictated by reprocessing design, desired product constitution and environmental/safety considerations.

One of the major problems of the PUREX process is the coextraction of technetium. In aqueous environments it usually occurs as the pertechnetate anion (TcO_4^-) and is believed to act as a counter ion to the U/Pu-TBP complex.[15] Ideally pertechnetate would be removed early on in the process, remain in the aqueous phase without

interaction with the extracted complexes or be held back in the aqueous phase during extraction by a separate reagent.

The dissolved nuclear waste is highly radioactive and will degrade solvents and extractants as well as components of the processing machinery.[11,26] The heavier the core of an atom, the more likely it is to absorb radiation (especially neutrons) and cause the destruction of the molecule, in the case of TBP the phosphorus atom. The development of novel extractants is restricted to light, first and second row elements, namely carbon, hydrogen, oxygen and nitrogen. Accordingly, these extractants are commonly called CHON ligands. Beside their light weight they can also be completely incinerated to harmless compounds without residue.[27]

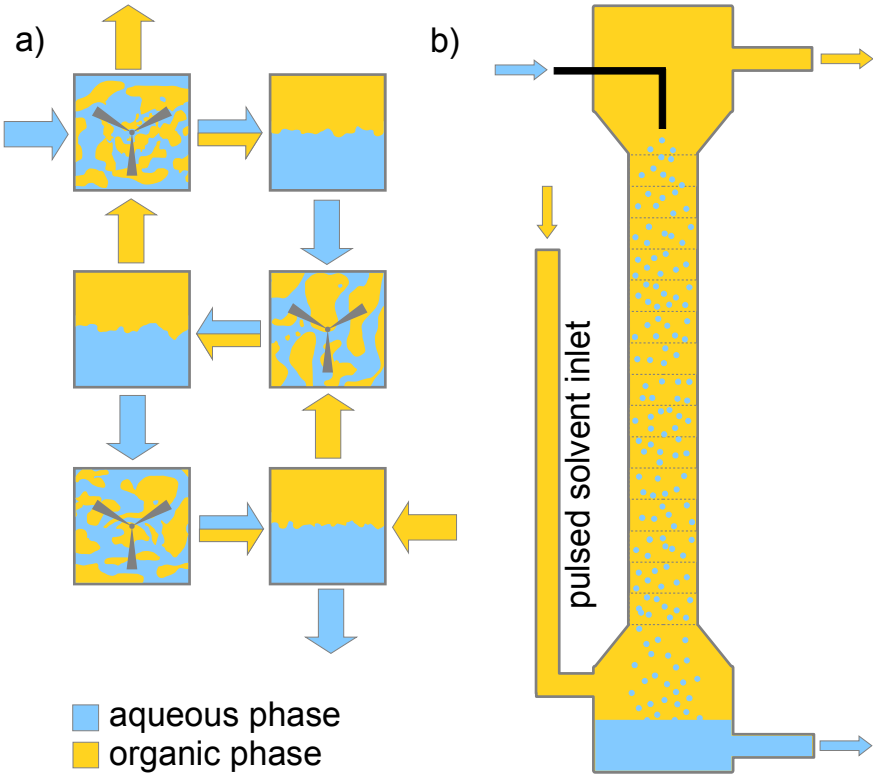

Figure 1.12: Industrial extraction instrumentation: a) mixer-settler, series of 3 stages, b) pulsed column.[15]

With high levels of radioactivity, oxidising solutions and degradation of extractants, time is of the essence. Many processes, especially after the removal of U and Pu, require very long equilibration times.[28] With the currently available instruments for continuous extraction, mixer-settlers and pulsed columns (Figure 1.12), contact times are short and require fast extraction kinetics. Future extractions

need to show significantly improved kinetics to achieve equilibrium or be under kinetic product control.

Furthermore, as this is an industrial application, production cost of solvents and extractants will be considered before a candidate is implemented into the processes.

1.3 Goal of the project

In order to design the future procedures for spent nuclear fuel reprocessing, the molecular processes that govern the extractions need to be well understood. So far many studies concentrated on achieving the best possible separation between lanthanides (often Eu as standard[28,29]) and the minor actinides by extraction studies and a few binding studies. The underlying processes, interactions with contaminants and the way conditions affect the extractions are poorly understood.

By far the biggest challenge in minor actinide separations is to find ligands and conditions that will favour the binding of actinides over the lanthanides. They all are commonly encountered as M^{3+} ions, all of similar size and charge distribution. Chemically relatively inert, they cannot be separated by specific chemical reactions in an aqueous solution. To distinguish them, one has to make use of the more subtle differences.

For one, actinides are known to form somewhat more covalent bonds than lanthanides and favour softer donor sets. Where the latter are strongly bound by hard anionic ligands, for example by carboxylic acid functionalities, their interaction with softer donors such as nitrogen or sulphur is much weaker. The actinides however are likely to form more stable complexes with softer donors.

Even though their size is very similar, the actinides are slightly larger as shown in

Figure 1.13. The focus being on the early actinides up to curium, the early lanthanides from lanthanum to samarium will be of the most concern in terms of similar size. An(IV) ions are significantly smaller and are highly unlikely to bind to the same ligand types that were optimised to early Ln(III) and An(III). Even less so as many of them lie in an equilibrium with the even smaller An(VI) ions, that tend to form molecular species instead of spherical ions.

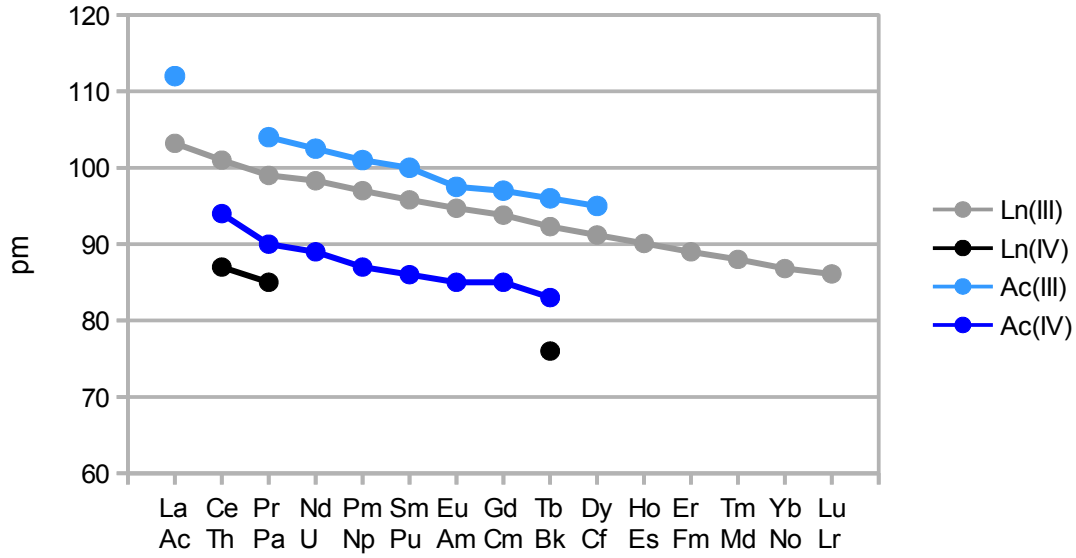

Figure 1.13: Ionic radii of Ln and An cations in a hexacoordinated environment[32]

Non-ionic functionalities form charged complexes with the f-elements, which could potentially be an issue when it comes to extraction into a non-polar phase. The coextraction of anions to balance the charge needs to be investigated and potentially be optimised.

In the following chapters several aspects of minor actinide extractions will be discussed. The speciation of metal complexes, their interaction with anions and the competition with protonation processes were evaluated in a range of systems and conditions, including extraction studies.

References

[1] S. Cotton, *Lanthanide and Actinide Chemistry*, Wiley, Chichester, **2007**.
[2] L. Pauling, E. B. Wilson, *Introduction to Quantum Mechanics: With Applications to Chemistry*, Courier Corporation, **1985**.
[3] J. C. Slater, *Phys. Rev.* **1930**, *36*.
[4] P. W. Atkins, R. Friedman, *Molecular Quantum Mechanics*, Oxford University Press, Oxford ; New York, **2011**.
[5] P. Jacob, P. S. Callery, A. T. Shulgin, N. Castagnoli, *J. Org. Chem.* **1976**, *41*, 3627–3629.
[6] S. Aime, M. Botta, M. Fasano, E. Terreno, *Chem Soc Rev* **1998**, *27*, 19–29.
[7] D. F. Shriver, P. W. Atkins, *Inorganic Chemistry*, Oxford Univ. Press, Oxford, **2002**.
[8] P. Hänninen, H. Härmä, T. Ala-Kleme, Eds. , *Lanthanide Luminescence: Photophysical, Analytical and Biological Aspects*, Springer, Berlin; New York, **2011**.
[9] A. de Bettencourt-Dias, Ed. , *Luminescence of Lanthanide Ions in Coordination Compounds and Nanomaterials*, Wiley, Chichester, West Sussex, United Kingdom, **2014**.
[10] F. Xie, T. A. Zhang, D. Dreisinger, F. Doyle, *Miner. Eng.* **2014**, *56*, 10–28.
[11] G. Choppin, C. Ekberg, J.-O. Liljenzin, J. Rydberg, Eds. , *Radiochemistry and Nuclear Chemistry*, AP, Academic Press/Elsevier, Amsterdam, **2013**.
[12] S. M. Mansell, N. Kaltsoyannis, P. L. Arnold, *J. Am. Chem. Soc.* **2011**, *133*, 9036–9051.
[13] A. R. Fox, S. C. Bart, K. Meyer, C. C. Cummins, *Nature* **2008**, *455*, 341–349.
[14] T. Andrea, M. S. Eisen, *Chem Soc Rev* **2008**, *37*, 550–567.
[15] P. D. Wilson, Ed. , *The Nuclear Fuel Cycle: From Ore to Waste*, Oxford University Press, Oxford; New York, **1996**.
[16] H. Feiveson, Z. Mian, M. V. Ramana, F. von Hippel, **2011**.
[17] *NUCLEAR WASTE: DOE Lacks Critical Information Needed to Assess It's Tank Management Strategy at Hanford*, US Government Accountability Office, **2008**.
[18] A. Mascarelli, *New Sci.* **2013**, *220*, 42–45.
[19] E. Gibney, *Nat. News* **2015**, *December 2nd*.
[20] Greig Watson, *BBC News* **2016**.
[21] M. I. Ojovan, W. E. Lee, *Metall. Mater. Trans. A* **2011**, *42*, 837–851.
[22] International Atomic Energy Agency, *Spent Fuel Reprocessing Options.*, International Atomic Energy Agency, Vienna, **2008**.
[23] Y. S. Fedorov, B. Y. Zilberman, A. A. Kopyrin, S. A. Arkhipov, *Radiochemistry* **2001**, *43*, 166–171.
[24] P. Sahu, S. M. Ali, K. T. Shenoy, *Phys Chem Chem Phys* **2016**, *18*, 23769–23784.
[25] Z. Kolarik, E. V. Renard, *Platin. Met. Rev.* **2003**, *47*, 74–87.
[26] M. H. Lloyd, R. L. Fellows, *Alpha Radiolysis and Other Factors Affecting Hydrolysis of Tributyl Phosphate*, Oak Ridge National Laboratory, **1985**.
[27] C. Madic, O. Courson, R. Malmbeck, K. Römer, G. Pagliosa, B. Sätmark, J.-P. Glatz, P. Baron, **1998**.
[28] F. W. Lewis, L. M. Harwood, M. J. Hudson, M. G. B. Drew, J. F. Desreux, G. Vidick, N. Bouslimani, G. Modolo, A. Wilden, M. Sypula, et al., *J. Am. Chem. Soc.* **2011**, *133*, 13093–13102.
[29] A. Afsar, L. M. Harwood, M. J. Hudson, P. Distler, J. John, *Chem Commun* **2014**, *50*, 15082–15085.
[30] L. S. Natrajan, N. M. Khoabane, B. L. Dadds, C. A. Muryn, R. G. Pritchard, S. L. Heath,

A. M. Kenwright, I. Kuprov, S. Faulkner, *Inorg. Chem.* **2010**, *49*, 7700–7709.
[31] JWB, "Thermal Fission Yield," can be found under https://en.wikipedia.org/wiki/File:ThermalFissionYield.svg, **2008**.
[32] R. D. Shannon, *Acta Crystallogr. Sect. A* **1976**, *32*, 751–767.

Chapter 2: Ligand Synthesis

2.1 Choosing model ligands

The main challenge for future nuclear fuel cycles is the development of a procedure capable of separating lanthanides and actinides to allow transmutation of the highly radioactive minor actinides.

In the introductory chapter it was already mentioned that the goal of this project was to provide more knowledge to base the design of novel extractants on for industrial nuclear fuel reprocessing. This involved the study of the molecular processes involved with metal binding, extraction between organic and aqueous phases and how these processes are influenced by the presence of other species.

To investigate these processes, model ligands were required that form well defined complexes with M(III) ions of the f-elements. They should have structural features enabling their study in solution, and should comply with the general requirements for compounds to be used in the nuclear fuel cycle as discussed in chapter 1.

Whereas most ligands presented in recent literature focus on an efficient separation of the minor actinides from model lanthanides (often Eu(III))[1,2], the design of the ligands presented here is focused on their potential to aid the identification of important processes relevant for industrial application and to understand how certain ligand properties affect them.

In this chapter the two model ligands used in the project are introduced, the reasoning behind their design explained and their synthesis and properties discussed.

The ligand used for the major study of the project was 1,4,7,10-tetrapicolyl-1,4,7,10-

tetraazacyclododecane (12N4Py4, Figure 2.1), that was chosen on the basis of several characteristics that make it an excellent model extractant.

1. polydenticity. The ligand provides eight binding sites for the lanthanide and actinide ions, reduces the influence of solvent molecules and other monodentate ligands, and increases the binding strength by exploiting the chelate effect. By combining several binding sites within one ligand molecule, the entropy decrease that has to be overcome to form the metal complex is significantly reduced. Additionally, polydentate ligands may dissociate at one coordination site but are kept in close proximity of the metal centre through the coordination at the other donor atoms. With the large amount of donor atoms, formation of complexes with different metal to ligand ratios can be avoided, as the octadentate 12N4Py4 satisfies the f-elements need for high coordination numbers and a 1:1 coordination is favoured.

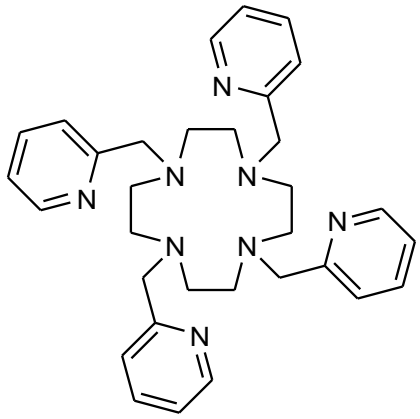

Figure 2.1: 1,4,7,10-Tetrapicolyl-1,4,7,10-tetraazadodecane (12N4Py4)

2. macrocyclic base: It is well known that the correct size of macrocyclic ligands facilitate the formation of complexes.[3] By forming a cyclic structure some degrees of freedom within the ligand are removed and the macrocyclic binding sites are prearranged close to the conformation necessary to bind the metal ions. Its rigidity avoids the formation of binuclear complexes through bridging coordination and supports the formation of 1:1 complexes and should cause a strong preference for spherical ions over the linear actinyl ions (UO_2^{2+}, NpO_2^{+}). In comparison to cryptands, armed macrocycles retain enough flexibility to accommodate several similar ions, as

both An(III) and Ln(III) slightly vary in size across the series.

3. CHON principle: Restriction to these elements ensure it can be incinerated and reduces the radiolysis commonly encountered with heavier nuclei. These problems are encountered with the traditional extractant TBP in PUREX due to its phosphorus content and are one of the reasons for the development of a new generation of ligands.[4]

3. Softer donors: Nitrogen donors are considerably softer than oxygen donors often used to produce highly stable lanthanide complexes. They favour metal cations that are able to interact covalently with their ligands, which should lead to stronger binding constants for actinides than for lanthanides and enable their separation. A decrease in binding strength also should allow f-element complexes to be kinetically labile to be able to form a thermodynamic equilibrium.

4. Aryl chromophores: By adding a chromophore as a functional group new ways of detecting formed species emerges. UV-spectra will show the presence of ligands and complexes. Especially with the f-elements intense emission and long life-times can be expected for the complexes, giving an additional detection method.

5. symmetry: The presence or a C4 rotation axis facilitates the observation of species using various spectroscopic methods. Especially in NMR spectra of paramagnetic complexes a well defined molecular axis significantly simplifies interpretation of signals.

6. simplicity. Beside the functional groups involved in binding metal ions and the basic backbone of the ligand, no other moieties are present. Optimisations to improve solubility, phase transfer or to make the synthesis cheaper were not of primary concern. This makes 12N4Py4 a simple ligand based on the amount of

binding sites it provides.

The binding strength between ligands and metals is not only based on functional groups, but also on the size of the binding pocket. The octadentate 12N4Py4 is of ideal size to fit lanthanide 3+ ions, which has been previously shown.[5] While actinide 3+ ions are of comparable size (see chapter 1), the early actinides are readily oxidised to smaller An(IV) ions that might bind more strongly to ligands with smaller binding cavities.

The smaller hexadentate analogue of 12N4Py4, tripicolyl-triazacyclononane (9N3Py3, Figure 2.2) was chosen as a second ligand. It only provides 6 nitrogen donors but might still be able to make use of the macrocyclic effect to bind some of the smaller metal ions and allow insight into their extraction as well as the extent of size selectivity of macrocyclic ligands. Generally it was assumed that the rigidity of the macrocycle and the pyridyl rings favours metal ions of a certain size and excludes larger ions as it can no longer wrap around the metal in a stable conformation. 9N3Py3 might be of an appropriate size to bind to the smaller late Ln(III) ions such as ytterbium or some of the An(IV) ions. An(VI) are even smaller, but commonly not found as spherical ions but as molecular species such as uranyl, it was not expected that they would be coordinated by one of the macrocyclic ligands.

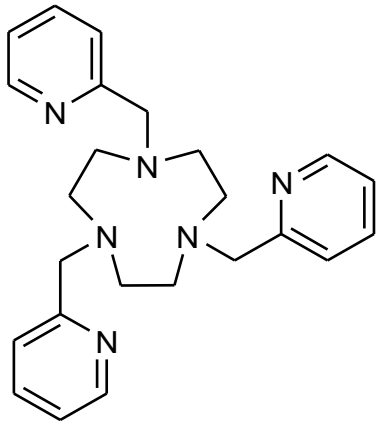

Figure 2.2: 1,4,7-Tripicolyl-1,4,7-triazacyclononane (9N3Py3)

2.2 Synthesis of the macrocycles

The desired ligands can be accessed from the unsubstituted macrocycles 1,4,7,10-tetraazacyclododecane (cyclen) and 1,4,7-triazacyclononane (TACN).

Cyclen is commercially available and was used as purchased in this project.

TACN is also commercially available, however due to its high price it was synthesised following a literature procedure.[6] N,N',N''-tritosyldiethylene triamine disodium salt was reacted with ethylene glycol ditosylate to form the macrocyclic ring (Scheme 2.1), followed by detosylation of tosyl-TACN in concentrated sulfuric acid. Precipitation with ethanol yielded the polyhydrosulfate salt of the product that was worked up in aqueous hydrochloric acid.[6]

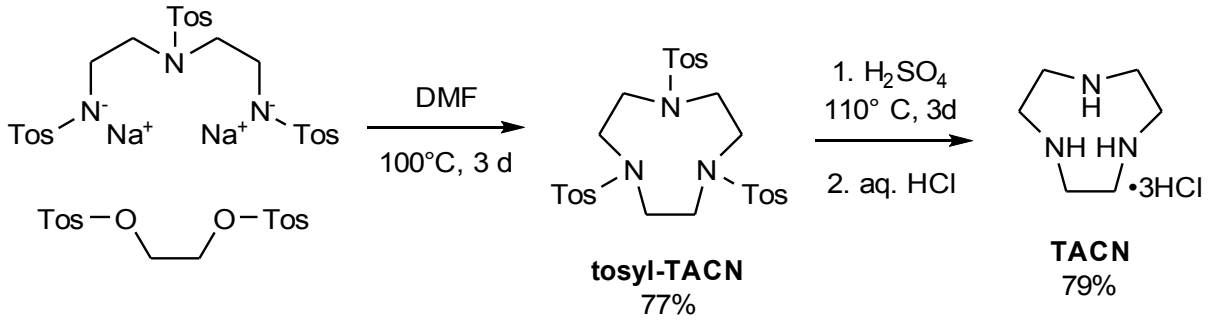

Scheme 2.1: Synthesis of 1,4,7-triazacyclononane (TACN)

The free TACN base can be obtained directly by a second basic work up, but storage, handling and weighing was significantly easier when the hydrochloride salt was produced. As most of the subsequent reactions require the addition of base, deprotonation can occur *in situ*.

2.3 Tetrapicolyl-cyclen (12N4Py4)

12N4Py4 has been previously studied with various lanthanides, although in a different context.[5] Its affinity for An(III) ions should theoretically be higher due to the softer donor sets, being more compatible with the greater covalency of the actinides.

The synthesis of 12N4Py4 was short and efficient and was conducted using a previously described procedure.[5] Heating cyclen and picolyl-chloride hydrochloride in acetonitrile over cesium carbonate overnight (Scheme 2.2) yielding the desired product through a substitution mechanism. Purification was achieved by recrystallisation from hot acetonitrile, producing pale orange needles.[5]

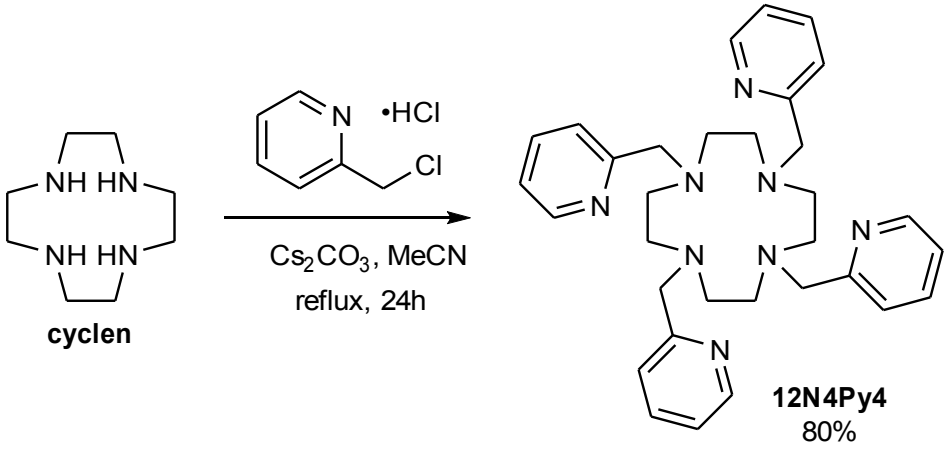

Scheme 2.2: Synthesis of 12N4Py4

It was also established that 12N4Py4 could be prepared in aqueous conditions. Cyclen and the picolyl-chloride hydrochloride were dissolved in water, adding a few drops of HCl to improve the solubility of cyclen. Solid KOH was then slowly added to deprotonate the cyclen amines, until a pH of 11 was achieved. The product was formed as the free base and was found to have limited solubility in water, precipitating as a colourless solid of sufficient purity to be used in subsequent reactions.

2.4 Tripicolyl-TACN (9N3Py3)

The synthesis of 9N3Py3 followed the literature as described by Wieghardt et al.[7]

The hydrogenchloride salts of both TACN and 2-picolyl-chloride were dissolved in water and NaOH was slowly added (Scheme 2.3). The pH was adjusted to between 9 and 11 and maintained until precipitation of a red oil was complete.

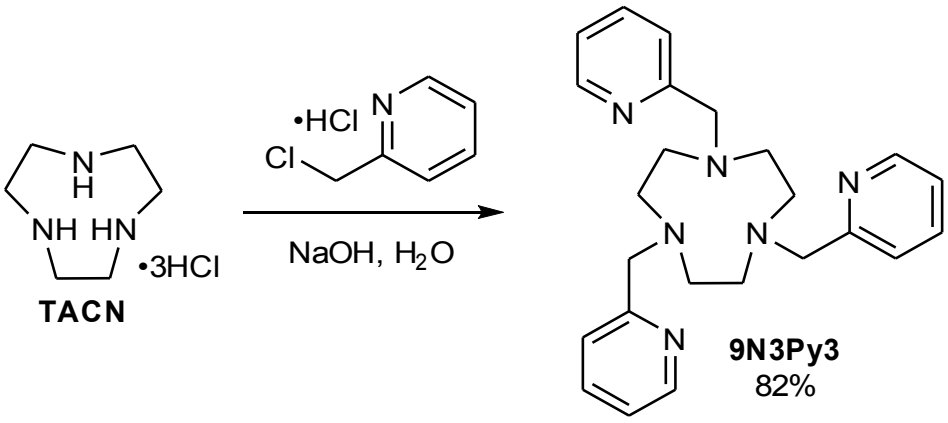

Scheme 2.3: Synthesis of 9N3Py3

Generally the purity of the oil produced was sufficiently pure to be used in subsequent reactions. It was stored in a freezer, as at room temperature it darkened in colour and slowly decomposed. Partially decomposed product was purified by column chromatography, yielding a highly pure product of a yellowish colour.

2.5 Spectral properties of 12N4Py4 and 9N3Py3

The benefits of simple model ligands are already revealed in the ^{1}H-NMR spectrum, where the 40 hydrogen atoms of a 12N4Py4 molecule combined to give 6 signals (Figure 2.3) corresponding to distinct proton environments, for 9N3Py3 6 signals were also observed for the 30 hydrogen atoms present.

Ring and relative arm conformation do produce different environments for the

involved protons (axial and equatorial protons, different steric interactions), however interconversions between conformers of the free ligand have low energy barriers and occur sufficiently fast to give averaged signals in the spectrum.

Some minor differences between the spectra can be found in terms of shift. Due to their different sizes the two compounds take on slightly different geometries in solution leading to a change in the local environment of the proton nuclei.

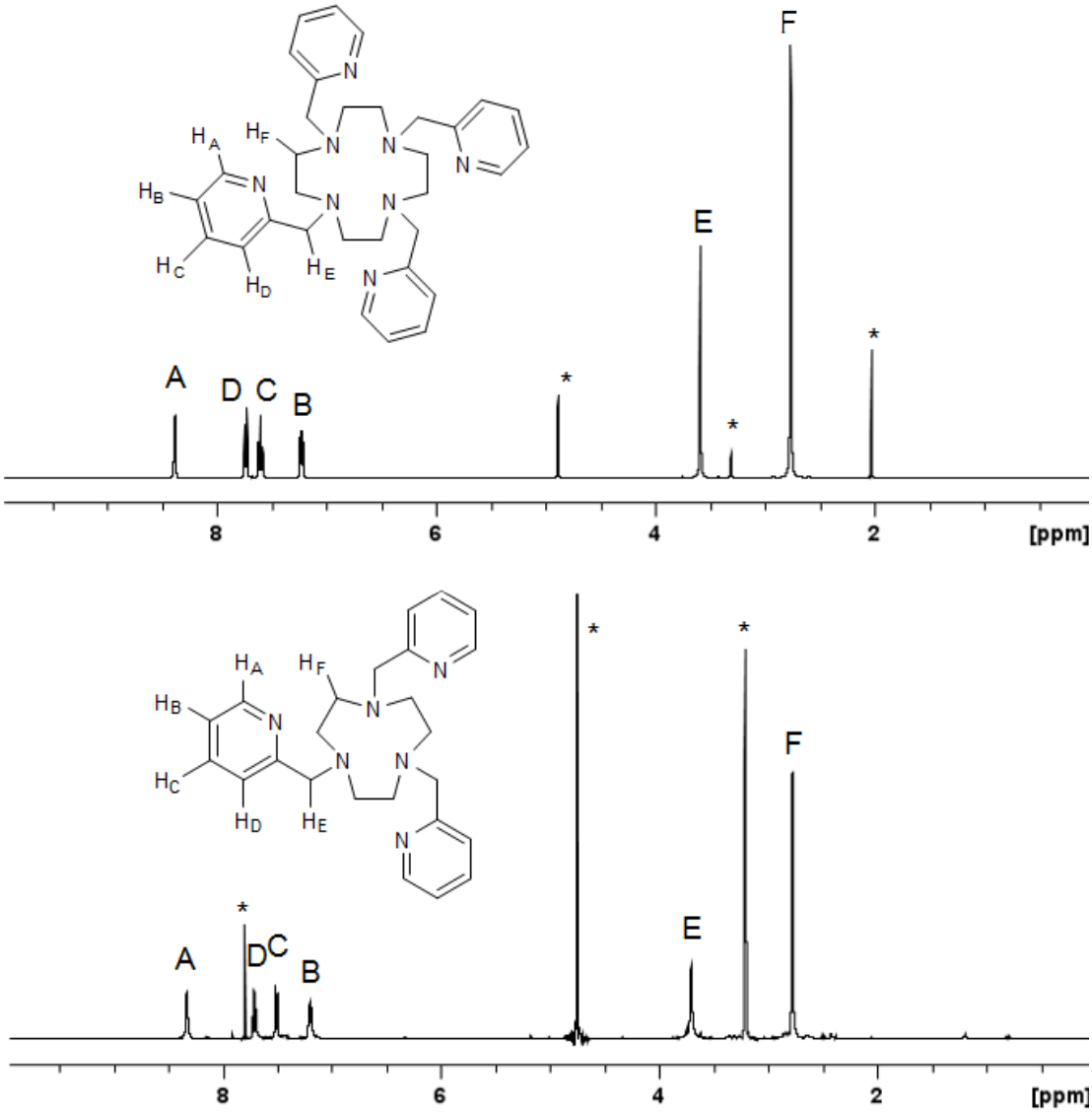

Figure 2.3: ^{1}H-NMR of 12N4Py4 and 9N3Py3 in MeOD

2.5.1 Photophysical properties of 12N4Py4

The presence of pyridyl functionalities offers the possibility to analyse 12N4Py4 and 9N3Py3 by UV-absorption and luminescence. In theory all pyridine derivatives have three π→π* absorption transitions, two corresponding to an aryl E-band below 200 nm and a B-band at 250-270 nm.[8,9] In most solvents, the E-bands are not or only partially visible due to the absorption of the solvent molecules themselves.

The B-band in 12N4Py4 was observed at 260 nm in methanol (Figure 2.4) and shows a weak fine structure of three underlying bands originating from vibrational states. Pyridine and its derivatives also have the possibility for a n→π* transition from the lone pair orbital (n for non-bonding orbital). In polar solvents however it is shifted and commonly masked by the π→π* transition, protic solvents additionally form hydrogen bonds with the lone pair which decreases the intensity of the n→π* absorption, as would be the case for the measurement in methanol. The extinction coefficient of 12N4Py (11568 M^{-1} cm^{-1} in methanol) was found to be significantly larger than in pyridine (2750 M^{-1} cm^{-1} in ethanol[9]), due to the increased number of chromophores per molecule.

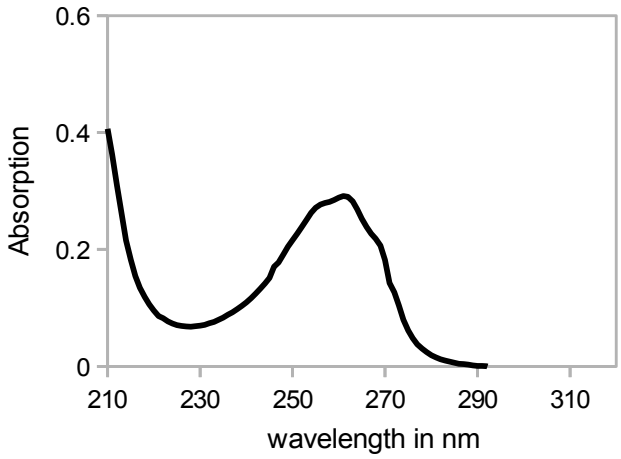

Figure 2.4: UV-Absorption of 12N4Py4 in MeOH

In the emission spectra a weak signal could be observed at 450 nm (Figure 2.5). It was broad and featureless as is typical for organic chromophores. Based on signal

assignment of pyridine in literature[10], the 450 nm emission corresponds to the $T_1 \rightarrow S_0$ transition and was in fact a phosphorescence signal. Fluorescence would be observed at around 330 nm, but is known to be very weak or not observed for pyridine compounds at room temperature and condensed phases.[10]

The excitation spectrum measured by observing emission at 450 nm overlaps with the absorption spectrum.

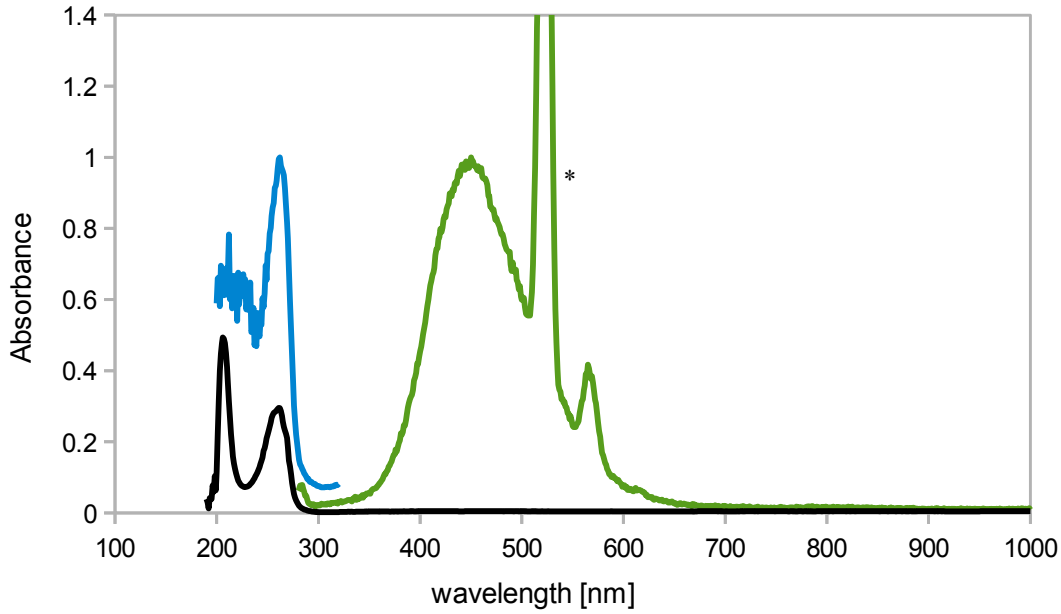

Figure 2.5: Luminescence spectra of 12N4Py4, absorption (black), emission (green, normalised, λ_{ex} 260nm) and excitation (blue ,normalised, λ_{em} 455 nm), recorded in MeOH, $5*10^{-5}$ M. 2λ artefact present (*).

The singlet and triplet states of excited pyridine chromophores are composed of several components (Figure 2.6).[11] As mentioned before, the n→ π* transition is often weak, due to the limited overlap between the orbitals, even though the lone pair orbital n is the highest occupied molecular orbital in the ground state S_0.

A low probability of transition affects both directions and makes the fluorescence from the ^{1}nπ* state comparatively long lived. This allows time for intersystem crossing to the triplet state ^{3}nπ* to occur. Similarly there is the possibility for the ^{1}ππ* state to

undergo intersystem crossing to $^3\pi\pi^*$.

Both the π and the π* orbitals occupy a similar space, while the lone pair orbital is positioned perpendicular to the aromatic system. The difference between the singlet and triplet excited states is therefore much larger for the ππ* states than the nπ* states, which causes the ^{3}nπ* to be of higher energy than ^{3}ππ*, making the later the lowest energy excited state achievable.[11] It was suggested that the ^{3}nπ* state undergoes internal conversion to form a ^{3}ππ* state, from which the phosphorescence of pyridine is observed.[11]

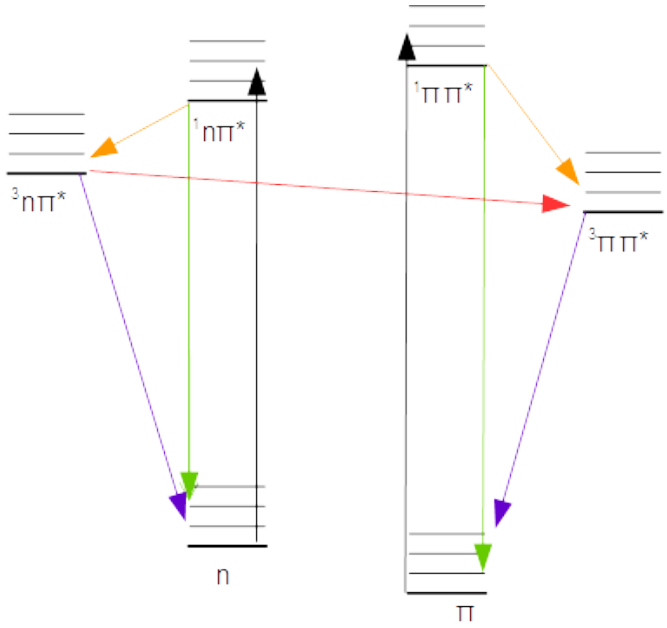

Figure 2.6: Processes involved in pyridine luminescence: absorption (black), fluorescence (green), intersystem crossing (orange), internal conversion (red) and phosphorescence (purple).[11]

In 12N4Py4, the rigid pyridyl chromophore is coupled to a tertiary amine that can potentially contribute to additional nπ excited states, their relative energies changing with the conformation of the molecule. It is very likely that several of the achievable excited states relax via a radiationless pathway to the ground state S_0 and reduce the total emission of 12N4Py4. Measurement in solution adds several intermolecular interactions that can further reduce emission intensity, including energy and electron transfer.

2.5.2 Photophysical properties of 9N3Py3

Both 12N4Py4 and 9N3Py3 contain the same chromophores in a near identical environment. It was expected to find very similar behaviour in absorption and luminescence.

9N3Py3 shows a very similar absorption spectrum (Figure 2.7) with the B-band at 260 nm with a vibrational fine structure as described for 12N4Py4. Due to the reduced number of pyridyl chromophores present per molecule, the molar extinction coefficient was reduced as expected to roughly three quarters (8819 M^{-1} cm^{-1}) of the extinction coefficient of 12N4Py4.

Excitation at 260 nm gives an emission spectrum with a main emission around 430 nm that consists of two peaks and a shoulder around 370 nm.

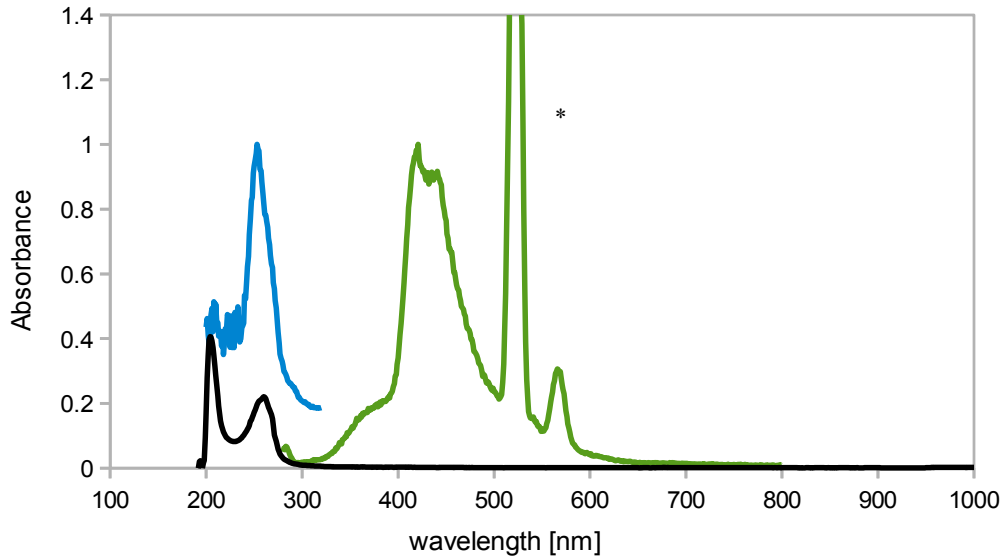

Figure 2.7: Luminescence speactra of 9N3Py3, absorption (black), emission (green, normalised, λ_{ex} 260nm) and excitation (blue, normalised, λ_{em} 419nm), recorded in MeOH, $5*10^{-5}$ M. 2λ artefact present (*).

In principle there is no reason why there would be any difference between the phosphorescence of 12N4Py4 and 9N3Py3 in terms of shape and Stokes shift. It was observed however that 12N4Py4 was stable as a solid as well as in solution, while

9N3Py3 tended to slowly decompose, the colour changing from yellow to brown over time.

Pyridine emission is known to be very sensitive to the presence of impurities.

Excitation spectra recorded while observing the emission at both peak maxima (419 and 439 nm) were identical with a maximum at 255 nm. The absorption spectrum in comparison however showed a maximum at 260 nm (Figure 2.8). This partially overlaps with the absorption spectrum but could also be an indicator of the presence of decomposition products of 9N3Py3. As the luminescence of 9N3Py3 was not used in any measurements later on, the reasons for the particular shape of the emission spectrum were not investigated further.

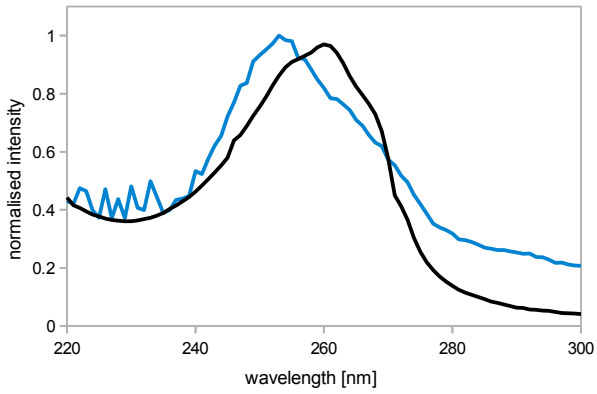

Figure 2.8: Shift of excitation maximum in relation to absorption maximum, normalised

References

[1] F. W. Lewis, L. M. Harwood, M. J. Hudson, M. G. B. Drew, J. F. Desreux, G. Vidick, N. Bouslimani, G. Modolo, A. Wilden, M. Sypula, et al., *J. Am. Chem. Soc.* **2011**, *133*, 13093–13102.

[2] A. Bremer, D. M. Whittaker, C. A. Sharrad, A. Geist, P. J. Panak, *Dalton Trans* **2014**, *43*, 2684–2694.

[3] C. E. Housecroft, A. G. Sharpe, H. Bera, A. Rompel, *Anorganische Chemie*, Pearson Studium, München, **2008**.

[4] P. D. Wilson, Ed. , *The Nuclear Fuel Cycle: From Ore to Waste*, Oxford University Press, Oxford; New York, **1996**.

[5] L. S. Natrajan, N. M. Khoabane, B. L. Dadds, C. A. Muryn, R. G. Pritchard, S. L. Heath, A. M. Kenwright, I. Kuprov, S. Faulkner, *Inorg. Chem.* **2010**, *49*, 7700–7709.

[6] S. H. Eitel, M. Bauer, D. Schweinfurth, N. Deibel, B. Sarkar, H. Kelm, H.-J. Krüger, W. Frey, R. Peters, *J. Am. Chem. Soc.* **2012**, *134*, 4683–4693.

[7] K. Wieghardt, E. Schoeffmann, B. Nuber, J. Weiss, *Inorg. Chem.* **1986**, *25*, 4877–4883.

[8] L. D. S. Yadav, *Organic Spectroscopy*, Kluwer; Anamaya Publishers, Dordrecht [Netherlands]; Boston: New Delhi, **2005**.

[9] J. A. Joule, K. Mills, *Heterocyclic Chemistry*, Wiley, Hoboken, N.J, **2009**.

[10] K. Sushida, M. Fujita, T. Takemura, H. Baba, *J. Chem. Phys.* **1983**, *78*, 588–589.

[11] A. R. Katritzky, *Physical Methods in Heterocyclic Chemistry. Volume VI Volume VI*, Academic Press, New York, **1974**.

Chapter 3: Protonation of 12N4Py4

3.1 Introduction

During the development of novel strategies to reprocess nuclear waste, many of the conditions and techniques can be changed. Some of them however will have to remain in place. One of them is the acidic nature of the first solution produced by dissolving the spent fuel in nitric (or any other) acid, as this solution cannot be completely neutralised to avoid precipitation of components. For large scale operations, separation techniques such as precipitations are unfavourable from an engineer's point of view, meaning that the use of extraction techniques will probably remain firmly in place.

On this basis, all developed extractants have to be operational in aqueous media and the presence of hydroxonium ions.

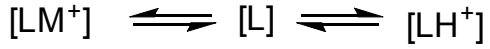

Figure 3.1: Competition between protonation and metal binding

The ligands presented in the previous chapter both contain amine functionalities as binding sites. It has to be considered to what degree they are protonated in acidic solutions, as protonation will directly compete with the metal binding process.

Binding constants (K_c) to metals depend on the solvent, so the presence and competition of hydroxonium ions cannot be avoided when meaningful values for K_c should be obtained. For nuclear reprocessing this means constants have to be determined for aqueous conditions. As binding strength is an important factor to extraction separations, this competition needs to be quantified.

In aqueous conditions only relative binding strengths (K') could be determined.

$$K' = K_a \times K_c = \frac{[LM^+][H_3O^+]}{[LH^+][M^+]} \qquad 3.1$$

If however the proton dissociation constant K_a can be determined for the ligands in the absence of metals the actual binding constant K_c could be determined from the relative K'. It was decided to conduct pK_a determinations in preparation for metal binding studies. Even though equation 3.1 indicates only one protonation event, the presence of higher protonated species was expected (Figure 3.2).

$$[L] \rightleftharpoons [LH^+] \rightleftharpoons [LH_2^{2+}] \rightleftharpoons [LH_x^{x+}]$$

Figure 3.2: Equilibria for protonation of 12N4Py4

It quickly became evident that the large number of basic functionalities cause traditional pK_a determination methods to fail and more advanced techniques had to be explored. The details of the development of these methods are described in this chapter.

3.2 Titration in non-aqueous solvents

The model ligand 12N4Py4 was found to be poorly soluble in water. First it was established whether the pK_a could also be determined in a different solvent such as methanol or acetonitrile, in which the metal complexes would also be soluble.

Several NMR titrations were performed, as pH-meters do not work reliably in other solvents than water. The usual acid of choice for pK_a titrations is hydrochloric acid. Its deuterated equivalent, DCl, is commercially only available as aqueous solutions. Use of aqueous DCl would cause the solution to gradually accumulate water, changing NMR shifts of individual species as well as the dissociation constant to be measured. Other acids available in pure form could be used, such as sulfuric acid or triflic acid,

even in undeuterated form. Unfortunately the term "strong acids" and its complete deprotonation in dilute solution is only valid in water, therefore in non-aqueous solution their pK_a has to be known. These values were not available for the preferred conditions.

Methanolic HCl thus was prepared as the titrant. The main problem was that the concentration of the acid could not be determined with the necessary accuracy.

The idea to use a non-aqueous solvent for the pK_a determination was soon abandoned, as the eventual application will use water and constants determined in other solvents cannot easily be transferred to aqueous conditions. Nevertheless, the first few experiments gave some important insight into the nature of the protonated species.

Following the proton shifts in NMR spectra during the titration in methanol with trifluoroacetic acid (Figure 3.3) showed a stronger shift in the peaks associated with

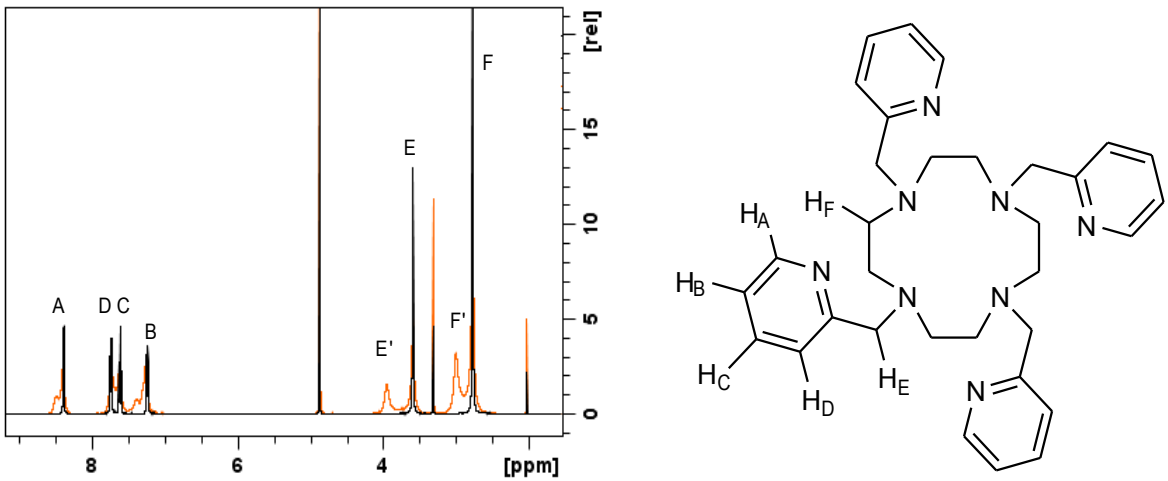

Figure 3.3: NMR-titration of 12N4Py4 in methanol with trifluoro acetic acid, pure ligand (black) and with 0.4 equivalents of acid (orange)

the CH_2 groups around the aza-nitrogens (E and F), suggesting the first protonation occurs within the macrocycle. This is also consistent with typical pK_a values for amines in water, where tertiary amines (triethylammonium pK_a = 10.75[1]) are slightly more basic then pyridines (pyridinium pK_a = 5.21[1]). Also a second protonation event

seemed to affect the shift of the CH_2 groups more than the aromatic ones, so another proton can probably fit into the macrocycle without interfering with the first one. This is further supported by crystal structures of a diprotonated 12N4Py4 measured previously by Natrajan et al.[2] and several crystal structures obtained in the anion study presented in Chapter 8.

The protonation was found to be slow on the NMR time scale, as instead of a steady peak shift a second set of peaks appeared while the original ones disappeared. For an acid-base reaction this is unusual, as they commonly are among the fastest reactions known.[3] At the same time there occurred no splitting of the CH_2 peak, meaning all 16 macrocycle protons experienced the same chemical environment averaged over the NMR time scale. The first proton bound within the ring probably is capable of switching between the nitrogen donors in a fast reaction or it may even be shared between two or more nitrogens simultaneously, making the complete dissociation less likely and thereby slower.

3.3 Back-titration in water

Considering that eventual applications will always contain an aqueous phase, only aqueous pK_a values will be significant. To overcome the solubility issue, 12N4Py could be protonated and then titrated with base, instead of the usual direct titration with acid.

Some consideration had to be put into the choice of base. Strong bases are required to ensure a complete reaction in all pH ranges and they are commonly metal hydroxides. 12N4Py4 however was designed to bind metals, so bases with cations that bind to the ligand are unsuitable for the titration. Several alkali and earth alkaline

metal hydroxides were tested with 12N4Py4 by NMR spectroscopy like Li, Na, K, Ba and Cs. The smallest change in chemical shift in the proton signals was observed with KOH, suggesting the least amount of interaction between the ligand and the cation. Accordingly it was used as the source of hydroxide in all further titrations.

Protonation can be followed with several measurement techniques. Absorption or luminescence measurements could be an option, but tests on 12N4Py4 showed that different protonated species barely differ in their spectra.

NMR techniques could also be employed as used in the investigation with methanol. However, pK_a values also differ for H_2O and D_2O solutions, so undeuterated water would be required to get an accurate measurement. This caused a strong solvent signal in proton spectra, that distorted the ligand signals. While carbon spectra are not affected by the undeuterated solvent, their response to changes in protonation states is also smaller. Additionally concentrations need to be significantly higher than would be required for diluted solutions. Ideally metal binding was to be investigated using the same technique and obtaining carbon spectra of paramagnetic compounds can be difficult due to peak broadening.

Instead, the traditional measurement with a pH-meter was chosen. Figure 3.4 shows a typical pH curve obtained this way.

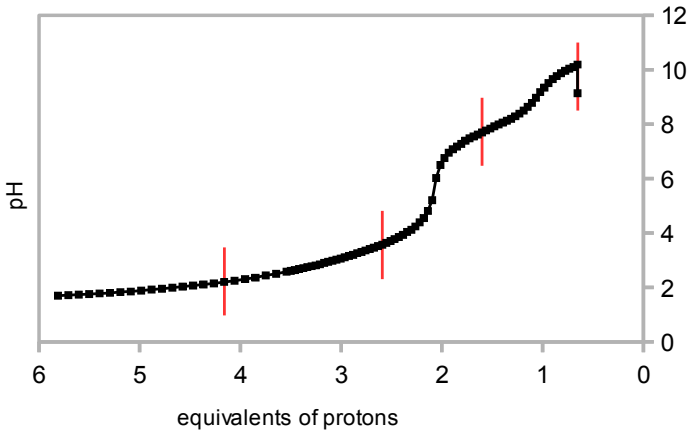

Figure 3.4: Titration curve for 12N4Py4 in water, approx. pK_as shown in red

The curve of the titration is limited on either side. In the acidic range, the pH-electrode used became increasingly

imprecise, values below pH 2 are no longer linear with the addition of acid/base. Into the basic range the ligand became completely deprotonated and started precipitating from solution, removing it from the equilibrium. The two limitations caused two protonation events to be depicted incompletely, the respective equivalence points could not be determined. The four protonations were not distributed uniformly across the pH range but in two pairs, each of them overlapping with their neighbour. Traditionally, pK_a values are calculated as the middle point between two equivalence points. With four of the five equivalence points missing, a different technique had to be used.

A pH-electrode directly measures the actual amount of hydroxonium ions in solution, but in contrast to other measurement techniques gives no information about other species. Their concentrations would have to be determined by calculation through various equilibria and dependencies.

Arno Kraft[4] published a fitting procedure based on the concentration of ions involved in a titration. The equation used and implications for the execution of titrations are discussed in detail in this section.

Logically in a non-charged solution the number of negative charges (anions) is equal to the number of positive charges (cations). In the presented titrations, the anions were hydroxide and chloride (from protonating the solution first with HCl). Cations present were protons/hydroxonium ions, potassium and all possible species of protonated 12N4Py4. With the determination of hydroxonium ions, the concentration of hydroxide was imminently known through the autoprotolysis constant of water. Both chloride and potassium did not participate in any reaction through the titration,

the concentration could be directly calculated from the quantity added. All that remains are the protonated species of 12N4Py4, that can be combined to the concentration of bound protons [H_b] as shown in equation 3.3.

$$[Cl^-] + [OH^-] = [K^+] + [H_3O^+] + [LH^+] + 2[LH_2^{2+}] + 3[LH_3^{3+}] + 4[LH_4^{4+}] \quad 3.2$$

$$[Cl^-] + [OH^-] - [K^+] - [H_3O^+] = [H_b] \quad 3.3$$

The total concentration of 12N4Py4 (L_{tot}) was known, [H_b] can be transformed to the average number of bound protons per molecule nH_b by division by L_{tot}.

$$\frac{[Cl^-] + [OH^-] - [K^+] - [H_3O^+]}{L_{tot}} = nH_b \quad 3.4$$

Meanwhile the known concentrations [H^+], [OH^-], [K^+] and [Cl^-] were combined and nH_b was calculated for each point of the titrations to produce a Bjerrum plot in dependence of the pH of the solution. Transforming the data of Figure 3.4 gives the plot shown in Figure 3.5.

Regions of pH where the electrode accuracy was poor (below pH 2.5) and areas where precipitation was observed were omitted as they did not depict the equilibria correctly. pK_a values could be deduced by finding the pH values where nH_b takes on values of n.5 (n = natural number). However, more precise results were obtained by following the fitting procedure described below.

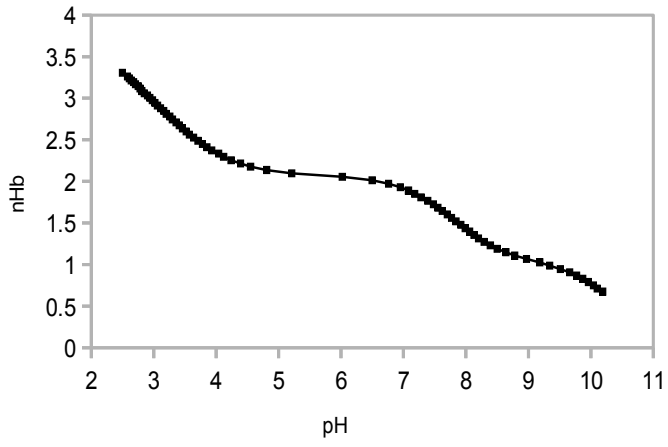

Figure 3.5: Bjerrum plot for a 12N4Py4 titration curve using equation 3.4

In order to obtain an equation that can be fitted to the experimental data that produces the dissociation constants,

nH_b in dependence of all contributing species is transformed as shown below. Hereafter $[H_3O^+]$ is described as [H] and charges are omitted hereafter.

$$nH_b = \frac{[H_b]}{[L_{tot}]} = \frac{[LH] + 2[LH_2] + 3[LH_3] + 4[LH_4]}{[L]+[LH]+[LH_2] + [LH_3] + [LH_4]} \quad 3.5$$

The ligand species are interconnected through the equilibrium constants K_1 to K_4.

$$K_1 = \frac{[L][H]}{[LH]} \quad ; \quad [LH] = \frac{[L][H]}{K_1} \qquad etc \quad 3.6$$

Substitution of the higher protonated species with the equilibrium constants removes several unknown species from the equation.

$$nH_b = \frac{[L]\frac{[H]}{K_1} + 2[L]\frac{[H]^2}{K_1K_2} + 3[L]\frac{[H]^3}{K_1K_2K_3} + 4[L]\frac{[H]^4}{K_1K_2K_3K_4}}{[L] + [L]\frac{[H]}{K_1} + [L]\frac{[H]^2}{K_1K_2} + [L]\frac{[H]^3}{K_1K_2K_3} + [L]\frac{[H]^4}{K_1K_2K_3K_4}} \quad 3.7$$

The term [L] cancels from the fraction, thereby removing all unknown species and leaving only the constants.

$$nH_b = \frac{\frac{[H]}{K_1} + \frac{2[H]^2}{K_1K_2} + \frac{3[H]^3}{K_1K_2K_3} + \frac{4[H]^4}{K_1K_2K_3K_4}}{1 + \frac{[H]}{K_1} + \frac{[H]^2}{K_1K_2} + \frac{[H]^3}{K_1K_2K_3} + \frac{[H]^4}{K_1K_2K_3K_4}} \quad 3.8$$

Equation 3.8 is based on the 12N4Py4 system with an expected number of 4 protonation reactions, but can also be described in a more general form:

$$nH_b = \frac{\sum_{j=1}^{n} \frac{j*[H]^j}{\prod_{i=1}^{j} K_i}}{1+\sum_{j=1}^{n} \frac{[H]^j}{\prod_{i=1}^{j} K_i}} \quad 3.9$$

with n = the number of protonation events to be fitted.

The goodness of fit strongly depended on the accuracy of concentrations and quality

of the used chemicals. HCl was obtained as a concentrated aqueous solution and diluted as needed. As HCl can evaporate from solution and the solution was diluted by humidity over time, concentrations tend to be lower than anticipated. KOH was obtained in pellet form. It is strongly hygroscopic and binds both water and carbonate from the atmosphere, so the outer part of the pellets contained potassium carbonate. Because carbonate effectively buffers the titration curve it needed to be removed, which was achieved by stirring the initial KOH solution with CaO overnight.[5] To avoid contamination by atmospheric carbon dioxide, all solutions were prepared with previously boiled water and used freshly. HCl and KOH solutions were standardised by titration using potassium hydrogen phthalate as a primary standard and against each other. All other chemicals were dried or their solvent content determined by NMR.

Further consideration had to be put into the value of the water autoprotolysis constant. For most applications the well known expression pH + pOH = 14 is sufficient. But this is only completely true for standard conditions without any dissolved compounds. There are however equations to better estimate the value for different conditions, used was the one published by Sweeton[6] with a saturation pressure obtained from the Antoine-equation.[7]

To further increase accuracy, all measurements were performed twice and a global fitting procedure performed.

Using these methods the fitted parameters describe the experimental data remarkably well (Figure 3.9). The main deviation from the data was in the very basic region, where precipitation sets in, but adjusted R^2 values are very high between

0.993 and 0.999, while the reduced chi-square is low between 0.005 and 0.0003[1]. The measured pK_as (10.31, 7.72, 3.57, 2.22) give more insight into the binding mode. Two protonation events with constants very similar to the pK_a of tertiary amines (triethylammonium 10.75[1]) in close proximity in the basic region suggest that two of the aza-nitrogens get protonated on opposite positions of the macrocycle. They are very likely stabilised by a second nitrogen as previously observed in methanolic solutions The third and fourth protonations are more likely to occur on the pyridyl arms, so the positive charges are spread out over the molecule. Figure 3.10 depicts this proposed sequence of protonation. Structures are however highly labile in solution and protons quickly redistribute within the molecule.

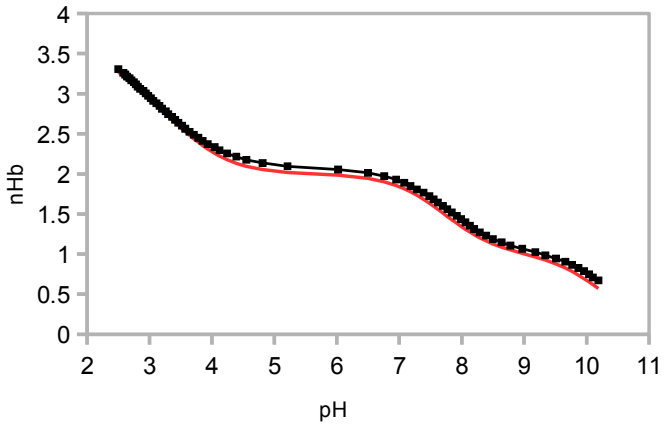

Figure 3.6: Bjerrum plot of the pH titration of 12N4Py4 (black) with the fitted equation (red)

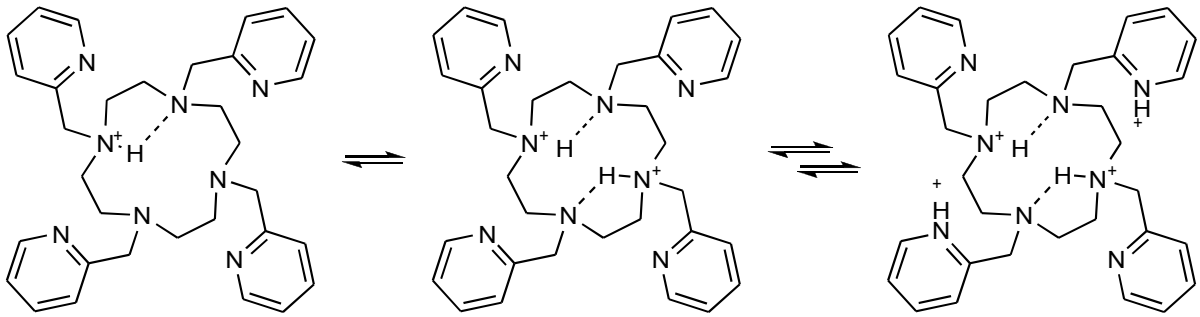

Figure 3.7: Proposed sequence and structure of protonated 12N4Py4

1 OriginPro® 9.1 uses an alternative definition of reduced chi-square = residual sum of square divided by degrees of freedom making numbers approaching 0 desirable.

3.4 Expanding the set of conditions

pK_a values generally depend on the conditions and change with temperature, pressure and polarity or ionic strength of the solution. In order to be able to use the pK_a values to calculate binding constants of 12N4Py4 to various metals, they had to be measured in the same conditions as the complexation will occur. With regard to industrial application, it might be of interest to heat or cool solutions in order to get a more efficient separation. Measurement of binding constants at different temperatures also gives a good estimation of thermodynamic constants of individual reactions and allows predictions of ideal conditions for separation.

The original set of pK_as was recorded at 22°C (slightly above room temperature), additional measurements were performed at 0° and 40°C. A systematic error in temperature measurement caused the actual temperatures to be 0° and 38°, the data was corrected accordingly.

While 0°C is certainly interesting for pK_as, difficulties in maintaining the temperatures for longer periods of time (see chapter 5) lessen its value for further investigations. Higher temperatures than 40°C are also impractical as the evaporation of the solution decreases the accuracy of volume determinations significantly. A fourth temperature set was chosen at 30°C in order to allow three temperature sets to be measured with metals and their thermodynamic constants to be estimated.

Depending on the sequence of separations in spent nuclear fuel reprocessing and the dilution of solutions the ionic strength may vary quite significantly. To investigate the influence of concentrations of non-coordinating ions on the pK_a, sets of measurements at different ionic strengths were performed. Ionic strength was increased by addition of KCl to give concentrations of 0, 0.5, 1 and 2M). In

combination with the different temperatures, this gives a total of 16 different conditions, in which pK_a values were determined (Table 3.1).

Table 3.1: pK_a values of 12N4Py4 for different conditions

Temp.	[KCl] in M	pK_a 1	pK_a 2	pK_a 3	pK_a 4
0°C	0	10.77	8.26	3.67	1.85
0°C	0.5	10.71	8.59	4.24	2.86
0°C	1	10.87	8.70	4.39	3.07
0°C	2	10.86	8.79	4.50	3.20
22°C	0	10.31	7.72	3.57	2.22
22°C	0.5	10.32	7.98	3.96	2.69
22°C	1	10.57	8.19	4.19	2.90
22°C	2	10.19	8.21	4.30	3.09
30°C	0	10.53	7.60	3.48	1.88
30°C	0.5	10.50	7.93	3.97	2.65
30°C	1	10.92	8.20	4.14	2.83
30°C	2	12.16	8.40	4.44	3.04
38°C	0	9.89	7.34	3.36	2.03
38°C	0.5	9.88	7.53	3.74	2.45
38°C	1	10.42	7.88	4.00	2.67
38°C	2	9.90	7.98	4.27	3.05

A graphical representation of the dissociation constants of 12N4Py4 is shown in Figure 3.8, the four planes representing the four pK_as in dependence of KCl concentration and temperature. Cross sections give two dimensional graphs that are significantly easier to interpret for dependencies on either temperature or ionic strength (Figure 3.5, left, section 3.5).

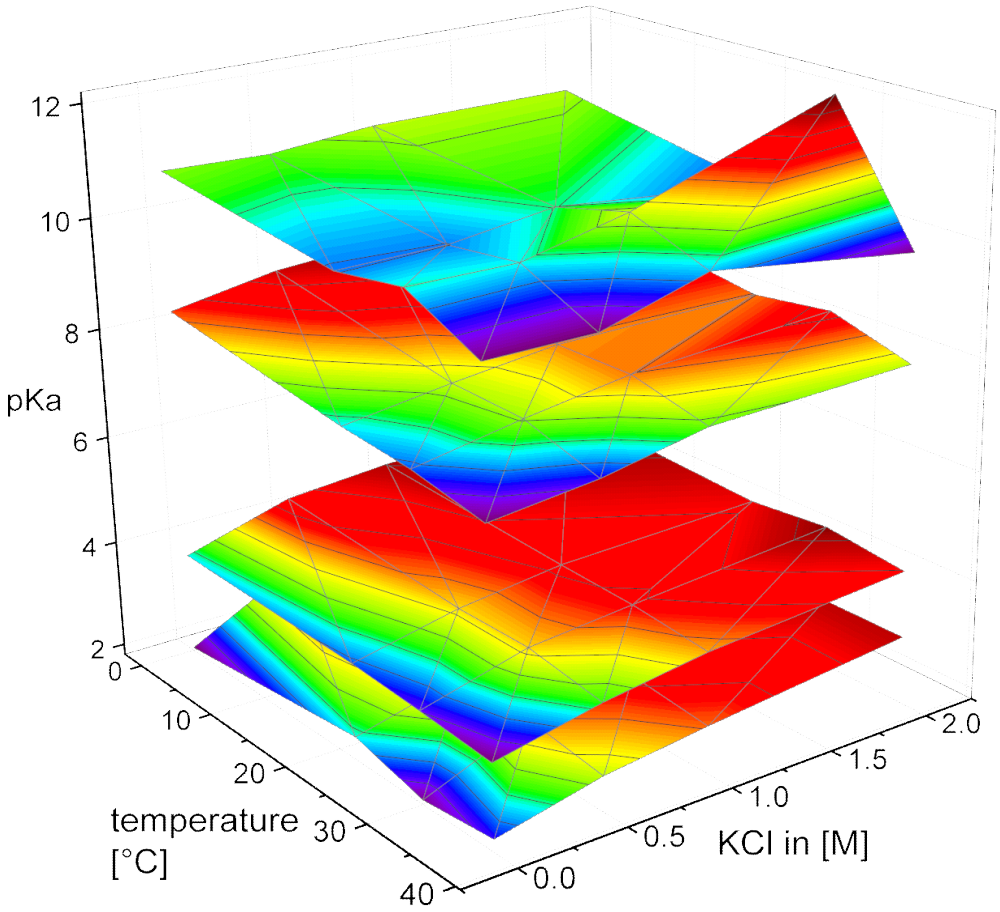

Figure 3.8: Graphical representation of 12N4Py4 pK_{ap} values

3.5 Thermodynamic analysis

The connection between equilibrium constants and thermodynamic constants is given by

$$\Delta G = -RT \ln K \qquad 3.10$$

and

$$\Delta G = \Delta H - T \Delta S \qquad 3.11$$

Values for entropy and enthalpy changes were obtained by plotting ΔG against the temperature and applying a linear fit. The resulting cross section for data of all four

temperatures at 0M [KCl] is shown in Figure 3.9 as well as the ΔG values calculated from the pK_as.

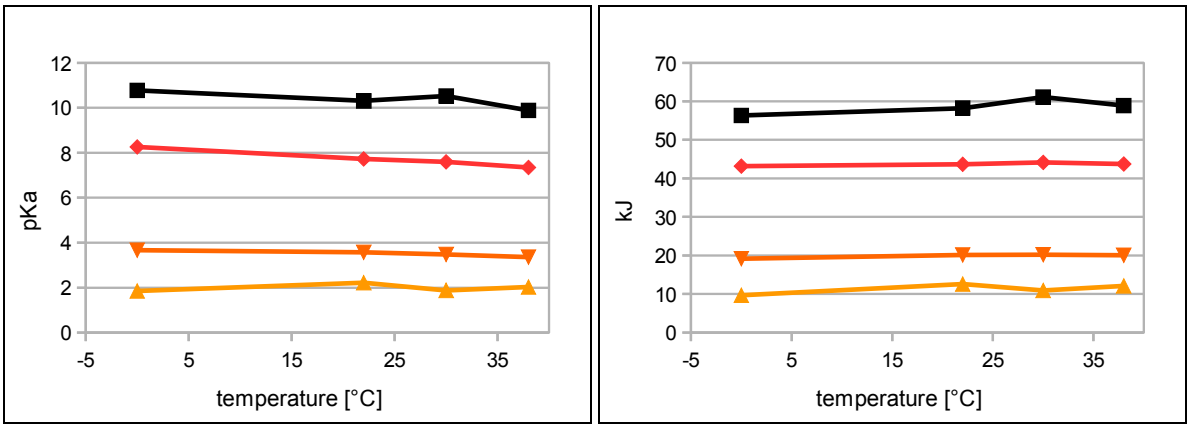

Figure 3.9: pK_a values of 12N4Py4 in dependence of temperature without added KCl (left) and the respective ΔG values (right),corresponding to K_1 (black), K_2 (red), K_3 (orange) and K_4 (light orange).

Table 3.2 shows entropy and enthalpy values obtained for all deprotonation reactions at the four ionic strengths measured.

For the second pK_a (LH_2 to LH, K_2) at [KCl] = 0M the linear fit gives a ΔH of approx 38 kJ/mol and a ΔS of -18 J/mol. The reaction is therefore both endothermic and endergonic. As these values were calculated for the dissociation reaction, the enthalpy shows that protonated species are clearly favoured over deprotonated ones in aqueous solution. The entropy contribution is very small in comparison, the reaction is therefore not highly dependent on temperature. However cooling of solutions would be expected to alter equilibria to slightly favour less protonated species.

The same trends were seen over all equilibrium constants and ionic strengths.

It should be remarked that while the fitting of pK_a values was of high accuracy, the thermodynamic constants given here should only be seen as estimates, as they are based on only four values.

Table 3.2: Thermodynamic constants for pK_as in 12N4Py4, values in J/mol

M KCl		K_1	K_2	K_3	K_4
0	ΔH	31000	38000	12000	-5200
0	ΔS	-92	-18	-25	-56
0.5	ΔH	29000	42000	19000	16000
0.5	ΔS	-99	-10	-11	4
1	ΔH	13000	33000	16000	16000
1	ΔS	-160	-47	-26	0
2	ΔH	10000	30000	7800	6900
2	ΔS	-170	-57	-57	-36

Comparing thermodynamic values for different ionic strengths revealed that ΔH rises for increasing KCl concentrations, the protonated species seem to become stabilised in a more polar solution. It is likely however that for extremely high ionic strengths this trend would reverse as protonated 12N4Py4 species would compete for solvent molecules with other dissolved ions. ΔS showed a a trend towards more negative values for all but K_4. This could mean that while temperatures has a small effect on the equilibria, ionic strength/dilution could be a useful tool to control complexation of metal ions in the presence of hydroxonium ions.

3.6 Error estimation

As published by A. Avdeef et al. in 1982, Bjerrum plots can also be used to check for systematic errors in titrations.[8]

Electrode errors can reveal themselves in curves that strongly deviate from the expected curve form on one or two ends of the titration curve. This has been found for pH values below 2.0 (Figure 3.10 a), accordingly only values above this pH have been used for the fitting procedure.

Among the most common systematic errors are incorrectly determined concentrations of acid and base solutions. The effect on the titration curve can be seen most strongly around the middle inversion point (for 12N4Py4) that appeared as a broad plateau in the Bjerrum plot. Logically, this plateau should be level with an integer for nH_b. Some smaller deviations were found in some of the titration curves, therefore the HCl and KOH solutions represent the main source of systematic errors for this method. Avdeef et al. advise correcting for the acidity error by means of the end point of the titration, where nH_b should be 0. Unfortunately this endpoint is not available due to precipitation, this systematic error remains uncorrected.

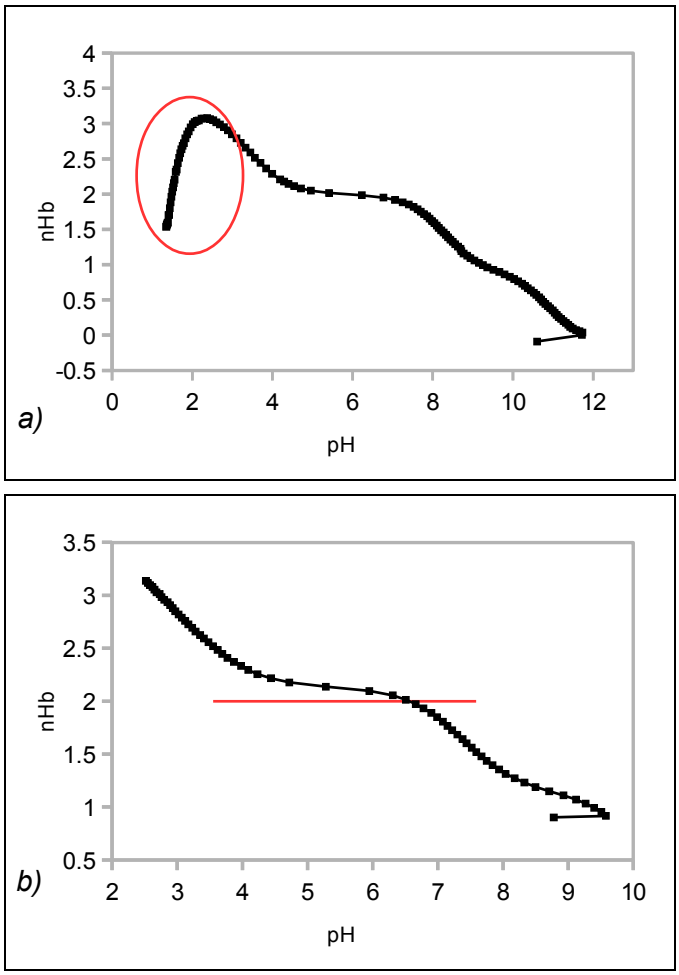

Figure 3.10: Systematic errors in titrations. a) electrode error in low pH range, b) acid/base error causes inversion point plateau to lie above expected level (red line). Data was not used for fitting.

Whereas acid-base errors manifest themselves in deviation from the expected curve with approximately equal distribution along the curve, ligand concentration error does so with increasing deviation towards the end of the experiment. To obtain the ligand concentration as accurately as possible, the purity of the sample was analysed by both CHN elemental analysis and proton NMR. The primary contaminant in 12N4Py4

is residual acetonitrile that was used for recrystallisation. As acetonitrile (MeCN) has a similar distribution of C, H and N as the ligand itself, CHN values obtained indicate slightly too high purities. Instead the NMR based purity was used which integrated the ligand signals against residual MeCN. When the experimental data was corrected for the ligand purity, curves obtained do not show significant deviation from expected curves that would be caused by ligand concentration errors.

It was observed that precipitation sets in earlier and at lower pH values for samples at raised temperatures, the solubility of the free base in warm solution seems to be lowered.

The precipitation also cuts off an important part of the titration curve, meaning values obtained for K_1 are less accurate that the other dissociation constants. This is particularly true for warm solutions.

3.7 Conclusion

In extractions from acidic aqueous solutions, the protonation of 12N4Py4 will play a major role. Dissociation constants for the four protonation events seen between pH 2 and 14 were determined using a fitting procedure. The results are of high quality and can be further used to investigate the binding of metal cations. It also became evident that the free ligand only has a limited solubility in water. The equilibrium overview shown in Figure 3.2 can therefore be expanded as shown in Figure 3.11.

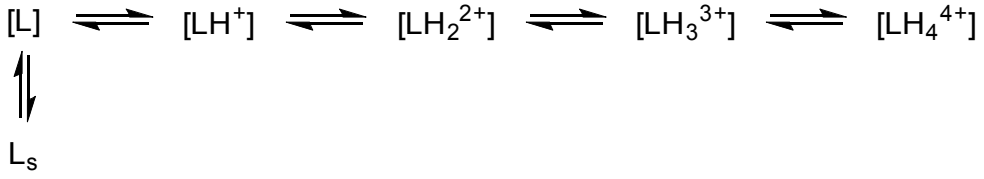

Figure 3.11: Overview of equilibria established in this chapter

References

[1] D. H. Ripin, D. A. Evans, "Evans pKa table," http://evans.rc.fas.harvard.edu/pdf/evans_pKa_table.pdf, accessed 16.6.2017.
[2] L. S. Natrajan, N. M. Khoabane, B. L. Dadds, C. A. Muryn, R. G. Pritchard, S. L. Heath, A. M. Kenwright, I. Kuprov, S. Faulkner, *Inorg. Chem.* **2010**, *49*, 7700–7709.
[3] M. Eigen, *Discuss. Faraday Soc.* **1965**, *39*, 7–15.
[4] A. Kraft, *J Chem Educ* **2003**, *80*, 554.
[5] P. Sipos, P. M. May, G. T. Hefter, *The Analyst* **2000**, *125*, 955–958.
[6] F. H. Sweeton, R. E. Mesmer, C. F. Baes Jr, *J. Solut. Chem.* **1974**, *3*, 191–214.
[7] L. C. Antoine, *Comptes Rendus* **1888**, *107*, 681–684.
[8] A. Avdeef, D. L. Kearney, J. A. Brown, A. R. Chemotti, *Anal. Chem.* **1982**, *54*, 2322–2326.

Chapter 4: Lanthanide, Calcium and Sodium Complexes of 12N4Py4

The lanthanides have been intensely studied for their potential in a wide variety of applications, including magnetic resonance imaging, luminescent dyes and single molecule magnets, due to the properties arising from the 4f-orbitals being both diffuse and well shielded. While lanthanide compounds and complexes are well established as tools in many fields[1–3], the fundamental mechanisms within the ion that produce these sought after effects is subject of continuous investigation.[4–6]

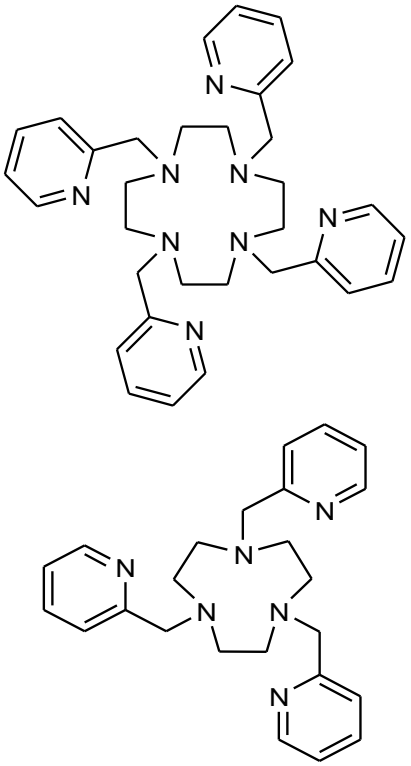

Figure 4.1: 12N4Py4 and 9N3Py3, the ligands chosen for the study of lanthanide binding

To study the interaction between lanthanide ions and their physical and chemical environment, simple and symmetric model ligands are commonly used. While in many areas a high kinetic and thermodynamic stability is desired and ligands containing oxygen donors are favoured, softer N-donors allow for more uniform ligand fields. Nitrogen can be both functional group as well as an integral part of the ligand back bone, so compact encapsulating ligands can be designed.

Both 12N4Py4 and 9N3Py3 fulfill these basic requirements, making them suitable model systems for the study of lanthanide binding, as discussed in chapter 2. Furthermore, many lanthanide complexes of 12N4Py4 are already known and published.[5,7,8] While they focus on specific aspects of 12N4Py4 complexes, this study aims at providing a detailed understanding of

equilibrium thermodynamics and a general overview of the involved reactions involving or interfering with 12N4Py4 lanthanide complexes. A detailed understanding of the properties of the compounds is vital for designing equilibrium experiments and understanding the measurement results. In this chapter, several aspects of 12N4Py4 lanthanide complex synthesis and characterisation, including luminescence, are discussed and compared to findings in recent literature.[4,5,7,8] Furthermore it is also described how the approach can be extended to calcium and sodium. The influence of their lower charge and larger radii on complex formation and properties are compared to the lanthanide complexes.

4.1 Synthesis of Ln(III)-12N4Py4 complexes

The Ce(III), Pr(III), Nd(III) and Yb(III) complexes of 12N4Py4 were synthesised following a procedure described in the literature[7], through the reaction of the lanthanide triflate salt and the free ligand in methanol at 40°C (Scheme 4.1). Crystals were grown from a MeCN/Et_2O system.

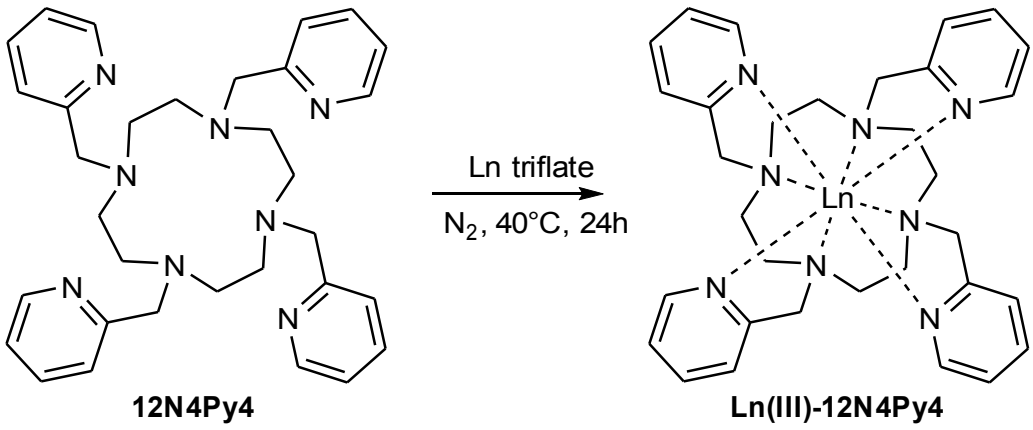

Scheme 4.1: Synthesis of 12N4Py4 lanthanide complexes

While for most lanthanides the reaction time of 24 h proved sufficient, ytterbium was

found to form the complex significantly slower and up to 11 days were required for the reaction to reach completion. Attempts to accelerate the reaction using higher temperatures or acetonitrile as solvent proved unsuccessful. The lanthanide complexes are usually colourless or retain some of the pastel colour of the lanthanide triflate salts. All proved to be stable when stored as solids and no decomposition was observed.

In the synthesis of the Ce(III) complex, a white precipitate was formed when the solvent is not kept dry and/or the ligand is added too quickly to the metal solution. However, this behaviour was not observed with any of the other lanthanides investigated. This precipitation is discussed in more detail later on in this chapter.

Attempts were made to synthesise the Ce(IV) complex of 12N4Py4. NMR spectroscopy did show evidence of complexation, some of the signals are however congruent with the Ce(III) complex. It is formed by reduction of Ce(IV), which itself does not seem to form any complexes with 12N4Py4. It appears that the smaller Ce(IV) core is too small to fit into the binding cavity or the sulfate/nitrate counter ions used were better ligands that the N-donors for the fourfold cation. Both anions can act as bidentate ligands to Ce(IV) as known from solid structures[9,10] and are known to bind to lanthanides quite strongly.[11] Slightly more of the Ce(III) complex was found to have formed when Ce(IV) triflate was used as the starting material.

Ce(IV) would have been very interesting in order to investigate redox reactions on the formed complexes. Even though it is a strong oxidising agent, it is stable in aqueous solutions at low pH. In the raffinate of nuclear reprocessing it might be encountered depending on the conditions. To extract it or hold it back in a solution different ligands than 12N4Py4 would be required.

4.2 Crystal structure and geometry

Crystal structures of the triflate salts of 12N4Py4-Ln complexes have been previously published for all discussed lanthanides[7] except for the Ce(III) complex, which is presented here.

The crystals were grown from a freshly synthesised batch of Ce(III)-12N4Py4 from acetonitrile layered with diethyl ether over several days and its structure (measured, solved and refined by Dr. L. Pfeifer and Dr. A. Thompson) is shown in Figure 4.2. The cerium ion is tightly encapsulated by 12N4Py4 in a conformation expected from known 12N4Py4-Ln structures. The macrocycle is slightly twisted to allow all four aza-nitrogen atoms to coordinate to the metal, while the pyridyl arms are rotated around the central axis of the complex.

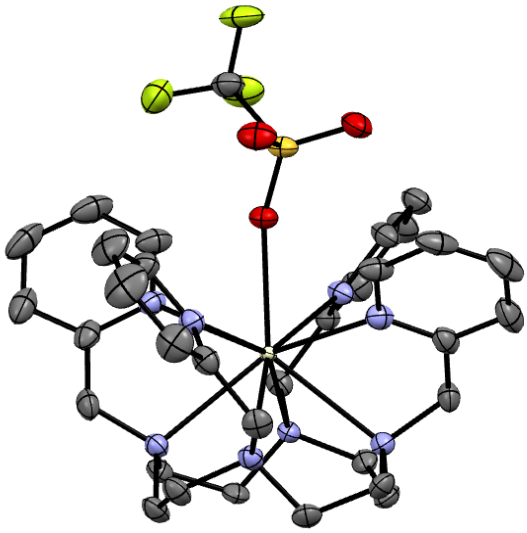

Figure 4.2: Crystal structure of Ce(III)-12N4Py4 complex as triflate salt (WTS01). Hydrogen atoms, two triflate ions, one water, one MeOH and two MeCN molecules are not displayed, probability level at 50%.

Cerium is known to prefer conformations where it is surrounded by 9 ligands, 8 of which are filled by the nitrogen donors of 12N4Py4, the remaining site is commonly taken by one of the triflate counter ions. The remaining anions are arranged around the complex and do not seem to participate in any direct interaction with the metal centre. Additionally two acetonitrile, one methanol and one water molecule are also contained in the solid per complex.

The space group of the crystal is the orthorhombic Pbcn, just as is also seen in

neodymium and europium complexes of the corresponding conformation. Bond lengths between the nitrogen atoms and the metal centre are on average 2.70 Å for the ring nitrogens and slightly shorter for the pyridyl nitrogens at 2.68 Å. This is in agreement with corresponding structures of Pr(III) (2.69 Å, 2.67 Å), Nd(III) (2.67 Å, 2.65 Å) and Eu(III) (2.65 Å, 2.60 Å) complexes,[7] where the distance to the ring nitrogens is generally longer than the distance to the pyridyl nitrogens. It also fits nicely into the series to show that the bond lengths gradually decreases for the later lanthanides as a consequence of the lanthanide contraction. The distance to the triflate oxygen atom is somewhat shorter at 2.53 Å, but again longer than the equivalents for later lanthanides (2.52 Å for Nd and 2.51 Å for Eu).

Lanthanide complexes based on tetra-substituted cyclen rings commonly appear in two pairs of enantiomeric diastereoisomers.[12] Due to the twisting of the macrocycle and the rotation of the pendant arms two helical elements of chirality are introduced. Figure 4.3 shows the four encountered conformations. Transition from one isomer to another occurs either through ring inversion or arm rotation; however the transition states are considerably less stable and therefore short lived. The handedness of the

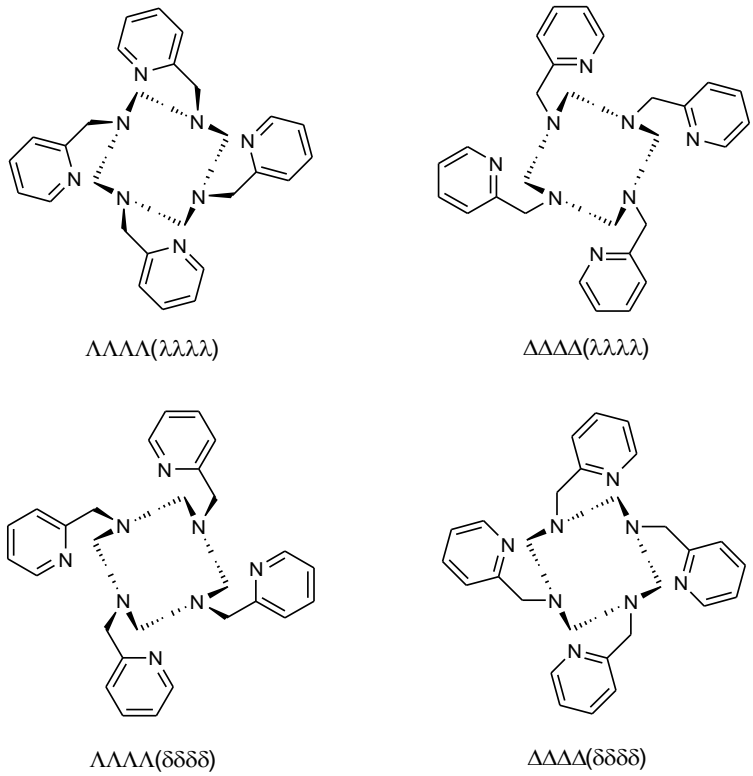

Figure 4.3: Representation of conformations of 12N4Py4-Ln complexes

pyridyl arms is described by the established symbols Δ (right-handed) and Λ (left-handed) when the molecule is viewed along the C4 axis with the pendant arms in front and the macrocycle in the back.[13] To avoid confusion between the handedness of the pyridyl ring rotation and the twisted macrocycle, the later is described with the lower case letters δ (right-handed) and λ (left-handed). Overall conformation is then for example ΛΛΛΛ(δδδδ).[7] The relative handedness of the two elements produces a square-antiprismatic geometry (SAP, for ΔΔΔΔ(λλλλ) and ΛΛΛΛ(δδδδ)) or a twisted square-antiprismatic geometry (TSAP, for ΔΔΔΔ(δδδδ) and ΛΛΛΛ(λλλλ)) in lanthanide complexes.

The presented structure contains the cerium complex in the twisted square-antiprismatic geometry as a racemic mixture of both enatiomers. Figure 4.4 shows another angle of the structure to demonstrate the conformation. The same conformation is also seen for Pr(III), Nd(III) and Eu(III).[7] Other, later lanthanides such as Gd, Tb, Er and Yb were crystallised in the square-antiprismatic form. This however does not mean that they exclusively exist in these respective geometries.

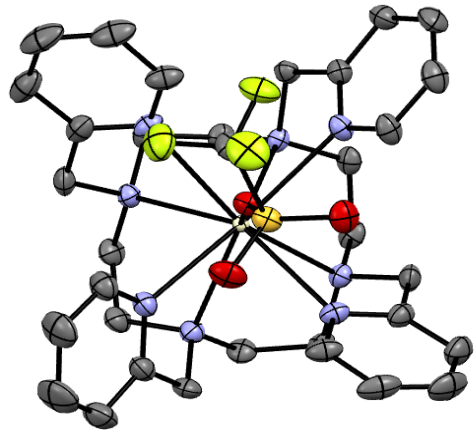

Figure 4.4: Crystal structure of Ce(III)-12N4Py4 complex as triflate salt (WTS01). Hydrogen atoms, two triflate ions, one water, one MeOH and two MeCN molecules are not displayed, probability level at 50%.

4.3 NMR spectroscopy

Lanthanides are frequently employed in NMR spectroscopy as shift reagents.[1] Their paramagnetic properties add an additional magnetic field component for the nuclei in

direct contact or close proximity (pseudo-contact) to the lanthanide centre. The observed shifts of proton signals are generally spread out over a wider range as commonly observed for non-paramagnetic samples, the effect depends on the lanthanide and the number of unpaired electrons.[1] A slight broadening of the signals is observed that causes the multiplicities to disappear. Carbon signals are often less affected by the paramagnetic lanthanide centre in terms of their shifts, but also broaden and decrease in intensity. Slight shift changes occur during complexation. Figure 4.5 shows the ^{1}H-spectrum of Ce(III)-12N4Py4 and their corresponding signals of the free ligand.

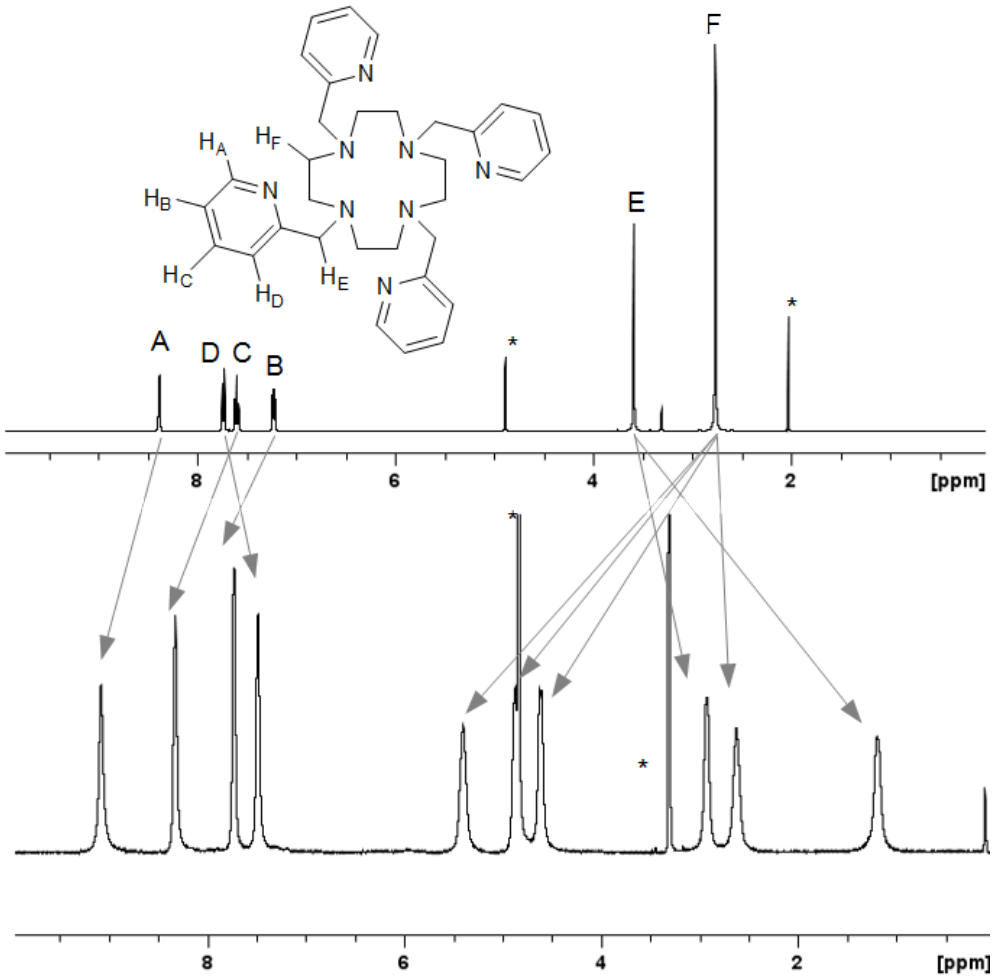

Figure 4.5: ^{1}H-NMR of 12N4Py4 and its Ce(III) complex in MeOD (residual solvent)*

The diastereoisomers described in the previous paragraph have different proton spectra, but for most of the lanthanides one of the two isomers clearly dominates in solution. At high concentrations a second set of signals that otherwise are not distinguishable from the baseline (Figure 4.6) is revealed. This was not expected, as many lanthanide complexes such as with europium have to be cooled in order to obtain two sets of NMR signals.[7] For the cerium complex the two species were observed at room temperature, indicating that the conversion of one isomer to the other is slow and the transition states high in energy.

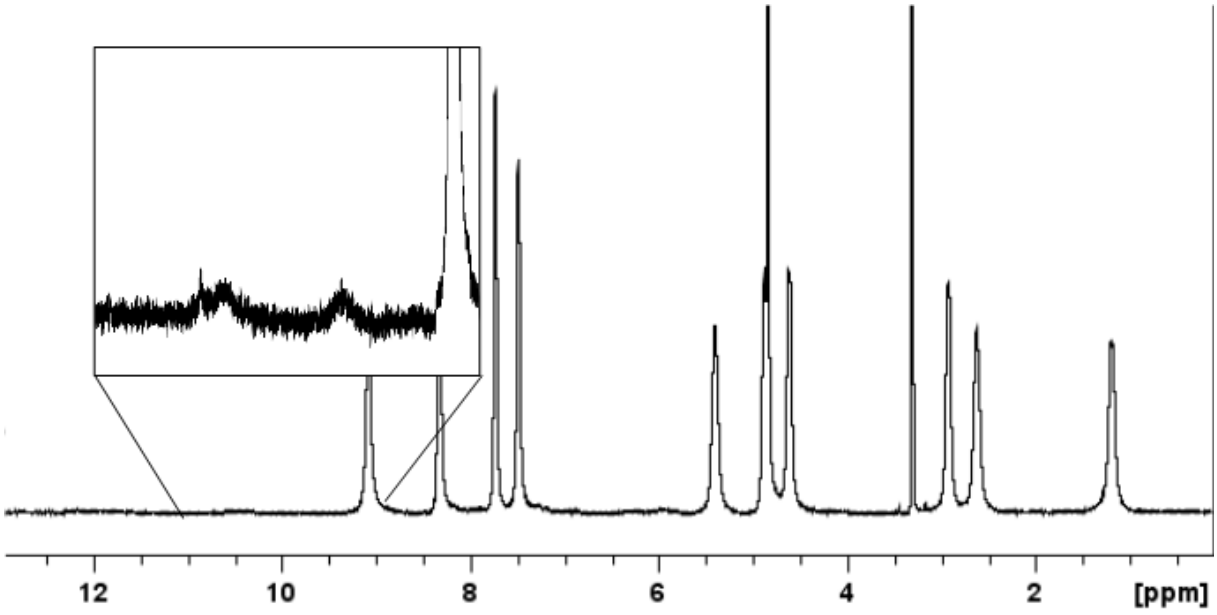

Figure 4.6: Signals of minor isomer in Ce(III)-12N4Py4 (MeOD)

Through intensive study of the NMR and luminescence spectra of several lanthanide complexes in the combination with computational methods Natrajan et al.[7] established that the early lanthanides up to samarium and europium primarily take on the twisted square-antiprism conformation in solution, which is slightly more stable. For the smaller later lanthanides the square-antiprism becomes more accessible.

Shifts observed in lanthanide complexes are often described as being produced by the sum of a diamagnetic shift and a paramagnetic shift.[14] The diamagnetic shift

itself is thought of being composed of the chemical shift produced by the chemical structure of the ligand, a factor introduced by the coordination of a metal ion and potentially influences by coordinated anions. The paramagnetic shift is described by a contact (through bonds) and a pseudocontact (through space) component.[15] Contact shifts for lanthanide ions in solution are thought to be small, leaving the angle and distance dependent pseudocontact shift to cause the large shifts typical for lanthanide NMR spectra. Investigations of these shifts commonly refer to a modified equation based on the work of McConnell and Robertson[15] and of Bleaney[16,17] to describe the lanthanide induced shift in proton NMR spectra:

$$\delta_{pc} = D\frac{3\cos^2\theta - 1}{r^3} \qquad 4.1$$

It consists of a term D, containing several measurement and nuclei specific parameters, the angle θ of the position of a nucleus from the symmetry axis of the compound and its distance r from the lanthanide nucleus. If complexes of lanthanides are compared to each other, the free ligand or other non-covalent complexes such as the corresponding calcium compounds, the term D can be assumed constant, making the predicted shift solely dependent on the distance r and the angle θ from the central axis of the complex, which in the case of 12N4Py4 is the C_4 axis.

The difference between the ^{1}H-NMR spectra of the non-paramagnetic Ca-12N4Py4 complex (see section 4.6) and the paramagnetic Ce(III)-12N4Py4 should therefore correlate to distances and angles of the protons to the lanthanide centre determined from the crystal structure. Entering the geometric values into equation 4.1 and plotting it against the measured NMR shifts is expected to show a linear relationship with the term D corresponding to the slope of the graph (Bleaney plot). The exact

assignment of Ce(III)-12N4Py4 proton signals is challenging as the paramagnetic metal both strongly influences the shift of the signals and removes the coupling patterns.

There are several different ways to assign the CH_2 proton peaks, but none of them produced a straight line in the Bleaney plot. The closest to a linear relation (Figure 4.7) still only gave an R^2 value of 0.62. For Ce(III) the assumption that contact shift is insignificant does not hold true, as the metal also shows considerable contribution of the 5d-orbital.

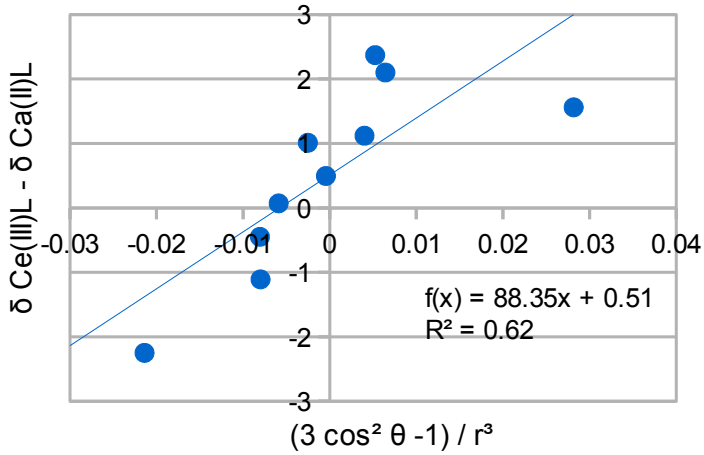

Figure 4.7: Bleaney plot for Ce(III)-12N4Py4 in comparison to Ca(II)-12N4Py4

4.4 Luminescence

As described in chapter 1, lanthanides on their own do not show intense emission as their f-f transitions are parity forbidden.[18] In combination with strongly absorbing ligands however the lanthanides can be excited through energy transfer from the excited state of the ligand chromophore, producing intense, lanthanide specific and long lived emission.[18] This antenna effect has also been observed for most of the lanthanide complexes of 12N4Py4. Initially the binding constant of 12N4Py4 to cerium should have been determined with luminescence experiments. Ce(III) however is a bad model for lanthanide emission. Its only f-f transition ($^2F_{7/2} \rightarrow {}^2F_{5/2}$)

lies so far into the infrared (approx. 5000 nm) that it is not observed in solution.[18]

The absorption around 265 nm (Figure 4.8, black line) is slightly red-shifted in comparison with the free ligand (260 nm), consistent with the polarisation of the pyridyl ring through coordination of a trivalent ion.

In the luminescence measurement an emission spectrum (Figure 4.8, green line) was observed that shows one signal, its form and position is nearly identical to the emission spectrum of the free ligand. The excitation spectrum obtained by observing the emission at 480 nm (Figure 4.8, blue line) contains two peaks, one at 265 nm, which overlaps with the absorption spectrum, and a second one at 370 nm. While in Ce(III) f-f transitions are not observed, it is the only lanthanide that can alternatively undergo a formally allowed f-d transition. Based on the red-shift of the emission (445 nm to 490 nm) and the presence of a second, red-shifted excitation signal it is suggested that such a f-d transition takes place in the Ce(III)-12N4Py4 complex.

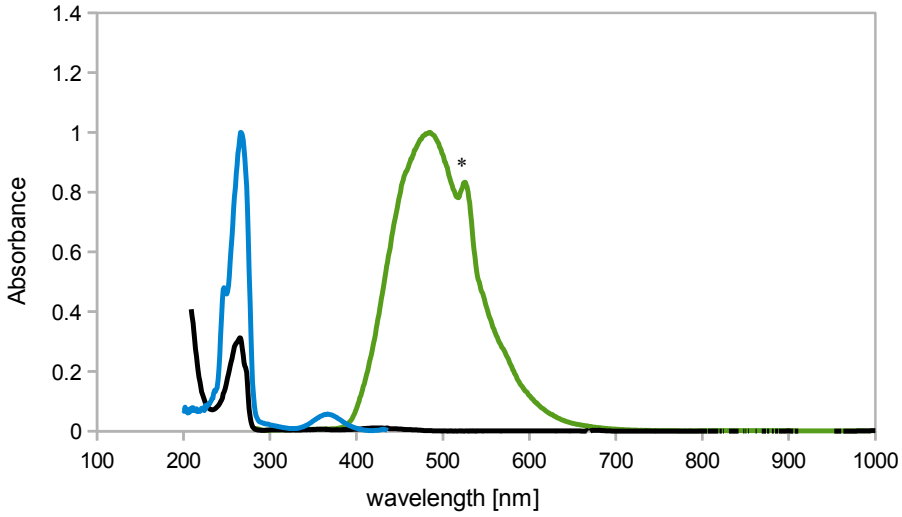

*Figure 4.8: Luminescence of Ce(III)-12N4Py4 in MeOH. Absorption (black), emission (green, λ_{ex} 260 nm, normalised) and excitation (blue, λ_{em} 480 nm, normalised) at 2.5*10-5 M. 2λ artefact (*).*

An emission spectrum with an excitation wavelength of 370 nm produced a spectrum similar to the one shown in Figure 4.8 with a decreased intensity, which is assigned to the direct excitation of the f-d transition in Ce(III). This illustrates that sensitisation

via the ligand absorption is more effective. From the wavelength (370 nm) of this direct excitation it can further be deduced that the energy transfer to the metal occurs from the $^{1}\pi\pi^{*}$, as the ligand phosphorescence at 450 nm indicates that the $^{3}\pi\pi^{*}$ state is already be too low in energy.

By coordinating all nitrogen lone pairs to the metal centre, they can no longer participate in the formation of $^{1}n\pi^{*}$ and $^{3}n\pi^{*}$ states. The coordination also locks the ligand conformation, disabling rotations required for energy minimisations that promote non-radiative relaxation. This leads to an increase in the emission intensity (factor 13.8 relative to free ligand)

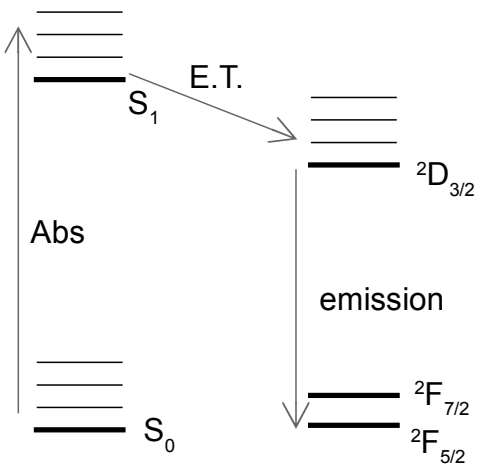

Figure 4.9: Jablonski Diagramm of Ce(III) luminescence

No lifetimes could be recorded due to instrument limitations at the excitation wavelength used, meaning they are below 0.015 ms.

12N4Py4 complexes of Pr(III), Nd(III) and Yb(III) were previously reported to show f-f transitions with emission wavelengths in the near-IR region.[5,7]

4.5 Precipitation in solution

During the synthesis of the Ce(III)-12N4Py4 complex a white precipitate can form that is also encountered in solutions after prolonged storage. Initially it was believed that precipitates of a carbonate phase might cause these observations. However, its formation could not be forced by exposing it to air/CO_2. Precipitation from solution was observed in aqueous solutions and also (to a lesser degree) in other protic

solvents. The precipitate did not redissolve in any common solvent except acidic aqueous solutions.

When metal complexes were titrated with acid/base, as discussed in chapter 5, this precipitation occurred for all four lanthanides (Ce, Pr, Nd and Yb) at pH values approaching neutral/basic pH. The occurrence of this precipitate is the major limiting factor to the determination of binding constants. It appears likely that the precipitates consist of species of lanthanide hydroxides, oxides or a lanthanide oxide/hydroxide cluster capped by 12N4Py4 units.

The precipitation of simple lanthanide hydroxides was studied in the 1970s; however exact formulations of precipitates remain elusive and highly dependent on the exact circumstances of their formation.[19–21]

In the presence of ligands, polynuclear lanthanide clusters can be formed. Such systems have been described before and come in a variety of shapes and sizes.[22] Figure 4.10 shows a few of the very basic building blocks frequently encountered. A core cluster forms from lanthanide ions, hydroxides and oxides that can be capped by coordinating the ligand, inhibiting further growth from this position. As such, the ligand can define cluster growth and overall cluster size.

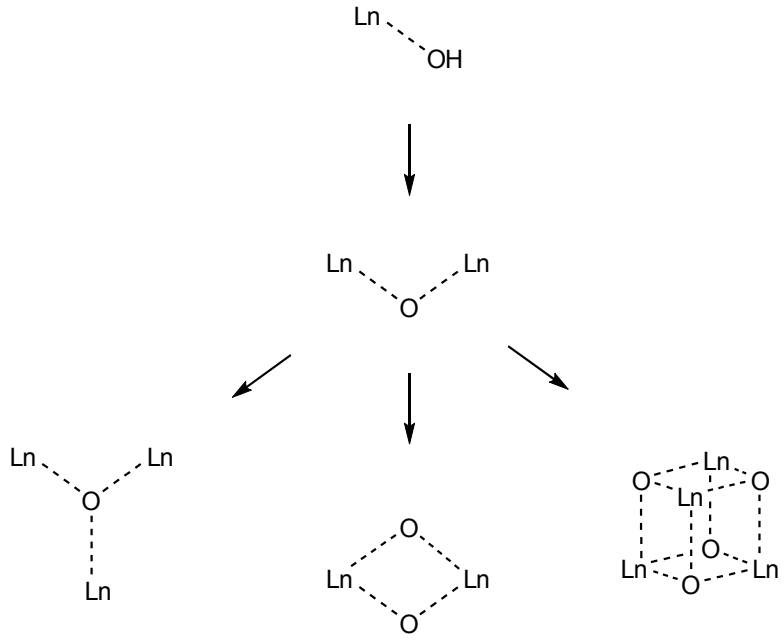

Figure 4.10: Selection of lanthanide hydroxide and oxide binding and cluster motifs

Even though in neutral

aqueous solutions and organic solutions hydroxide concentrations are small to negligible, the extremely low solubility of lanthanide hydroxides aids in the formation of precipitate. Lanthanide ions are also hard Lewis acids and can coordinate water. The hydroxide complex is then formed by deprotonation of the coordinated H_2O.

This theory is further supported by an observation made during one synthesis of 12N4Py4-Ce(III), where both a colourless precipitate as well as colourless crystals were isolated. The crystal contained the protonated ligand with triflate as counter ions even though methanol was used as a reaction medium and 12N4Py4 should not be able to deprotonate methanol. It is therefore likely that traces of water in the employed solvent dissociated to form protonated ligand and cerium hydroxide.

Some of the precipitate obtained from pH titration in the presence of metal was isolated and washed with water and methanol, the dry powder then measured by solid state NMR. The carbon spectrum (see Figure 4.11) shows a pattern consistent

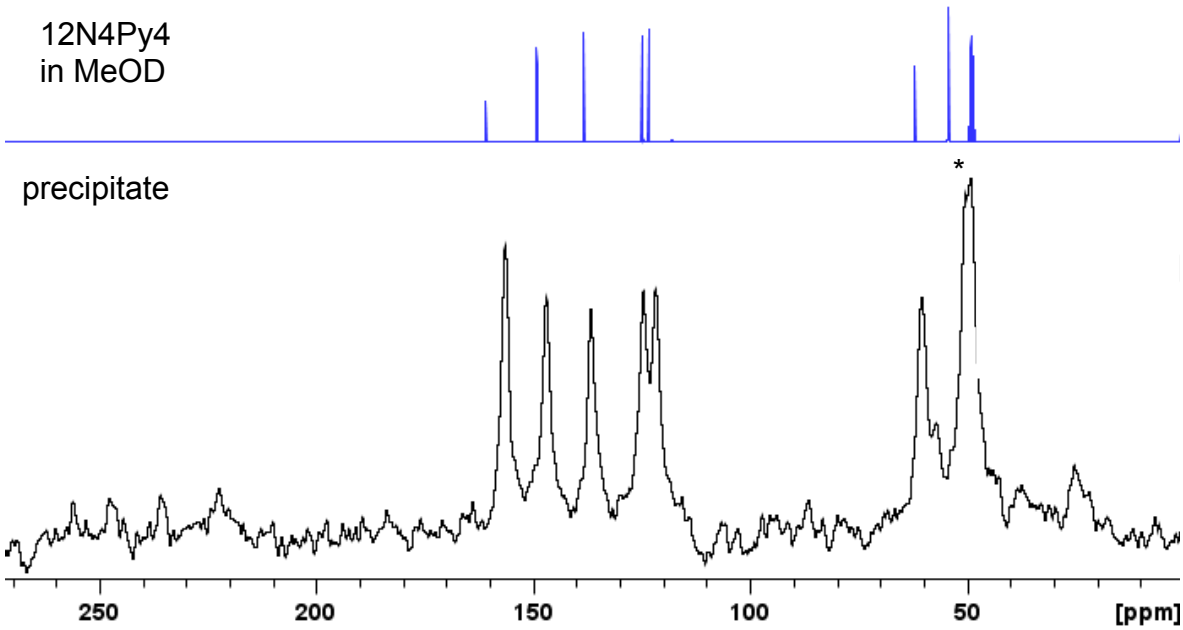

Figure 4.11: Solid State ^{13}C-NMR of Nd precipitate (black) in comparison to the ^{13}C-NMR of the free ligand (blue, in MeOD). Splitting in three peaks observed (*)

with 12N4Py4 with some splitting of peaks observed in one of the peaks (marked

with *), which in the free ligand is associated with the CH_2 groups of the macrocycle.

A possible interpretation is that the ligand coordinates to a metal cluster via the four aza nitrogens, the pyridyl groups however do not and can freely rotate. Poor resolution as a consequence of the solid state and the small influence of complexation on the chemical shift however require that the proposed structure is supported by further analysis.

ICP-MS analysis of precipitate obtained in a Ce(III)-12N4Py4 synthesis gave an approximate cerium content of 37%, which is significantly higher than would be expected for the 1:1 12N4Py4 complex (approx. 13%) but lower than pure Ce(OH)3 (73%). Structures of hydroxide/oxide clusters with 12N4Py4 could then produce such an intermediate cerium content.

For cerium it is also possible that the metal is oxidised to Ce(IV) and that the non-innocence of the pyridine ligand contributes to further complicate the picture.

Unfortunately the available methods to analyse insoluble solids only gave limited information about connectivities within the potential lanthanide cluster and how 12N4Py4 might coordinate to it, so the exact structure remains unknown.

4.6 Calcium binding

4.6.1 Synthesis

In the early phase of the project experiments were performed to see if the 12N4Py4 cerium(III) complex can be synthesised in aqueous solution. NMR and mass spectrometry revealed the presence of an unexpected species, which soon was identified to be the calcium complex of 12N4Py4. The source of calcium in this

experiment was a water sample of low purity. A synthesis of Ca-12N4Py4 and its characteristics has been previously published.[23]

Even though calcium is not a fission product encountered in nuclear power production, it could enter the reprocessing stream if non-deionised water is added to the waste to dilute the raffinate. From this single experiment it became evident that calcium binds 12N4Py4 quantitatively, quickly and the produced complex is stable to the analysis conditions. If calcium is effective in competing with lanthanides and possibly lanthanides it is essential to evaluate the binding strength of the complex.

4.6.2 Properties

Calcium(II) can serve as a simplified model of a Ln(III) being comparable in size, although it carries a lower charge. Furthermore, it does not have any valence electrons to interact with surrounding crystal fields. The great advantage of calcium is that its hydroxide complexes only form at high pH, meaning that precipitation is rarely encountered, however carbonate precipitates are common.[19]

In the titration experiments, that are discussed in detail in chapter 5, calcium was investigated alongside the lanthanides. It was observed that the calcium complex is only sparingly soluble in water, crystallising as a chloride salt at elevated pH. The structure depicted in Figure 4.12 (measured, solved and refined by Dr. L. Pfeifer and Dr. A. Thompson) was measured from one of these crystals obtained in titration experiments.

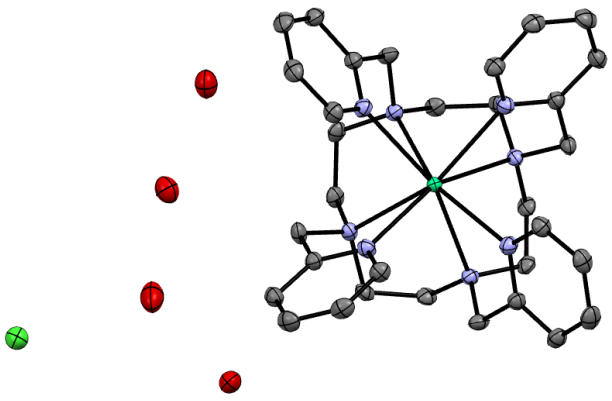

Figure 4.12: Crystal structure of Ca(II)-12N4Py4 complex as hydrated chloride salt (WTS02). One chloride in disorder with water. Hydrogen atoms not displayed, probability level at 50%.

In the measured crystal calcium is bound in an equivalent symmetry to the lanthanide complexes previously discussed and takes on the twisted square anti-prismatic (TSAP) conformation. Both enantiomers of the TSAP geometry are present in the crystal to produce the space group P4/n. Clusters of water and chloride anions fill the space between complexes. One of the chlorides is positioned above the calcium centre with all angles between Cl-Ca-N identical for the pyridyl nitrogens at 63°, but the long distance of 5.23 Å makes it highly questionable if this chloride can be considered coordinated to the complex. A coordinated chloride was found in the Pr(III)-12N4Py4 structure[7] with a more reasonable distance of 2.77 Å .

The distance between the nitrogen donors and the metal centre (2.58 Å for ring N, 2.58 Å for arm N) are shorter than the corresponding measurement in the cerium complex (2.70 Å ring N, 2.69 Å arm N) in paragraph 4.2. This is probably due to the reduced size of the Ca(II) ion (1.12 Å radius[24]) in comparison to the lanthanides (Ce(III) 1.14 Å radius[24]) in compounds of coordination number 8. Crystal structures of Ca(II)-12N4Py4 have been previously published[23] and the motif of an coordinated Ca(II) with a cyclen based ligand is well documented.[23,25–28]

NMR spectra of the triflate salt of Ca(II)-12N4Py4 were recorded (Figure 4.13). Calcium is not paramagnetic and provides further insight into the properties of 12N4Py4 complexes. The aromatic peaks are very similar to those of the free ligand, with a slight upfield shift. While in the free ligand the CH_2 groups are equivalent and observed as singlets due to rapid rotation around single bonds, the complexation to a metal center locks them into one geometry.

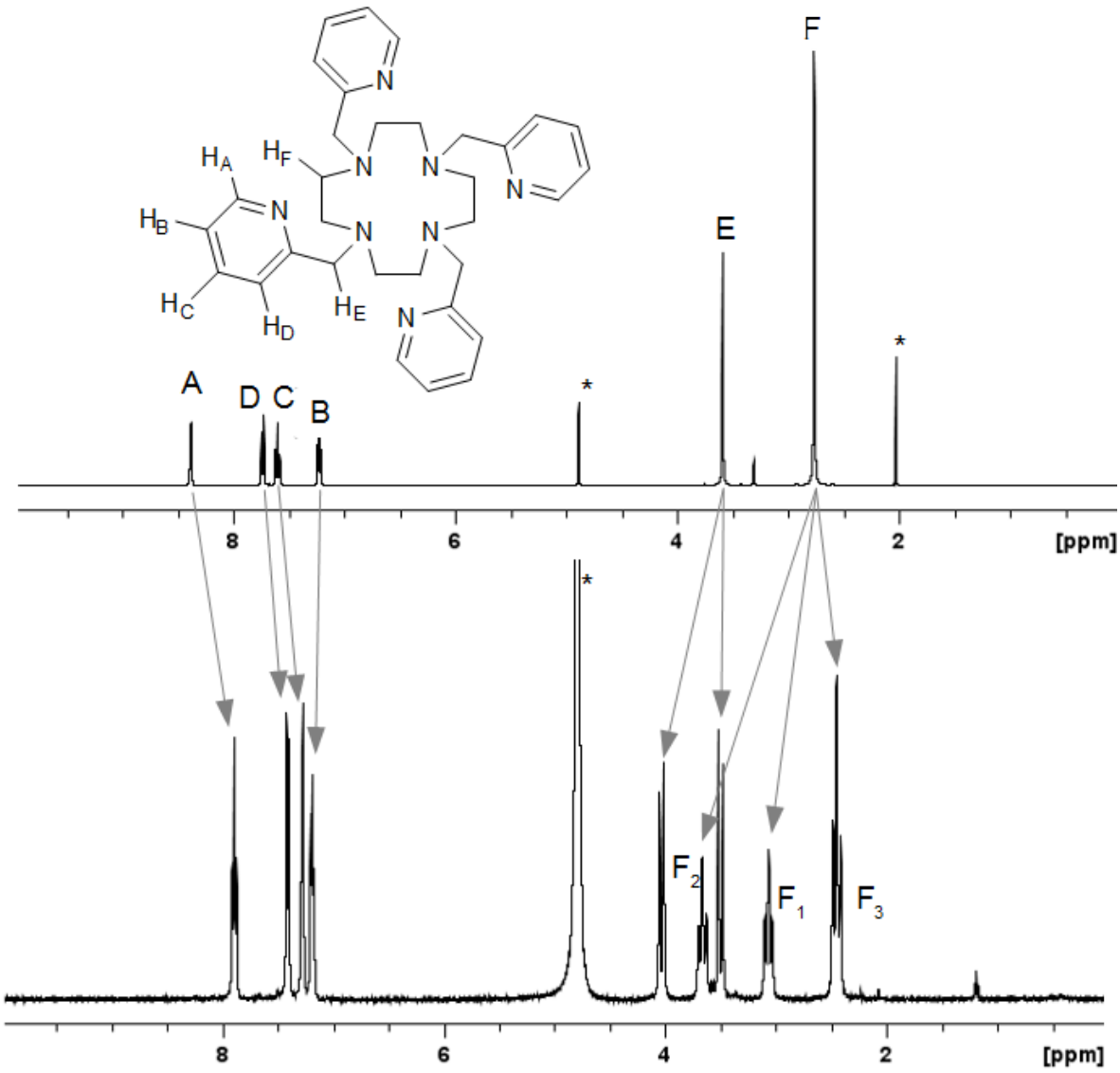

Figure 4.13: ^{1}H-NMR of Ca(II)-12N4Py4 (D2O) in comparison to the free ligand (MeOD)

From the crystal structure it is known that the CH_2 bridges of the macrocycle form a five membered ring with the adjacent nitrogens and the central calcium atom in a twisted conformation. Due to the long N-Ca bonds and the small angle at the metal ions the other angles are larger (110-112°) than in cyclopentane (105° [29]) and the protons can achieve a staggered conformation in which for each CH_2 group one protons takes on an axial conformation and the other an equatorial (Figure 4.14).

The two equatorial proton have highly similar chemical and magnetic environments, causing them to overlap to give a signal that resembles a triplet, but is instead two *ddd* signals. Axial protons experience some sterical interactions that lead to deshielding, their signals are observed at a higher shift than the equatorial protons. As the free ligand signals represent an averaged shift between both conformations, the equatorial protons appear at a lower shift relative to the corresponding signal of the free ligand. The axial proton that is directed towards the pyridyl arms also experiences the effect of the ring current in the aromatic ring and is slightly more shielded than the other axial proton. All these effects lead to the observed 1:1:2 pattern in Figure 4.13.

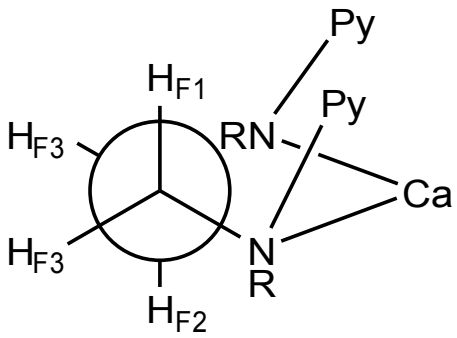

Figure 4.14: Fisher projection of macrocycle bridge of Ca-12N4Py4, viewed along C-C bond

In luminescence, the absorption of Ca(II)-12N4Py4 with a maximum at 263 nm (Figure 4.15 represent an intermediate between the free ligand and the Ce(III) complex, as the lower charge and larger size of Ca(II) polarises the pyridyl to a lesser degree than the Ce(III) ion.

Calcium does not have any luminescence transitions, all processes therefore have to be ligand based. The emission spectrum obtained upon irradiation at 263 nm shows a broad peak at 445 nm and matches the ligand emission in shape and position. The increase in emission intensity (9.42 relative to free ligand) is comparable with that of the cerium complex (13.8 relative to free ligand). Even though the coordination of

calcium does not offer alternative emissive transitions, it occupies the pyridyl lone pair and prevents their interference with π* states.

The lifetime of the calcium complex is expected to be similar to the free ligand and could not be recorded with the available instrumentation.

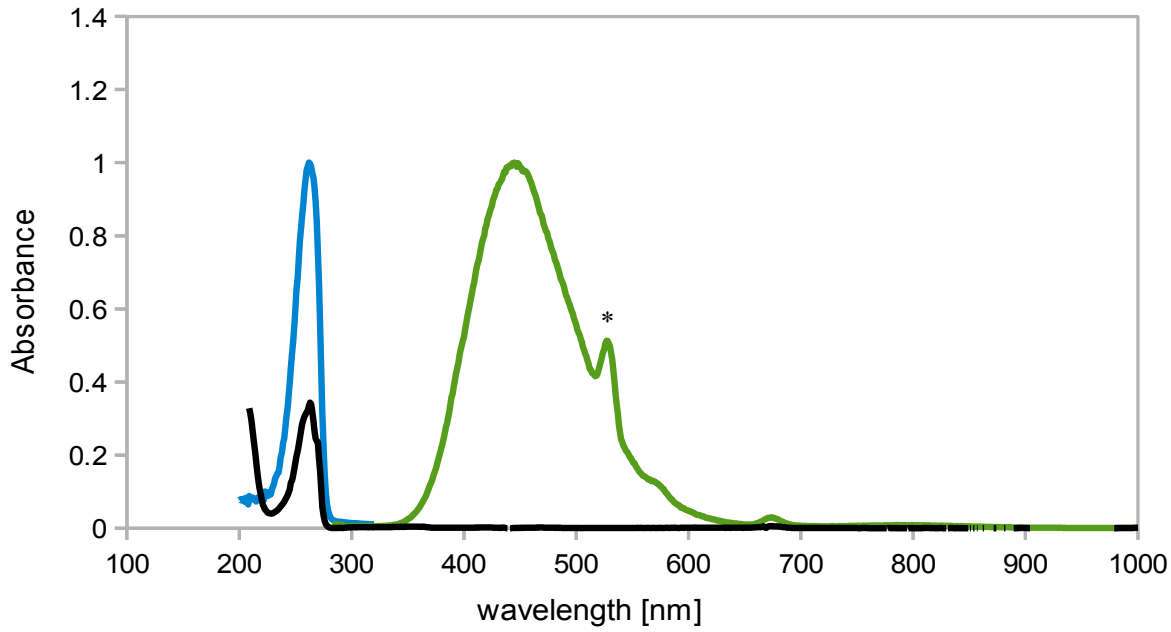

*Figure 4.15: Luminescence of Ca(II)-12N4Py4 in MeOH. Absorption (black), emission (gray, λ_{ex} = 263 nm, normalised) and excitation (light gray, λ_{em} = 445 nm, normalised) spectra at 2.5*10^{-5} M. 2λ artefact (*)*

4.7 Sodium

Another common impurity in water are sodium ions; these have been established to bind weakly to 12N4Py4 when it was evaluated which base could be used for the pK_a titrations (chapter 3). The literature procedure describes the formation of the sodium complex of 12N4Py4 as a chloride salt when the substitution of the cyclen ring with 2-picolyl chloride is performed in the presence of NaCl.[7] It can however also be synthesised from the isolated ligand with sodium triflate in acetonitrile (Scheme 4.2).

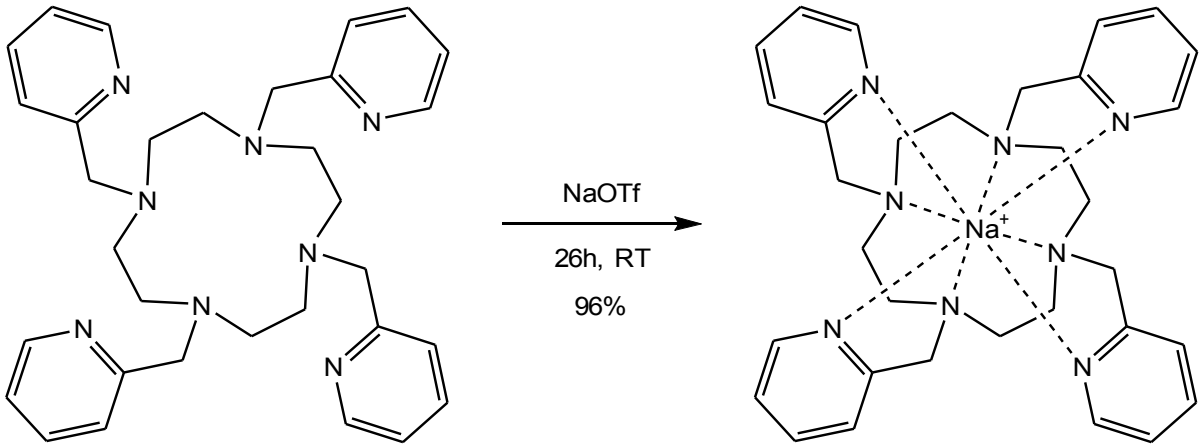

12N4Py4 **Na(I)-12N4Py4**

Scheme 4.2: Synthesis of Na(I)-12N4Py4 as triflate salt

NMR spectra of Na(I)-12N4Py4 (Figure 4.16) showed sharp signals for the aromatic protons that were shifted upfield and broad peaks for the CH_2 groups. A first theory was that the aza nitrogens might only coordinate weakly and an averaged signal of coordinated and uncoordinated sites was recorded. The pyridyl protons however are very sharp and clearly shifted upfield compared to the free ligand. When the pyridyl nitrogen are coordinated to the metal, dissociation of the macrocycle is highly unlikely.

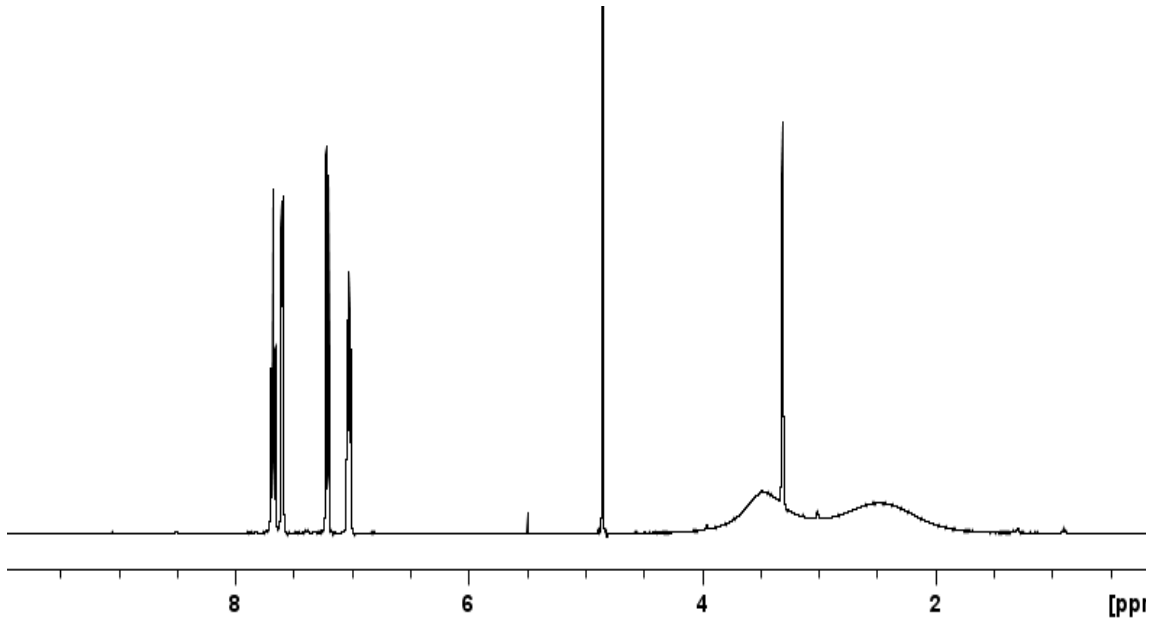

Figure 4.16: ^{1}H-NMR of Na-12N4Py4 in MeOD

Coordination to a metal would however produce two isomers rendering the two protons of each CH_2 groups inequivalent, as discussed for Ce(III)-12N4Py4 and Ca(II)-12N4Py4. Fast ring inversion or arm rotation interconverts the two isomers and could produce the observed broad signals as an averaged signals of the two protons. Spectra recorded for 12N4Py4 in D_2O in the presence of either NaCl or NaOH showed signs of interaction, but suggest weaker binding strengths than for Ca(II)-12N4Py4 and the lanthanide complexes.

A crystal structure of Na-12N4Py4 was obtained (measured, solved and refined by Dr. L. Pfeifer and Dr. A. Thompson) from an aqueous solution in the presence of sodium perrhenate (Figure 4.17). The metal center is 8 coordinated and well defined as found with Ca and the lanthanides. Distances between the nitrogens and the metal are somewhat shorter in the case of the ring nitrogens (2.57 Å) than for the previously discussed complexes, while in the case of the pyridyl nitrogens the difference is less pronounced (2.63 Å). The crystal is composed of a racemic mixture of the two twisted square anti-prismatic stereoisomers.

In comparison to the other structures, the torsion angle within the cyclen ring is not unusual at 59°. The pyridyl arms meanwhile show two sets of torsion angles. Two diagonal arms are rotate to 30 and 43° while the other two show angles of 11 and 13°. Such a large

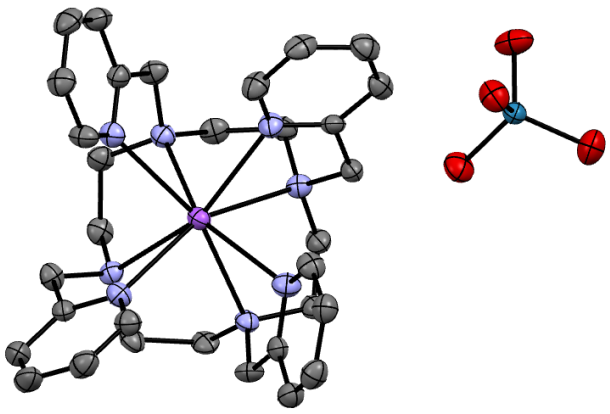

Figure 4.17: Crystal structure of Na(I)-12N4Py4 complex as perrhenate salt (WTS03). Hydrogen atoms not displayed, probability level at 50%.

difference might be caused by the packing in the solid. It is not sure wether the same would apply to the complex in solution or an averaged angle would be approached. This would at 24° be considerably smaller than the 30 to 40° observed for the calcium and lanthanide complexes.

The ligand is forced to adopt this confirmation due to the size of the sodium ion. Even though sodium is a considerably lighter atom than calcium or the lanthanides, its lower charge produces a cation that is just slightly larger (1.18 Å) than Ca(II) (1.12 Å) and the lanthanides (1.16 Å for La(III) to 0.98 Å for Lu(III)). Angles between carbon and nitrogen atoms in the macrocycle approach an average of 113°, whereas Ca(II) and Ce(III) complexes show 112° for the same angles.

In the solid phase sodium can comfortably sit in the 12N4Py4 cavity, but the large angles allow for change in conformation in solution as is reflected by the peak broadening in the NMR spectrum. It seems the sodium ion is at the upper limit in terms of size before a metal ion can no longer be accommodated by 12N4Py4.

Observations made in luminescence studies of Na(I)-12N4Py4 are in alignment with those for Ca(II)-12N4Py4. The absorption in UV (262 nm, Figure 4.18) is minutely red shifted in comparison to the free ligand, slightly less than in the Ca(II) complex due to the lower charge of sodium.

Emission is observed at 455 nm, slightly red shifted in comparison to both the free ligand and the calcium complex. The intensity is lower (1.9 relative to free ligand) than observed for Ca(II)-12N4Py4, possibly due to weaker binding of the pyridyl nitrogen donors.

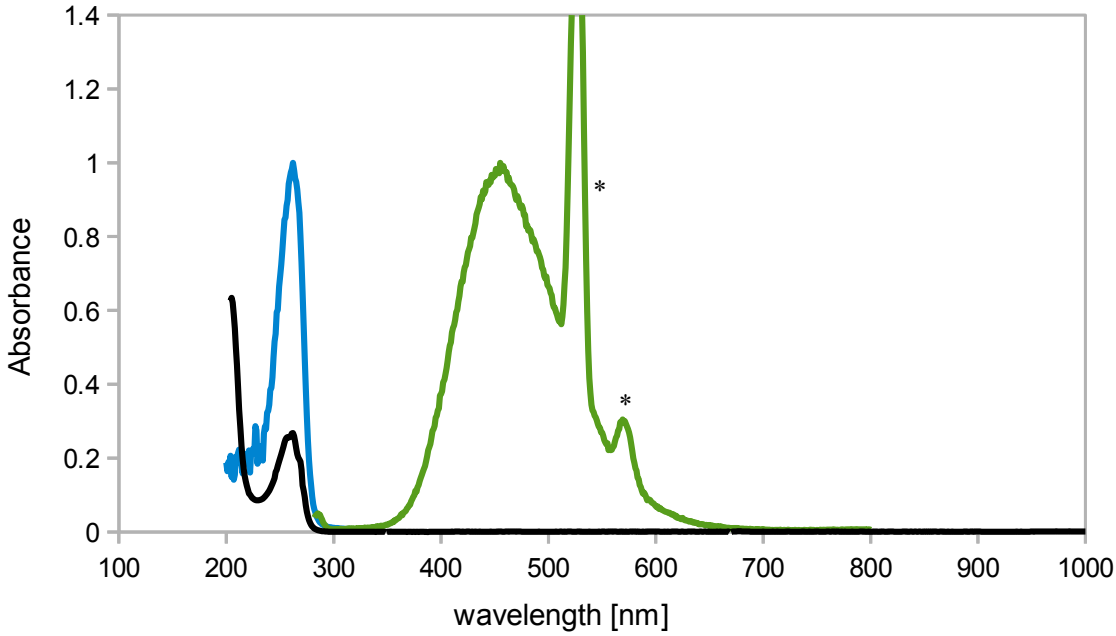

Figure 4.18: Luminescence of Na(I)-12N4Py4: absorption (black), emission (green, λ_{ex} = 262 nm, normalized) and excitation (blue, λ_{em} = 455 nm, normalized). 2λ artefact (*)

4.8 Conclusions

In this chapter it was shown that 12N4Py4 binds lanthanides as well as the alkali and earth alkali cations sodium and calcium in a predictable manner and forms stable complexes. The form two isomers, the twisted square anti-prism and the square anti-prism, their relative population depending on the size of the metal ion. Ce(III), Ca(II) and Na(I) complexes all crystallised as the TSAP. The large size of Na(I) however forces 12N4Py4 to adopt a more open conformation and appears to allow conversion between isomers in solution.

Figure 4.19 shows how the position of Ca(II) and Ce(III) in the complex are very similar, the larger Na(I) however takes on a position much further towards the macrocycle. It forces the ring into unfavourable angles and the pendant arms to

rotate less, further straining the structure. This causes significantly weaker binding.

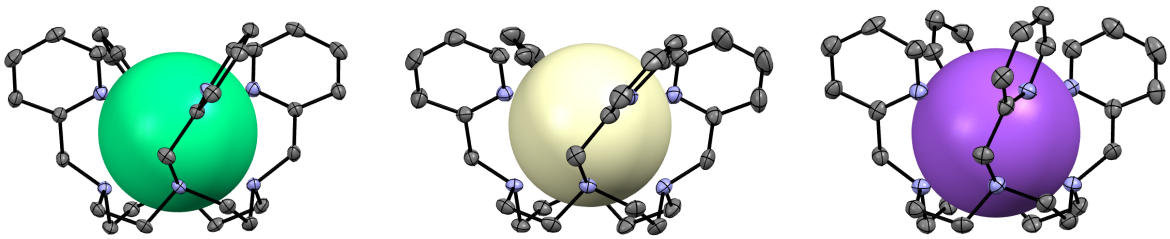

Figure 4.19: Effect of metal ion size on ligand structure, from crystal structures 6748, 6653 and 6746, van der Waals radii metals = 2x ionic radii[24]

Fluorescence is observed for these three complexes, in the case of Ca(II) and Na(I) it is mainly ligand based. Occupation of nitrogen lone pairs by coordination seems to remove non-radiative transitions from excited states and increases overall emission. Ce(III) also shows sensitisation of d-f transitions from ligand excited states.

In the presence of water metal cations also form hydroxo and oxo complexes, in the case of the lanthanides with low solubilities. This adds another aspect to the potential application, as precipitation removes species from equilibrium. It may also cause problems in applications during extraction. Selective precipitation can however also be encouraged in order to isolate one or several species as solids. There is indication that the ligand can be a component of the precipitation.

Figure 4.20 gives an overview of the equilibria established in this chapter.

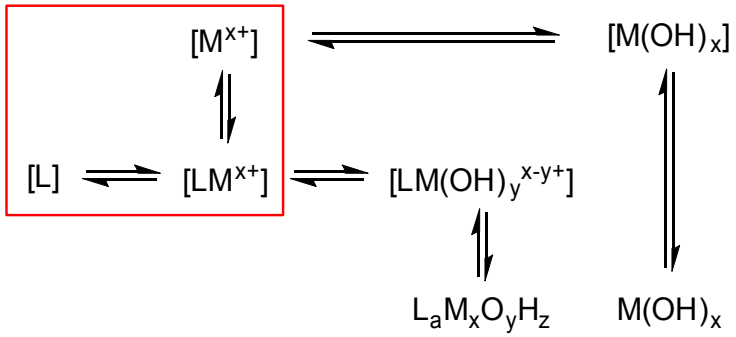

Figure 4.20: Metal complexation under consideration of hydroxide formation and precipitation

References

[1] B. C. Mayo, *Chem. Soc. Rev.* **1973**, *2*, 49.
[2] P. Caravan, J. J. Ellison, T. J. McMurry, R. B. Lauffer, *Chem. Rev.* **1999**, *99*, 2293–2352.
[3] F. Hulliger, H. R. Ott, *Z. Für Phys. B Condens. Matter* **1987**, *67*, 291–298.
[4] O. A. Blackburn, N. F. Chilton, K. Keller, C. E. Tait, W. K. Myers, E. J. L. McInnes, A. M. Kenwright, P. D. Beer, C. R. Timmel, S. Faulkner, *Angew. Chem. Int. Ed.* **2015**, *54*, 10783–10786.
[5] O. A. Blackburn, A. M. Kenwright, A. R. Jupp, J. M. Goicoechea, P. D. Beer, S. Faulkner, *Chem. – Eur. J.* **2016**, *22*, 8929–8936.
[6] X. Zhou, X. Zhao, Y. Wang, B. Wu, J. Shen, L. Li, Q. Li, *Inorg. Chem.* **2014**, *53*, 12275–12282.
[7] L. S. Natrajan, N. M. Khoabane, B. L. Dadds, C. A. Muryn, R. G. Pritchard, S. L. Heath, A. M. Kenwright, I. Kuprov, S. Faulkner, *Inorg. Chem.* **2010**, *49*, 7700–7709.
[8] J. J. Wilson, E. R. Birnbaum, E. R. Batista, R. L. Martin, K. D. John, *Inorg. Chem.* **2015**, *54*, 97–109.
[9] B. M. Casari, V. Langer, *Z. Für Anorg. Allg. Chem.* **2007**, *633*, 1074–1081.
[10] T. A. Beineke, J. Delgaudio, *Inorg. Chem.* **1968**, *7*, 715–721.
[11] R. Díaz-Torres, S. Alvarez, *Dalton Trans.* **2011**, *40*, 10742.
[12] G. Pályi, C. Zucchi, L. Caglioti, Eds. , *Organometallic Chirality*, Mucchi, Modena, **2008**.
[13] G. P. Moss, *Pure Appl. Chem.* **1996**, *68*, 2193.
[14] N. F. Ramsey, *Phys. Rev.* **1950**, *78*, 699–703.
[15] H. M. McConnell, R. E. Robertson, *J. Chem. Phys.* **1958**, *29*, 1361–1365.
[16] B. Bleaney, *J. Magn. Reson. 1969* **1972**, *8*, 91–100.
[17] B. Bleaney, C. M. Dobson, B. A. Levine, R. B. Martin, R. J. P. Williams, A. V. Xavier, *J. Chem. Soc. Chem. Commun.* **1972**, 791b.
[18] P. Hänninen, H. Härmä, Eds. , *Lanthanide Luminescence*, Springer Berlin Heidelberg, Berlin, Heidelberg, **2011**.
[19] J. Kragten, *Atlas of Metal-Ligand Equilibria in Aqueous Solution*, E. Horwood; Halsted Press, Chichester, Eng.: New York, **1978**.
[20] R. M. Smith, A. E. Martell, R. M. Smith, *Critical Stability Constants Volume 4: Inorganic Complexes*, Plenum Press, New York, **1976**.
[21] P. L. Brown, C. Ekberg, *Hydrolysis of Metal Ions*, Wiley-VCH Verlag GmbH & Co. KGaA, Weinheim, **2016**.
[22] Z. Zheng, in *Encycl. Inorg. Bioinorg. Chem.* (Ed.: R.A. Scott), John Wiley & Sons, Ltd, Chichester, UK, **2012**.
[23] H. Ito, H. Tsukube, S. Shinoda, *Chem. - Eur. J.* **2013**, *19*, 3330–3339.
[24] R. D. Shannon, *Acta Crystallogr. Sect. A* **1976**, *32*, 751–767.
[25] H. Misaki, H. Miyake, S. Shinoda, H. Tsukube, *Inorg. Chem.* **2009**, *48*, 11921–11928.
[26] H. Ito, H. Tsukube, S. Shinoda, *Chem. Commun.* **2012**, *48*, 10954.
[27] J. Platzek, P. Blaszkiewicz, H. Gries, P. Luger, G. Michl, A. Müller-Fahrnow, B. Radüchel, D. Sülzle, *Inorg. Chem.* **1997**, *36*, 6086–6093.
[28] H. Maumela, R. D. Hancock, L. Carlton, J. H. Reibenspies, K. P. Wainwright, *J. Am. Chem. Soc.* **1995**, *117*, 6698–6707.
[29] F. J. McQuillin, M. S. Baird, *Alicyclic Chemistry*, Cambridge University Press, Cambridge; New York, **1983**.

[30] P. D. Wilson, Ed. , *The Nuclear Fuel Cycle: From Ore to Waste*, Oxford University Press, Oxford; New York, **1996**.

Chapter 5: 12N4Py4 metal binding constants

5.1 Introduction

The determination of pK_a values of 12N4Py4 (see chapter 3) allows the measurement of metal binding constants in water. In this chapter several different methods to obtain metal binding constants are explored and the results from each are compared. The previously discussed issues with formation of lanthanide hydroxides were encountered again and their influence on the measurements and the obtained results were evaluated. Later in this chapter it will also be discussed how equilibria are influenced by ligand metal ratios and dilutions.

5.2 Titration experiments and general observations

Initially it was planned to determine the binding constants by luminescence. The f-f transition of most lanthanides is a valuable tool to follow complexation of the metal in solution.[1] At the beginning of the project Ce(III) was chosen as the primary model lanthanide. Unfortunately the f-d transition proved to be less useful to monitor speciation, as the emission spectrum overlaps with that of the free ligand. Initial measurements on the complex in water gave inconclusive and poorly reproducible results, which can be partly attributed to the competition between metal and protons. The challenge of luminescence measurement is further complicated by differences in emissive quantum yield between species, which means that observed data is a quantum yield weighted average.

Before extensive equilibrium studies were performed, it was briefly considered performing kinetic measurements of lanthanide binding; early experiments with neodymium however suggested that the complexation is very slow at room temperature and may take up to a week to properly equilibrate. The instrumentation could not easily be heated and is not meant to be running for such a long time, therefore no detailed kinetic data were recorded. The slowness of the reaction does however have an effect on how equilibrium measurements have to be planned. It also explains the non-reproducibility of the measurements of the cerium complex, as the amount of complex present in solution is dependent on the age of the solution and the slow dissociation of the metal from 12N4Py4.

It was at this point in time that it became apparent that the competition with protonation is an essential component of the equilibrium system and the focus was temporarily diverted to pH titrations. Measurement of the pK_as that followed were discussed in chapter 3.

5.2.1 Experimental considerations

Several considerations have to be made before performing the titration. These will be discussed in general terms here as they also have an influence on the accuracy on the data and the results obtained from them.

Binding constants between metal ions and ligands can be determined through the titration of one species with the other.[2] With the involvement of competing protonation processes, a pH titration becomes preferable. In chapter 3 several considerations concerning the set up of pH titrations were discussed, these can also be used for the titration in presence of metal ions.

As mentioned earlier, complexation reactions at room temperature were observed to

be very slow. However, measuring samples over a long period of time causes them to accumulate dissolved CO_2 from the atmosphere, which would interfere with a precise measurement, owing both to potential coordination and precipitation of metal carbonates and the buffering capacity of the carbonate ion. It would also require an unreasonable amount of time to leave each solution to equilibrate for a week after each addition of acid or base. Thus, instead of titrating one solution with acid or base, each point of the titration was prepared as an individual sample with varying acid/base content. Each series of samples was allowed to equilibrate for 6-8 days at a constant temperature before its pH was determined.

Increasing the number of samples studied requires more of each compound as well as increased preparation time, so only a limited amount of samples could be prepared for each series. On average a total of 10 to 20 samples were made per series.

The influence of ionic strength and temperature was investigated for the pK_a determination. To provide an equally comprehensive study on metal binding, these conditions were reproduced. Of the four temperatures (0°, 22°, 30° and 38°C) three were also used in this titrations (22°, 30° and 38° C), as the low temperature at 0°C could not be maintained controllably for such long periods of time with the equipment at hand. Ionic strength was controlled by using potassium chloride solutions of different concentrations (0.5, 1.0 and 2.0 M). No measurement without addition of KCl (ionic strength ~ 0 M) was incorporated in the investigation, as the changing concentrations of protonated ligand and metal complexes would have a too large relative effect on the total ionic strength.

From the structure of lanthanide (and other) complexes of 12N4Py4 it is known that

the ligand encapsulates the metal centre very effectively and it is not likely that more than one molecule of 12N4Py4 would bind on each metal centre, therefore 1:1 metal to ligand concentrations were used as a first approximation when modelling binding. In all cases this approach was found to be satisfactory.

5.2.2 Data treatment

The data obtained was treated using a methodology derived from that described in chapter 3. Differences between concentrations of hydroxide, protons, chloride and potassium were used to determine the concentration of bound protons [H_b]. From equations 3.2 - 3.4 it is known that [H_b] can be described using the concentration of the free ligand and all involved proton dissociation constants (K_1 to K_4).

$$[H_b] = [LH] + 2[LH_2] + 3[LH_3] + 4[LH_4] \qquad 5.1$$

$$[H_b] = [L]\left(\frac{H}{K_1} + \frac{2H^2}{K_1K_2} + \frac{3H^3}{K_1K_2K_3} + \frac{4H^4}{K_1K_2K_3K_4}\right) \qquad 5.2$$

As dissociation constants (K_1 to K_4) have been determined (see chapter 3), [L] can be determined for each titration point. The respective concentrations of the protonated 12N4Py4 species can be obtained directly from the individual dissociation constants. This leaves the complex concentration [LM] to be determined from the total ligand concentration L_{tot} and the free metal concentration [M] from the total metal concentration M_{tot}.

$$L_{tot} = [L] + [LH] + [LH_2] + [LH_3] + [LH_4] + [LM]$$

$$[LM] = L_{tot} - [L] - [LH] - [LH_2] - [LH_3] - [LH_4] \qquad 5.3$$

$$M_{tot} = [M] + [LM]$$

$$[M] = M_{tot} - [LM] \qquad 5.4$$

Plotting all calculated concentrations gave an overview over the composition of the mixture at different pH values (Figure 5.1).

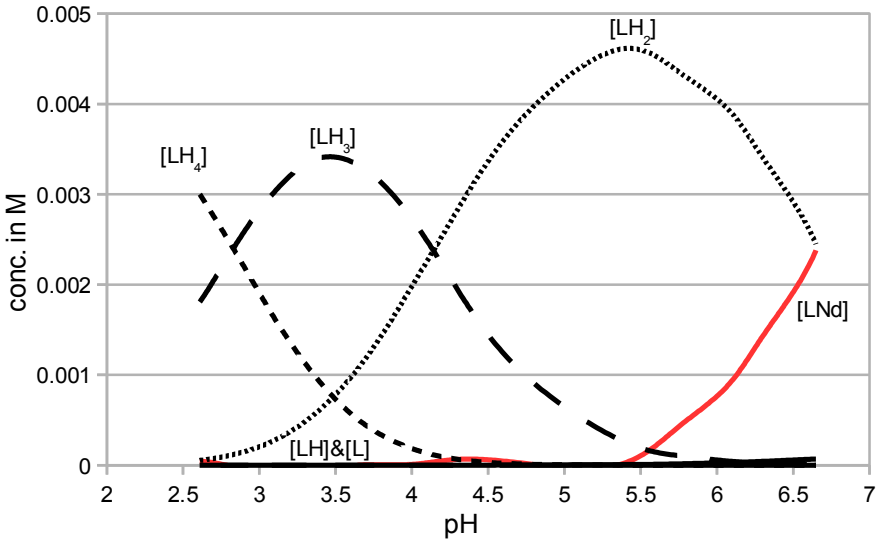

Figure 5.1: Concentrations of species in pH titration with 12N4Py4 and $Nd(OTf)_3$ at 30°C and 1M KCl.

The speciation curve for neodymium binding (Figure 5.1) also shows that, with individually prepared samples for each titration point, the range of the titration had to be determined beforehand, without knowledge of the binding strength and could not be adjusted during measurement. Several titrations showed an incomplete binding curve or were in the wrong pH range all together and had to be repeated. However as long as a good portion of the complexation is recorded, the binding constant could still be determined with confidence.

For all investigated lanthanides (cerium, praseodymium, neodymium and ytterbium) precipitation was observed in samples towards the neutral/basic pH range. Species contained in the precipitate can no longer participate in solution equilibria, thus further limiting the range where binding constants can be determined. As such all raw data had to be treated with caution.

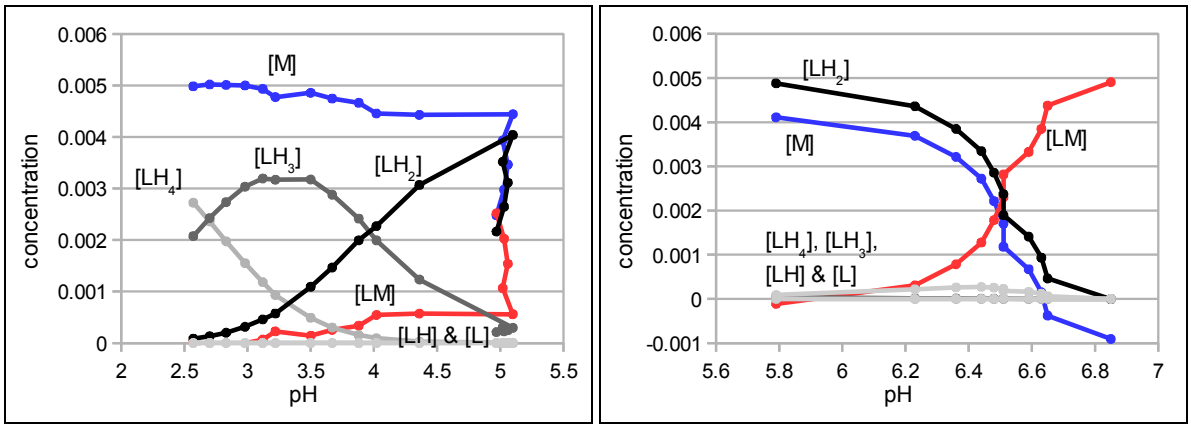

Figure 5.2: Speciation diagrams for Ce(III) (0.5 M KCl at 22°C) and Yb (III) (0.5 M KCl at 38°C) with disturbances caused by precipitation towards the righthand end of the titration.

Beside visible precipitation, formation of colloidal precipitates is also indicated by strongly fluctuating data points from the mean curve or whose species concentrations are not physically possible (such as negative concentrations or [LM] > L_{tot}) as highlighted in Figure 5.2. Data points affected by precipitation can not be considered in the determination of the binding constant.

Calcium and sodium did not produce any precipitation problems of the kind described for the lanthanides and therefore binding constants are somewhat easier to measure for them as there are less limitations. In the case of calcium however it was observed that the complex itself has a reduced solubility in water and crystallises from solution. This also influences the region of reliable data, however is also indicative of fast crystallisation/redissolution processes that allow equilibrium to be established more quickly. Furthermore, it gives a promising outlook for the extractability of the complexes into less polar solvents.

5.3 Estimation of binding constants

Theoretically the binding constant K_c to the metal could be determined from a single point in the titration:

$$K_c = \frac{[LM]}{[L][M]} \qquad 5.5$$

As the experimental data undergoes several mathematical transformations, minor inaccuracies in the sample concentrations as well as truncation of decimal places in spreadsheet programs can lead to much bigger errors in the binding constant obtained. Therefore it is better that binding constants be calculated for several points and an average taken. Table 5.1 shows an excerpt of the values for $\log K_c$ that have been estimated for lanthanide complexes. A more extensive table can be found in the experimental part of this thesis. Inaccuracies have an increased effect on very low concentrations of any species involved in equation 5.5. So only values where the percentage of complexed metal is between 20% and 80% of the total metal concentration/ ligand concentration were considered.[2]

This condition was not met by any data point of the cerium series as well as a few series of the other metals.

Table 5.1: $\log K_c$ of lanthanides estimated directly from [Hb] at 1 M KCl

metal	$\log K_c$ at 22°C	$\log K_c$ at 30°C	$\log K_c$ at 38°C
cerium	10.97[a]	11.92[a]	11.73[a]
praseodymium	6.74	8.74	8.82
neodymium	6.73	8.49	8.97
ytterbium	8.08	9.08	8.99

a obtained from samples containing precipitation, have to be rejected.

It also has to be mentioned that in many cases only 2-4 data points fulfilled the necessary requirements to be used in the determination of the constant, therefore the

accuracy of the method is lowered.

Most values for Pr(III), Nd(III) and Yb(III) all are within the range between 6 and 9. Literature values for lanthanide complexes of EDTA, DOTA and other oxygen donor ligands are considerably larger (logK 10 - 30) due to the oxygen affinity of the lanthanides and the electrostatic attraction of negative counter charge provided by the ligand.[3] Octadentate ligands offering purely N-donor atoms are rare, though the stability constant of comparable tri- and tetradentate ligands are reassuringly lower (log K 3-5) than found in this study.[4] Their 1:2 complexes then show stability constants of comparable to 12N4Py4.

Values determined for Ce(III) were obtained from data that was heavily compromised by precipitation. No data point was measured that fully complies with the conditions laid out earlier. This may be the main reason why cerium binding constants are significantly larger than for the other lanthanides, even though there is no chemical basis to explain such an effect. These values therefore have to be rejected on the basis that in the presence of precipitation equilibrium cannot be achieved.

Table 5.2 gives the $\log K_c$ values obtained for Ca(II) and Na(I). Values for Ca(II) are similar to those obtained for Ce(III), in this case however the absence of precipitate suggests the accuracy of these results. It is possible that the low solubility of Ca-12N4Py4 suggests a higher binding constant than would be observed at lower

Table 5.2: $\log K_c$ of calcium and sodium estimated directly from [Hb] at 1 M KCl

metal	$\log K_c$ at 22°C	$\log K_c$ at 30°C	$\log K_c$ at 38°C
calcium	11.87	12.63	11.94
sodium	5.26	7.72	5.04

concentrations, this is however more likely to be the case for low temperatures (22°C) and high ionic strengths, for which in some combination even higher

constants were calculated (14.52 at 30°C, 2 M KCl).

12N4Py4 as a neutral ligand cannot balance the high charge of lanthanide ions as well as an anionic ligand such as DOTA, while the lower charge of Ca(II) allows more stable complexes. Technically, 12N4Py4 has to compete for the metal ions against water as one of the simplest ligands and lanthanides have a significantly higher hydration enthalpy than both Ca(II) and Na(I)[5], which are therefore more readily available to bind an N-donor ligand. Sodium should by these standards show constants even higher than Ca(II), its larger size however cause it to fit less well into the binding cavity of 12N4Py4, decreasing the complex stability.

5.4 Fitting procedure for metal binding constants

When discussing the determination of deprotonation constants in chapter 3 it was mentioned already that values determined directly from the Bjerrum plot can merely be seen as an estimate, especially for systems where transitions between species overlap. Similarly, the accuracy of binding constants of metals could greatly be increased by using a fitting procedure. Fitting procedures can also take into account data points where metal complex concentrations are very small and instead use the change seen in the dissociation constants to determine the strength of binding to the metal.

5.4.1 Finding an equation to describe the system

A fitting procedure can be found for any system given that it is completely described by mathematical equations, there are at least as many equations as unknown quantities (constants and concentrations) and a dependency can be established that

relates all species to a measurable quantity (for example [H] or [H_b]). On the assumption that 12N4Py4 is either protonated (in one of four different protonation states), present as the free ligand or the metal complex, while the metal is either free or bound to 12N4Py4, the system is described by a set of eight equations.

Relations between different protonated states are defined by the four dissociation constants:

$$K_1 = \frac{[L][H]}{[LH]} \quad 5.6$$

$$K_2 = \frac{[LH][H]}{[LH_2]} \quad 5.7$$

$$K_3 = \frac{[LH_2][H]}{[LH_3]} \quad 5.8$$

and

$$K_4 = \frac{[L_3][H]}{[LH_4]} \quad 5.9$$

The equilibrium under investigation is defined as

$$K_c = \frac{[LM]}{[L][M]} \quad 5.10$$

From the measured pH value the concentration of protons bound can be calculated to give [H_b]

$$[H_b] = [LH] + 2[LH_2] + 3[LH_3] + 4[LH_4] \quad 5.11$$

And finally the sum of all species containing ligand or metal respectively.

$$M_{tot} = [LM] + [M] \quad 5.12$$

$$L_{tot} = [L] + [LH] + [LH_2] + [LH_3] + [LH_4] + [LM] \quad 5.13$$

These equations were combined as is described in detail in the appendix to produce a function of $[H_b]$ that is only dependent on the binding and dissociation constants K_1, K_2, K_3, K_4 and K_c.

$$[H_b] = \frac{-(B - K_c\Delta_{tot}) + \sqrt{(B - K_c\Delta_{tot})^2 - 4BK_cL_{tot}}}{\frac{2BK_c}{A}} \qquad 5.14$$

with

$$\Delta_{tot} = L_{tot} - M_{tot}$$

$$A = \frac{[H]}{K_1} + 2\frac{[H]^2}{K_1K_2} + 3\frac{[H]^3}{K_1K_2K_3} + 4\frac{[H]^4}{K_1K_2K_3K_4}$$

$$B = 1 + \frac{[H]}{K_1} + \frac{[H]^2}{K_1K_2} + \frac{[H]^3}{K_1K_2K_3} + \frac{[H]^4}{K_1K_2K_3K_4}$$

5.4.2 Restrained fitting of 12N4Py4 metal titrations

With the newly developed equation it is possible to fit experimental metal titration data to obtain the binding constant. As the dissociation constants K_1 to K_4 have been previously established (chapter 3), the corresponding values were entered and kept constant during the fitting procedure, only allowing the program (OriginPro® 9.1) to vary K_c to find the best fit. Table 5.3 show some of the binding constants obtained using the fitting procedure in comparison to the previously calculated values.

In general, the binding constants obtained through the fitting procedure are within one order of magnitude of the estimated values, meaning that the quality of their output is very similar. The data measured for cerium, as discussed for the estimation, is too severely affected by precipitation to contain enough information on the complexation event. From the remaining data, the fitting procedure is not capable to

extract any additional information, the results are equally far from expected and reasonable values.

Table 5.3: $logK_c$ of lanthanides estimated directly from $[H_b]$ at 1 M KCl

metal	$logK_c$ at 22°C		$logK_c$ at 30°C		$logK_c$ at 38°C	
	estim.	fit	estim.	fit	estim.	fit
cerium	10.97[a]	10.70	11.92[a]	11.30	11.73[a]	11.11
praseodymium	6.74	6.52	8.74	8.82	8.82	8.78
neodymium	6.73	6.71	8.49	8.52	8.97	8.82
ytterbium	8.08	7.34	9.08	8.30	8.99	8.25
calcium	11.88	11.89	12.63	12.69	11.94	11.97
sodium	5.26	5.16	7.72	7.63	5.04	5.10

a values rejected as precipitation interfered

For calcium, sodium and neodymium the fitted curve matches the experimental data very well, as is reflected in high adjusted R^2 values (above 0.95 with a few exceptions). The values for praseodymium are slightly lower, while in ytterbium the fit does not seem to be particularly good with adjusted R^2 values as low as 0.53.

5.4.3 Unconstrained fitting

In chapter 3 it was already discussed that in the fitting of dissociation constants the final deprotonation step (K_1) contained the largest error, as it coincided with the precipitation of the free ligand and only few data points where available for an accurate fit of this constant. This also means that the pK_a values used for the fitting of the metal titration are not perfect values.

The fitted binding constants were reentered as initial values for a second fitting, in which all binding constants (K_1, K_2, K_3, K_4 and K_c) where allowed to vary in turns until the fit converged. Table 5.4 gives the new fitted binding constants obtained with these second procedure in comparison with the results of the restricted fitting for the same

data sets. For most cases K_c remains exactly the same, the adjusted R^2 is generally increased. In many cases however the removal of the constraints caused the dissociation constants to drift off to values that are clearly not in relation to the chemical situation. Often K_4 would drop down to 10^{-8} or 10^{-9} and therefore below K_1 and K_2. This of course is not in agreement with our chemical understanding of polyprotic acids. It is also an indicator for the data set being too small for the complexity of the fitting function and there are too many ways of choosing the constants to obtain a mathematically good fit.

Table 5.4: logK_c determined by unconstrained fitting procedure at 1 M KCl

metal	logK_c at 22°C		logK_c at 30°C		logK_c at 38°C	
	fit 1	**fit 2**	**fit 1**	**fit 2**	**fit 1**	**fit 2**
Cerium	10.70	10.70	11.30	11.30	11.11	11.12
Praseodymium	6.52	6.52[b]	8.83	8.82[b]	8.79	8.78[b]
Neodymium	6.71	6.71	8.52	8.52	8.83	8.82
Ytterbium	7.34	7.34[b]	8.30	8.30[b]	8.26	8.25[b]
Calcium	11.89	11.77[b]	12.68	12.53[b]	11.97	11.87[b]
Sodium	5.18	5.16	7.63	7.63[b]	5.11	5.10[b]
[b]*strong deviation of K_1-K_4 observed,*						

It should also be mentioned that the exact outcome of this fitting procedure, especially the changes made to the dissociation constants, is dependent on the sequence in which the constants were fitted, further lowering confidence in the accuracy of these values.

Generally it seems that this unconstrained fit does not offer an improvement over the constrained fit but might in fact be less appropriate to these data sets. Both fitting methods use a highly complex equation and were used to fit a very limited data set. If a a more extensive data set was available, the accuracy of the fitting procedure could be greatly increased. Preceding pK_a measurements might become redundant, if the

metal titration includes data point for the complete range of pH of interest. It has the advantage that precipitation of the free ligand is circumvented by formation of the metal complex. There remains however the precipitate of putative lanthanide hydroxide phases, that again limits the applicability of the technique.

Large deviations from physically possible concentrations (e.g. in Figure 5.2) caused by the presence of precipitate are only reflected by small changes in $[H_b]$. The estimation technique therefore helps identifying samples that need to be excluded from the fitting procedure due to small amounts of precipitate. When the fitting technique is used as the sole determination method, such samples might be wrongly included in the procedure. This might be a challenge when systems are fitted and the pK_a values of the ligand weren't or couldn't be determined beforehand.

5.5 Including hydroxide formation in binding constant determination

Already in chapter 4 it was mentioned that lanthanides readily bind hydroxide anions, forming compounds of low solubility. In all lanthanide titrations the corresponding precipitate was observed. The formation of simple lanthanide hydroxides is pH dependent. Simple $Ln(OH)_3$ accordingly has three formation constants, that were already determined in the 1970s.[..]

The binding constants are generally presented in the form

$$K_{OH} = \frac{[M(OH_x)][H]^x}{[M]} \qquad 5.15$$

reflecting the reaction pathway (Scheme 5.1), whereas a water molecule coordinates to the metal and undergoes dissociation. In aqueous solution the concentration of

water is assumed constant and therefore does not appear in the equation.

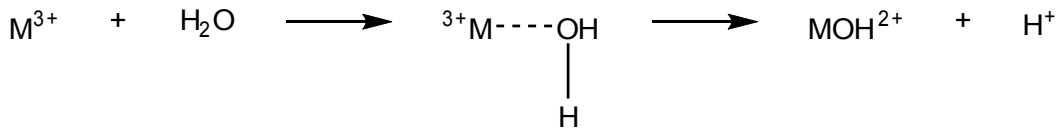

Scheme 5.1: Suggested mechanism of metal hydroxide formation

During the formation of the precipitate, the concentration of free protons is increased through the dissociation of water to form the hydroxides. With the current model these protons are not accounted for. This decreases the value of $[H_b]$ calculated from experimental data, indicating formation of the metal complex and thereby suggesting a binding constant that is too large.

The effect can also be seen when looking at the individual binding constants determined for each of the data points along a titration curve. If the precipitation sets in during the complexation event, binding constants gradually increase for data points with more precipitation. Whereas precipitation was found to be most common in cerium titrations, similar consideration has to be applied to all other lanthanides.

Even though the integration of hydroxide formation constants into the fitting procedure is theoretically and mathematically possible, the function gets increasingly complex with each added species. The data sets of this study are too small to deduce a fitting function and get an improved result. It is however possible to use the hydroxide formation constants to obtain an improved estimation similar to the one in section 5.3. It is not necessary to include all equations describing the system and instead developing an equation that describes one unknown species as a function of pH and $[H_b]$. This is basically the same method as the estimation of fitting function, but this time based on an extended set of species. The derivation of the equation is presented in detail in the appendix and takes on the following form for M(III) ions.

$$\frac{[H_b] + 3M_{tot} - 3L_{tot} - C\frac{M_{tot} - L_{tot}}{D}}{A - 3B + \frac{CB}{D}} = [L] \qquad 5.16$$

with

$$C = 3 + 2\frac{K_{OH}}{[H]} + \frac{K_{OH2}}{[H]^2}$$

$$D = 1 + \frac{K_{OH}}{[H]} + \frac{K_{OH2}}{[H]^2} + \frac{K_{OH3}}{[H]^3}$$

Alternative functions were derived for Ca(II) and Na(I) (see appendix).

This equation allows the calculation of [L] for each point in the titration, subsequently all other concentrations can be deduced using the equilibrium equations 5.6 - 5.10. The stability constants of the metal complexes of 12N4Py4 was then calculated for all data points and an average taken. Table 5.5 summarises some of the results obtained using this technique in comparison with the estimated constants of section 5.3.

Table 5.5: Estimation of logK_c including hydroxide formation compared to section 5.3

metal	**logK_c at 22°C**		**logK_c at 30°C**		**logK_c at 38°C**	
	estim. 1	**with K_{OH}**	**estim. 1**	**with K_{OH}**	**estim. 1**	**with K_{OH}**
Cerium	*10.97*[a]	*10.97*	*11.92*[a]	*11.92*	*11.73*[a]	*11.73*
Praseodymium	*6.74*	*6.45*	*8.74*	*8.89*	*8.82*	*8.88*
Neodymium	*6.73*	*6.68*	*8.49*	*8.48*	*8.97*	*8.97*
Ytterbium	*8.08*	*7.31*	*9.08*	*8.32*	*8.99*	*8.20*
Calcium	*11.89*	*11.87*	*12.68*	*12.64*	*11.94*	*11.94*
Sodium	*5.26*	*5.26*	*7.72*	*7.73*	*5.04*	*5.09*

[a] *determined from data where precipitation interfered.*

For most of the titrations, these new values are again very close to the estimated values of section 5.3. The largest deviations are observed for ytterbium. Interestingly, the new estimation gives results that are closer to the results of the fitting

procedures. Meanwhile in the cerium series there is little difference, again due to the interference of the precipitate.

While this new method includes more species and therefore presents a more comprehensive theory of the equilibrium situation in solution, it does not cover every possibility. From various crystal structures (the reader is referred to chapter 4 and the literature[8]) it is known that the 12N4Py4 complex allows solvent molecules or anions to coordinate to the metal centre, which could also be a hydroxide. This in turn can also lead to cluster formation of various compositions. Without the knowledge of their structure however it is not possible to include them into the determination of binding constants.

However the fact that estimation of binding constants give very similar results with or without the consideration of metal hydroxides suggests that their influence is small. This new estimation method does not show a significant improvement over the other methods for this system.

5.6 Consideration of the precipitate

Effects upon the titration caused by precipitation has so far only been discussed briefly. It is a result of the solution reaching concentrations of metal and hydroxide above the solubility limit for $M(OH)_x$, the corresponding solubility product is commonly expressed as

$$K_s = [M][OH]^x \qquad 5.17$$

Precipitation of lanthanide hydroxide has very similar effects on the titration data as the formation of hydroxide in solution, it increases pH, but also removes species from

solution and inhibits them from taking part in the equilibrium.

The nature of solubility constants do not allow their integration into equilibrium calculation, as they represent a solubility limit, not a gradual transition from one species to another. Under these circumstances no improved equation for data fitting can be developed. Still it is important to understand how the precipitate fits into the system.

The solubility of lanthanide hydroxides is generally very low with K_s between 15.43 for lutetium and 19.72 for lanthanum.[9]

Using the solubility limit and the equilibrium constants, a phase diagram can be produced that shows the main species in dependence of pH and the metal concentration, in absence of any ligand. Figure 5.3 (top) shows such a diagram for Nd(III) ions in water. Sources of binding constants also often give formation constants for additional species, such as $Ln(OH)_4^-$ and polynuclear hydroxides.[7] If they are included in the graph the region of precipitation changes its shape (Figure 5.3, bottom graph). It becomes clear that in the concentration region of the titrations ($5*10^{-3}$ M) performed, the precipitate sets in before the metal hydroxides reach significant percentages of the total metal concentration.

The formation of precipitate could be avoided by lowering the metal concentration, moving the solubility limit into more basic ranges. In order to still be able to follow complex formation by pH measurement, the ligand concentration would have to be lowered accordingly.

Metal binding directly competes with protonation, in low concentration scenarios however the available free protons then outnumber the metal ions, shifting the metal binding event into higher pH ranges. There they would meet again with the solubility limit. Only very low concentrations completely avoid precipitation at any pH, but also moving out of the range of detection with the available instrumentation. This would be the case for concentrations below 10^{-8} M as estimated from the species distribution graph (Figure 5.3), but even very sensitive luminescence measurements requires a minimal concentration of 10^{-6} M for a chromophore with the absorption of 12N4Py4 with the instrumentation at hand.

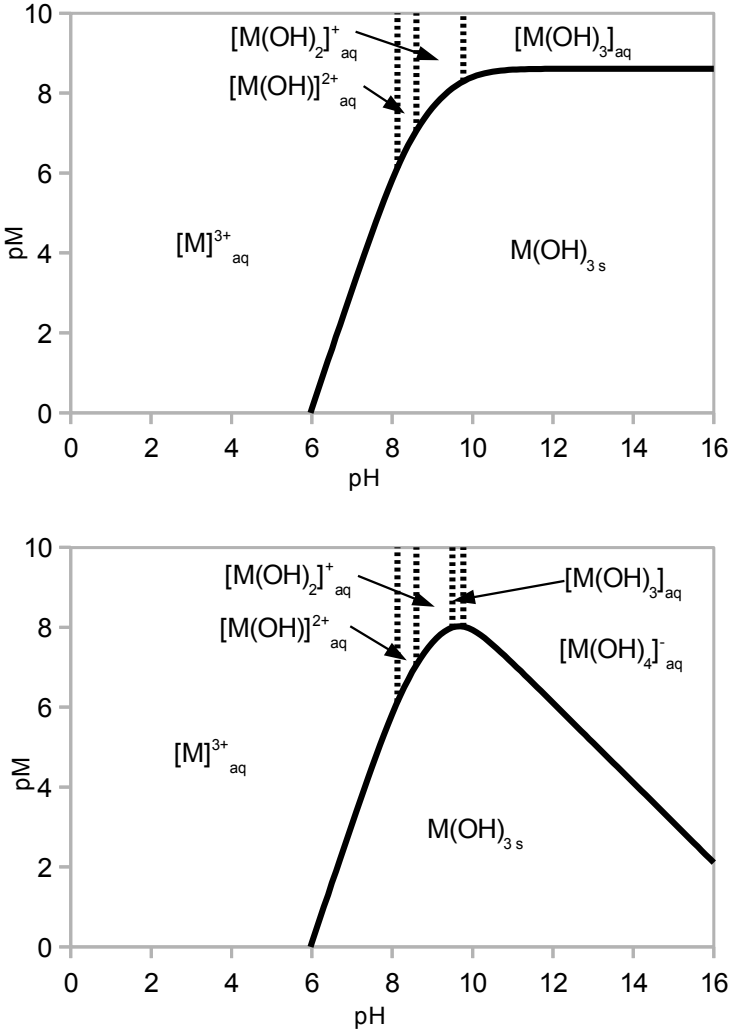

Figure 5.3: Species distribution for neodymium in dependence of pH and metal concentration (pM) with three (top) and four hydroxylation constants (bottom).[7]

Increasing the metal concentration moves the precipitation event into the acidic region, still effectively overshadowing the interaction of 12N4Py4 with the metal. This was tested with a series of titration using a tenfold excess of metal in comparison to the ligand. Precipitate occurred in close to all samples and the determined binding constants

were several orders of magnitude larger (Table 5.6) than those presented in section 5.3.

Table 5.6: Estimation of Kc for samples at tenfold metal excess (22°C, 1 M KCl)

metal	Ce(III)	Pr(III)	Nd(III)	Yb(III)
$\log K_c$	14.36	12.06	11.73	11.16

Precipitation is generally a sign of rapid solid formation, whereas slow processes promote crystal growth. Consideration of the kinetics of all involved processes offers more insight into the equilibrium near the solubility limit.

Protonation and deprotonation of 12N4Py4 was established to be slow in comparison compared to the NMR time scale, as an acid-base equilibria it can however be assumed to equilibrate within seconds. The metal hydroxide formation also is an acid-base reaction and assumed to be fast.

Complexation of the lanthanides by a polydentate ligand is slower however, as it consists of several individual binding events, one for each binding site, and the ligand has to replace water molecules around the metal ion. In the absence of precipitate, the complexation would be the rate determining step.

When the solubility limit of the metal hydroxide is reached, the precipitate acts as a kinetic trap. The remaining free metal may be complexed, allowing small amounts of the precipitate to redissolve. Due to the slow complexation of metal by 12N4Py4 the dissolution of precipitate and the subsequent formation of a thermodynamic equilibrium is very slow. This was also observed in an experiment where the quantity of precipitate in dependence of metal and ligand concentrations was estimated. Precipitate formed in most samples immediately upon the addition of base as a gel like white substance and increased in volume over the course of 8 weeks. After 8

months the precipitate condensed into a glass like substance, while in a few high pH samples large colloidal particles were observed. To reach an effective thermodynamic equilibrium, samples near the solubility limit of the metal hydroxide might therefore require significantly more time than the 7 days chosen for the binding constant titrations. It is absolutely essential to exclude these samples from the determination of K_c.

Calcium and sodium do not form insoluble hydroxides in the investigated pH range, however it was observed that 12N4Py4-Ca is not particularly soluble in water and crystallises from titration solutions as the chloride salt. Accordingly more crystals were formed in series at increased ionic strength.

The process of crystallisation is much slower than precipitation, and it can be assumed that the system did completely equilibrate. The relative insolubility of Ca-12N4Py4 is also an indicator that it might be well extractable into an organic solvent, a promising property with the extraction application in mind.

5.7 Prediction of behaviour in solution

Once binding constants have been measured, they can be used to simulate systems with different ligand and metal concentrations, which could be the case for alternative measurement techniques like UV- and luminescence measurements.

Simulations should line up with the experimental data, so significant deviations allow to single out measurements where the presented estimation and fitting procedures fail.

Solubility constants still cannot be worked into equilibrium equations, but it can be

predicted at which point the solubility limit would be reached and where it would affect measurement. They are represented in the simulations as a vertical dashed line, their position calculated from the pH value where the concentration of non-complexed metal and the concentration [OH] combined reach the solubility limit (equation 5.17, using values from the literature[9]). In the following, several scenarios are depicted to get a better understanding of what the determined binding constant mean for different systems.

5.7.1 Conditions as in the experimental titrations, $logK_c$ = 6-8

To start with, the pK_a of 12N4Py4 at 22°C in 1.0M KCl and the hydroxide constants for Nd(III)[9] were chosen as a representative for lanthanide binding. The titrations conducted for the determination of binding constants used L_{tot} and M_{tot} of 0.005 M, which was also used as initial amounts in the first simulation. For the binding constant, $logK_c$ of 6 and 8 were compared (Figure 5.4), a range where most lanthanide binding constant can be found. In both cases precipitation occurs during

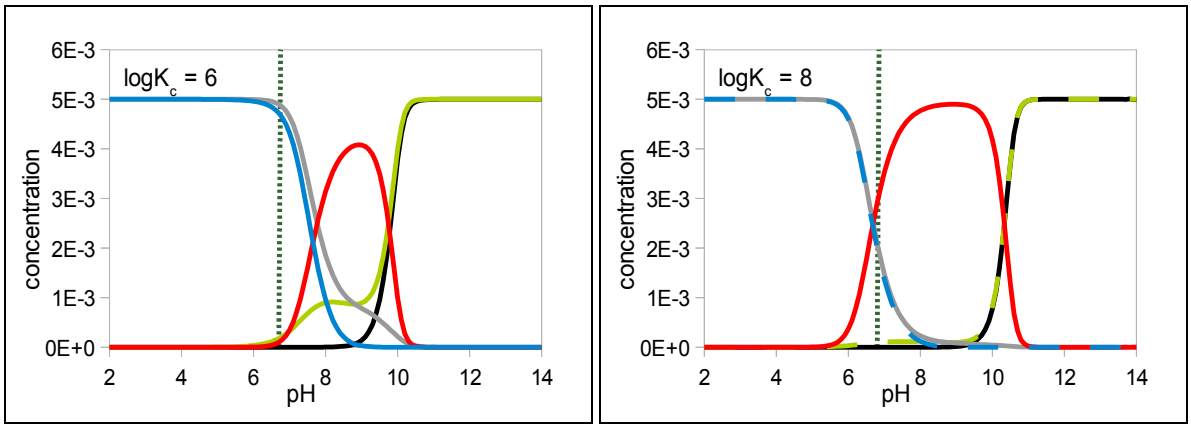

Figure 5.4: Simulation of species. pK_a 12N4Py4 at 22°C, 1M KCl, M_{tot} = L_{tot} = 0.005 M and $logK_c$ = 6 (left) and 8 (right). [L] black, [LM] red, [M] blue, [LH_x] grey, [$M(OH)_x$] green, solubility limit dashed.

the complexation event, but would leave a small window where the binding constant could be determined. It could also be claimed that at the very onset of precipitation

the amounts are still small enough to not significantly disturb the equilibrium measurement. From the simulation it is suggested that a $\log K_c$ of 6 is just around the lowest that could still be measured experimentally. All binding constants that were determined to be below $\log K_c = 7$ were indeed affected by precipitation (see Table 5.1).

5.7.2 $\log K_c$ significantly smaller (4) or larger (10)

If the binding constant was significantly lower ($\log K_c = 4$, Figure 5.5 left), no binding could be observed before the onset of precipitation. If binding constant where actually as high as determined for Ce(III) ($\log K_c = 10$, Figure 5.5 right), the measurement could follow complexation to completion before any solid would precipitate. It is therefore clear that such values have to be rejected. Very likely cerium binding is of similar strength to the other lanthanides, but because its hydroxides have the lowest solubility limit ($\log K_s = 18.5$[9]) of the investigated lanthanides no data points appropriate for binding constant determination could be measured.

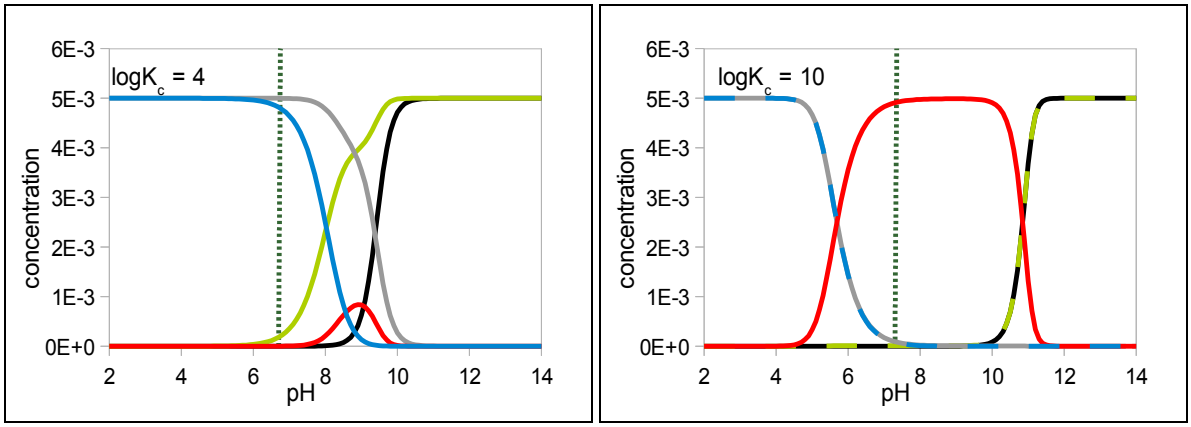

Figure 5.5: Simulation of species. pK_a 12N4Py4 at 22°C, 1M KCl, $M_{tot} = L_{tot} = 0.005$ and $\log K_c = 4$ (left) and 10 (right). [L] black, [LM] red, [M] blue, [LH_x] grey, [$M(OH)_x$] green, solubility limit dashed.

5.7.3 Excess of ligand

If the ligand concentration is increased (Figure 5.6), metal complexation is predicted to occur already at lower pH values. This would have been beneficial for the experimental work, however the influence of complexation on the total amount of bound protons $[H_b]$ would have been lowered and made the measurement less accurate.

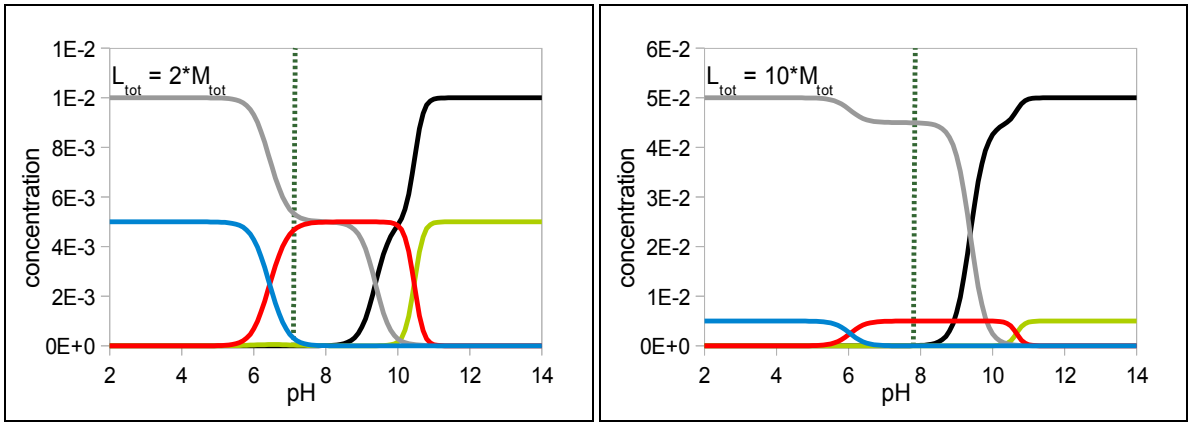

*Figure 5.6: Simulation of species. pK_a 12N4Py4 at 22°C, 1M KCl, $logK_c$ = 8, M_{tot} = 0.005, L_{tot} = 2*M_{tot} (left) and 10*M_{tot} (right). [L] black, [LM] red, [M] blue, [LH_x] grey, [$M(OH)_x$] green, solubility limit dashed.*

5.7.4 Excess of metal

Similarly the complexation event moves into an acidic pH range when the metal

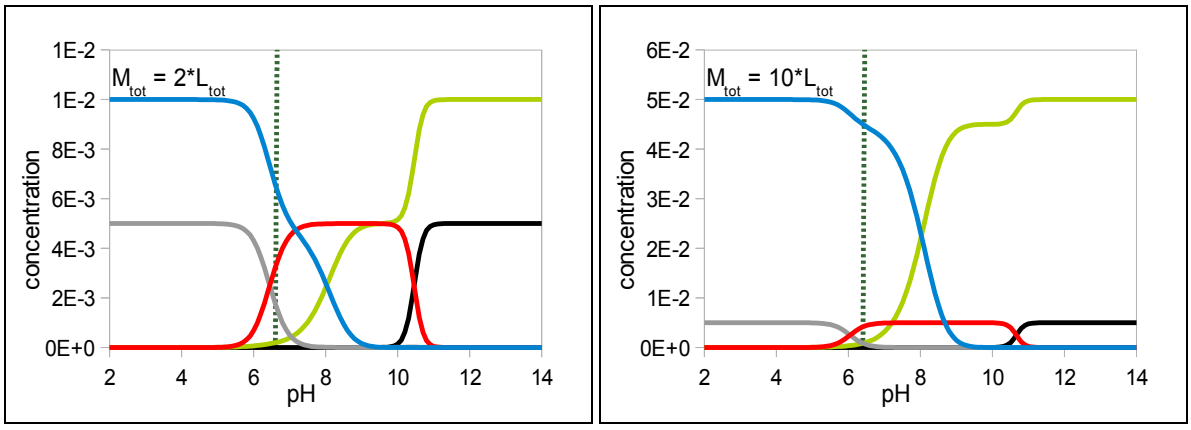

*Figure 5.7: Simulation of species. pK_a 12N4Py4 at 22°C, 1M KCl, $logK_c$ = 8, L_{tot} = 0.005 M, M_{tot} =2*L_{tot} (left) and 10*L_{tot} (right). [L] black, [LM] red, [M] blue, [LH_x] grey, [$M(OH)_x$] green, solubility limit dashed.*

concentration is increased, but so does the onset of precipitation (Figure 5.7). At higher metal concentration the volume of precipitate would also be increased, thereby slowing down the equilibration process.

5.7.5 Measurement at higher concentrations

If both metal and ligand concentrations are increased simultaneously, only slightly more of the complexation event is observable without the interference of precipitate. It is however possible that at increasingly high concentrations solubility limits of species other than metal hydroxides might be reached.

In nuclear reprocessing it is not expected that such high concentrations of lanthanides or actinides are reached due to the low content of them in spent nuclear fuel (see chapter 1).

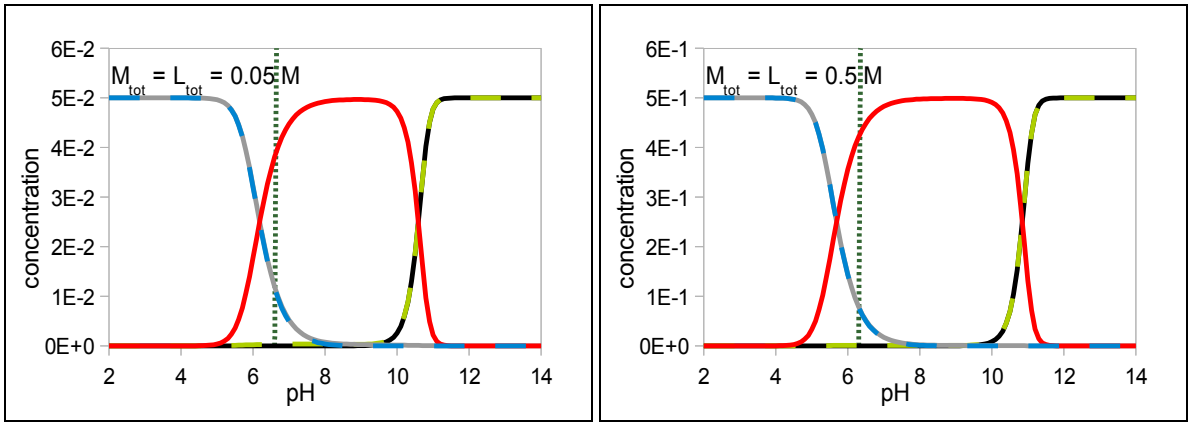

Figure 5.8: Simulation of species. pK_a 12N4Py4 at 22°C, 1M KCl, $logK_c$ = 8, $M_{tot} = L_{tot}$ =0.05 M (left) and 0.5 M (right). [L] black, [LM] red, [M] blue, $[LH_x]$ grey, $[M(OH)_x]$ green, solubility limit violet.

5.7.6 Measurement at lower concentrations

If the concentrations are simultaneously lowered, the opposite effect is observed. Less of the binding event is unaffected by precipitation. Additionally the low concentrations do not allow the metal to reach 100% complexation, as proton and hydroxide concentrations are high enough to effectively compete for ligand and metal at any pH.

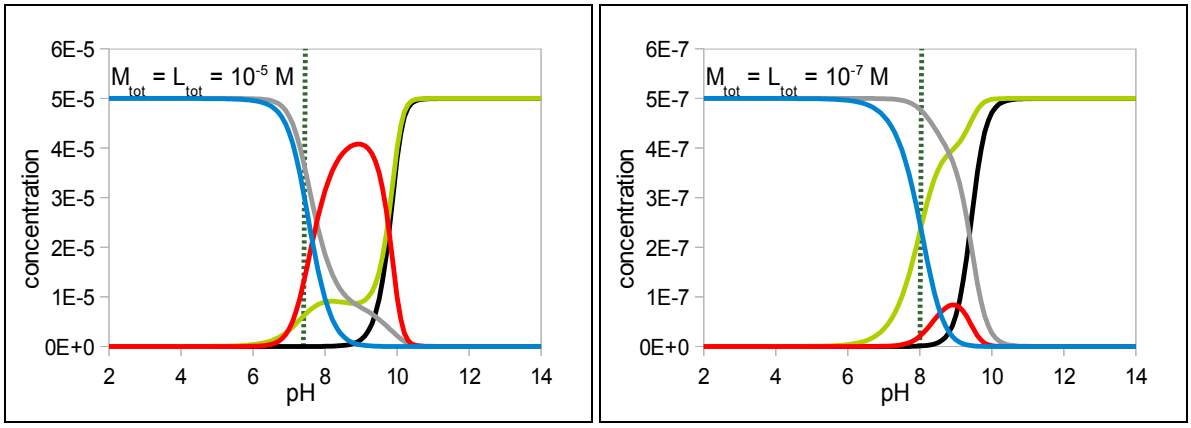

Figure 5.9: Simulation of species. pK_a 12N4Py4 at 22°C, 1M KCl, $logK_c$ = 8, $M_{tot} = L_{tot} = 5*10^{-5}$ M (left) and $5*10^{-7}$ M (right). [L] black, [LM] red, [M] blue, [LH_x] grey, [$M(OH)_x$] green, solubility limit violet.

Precipitation does occur at low metal concentrations, it can however be expected to be little in terms of volume and therefore harder to spot. Luminescence measurements, for Ln(III)-12N4Py4 complexes conducted at 10^{-5} M, are therefore not an appropriate tool for the determination of binding constants.

No precipitation would be expected for concentrations of metal below 10^{-8} M, unfortunately however data truncation by OpenOffice Calc 4.1.1 does not allow the calculation of such systems. From extrapolation of Figure 5.9 it is likely that virtually no Ln(III)-12N4Py4 complex would be formed at this concentration either.

The simulated graphs demonstrate why experimental determination of these binding constants is not straightforward. Most adjustments of concentrations lead to a

decrease in the size of the window where complexation can be followed. They are themselves a convenient tool to check measured constants.

5.8 Comparison of binding constant determination methods

The binding constants of 12N4Py4 can be determined by estimation based on the known dissociation constants of the protonated species and the simple binding equation for K_c. It is also possible to fit K_c to the experimental data using equation 5.14. Dissociation constants can be fixed or be allowed to change throughout the fitting procedure to get the best result possible. Hydroxide formation constants can be integrated to a certain degree into the estimation procedure, however with the present state of understanding of the solid structure of the precipitate it is not possible to produce a technique that includes all possible species in the system.

For the 12N4Py4 system all the determined binding constant are in reasonable agreement with each other. When pK_a values are known, estimating methods with or without the consideration of hydroxide formation are a useful tool. Fitting procedures, especially when a fitting equation has to be developed beforehand, show no significant advantages. They may however be a useful tool for systems where the pK_a values are unknown.

To obtain results of higher accuracy, an alternative measurement method that allows ligand concentrations to be in excess of the metal concentration would be needed. As seen from the simulated species distributions the exact value of the binding constant only has a minute influence on the overall distribution of species. For prediction of

extraction efficiency the results obtained are of sufficient accuracy.

For Calcium and Sodium, the influence of the hydroxides is much weaker and their inclusion into the determination of the binding constant is not effective or necessary. The binding constants can however be determined rather precisely due to the absence of precipitation.

With the level of accuracy of the determined binding constant it is unreasonable to calculate any thermodynamic constants like enthalpy or entropy or discuss the influence of ionic strength or temperature in depth. Generally it can be remarked that binding constants at 30°C were found to be higher than at 22°C or 38°C, suggesting that the temperature of maximum binding strength could be maintained in industrial application.

From simulations it can be seen that on increase or decrease of binding strength by less than one order of magnitude would have a small influence on the pH where binding occurs. Determination of binding constants with a significantly increased accuracy would be interesting from a basic and general research point of view, with respect to applications in nuclear reprocessing however it is not expected to give more information about these kinds of systems, unless of course they could include and quantify precipitation. Identification of other species so far not considered, such as metal complexes binding a hydroxide anion, might also be necessary for the development of such a procedure.

5.9 Conclusion

In this chapter it was shown that metal binding constants can be obtained from pH titration series and determined using different techniques. The most straight forward technique is the estimation based on species calculations using previously determined pK_a values, with or without inclusion of hydroxide species. It is also possible to run fitting procedures with the developed equations, either with or without simultaneously fitting pK_a values. For lanthanide complexes the occurrence of precipitate and experimental limitation leading to a small data set cause a simple estimation to be the best technique, given that the necessary care is given to exclude unfit data points.

References

[1] S. L. Wu, W. DeW. Horrocks, *J. Chem. Soc. Dalton Trans.* **1997**, 1497–1502.
[2] K. Hirose, *J. Incl. Phenom. Macrocycl. Chem.* **2001**, *39*, 193–209.
[3] R. M. Smith, A. E. Martell, *Critical Stability Constants: Volume 2: Amines*, Springer US, Boston, MA, **1975**.
[4] M. Miguirditchian, D. Guillaneux, D. Guillaumont, P. Moisy, C. Madic, M. P. Jensen, K. L. Nash, *Inorg. Chem.* **2005**, *44*, 1404–1412.
[5] D. W. Smith, *J Chem Educ* **1977**, *54*, 540.
[6] R. M. Smith, A. E. Martell, R. M. Smith, *Critical Stability Constants Volume 4: Inorganic Complexes*, Plenum Press, New York, **1976**.
[7] J. Kragten, *Atlas of Metal-Ligand Equilibria in Aqueous Solution*, E. Horwood; Halsted Press, Chichester, Eng.: New York, **1978**.
[8] L. S. Natrajan, N. M. Khoabane, B. L. Dadds, C. A. Muryn, R. G. Pritchard, S. L. Heath, A. M. Kenwright, I. Kuprov, S. Faulkner, *Inorg. Chem.* **2010**, *49*, 7700–7709.
[9] P. L. Brown, C. Ekberg, *Hydrolysis of Metal Ions*, Wiley-VCH Verlag GmbH & Co. KGaA, Weinheim, **2016**.

Chapter 6: 9N3Py3 and metal binding

6.1 Introduction

Following the success of complex synthesis, pK_a measurement and metal binding constant determination for 12N4Py4, attention was now directed at the second model ligand, 9N3Py3. In this chapter, its potential for binding metal cations of interest in this thesis is discussed. For the determination of equilibrium constants an unexpected property of the ligand was observed that lead to a readjusted procedure for the titration and fitting of the constants.

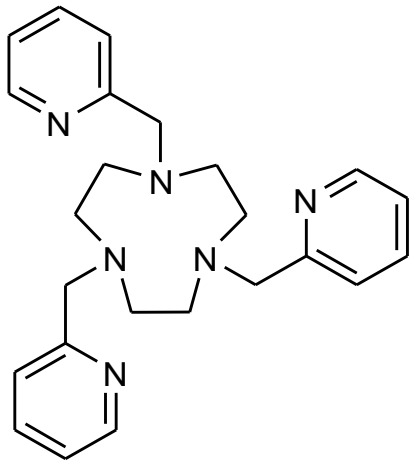

Figure 6.1: 1,4,7-Tripicolyl-1,4,7-triazacyclononane (9N3Py3)

6.2 Synthetic approach to 9N3Py3 metal complexes

As the hexadentate ligand 9N3Py3 offers a significantly smaller binding pocket than the previously discussed 12N4Py4, its potential to bind large metal cations is strongly affected. Experiments soon showed no evidence for complexation of the four lanthanides Ce(III), Pr(III), Nd(III) and Yb(III). Beside the size of the binding pocket, the reduced number of donor atoms may be a reason for the lack of complexation in solution. This seems confirmed by the successful synthesis of Ca(II)-9N3Py3, as calcium is about the same size (ionic radius 1 Å[1]) as the larger lanthanide cations (Ce(III) 1.01 Å , Pr(III) 0.99 Å, Nd(III) 0.983 Å , Yb(III) 0.868 Å[1]) in a six coordinate environment.

Ca(II)-9N3Py3 was synthesised by a method analogous to that used for to the 12N4Py4 complexes at 40°C in methanolic solution from the free ligand and calcium triflate (Scheme 6.1). After concentration of the reaction mixture, layering with diethyl ether directly produced the product as a crystalline powder.

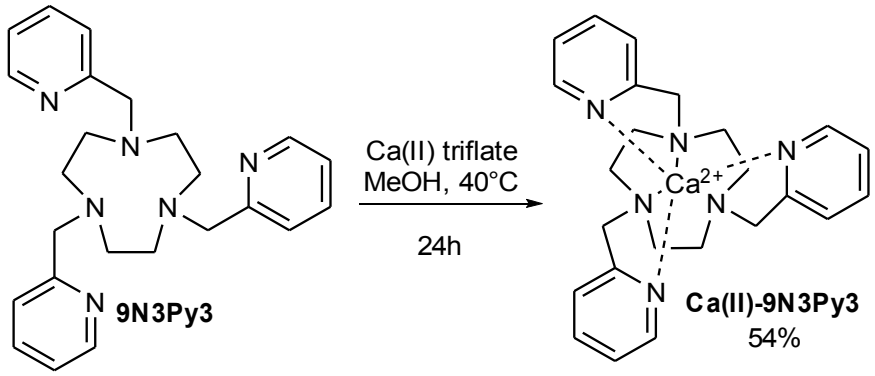

Scheme 6.1: Synthesis of Ca(II)-9N3Py3

Neither sodium nor potassium where found to be complexed by 9N3Py3, there is however evidence in the literature for some complexation in solution.[2]

6.3 Crystal structures

While cyclen based calcium complexes are well represented in literature[3–6], TACN based calcium complexes are rare. Of the 8 publications[7–15] found that describe such systems, none isolated the calcium complex but only studied them in solution. Accordingly no crystal structures have been previously published.

The structure obtained for the triflate salt of Ca-9N3Py3 is shown in Figure 6.3 (measured, solved and refined by Dr. L. Pfeifer and Dr. A. Thompson).

Whereas for all 12N4Py4 complexes two helical symmetry elements were observed in the ligand conformation, the rotation of the arms in 9N3Py3 is no longer symmetrical. Due to the low coordination and the restricted size of the ligand it cannot fully encase the metal. Two triflate counterions coordinate to fill the

coordination sphere of calcium and balance charge, one of them sitting on what could be considered the molecular axis, while the other coordinates alongside the pyridyl moieties. This however forces one of the pyridyl arms to rotate against the other two, breaking the symmetry.

The torsion angles of the other two pyridyl arms (37°, 43°) and the macrocyclic ring (-45°, -51°, -56°), which in terms of relative arrangement corresponds to the square anti-prism conformation of 12N4Py4. This was unexpected, as it was observed that 12N4Py4 adopts the TSAP geometry for larger metal ions and SAP for smaller ions. If the square anti-prismatic geometry for 8 coordinated metals was translated to a 6 coordinated system, a octahedral arrangement of the donor sites would be formed. 9N3Py3 however is too small to adopt this geometry around the large calcium atom. The presence of the coordinated triflate ions in Ca(II)-9N3Py3 increases the coordination number for calcium from 6 to 8. The geometry observed appears to be a compromise between the conformation requirements of the ligandand the attempt to achieve an overall symmetry distributing the 8 donor sites equally around the metal centre.

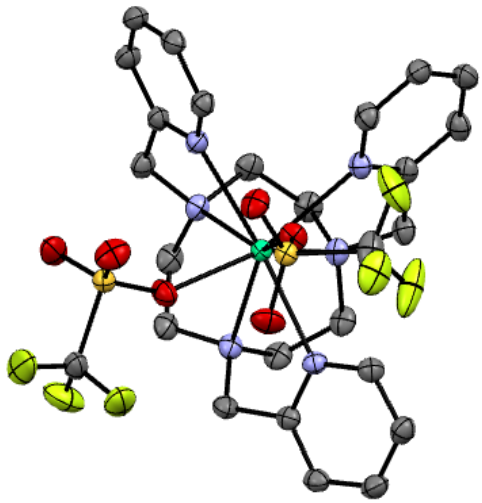

Figure 6.2: Crystal structure of Ca(II)-9N3Py3 complex as hydrated chloride salt (WTS04). Hydrogen atoms not displayed, probability level at 50%.

The open form of 9N3Py3 suggests that it might not coordinate as strongly to the metal in solution as it would for a smaller metal with a more ideal size for the binding cavity.

Distances between the metal center and the aza-nitrogen donors are longer (average 2.643 Å) in comparisons with the structure obtained for Ca(II)-12N4Py4 (2.591 Å), as is the case for the pyridyl nitrogens (2.592 Å for Ca(II)-9N3Py3, 2.575 Å for Ca(II)-12N4Py4).

6.4 Spectral properties

Ca(II)-9N3Py3 was compared to 9N3Py3 and metal complexes of 12N4Py4 by means of NMR spectroscopy and luminescence measurements.

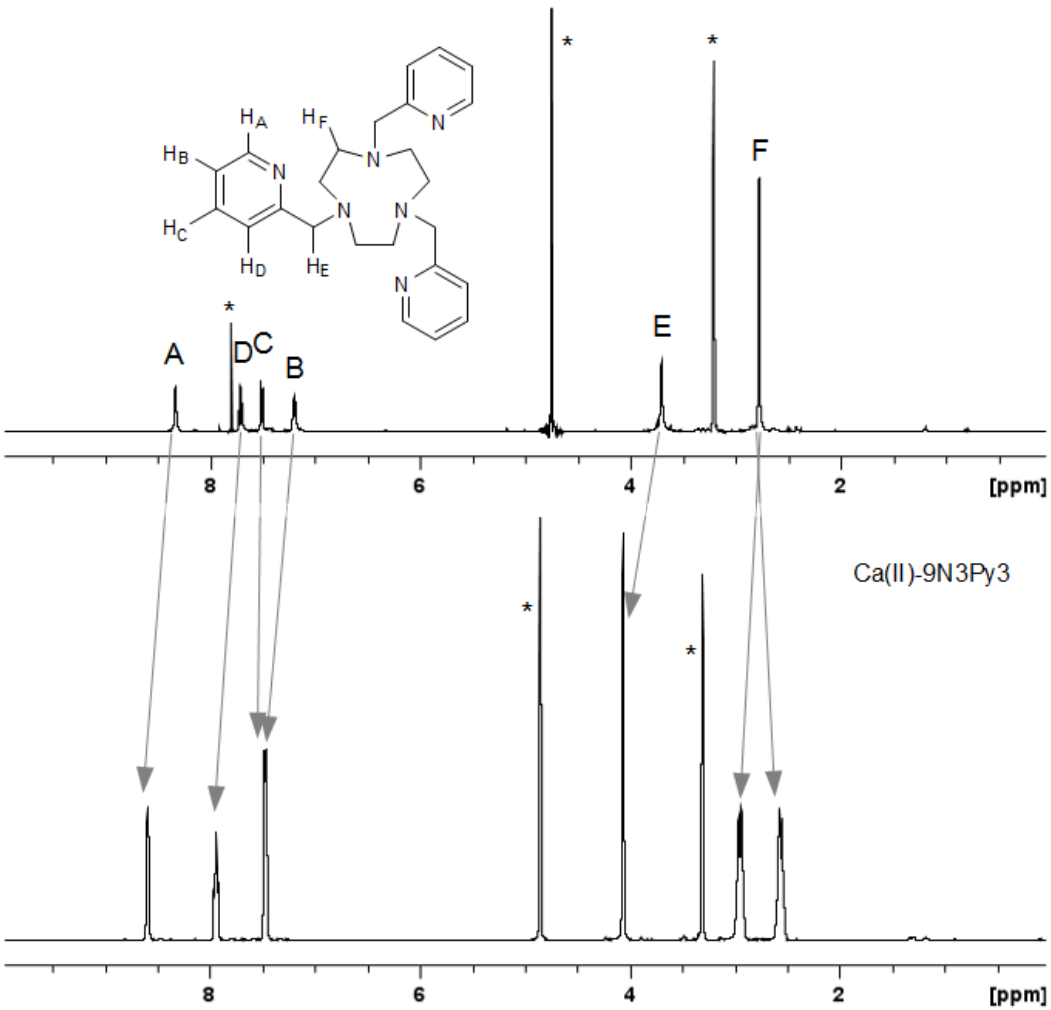

Figure 6.3: ^{1}H-NMR of Ca(II)-9N3Py3 in comparison to the free ligand and Ca(II)-12N4Py4, all measured in MeOD. (*) residual solvent peak

Figure 6.3 shows the proton NMR spectra of the free ligand and the calcium complex in comparison. In the aromatic region the protons were shifted due to the polarisation by the divalent metal, the protons experienced a slightly more symmetric environment along the symmetry axis of pyridine, causing protons B and C to overlap. It seems likely that the structure of this system reflects facile and rapid exchange of solvent and coordinated anions, giving rise to a time averaged structure in the NMR spectra.

It can be expected that in solution at least one of the triflate ions dissociates and is replaced by a solvent molecule. This allows the pyridyl arms to rotate more freely. In the ^{1}H-NMR spectrum (Figures 6.3 and 6.4) accordingly the signals for the pyridyl arm CH_2 were averaged to one shift (E) and no coupling between them is observed any more. Splitting of the signal is still present for the macrocyclic CH_2 groups (F) as

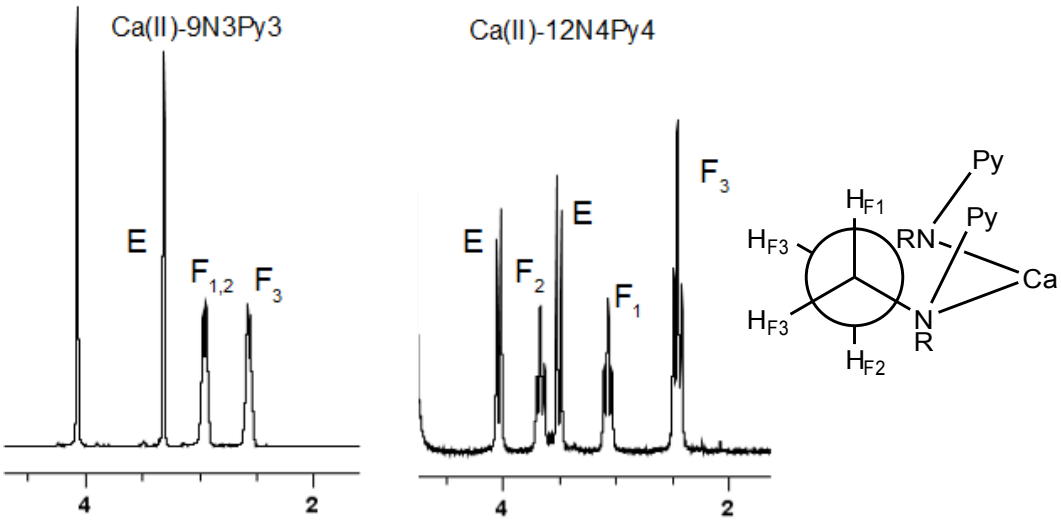

Figure 6.4: Comparison of CH_2 splitting pattern in Ca(II)-9N3Py3 and Ca(II)-12N4Py4

was previously observed in Ca(II)-12N4Py4 suggesting that ring inversion still is slow to occur. The two peaks correspond to the axial and the equatorial protons. Through the arm rotation however the influence of the ring current averages and the axial protons in the macrocycle can no longer be distinguished, in contrast to the three

signals observed for Ca(II)-12N4Py4, where the axial proton directed towards the pyridyl rings additionally experiences a high-field shift.

In the luminescence spectra a pattern comparable to Ca-12N4Py4 was observed. The absorption at 260 nm overlapped neatly with the free ligand and was only minutely more intense (8985 M^{-1} cm^{-1} compared to 8819 M^{-1} cm^{-1} for 9N3Py3). Emission and absorption spectra reflect what would have been also expected for 9N3Py3 (chapter 2), the maximum of the emission being at 455 nm, the excitation perfectly overlapping with the absorption. The intensity of the emission was significantly lower than for Ca(II)-12N4Py4 (0.17:1 relative intensity), suggesting that the coordination of the nitrogen lone pairs is less strong and they can interact with excited states of the pyridyl moiety, leading to non-radiative relaxation as discussed for 12N4Py4 complexes in chapter 4.

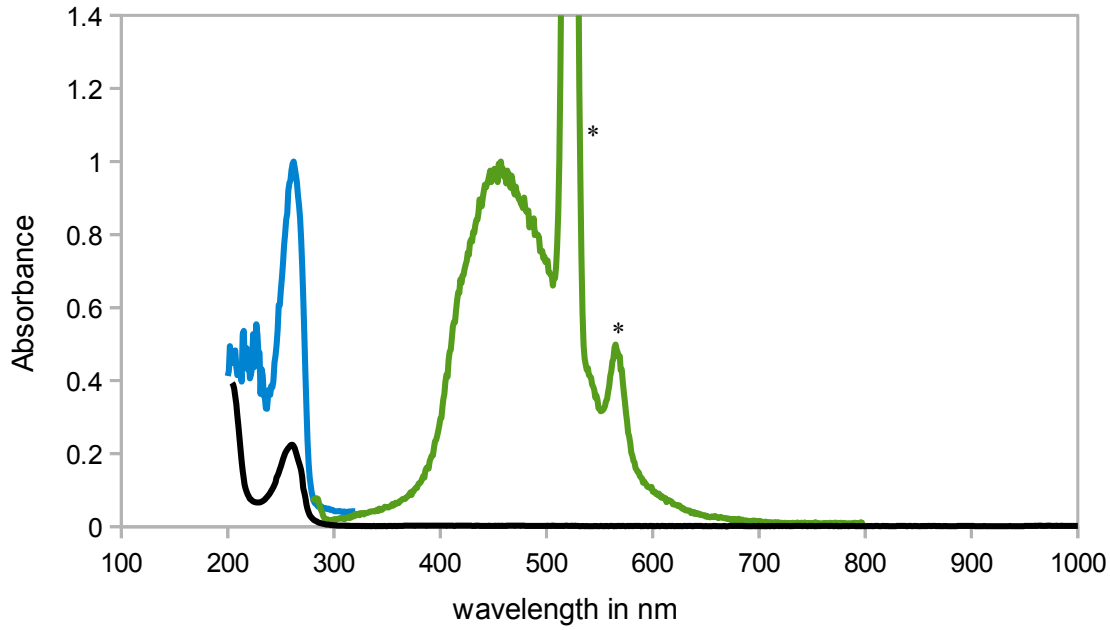

Figure 6.5: Luminescence of Ca(II)-9N3Py3: absorption (black), emission (green, λ_{ex} = 260 nm, normalised) and excitation (blue, λ_{em} = 455 nm, normalised). 2λ artefact (*)

6.5 pK_a determination for 9N3Py3

With the successful measurement of pK_a values for 12N4Py4 it was planned to conduct a similar, but smaller study on the pK_a values of 9N3Py3. It was already found that 9N3Py3 does decompose over time, so freshly columned product was used. Initial titrations gave Bjerrum plots that showed features associated with concentration errors (Figure 6.6). In particular, the plateau from pH 6 to 11 would be expected to align with nH_b = 1. A correction was added to estimate the purity of 9N3Py3 employed, data suggested it was as low as 75% pure.

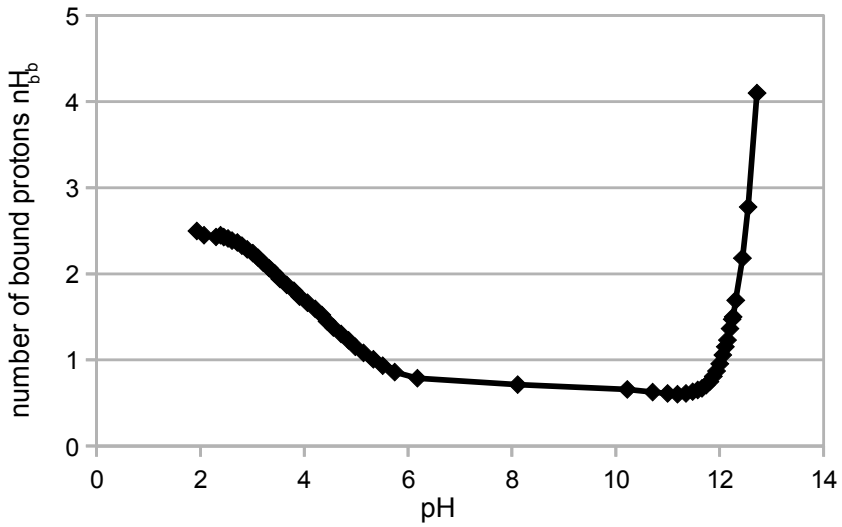

Figure 6.6: Number of protons bound by 9N3Py3 (nH_b) determined in early titration experiment

A second titration series was prepared with special focus on the purity and drying of the ligand. When dissolving 9N3Py3 in acidic solution, it became obvious what had caused the "impurity" of the ligand in the first titration. A white precipitate accumulated that did not redissolve in neutral water. A chloroform extract was measured by NMR, revealing signals indicative of decomposed 9N3Py3. It is highly likely that the ligand is not as stable in acidic solution as 12N4Py4. This makes the direct measurement of the pK_a values very difficult. It was abandoned in favour of the newly developed method of fitting equilibrium constants in the presence of metal ions that was used for the determination of binding constants of 12N4Py4 in chapter 5.

6.6 Fitting of Ca-9N3Py3

While the free ligand decomposes over time, its Ca(II) complex is stable and can be obtained in high purity through recrystallisation. This allowed a pH titration to be conducted of the metal complex in order to determine both the pK_a values and the metal binding constant simultaniously. A fitting function suitable for this purpose was developed in chapter 5 (also see appendix). It uses the assumption that negative charges and positive charges must balance themselves in solution. Differences between known concentrations of cations and anions therefore have to correspond to charge carried by protonated ligand species, expressed as $[H_b]$.

From the early pK_a titration experiment it was expected to observe 3 proton dissociation steps on any of the 6 basic nitrogen donors. The fitting function was adjusted accordingly. By using the preformed metal complex as a component, the total concentrations of metal (M_{tot}) and ligand (L_{tot}) are equal, accordingly Δ_{tot} becomes 0 and several terms disappear from the equation to give it a simpler form:

$$H_b = \frac{-B + \sqrt{B^2 + 4 B K_C M_{tot}}}{\frac{2 B K_C}{A}}$$

with

$$A = \frac{[H]}{K_1} + 2\frac{[H]^2}{K_1 K_2} + 3\frac{[H]^3}{K_1 K_2 K_3} \qquad 6.1$$

$$B = 1 + \frac{[H]}{K_1} + \frac{[H]^2}{K_1 K_2} + \frac{[H]^3}{K_1 K_2 K_3}$$

A program capable of non-linear fitting (OriginPro® 9.1) was used to determine the acid dissociation constants K_1, K_2 and K_3 as well as the metal binding constant K_c.

Figure 6.7 shows the Bjerrum plot calculated for the first titration performed with

Ca(II)-9N3Py3. The curve indicates two dissociation events to occur between pH 3 and 6 which overlap and a third in the basic region of about pH 10.

Upon approaching nH_b = 0.5 where pK_1 would be expected, the curve is strongly disturbed even though no visible precipitate was observed in the measurement. It is most likely that this is an indication of precipitation of the free base and not caused by hydroxide formation or low solubility of the calcium complex. 9N3Py3 as an oil is less likely to be detected by eye if small amounts of it separate from solution. This further implies that calcium does not bind very strongly in aqueous solution.

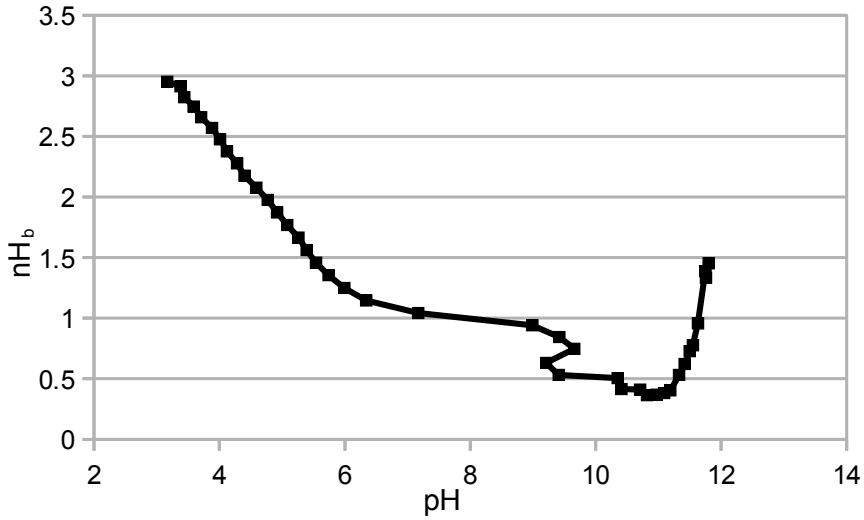

Figure 6.7: Bjerrum plot of 9N3Py3 titration, number of average bound protons per ligand molecule (nH_b) against pH

Even though it appears that complexation was not strong enough to inhibit separation of free base, it has to be assumed that small amounts of it still had formed. Therefore K_c has to be included into fitting procedures. Using equation 6.1, data unaffected by the separation of insoluble free base was fitted to obtain the pK_a values. Table 6.1 gives the results obtained.

Table 6.1: pK_as and calcium binding constant determined for 9N3Py3 at 22°C and 0.5 M KCl

pK_1	pK_2	pK_3	$logK_c$
9.98	5.45	4.03	-0.03

In contrast to the fitting of metal titrations of 12N4Py4, enough data points were

obtained for 9N3Py3 to allow the program to fit all constants simultaniously. A high adjusted R^2 value of 0.993 was obtained, confirming that the technique is well suited for an increased data set.

For 12N4Py4 it was established that the first two protons bind to the macrocyclic nitrogen atoms at high pH and two more coordinate to the pyridyl nitrogens in the acidic region, 9N3Py3 only showed one pK_a in the basic pH range, suggesting that the TACN ring cannot accommodate two protons that would necessarily be in close proximity and experience stronger mutual coulombic repulsion. pK_1 of 9N3Py3 is of intermediate strength between pK_1 and pK_2 of 12N4Py4. The pyridyl nitrogens however can achieve more distance between each other and so bind two protons as observed in 12N4Py4. Both pK_2 and pK_3 are higher than the corresponding pK_3 and pK_4 in 12N4Py4. By only binding one proton in the macrocycle, the pyridyl sites experience less coulombic repulsion.

The metal binding constant determined is very low. It has however also been established that the determination of binding constants from data where one of the involved species is only present in small amounts can be highly imprecise. In order to obtain a more reliable value for the metal binding, a second titration was conducted with an excess of metal and fitted with an equation previously used in chapter 5 (equation 5.14) that was adjusted to the 9N3Py3 system.

In order to maximise the probability to observe formation of the calcium complex, the total amount of metal was increased to 100 times the present ligand concentration. This has a significant impact on the ionic strength of the solution, increasing from 0.5 M to 2.9 M, which in turn influences the pK_as of 9N3Py3. The fitting was therefore performed for all equilibrium constants simultaneously. Table 6.2 gives the values

obtained using this technique.

Table 6.2: pK_as and K_c obtained for 9N3Py3 and Ca(II) at 100 fold metal excess

constant	22°C	30°C	38°C
pK_1	9.95	10.02	9.97
pK_2	5.59	5.48	5.35
pK_3	4.35	4.30	4.13
$logK_c$	2.55	3.02	3.03

The pK_a values all compare well between different temperatures and to those determined in the first titration experiment (Table 6.1). With the addition of more metal, more of the complex was able to form and the corresponding $logK_c$ values are significantly higher, although still lower than any of the metal binding constants determined for 12N4Py4. For the concentrations used, the last dissociation reaction from [LH] to [L] and the binding event of the metal severely overlap, the corresponding constants K_1 and K_c are highly dependent on each other as is reflected in the high standard error (e.g. K_1 9.95 ±1684, K_c 2.55 ±1696). Neverless, the values obtained for K_1 are in close agreement with those for the previous experiment at low M_{tot} and can therefore be accepted as an accurate representation. At high pH values where larger quantities of complex could form, some precipitation was observed. Due to its appearance (white solid) it is assumed that this precipitate consists of the intact metal complex, which would be similar to Ca(II)-12N4Py4 that also shows limited solubility.

Thermodynamic constants were calculated for the equilibrium constants, summarised in Table 6.3. It has to be remarked that due to the lower number of experiments these values are based on, they are not of the same accuracy as the values discussed for 12N4Py4 in chapter 3.

Table 6.3: Thermodynamic constants of 9N3Py3

constant	ΔH in kJ/mol	ΔS in J/molK
K_1	-1.5	-195.9
K_2	26.2	-18.3
K_3	24.9	0.6
K_c	51.9	226.3

Repetition of the experiments and measurement at different metal concentration would greatly increase the accuracy. Because 9N3Py3 has so far only shown calcium complexation at very low binding strength in combination with the results presented in chapter 5 it was decided to not pursue these investigations further. The thermodynamic constants presented are therefore only used as an indicator of the reaction mechanism.

K_1, K_2 and K_3 are dissociation constants and charged species usually are more stable in aqueous solutions than uncharged, it was expected to find positive values for the enthalpy, as was observed for 12N4Py4. ΔH for K_2 and K_3 fulfil this expectation, however ΔH for K_1 was found to be a negative value. By increasing the metal concentration to promote metal complexation the formation of free ligand [L] is suppressed and only small amounts are present throughout the titration. This makes the fitting of K_1 less reliable than that of the other equilibrium constants. Even minor deviations in one of the fitted K_1 values then causes rather large differences in the calculation of thermodynamic constants, as those are based on only three values. It is therefore highly likely that the low ΔH is a result of inaccuracies in the fitting of K_1 rather than a reflection of the physical situation in solution. Similarly the large value for ΔS would be caused the same way. ΔS for K_2 is again in agreement with the findings for 12N4Py4. The value for K_3 is just above 0. For K_4 in 12N4Py4 it had also

been observed that temperature dependency varies throughout the ionic strength series, indicating that this is also an effect of fitting inaccuracies.

The complexation reaction shows high positive values for ΔH and also a high and positive ΔS. As 9N3Py3 cannot fully encapsulate the metal ion the nitrogen donors cannot offer a stabilisation compared to the hydrated metal ion. The entropy however is influenced by the number of molecules on either side of the chemical equation. By binding the metal with the hexadentate ligand, the water molecules of the first hydration sphere of the metal are released. With an average water coordination number of 9 ($CaCl_2$ [16]) this is a significant decrease of ligands for Ca(II), even if it is assumed that two water molecules remain coordinated in place of the triflate ions found in the crystal structure.

An increase in binding strength primarily governed by entropy is highly interesting. The coordination and dissociation could be controlled by temperature in- or decrease, which is very easy to achieve in industrial application, although limited by the melting and boiling points of the solvents. It can be expected that the major contribution to the entropy change originates in the change of the number of molecules, as one polydentate ligand displaces several water molecules.

Trivalent lanthanides have been found to have large hydration numbers of 12-15 water molecules[17], while the larger and therefore less dense in charge An(III) ions have been determined to bind 9 water molecules on average.[18] While many ligand designs focus on finding a structure that binds one of the f-element series more strongly than the other and often targets the covalent nature of actinides, entropy controlled binding and release of ions with a difference in hydration number might allow a system that binds lanthanides more effectively than actinides. This would

allow exploitation of the greater solvent order imposed by charge dense lanthanide ions.

6.7 Summary

9N3Py3 was not observed to bind to lanthanide ions, which was not unexpected. It does however form complexes with Ca(II) ions, although the binding is weak in aqueous systems. A novel crystal structure was measured with the TACN motive unprecedented in solid state.

Even though the direct measurement of pK_as of 9N3Py3 represents a challenge due to low solubility and acid stability of the ligand, the fitting procedure developed for simultaneous determination of pK_as and metal binding constants proved highly effective for extended data sets and allowed the calculation of all relevant equilibrium constants of 9N3Py3 and its calcium complex.

The overall equilibrium system (Figure 6.8) observed for 9N3Py3 is significantly simpler than for 12N4Py4 due to the absence of lanthanide complexes and the hydroxide formation seen for them.

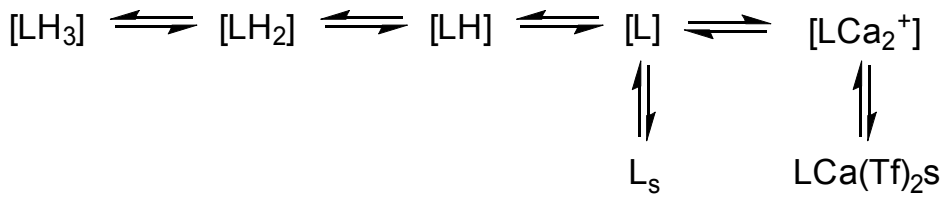

Figure 6.8: Equilibrium system for 9N3Py3

Even though 9N3Py3 is of very limited use to investigate lanthanide and possibly actinide binding, the thermodynamics of calcium binding offer a novel basis on which future ligands could be designed. Instead of exploiting the covalent character of actinide complexes, the difference in hydration numbers of lanthanides and actinides

could be used to produce a temperature controlled system for the selective binding and release of f-elements.

References

[1] R. D. Shannon, *Acta Crystallogr. Sect. A* **1976**, *32*, 751–767.
[2] H. Tsukube, K. Yamashita, T. Iwachido, M. Zenki, *J. Chem. Soc. [Perkin 1]* **1991**, 1661.
[3] H. Misaki, H. Miyake, S. Shinoda, H. Tsukube, *Inorg. Chem.* **2009**, *48*, 11921–11928.
[4] H. Ito, H. Tsukube, S. Shinoda, *Chem. Commun.* **2012**, *48*, 10954.
[5] J. Platzek, P. Blaszkiewicz, H. Gries, P. Luger, G. Michl, A. Müller-Fahrnow, B. Radüchel, D. Sülzle, *Inorg. Chem.* **1997**, *36*, 6086–6093.
[6] H. Maumela, R. D. Hancock, L. Carlton, J. H. Reibenspies, K. P. Wainwright, *J. Am. Chem. Soc.* **1995**, *117*, 6698–6707.
[7] A. Bevilacqua, R. I. Gelb, W. B. Hebard, L. J. Zompa, *Inorg. Chem.* **1987**, *26*, 2699–2706.
[8] C. J. Broan, K. J. Jankowski, R. Kataky, D. Parker, *J. Chem. Soc. Chem. Commun.* **1990**, 1738.
[9] R. Ramasamy, I. Lazar, E. Brucher, A. D. Sherry, C. R. Malloy, *FEBS Lett.* **1991**, *280*, 121–124.
[10] C. F. G. C. Geraldes, M. P. M. Marques, A. D. Sherry, *Inorganica Chim. Acta* **1998**, *273*, 288–298.
[11] J. Huskens, A. D. Sherry, *J. Am. Chem. Soc.* **1996**, *118*, 4396–4404.
[12] J. Huskens, A. D. Sherry, *J. Chem. Soc. Dalton Trans.* **1998**, 177–184.
[13] S.-S. Bao, Y.-X. Wu, N.-Z. Li, L.-M. Zheng, *Eur. J. Inorg. Chem.* **2016**, *2016*, 4476–4482.
[14] M. I. Kabachnik, T. Y. Medved', Y. M. Polikarpov, B. K. Shcherbakov, F. I. Bel'skii, E. I. Matrosov, M. P. Pasechnik, *Bull. Acad. Sci. USSR Div. Chem. Sci.* **1984**, *33*, 769–777.
[15] C. Gateau, M. Mazzanti, A. Nonat, *Novel Lanthanide Ligands and Complexes, and Use Thereof as Contrast Agents*, **2007**, WO2007083036 (A1).
[16] A. A. Zavitsas, *J. Phys. Chem. B* **2005**, *109*, 20636–20640.
[17] K. A. Gschneidner, L. Eyring, M. B. Maple, Eds. , *Handbook on the Physics and Chemistry of Rare Earths. Vol. 28*, North-Holland Publ, Amsterdam, **2000**.
[18] P. D'Angelo, F. Martelli, R. Spezia, A. Filipponi, M. A. Denecke, *Inorg. Chem.* **2013**, *52*, 10318–10324.

Chapter 7: Actinide binding

7.1 Introduction

Both 12N4Py4 and 9N3Py3 were chosen for their potential to investigate the characteristics of actinide binding. 12N4Py4 was expected to bind An(III) ions, which is the main oxidation state for the minor actinides, as their size (Figure 7.1) is very similar to the previously studied trivalent lanthanides. Meanwhile the earlier actinides, especially uranium, occur more commonly in higher oxidation states such as U(IV) and U(VI) in dependence of pH. Their smaller size might allow complex formation with 9N3Py3.

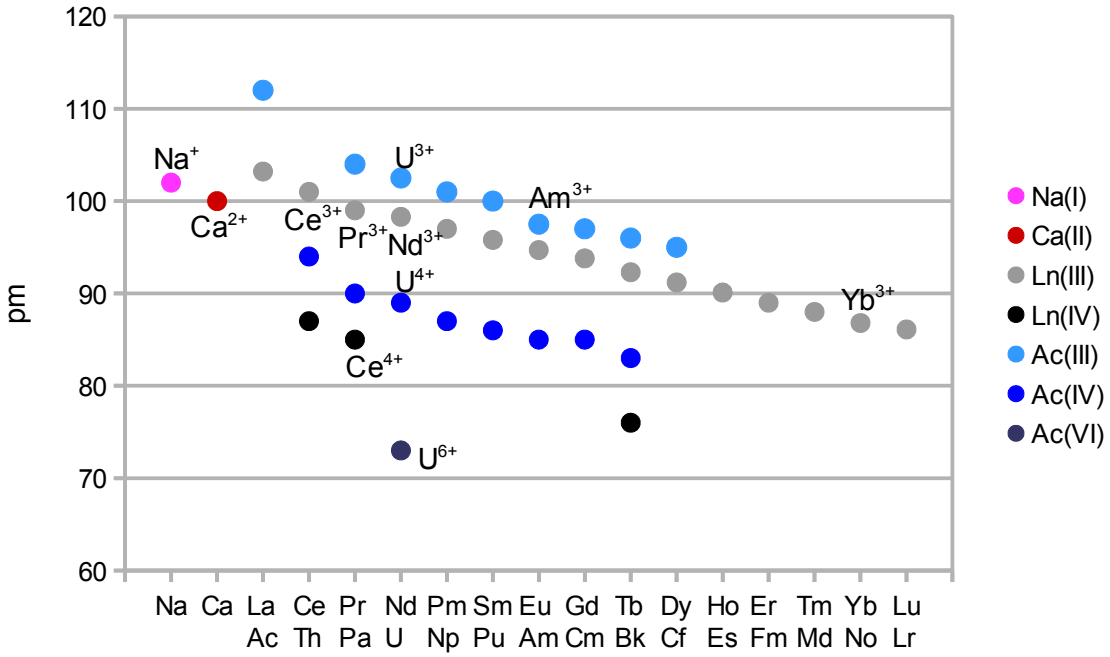

Figure 7.1: Ionic radii of cations in hexacoordinated environments.[2]

All actinide elements are radioactive and handling most of them is highly restricted. One of the few exceptions is uranium, which is accessible in a natural or a depleted state. Its main isotope ^{238}U is a long lived (half life 4.47 billion years) alpha emitter

with a low energy gamma component.[1] Safety considerations focus on reducing the risk of uptake of uranium compounds by inhalation or ingestion and spreading of radioactive material rather than external exposure by radiation.

Trivalent uranium, which has an ionic radius of 1.025 Å[2] (coord. no. 6) is of a size comparable to the early trivalent lanthanides (La 1.032, Ce 1.01, Nd 0.983, all coord. no. 6)[2], is highly sensitive to oxidation and not considered stable in aqueous solutions or in an oxygen rich atmosphere.[3,4] U(IV) is also readily oxidised, but is generally stable in acidic solutions and non-aqueous solvents as can be seen from Frost diagrams (Figure 7.2).[3] The most stable uranium oxidation state in aqueous solution is U(VI) which commonly exists as the uranyl ion UO_2^{2+}.[3,4] This non-spherical ion is not expected to be able to utilise all the donor atoms in ligands such as 12N4Py4 and 9N3Py3. For this project a sample of $U(IV)Cl_4$ was used to conduct uranium studies. It was expected that U(IV) would be too small to bind to 12N4Py4 but might form stable complexes with 9N3Py3.

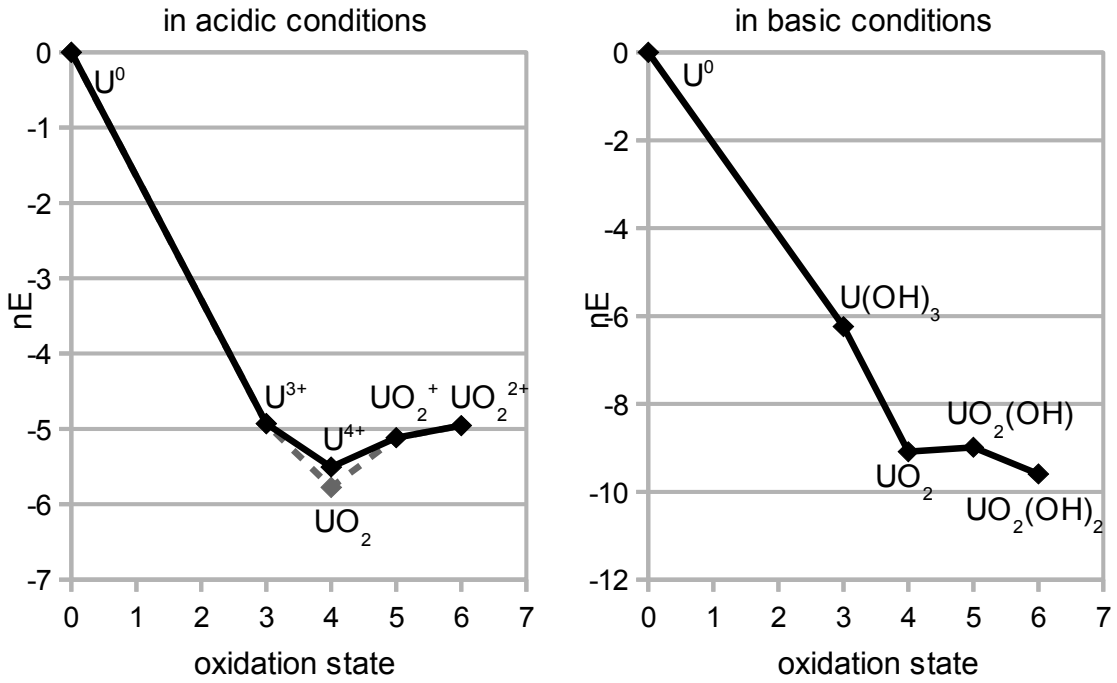

Figure 7.2: Frost diagrams for uranium, in acidic and basic conditions.[10]

While it is very useful to be able to work on an actinide element in a standard laboratory, U(IV) and U(VI) studies cannot truly reflect the behaviour of the minor actinides, which commonly appear as An(III) ions and do not show considerable redox behaviour in aqueous solutions. It was therefore essential to gain access to a facility where at least one of the minor actinides can be handled.

Studies on minor actinides were conducted by the National Nuclear Laboratory in Sellafield on Am-243 samples, one of the long lived minor actinides and an alpha emitter with gamma and beta components of low energy.[1]

7.2 U(IV)-12N4Py4

Experiments were conducted to investigate the potential of 12N4Py4 to bind the small U(IV) ion (Scheme 7.1). The methanolic solution of the ligand and UCl_4 initially was of a dark green colour, typical for the tetravalent uranium ion, but over the course of 24 h however it turned a yellow colour.

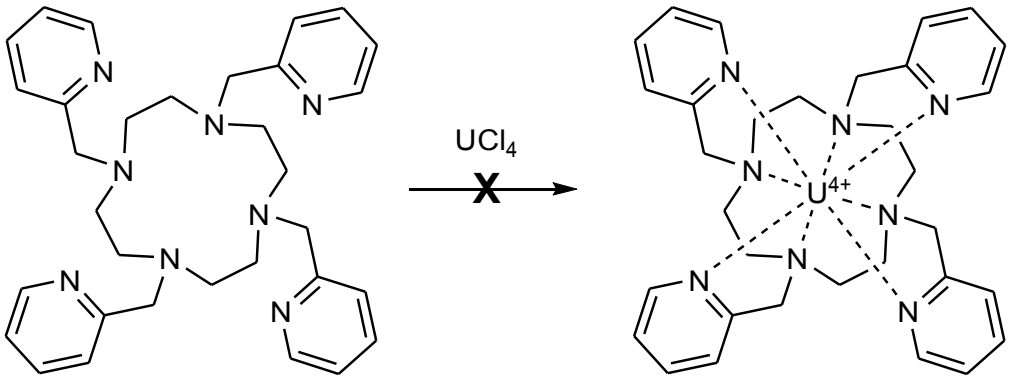

Scheme 7.1: Hypothetical complexation of U(IV) by 12N4Py4

Removal of the solvent and analysis by NMR spectroscopy showed no indication of complexation. UV(IV) complexes are paramagnetic and an increased shift range was expected for the hypothetical UV(IV)-12N4Py4 as a consequence of contact and

pseudo-contact contribution. This however was not observed. Instead the proton shifts matched those of protonated forms of 12N4Py4.

7.3 U(IV)-9N3Py3

The small size of U(IV) (Figure 7.1) suggests it might be complexed by the smaller cavity of 9N3Py3. The ligand was mixed with UCl_4 in methanolic solution and heated for 24 h (Scheme 7.2). As previously observed in the reaction with 12N4Py4, the solution turned yellow-brownish over the course of the reaction.

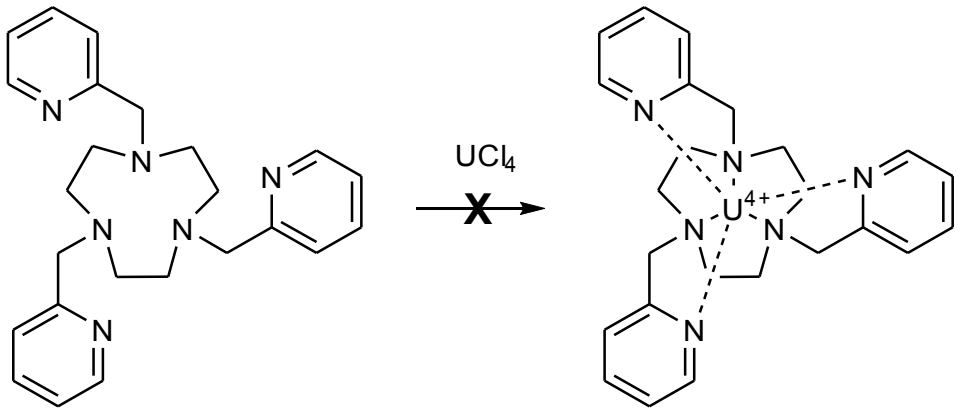

Scheme 7.2: Hypothetical complexation of U(IV) by 9N3Py3

After removal of the solvent the brownish powder was analysed by NMR spectroscopy. No signals indicative of paramagnetic compounds were observed. Instead the spectrum suggests that a considerable amount of 9N3Py3 had decomposed. In an attempt to see whether possibly a diamagnetic complex had formed, the crude product was washed with acetonitrile. Only some of the material dissolved and both parts were reanalysed by NMR spectroscopy. The spectrum of the solution showed a pattern suggesting the presence of protonated 9N3Py3.

Based on the NMR spectra in both the 12N4Py4 and the 9N3Py3 reactions combined with the observations of solubility and colour change, it is suggested that U(IV) reacts

with residual water in the solvent or atmospheric oxygen to $U(VI)O_2^{2+}$. In the redox reaction protons are released which bind to the ligands and cause the decomposition of 9N3Py3. The uranyl ion UO_2^{2+} is of linear shape and does not fit into the macrocyclic cavity, so no complex is formed.

7.4 U(IV)-CyMe$_4$-BTPhen

An additional ligand system, CyMe$_4$-BTPhen, was provided by Prof. Laurence Harwood. As with the macrocyclic ligands, CyMe$_4$-BTPhen was reacted with UCl_4 in methanol overnight, the solution turning from green to a yellowish colour.

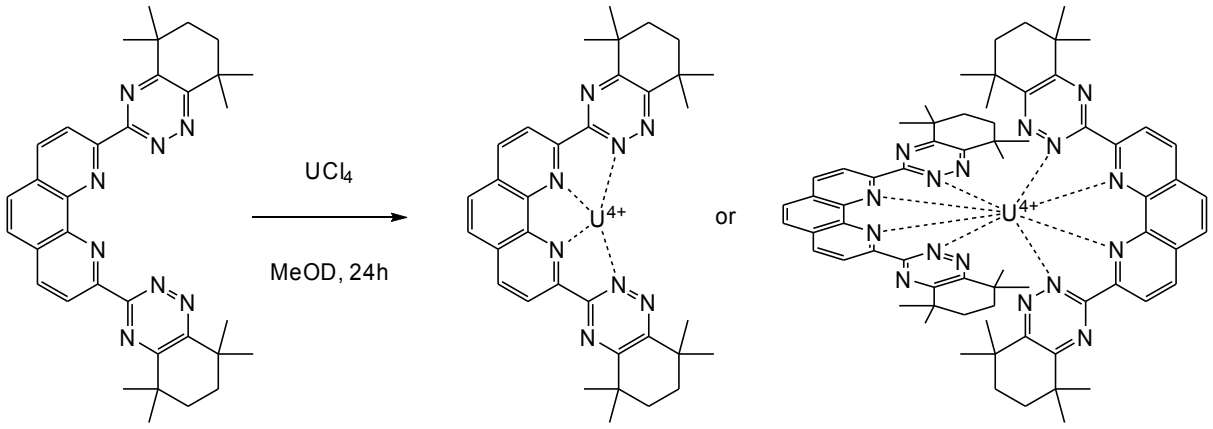

CyMe$_4$-BTPhen

Scheme 7.3: Hypothetical complexation of U(IV) by CyMe$_4$-BTPhen

The ^{1}H-NMR spectrum (Figure 7.3) taken of the crude mixture was dominated by signals corresponding to diamagnetic species, either free ligand, protonated ligand, decomposed material or diamagnetic complexes. There were however also several signals observed with chemical shifts indicative of paramagnetic species. BTPhen based ligands can form both 1:1 and 1:2 metal to ligand complexes as shown in Scheme 7.3. Protons in both complexes are symmetry related and the relatively small number of paramagnetic resonances does not distinguish between them.

Oxidation of U(IV) would likely lead to uranyl species, which could also be complexed by $CyMe_4$-BTPhen, forming a diamagnetic complex.

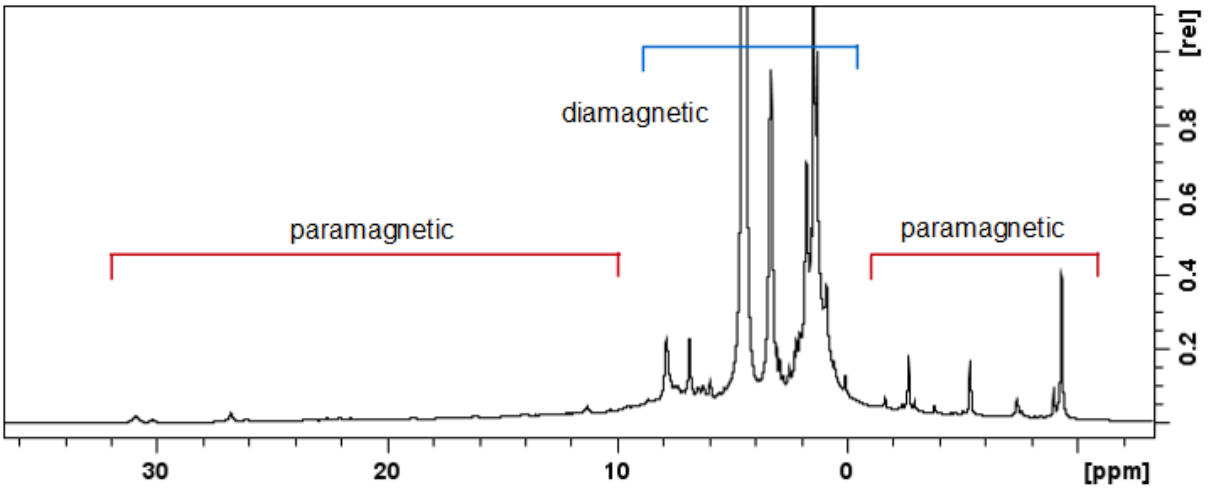

Figure 7.3: ^{1}H-NMR of crude mixture of UCl_4 and $CyMe_4$-BTPhen

Upon further work-up and reanalysis the paramagnetic signals disappeared. With the results of the reactions with 12N4Py4 and 9N3Py3 it had to be concluded that U(IV) is too readily oxidised to be used in speciation studies with the available equipment. Complex formation in aqueous solution is highly unlikely, as the high pH values necessary to stabilise U(IV) would keep the ligands from binding due to protonation. The study of U(IV) complexation was therefore abandoned.

7.5 Americium studies

Due to the radioactive characteristics of Am-243, only few facilities in the UK are allowed to handle it. One of these facilities is the National Nuclear Laboratory in Sellafield, which is also the industrial partner of this project. All studies on americium here presented were carried out in collaboration with Dr. Tamara Griffiths.

Due to the radioactive properties of ^{243}Am, its use is highly restricted and experiments had to be condensed to the absolutely essential studies. For this reason only

12N4Py4 was used, which in lanthanide studies had proven to be the better ligand for trivalent ions. The binding cavity of 9N3Py3 and the reduced number of coordination sites did not allow it to form stable Ln(III) ions, the same behaviour was expected for An(III) ions. Am(III) has an ionic radius (0.975 Å) very similar to that of Nd(III) (0.983 Å) and is more likely to show the same reactivities towards ligand systems.

The nature of the active area at the laboratory of NNL in Sellafield dictates the available characterisation methods, that were limited to luminescence measurements for speciation studies and gamma spectroscopy for quantification of americium.

UV-Vis spectra of ligands and complexes only showed small differences between species and were deemed not specific enough to follow complexation.

Gamma spectroscopy is a useful tool to determine isotopes and their concentration, but cannot give any information about the chemical species.

Luminescence can give very detailed information about a variety of species in solution. Whereas 12N4Py4 had been chosen on the basis of its capability to sensitise f-f transitions through its pyridyl chromophores, the Nd:YAG driven dye laser available for the study could not produce the excitation wavelength of 260 nm necessary for that purpose. Instead it was decided to excite the Am(III) directly at around 503-510 nm (assigned to the $^7F_{0'} \rightarrow {}^5L_{6'}$ f-f transition) and observe the emission around 660 - 740 nm ($^5D_1 \rightarrow {}^7F1$).[5–7] As f-f transitions are parity forbidden, they are generally weak, but may increase in asymmetric coordination species.[8]

In aqueous systems the complexation of metal ions competes with protonation of the ligand, making the process pH dependent. Whereas in the determination of binding constants for non-radioactive metals this was used to conduct pH titrations, no pH

meters were available in the active area for the americium study. Instead complexation studies were planned at constant pH controlled by a buffer solution. In this study, a Britton-Robinson buffer[9] consisting of phosphoric acid, boric acid and acetic acid was used.

The more covalent nature of the actinides mean that in theory they should bind to N-donors more strongly than the very ionic lanthanides. However, several other factors influence the binding strength between metals and ligand. Conditions were chosen so that complexation could also be observed in cases where binding strength was only minimally stronger than in the case of lanthanides, pH was set to 9.0.

The first experiment was designed to observe the kinetics of the formation of Am(III)-12N4Py4 and the characteristics of the complex, as luminescence properties were not yet known. A 1:1 solution of Am(III) chloride and 12N4Py4 in buffer was prepared and the emission spectrum measured over time. In the initial measurements, no emission was observed. This was unexpected as free americium usually exhibits a weak emission spectrum. It was suspected that some component of the solution, possibly the phosphate, must quench the luminescence of the free metal. Upon closer inspection of the sample however it was discovered that a precipitate had formed, much like the one known from lanthanide titrations. At the time, precipitation and its effect on the equilibrium had not yet been examined in depth. Further measurements after the sample was heated to encourage complexation did not produce a luminescent sample. In the hope that lowering of the pH would dissolve the precipitate and allow some complex to be formed, the pH was adjusted to 4-5 by addition of hydrochloric acid. Continued measurement did not show any changes in the emission spectrum.

A fresh solution was prepared at pH 5.5 and measured repeatedly over several days. Again, no luminescence emission was observed, though only minimal amounts of visible precipitate formed. The anions contained in the buffer might not only quench the emission of both free metal and the complex, it could potentially also form americium phosphates with high stability constants.

While the original plan was to use the first experiment to establish the properties of the complex in terms of emission spectra and lifetimes, further experiments would then be used to study complexation kinetics and competitive binding studies in the presence of calcium and neodymium. At this point however only enough Am(III) was left to conduct one further experiment and a new strategy had to be devised.

It was decided to focus on the determination of the binding constant of Am(III) to 12N4Py4. A non-buffered solution at 1 M KCl of $AmCl_3$ was prepared, which was titrated with increasing amounts of 12N4Py4. Initially it was confirmed that free Am(III) does indeed emit weakly in solution in the absence of buffer (Figure 7.4), so it was reasoned that complexation would change the emission spectrum, lifetimes or intensities.

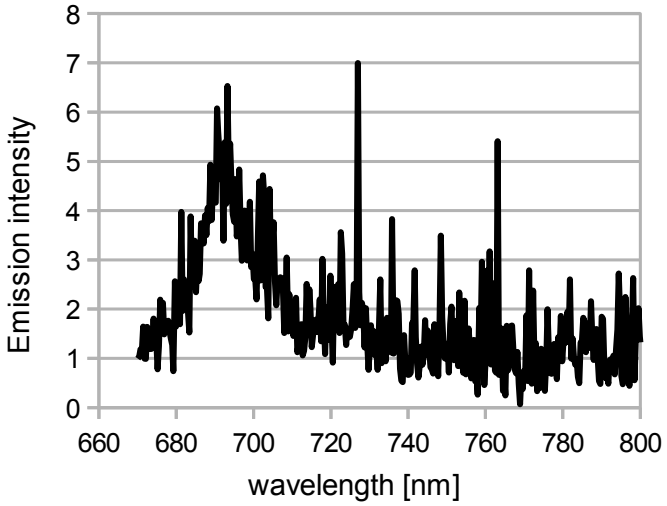

Figure 7.4: Emission of Am(III) in 1 M KCl, λ_{ex} = 503 nm

After addition of a total of 5 equivalents of 12N4Py4, the experiment was stopped as still no change in the luminescence was observed. It is unknown whether this is due to lack of complexation or the unsuitability of the measurement technique. The 8 N-

donors might not provide a ligand system asymmetric enough to increase americium luminescence.

Americium is expected to bind to amine ligands with a significantly higher affinity than lanthanides and complexation equilibrium constants could be expected to be up to 100 times larger, at room temperature and 1M KCl this will be approach approximately $\log K_c = 9$ compared to 6.45 to 7.31 measured for the Ln(III) ions. While this should increase the pH range where complexation can take place, it is again severely limited by hydroxide formation, which is considerably stronger for An(III) ions as can be seen from the speciation plot in Figure 7.5.

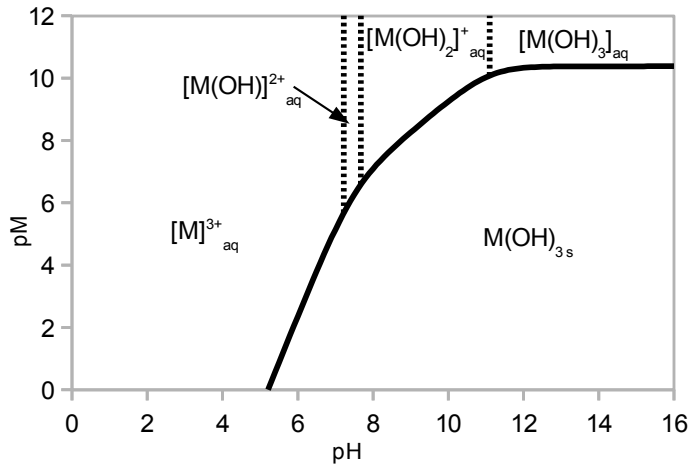

Figure 7.5: Speciation plot for Am(III) and hydroxides. [11]

Simulations for Am(III) binding for concentrations relevant for the experiments conducted at Sellafield with an assumed $\log K_c = 9$ revealed that the window where complexation can occur is effectively non-existent for 1:1 ligand to metal ratios. At a 5:1 ratio the complex can be observed (more than 20 % Mtot) between pH 6.1 and 6.4, at 10:1 ratio from pH 5.9 to 6.4. In these conditions large excess of ligand would have been necessary and a precise control of pH. In such large excess the ligand starts acting as a buffer reagent and pH control requires another buffer system, that does neither complex Am nor quench its luminescence, nor absorb at wavelengths used for Am(III) detection.

Monitoring of speciation using the ligand absorption and metal emission via the antenna effect would require lower metal concentrations, however this equally shifts

the window for binding into higher pH regions, keeping the window similarly small. If the minor actinides follow the trends of the lanthanides, complexation could be observed at 30°C, heating of the equipment was however equally unavailable. Alternatively, complexation could be studied in non-aqueous solvents and compared to the lanthanides. Unfortunately at this point no further americium luminescence experiments could be conducted and the equilibrium constant remains unknown.

7.6 Conclusion

Neither the uranium nor the americium showed complexation in the chosen conditions, uranium due to oxidation and americium due to hydroxide formation. Both U(IV) and Am(III) complexes of 12N4Py4 remain species of interest, even though their existence could not yet be verified. Investigation into their binding behaviour requires conditions and instrumentation not currently available at the Chemistry Department of the University of Oxford.

Nevertheless new insight was gained into how experiments need to be designed in order to potentially observe the desired minor actinide complexes of 12N4Py4.

References

[1] D. Delacroix, *Radionuclide and Radiation Protection Data Handbook 2002*, Nuclear Technology Publishing, Ashford, Kent, **2002**.
[2] R. D. Shannon, *Acta Crystallogr. Sect. A* **1976**, *32*, 751–767.
[3] N. N. Greenwood, A. Earnshaw, *Chemistry of the Elements*, Butterworth-Heinemann, Oxford ; Boston, **1997**.
[4] D. F. Shriver, P. W. Atkins, *Inorganic Chemistry*, Oxford Univ. Press, Oxford, **2002**.
[5] Z. Assefa, T. Yaita, R. G. Haire, S. Tachimori, *Inorg. Chem.* **2003**, *42*, 7375–7377.
[6] U. Resch-Genger, Ed. , *Standardization and Quality Assurance in Fluorescence Measurements I*, Springer Berlin Heidelberg, Berlin, Heidelberg, **2008**.
[7] L. R. Morss, Ed. , *The Chemistry of the Actinide and Transactinide Elements*, Springer, Dordrecht, **2010**.
[8] P. Hänninen, H. Härmä, Eds. , *Lanthanide Luminescence*, Springer Berlin Heidelberg, Berlin, Heidelberg, **2011**.
[9] H. T. S. Britton, R. A. Robinson, *J. Chem. Soc.* **1931**, 1456–1462.
[10] S. G. Bratsch, *J. Phys. Chem. Ref. Data* **1989**, *18*, 1–21.
[11] P. L. Brown, C. Ekberg, *Hydrolysis of Metal Ions*, Wiley-VCH Verlag GmbH & Co. KGaA, Weinheim, **2016**.

Chapter 8: Anion binding

8.1 Introduction

Due to the neutral nature of the ligands presented in this thesis, all their metal complexes are positively charged. In extraction applications, this leads to the coextraction of anions. There are several different way anions can interact with metal complexes or protonated ligand species. Anions might coordinate strongly to a specific site of the cationic ligand species; for example a small anion might coordinate to a metal complex of 12N4Py4 by acting as an axial donor atom from above the pyridyl face. Other ion pairs might only form loose association without a defined structural minimum. Depending on the characteristics of the anionic component the compound might become more lipophilic. And finally it is also possible that more complex structures arise from reactions of anions with other species, as already discussed for hydroxides in chapter 4. This chapter addresses the interaction of some anions with the ligands and complexes described earlier in this thesis.

8.2 Technetium

In aqueous solutions technetium occurs primarily as $Tc(VII)O_4^-$, also called the pertechnetate anion. One of the major problems encountered in PUREX is the coextraction of pertechnetate with U(VI)-TBP complexes. Technetium is therefore considered a contaminant. The exact structure of TBP-U(VI)-TcO_4 complexes is yet to be confirmed, but modelling with the structurally similar perrhenate ion (ReO_4^-) showed the anion to coordinate to the uranium centre in a monodentate fashion

(Figure 8.1).[2] This is also supported by recent investigation of alternative uranyl extractants and crystal structures.[3,4]

In this context it seems of great interest to look into the interactions between macrocyclic ligands and their metal complexes with present pertechnetate anions. Currently, technetium can only be handled as the meta-stable ^{99m}Tc in Oxford, which was deemed unsuitable for the study. ^{99}Tc could be used as part of a collaboration with the University of Zurich.

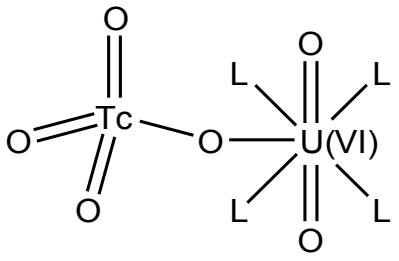

Figure 8.1: General structure expected for U(VII) pertechnetate complex with generic ligand L.

First, a solution of 12N4Py4 in methanol was mixed with an aqueous solution of ammonium pertechnetate and stirred for several hours. The solvent was removed and the sample analysed by NMR spectroscopy. None of the signals in both proton and technetium spectra indicated any interaction. Upon acidification with deuterium chloride the proton signals shifted in agreement with data obtained for protonated 12N4Py4, whereas the technetium spectrum showed no changes. However, after a few days a blueish compound crystallised from solution in the NMR tube. No crystal structure could be obtained and the compound slowly decomposed over time to TcO_2 in contact with air.

The colour and the formation conditions could suggest that pertechnetate was partially reduced by deuterium chloride to $[TcOCl_4]$, which is known to precipitate from aqueous solution in the presence of lipophilic ammonium cations, which is taken advantage of in the synthesis of $[TBA][TcOCl_4]$.[5–7] Reduction of pertechnetate to the tetrachloride Tc(V) in presence of protonated 12N4Py4 would equally cause the

formation of an insoluble salt. Similar formation of crystals and precipitate were found for 9N3Py3 and $CyMe_4$-BTPhen, however all eluded successful identification.

In nuclear reprocessing the conditions are generally not suitable for the formation of oxotetrachlorotechnetate due to the lack of chloride, so those reactions can be assumed not to be of any importance for the industrial application. It needs to be considered however if pertechnetate as a soft anion will not only interact with actinide and lanthanide complexes of novel extractants but also with protonated amine type ligands and affect partition coefficents in extractions.

8.3 Perrhenate and Iodide

Technetium is frequently modelled by perrhenate and there are significant similarities between pertechnetate and iodide.[8,9] Perrhenate is isoelectronic to pertechnetate and rhenium generally shows a similar chemistry as technetium[8,10], being in the same transition metal group together with manganese. Meanwhile iodide is preferred when size dependent behaviour of pertechnetate is to be modelled, as the two ions exhibit the same charge and very similar sizes (I^- 2.2 Å, TcO_4^- 2.5 Å) which is also exploited in medical imaging of the thyroid gland.[11,12]

8.3.1 Perrhenate

Attempts to produce a perrhenate salt of protonated 12N4Py4 from aqueous hydrochloric acids did not produce a precipitate or crystallisation as previously observed in the corresponding pertechnetate experiment. It might be that the significantly larger perrhenate anion does not form an ion pair with protonated 12N4Py4 of low solubility.

Perrhenate reacts with concentrated hydrochloric acid in the same way as technetium, forming oxotetrachlororhenate. No salt of it with protonated 12N4Py4 as a counter ion was found however. Perrhenate is less likely to be reduced than pertechnetate due to a difference in redox potential and might require harsher conditions.

If the reduction of perrhenate does take place in the presence of 12N4Py4 it is also conceivable that oxotetrachlororhenate reacts further with the nitrogen donors of the ligands to form the monooxo complex as portrayed in Scheme 8.1. Rhenium complexes of both cyclen and TACN have previously been synthesised from oxotetrachlorotechnetate,[13,14] however never *in situ* directly from perrhenate. Furthermore, the pyridyl arms could equally participate in substitution reactions, increasing the range of possible products.[15]

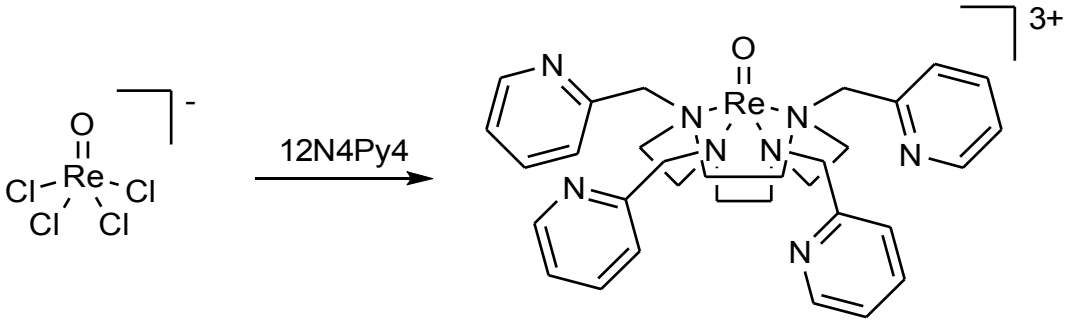

Scheme 8.1: Suggested substitution of chlorides by nitrogen donors exemplified by 12N4Py4.

Corresponding reactions of technetium have not been reported, and cyclen is a structural motif rarely encountered in technetium chemistry.[16,17]. Meanwhile, the smaller TACN based ligands for technetium are well studied.[18–20] It is conceivable that [$TcOCl_4^-$] obtained from TcO4- might react with TACN based ligands such as 9N3Py3 in a similar fasion as does [$ReOCl_4^-$] with cyclen.

When [$ReOCl_4^-$] or [$TcOCl_4^-$] are to be isolated, commonly tetrasubstituted ammonium counter ions like tetrabutylammonium are used that cause the product to precipitate

from the concentrated hydrochloric acid used to reduce perrhenate. Substitution reactions are not found due to the unreactive nature of tetrasubstituted ammonium ions. With protonated amines like 12N4Py4 or 9N3Py3 similarly insoluble salts are expected. As the proton can, however, be substituted easily, these amines are more likely to participate in substitution reactions.

In chapter 4 a crystal structure was presented of 12N4Py4 coordinating to sodium with a perrhenate as a counter ion. It originated from a failed attempt of replicating the pertechnetate experiments in acidic solution. Upon basifying of the solution with NaOH a colourless precipitate was observed, that was recrystallised from water to yield colourless crystals. The structure (Figure 8.2, measured, solved and refined by Dr. L. Pfeifer and Dr. A. Thompson) shows a sodium ion being coordinated to 12N4Py4. The perrhenate counter ion is not coordinated to the sodium complex due to its large size and only forms a loosely associated ion pair.

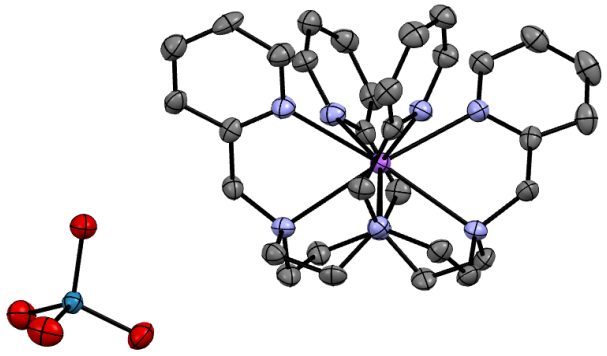

Figure 8.2: Crystal structure of Na(I)-12N4Py4 complex as perrhenate salt (WTS03). Hydrogen atoms not displayed, probability level at 50%

From metal binding studies it is known that the coordination of sodium is only effective at high pH values or in the presence of sufficient excess of sodium ions. The perrhenate salt could form simply because ReO_4^- is readily available as a counter ion. The immediate precipitation of large quantities of the salt however also suggest a particularly low solubility of the combination of the sodium complex and the perrhenate ion. Similar results can be expected for other metal complexes of

12N4Py4 and 9N3Py3. Further results supporting a particular low solublitiy of the salt are discussed in chapter 9.

8.3.2 Iodide

The solubility of salts greatly depends on size and charge distribution of the ions, where iodide is the better model for pertechnetate. An aqueous solution of KI and 12N4Py4 was acidified with concentrated HCl. Within a few days, dark red crystals formed. At the time it was speculated that the iodide (and the pertechnetate in the corresponding experiment) might sit in the protonated binding cavity of the ligand, which would greatly influence how the salt would extract in a possible application. To investigate weather that is the case, the crystals were analysed by single crystal X-Ray crystallography (measured, solved and refined by Dr. L. Pfeifer and Dr. A. Thompson). Surprisingly the crystal did not contain iodide counter ions, but incorporated three triiodide anions to balance each triprotonated ligand (Figure 8.3).

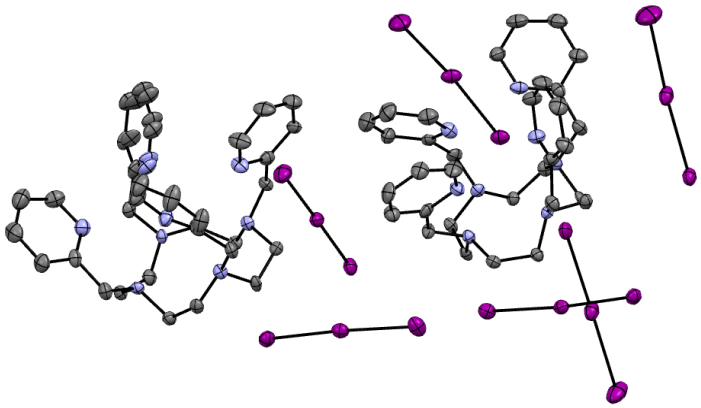

Figure 8.3: Crystal structure of 12N4Py4H3 triiodide (WTS05). Hydrogen atoms not displayed, probability level at 50%.

The bond lengths and angles of the triiodide moieties (Table 8.1) are in rough agreement with known values for triiodide ions.[21] It is known that the exact bond lengths between the iodine atoms strongly depend on the counter ion and the position of the anion within the crystal structure.

Table 8.1: Distances and angles of I_3^- ions

ion	I-I distance 1	I-I distance 2	I-I-I angle
triiodide 1	2.92 Å	2.95 Å	175.3°
triiodide 2	2.96 Å	2.89 Å	174.8°
triiodide 3	2.90 Å	2.96 Å	177.5°
ref[21]	2.82 Å	3.10 Å	180°

Iodide can be readily oxidised to iodine (Scheme 8.2), by oxygen from the atmosphere.[22] In acidic solution, iodine rapidly accumulates. It can then further react with excess iodide in an equilibrium reaction to triiodide and also higher polyiodides. The equilibrium however lies generally on the side of the starting materials.[23] The large and organic cation that is protonated 12N4Py4 however appears to form a sufficiently insoluble salt to stabilise the triiodide anion in a solid structure and act as a thermodynamic sink.

$$2I^- + {}^1/_2\,O_2 + 2H^+ \longrightarrow I_2 + H_2O$$

$$I^- + I_2 \longrightarrow I_3^-$$

Scheme 8.2: Reaction scheme of triiodide formation

The oxidation of iodide to iodine can be detected by the extraction into an organic phase. Acidification of a KI solution by HCl in the presence of a toluene phase caused it to indicate iodine formation by turning a pink colour, while the aqueous phase showed an intense yellow colour.

A similar experiment in the presence of 12N4Py4 also turned the toluene phase pink. After several days, the toluene phase slowly discolourised and dark red crystals formed on the interface of toluene and water. X-ray crystallography (measured,

solved and refined by Dr. L. Pfeifer and Dr. A. Thompson) confirmed it to be a triiodide salt of 12N4Py4. It was however surprising that the counter ion in this case was not a protonated form of 12N4Py4, but a potassium complex (Figure 8.4).

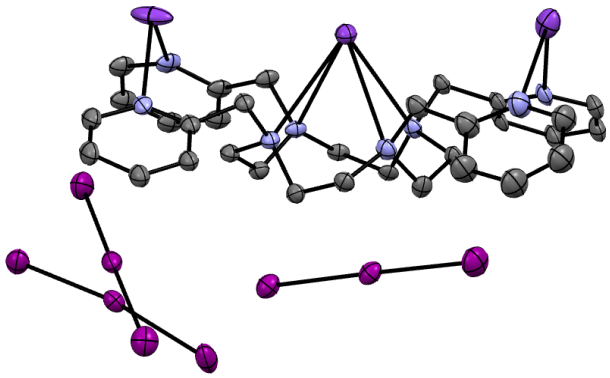

Figure 8.4: Crystal structure of K(I)3-12N4Py4 triiodide complex (WTS06). Hydrogen atoms not displayed, probability level at 50%.

In solution it was established that complexation of potassium is insignificant, due to the large size of the metal ion. Within the solid structure however one ligand molecule coordinates to three potassium ions, one sitting over the macrocycle being coordinated by 4 nitrogen atoms, two metals are cooordinated by two of the pyridyl arms each. The structure appears to be stabilised by a further complex of the same structure being positioned directly above in the packing of the crystals (Figure 8.5). Triiodide counter ions fill the spaces between the stacks of potassium complexes and balance the charge.

The bond between the central potassium ion and the coordinated nitrogens are very long (3.32-1.37 Å, Na(I)-12N4Py4 2.57 Å), even if the larger radius of the potassium ion (1.37 Å[24]) is considered, supporting the theory that the bond is rather weak.

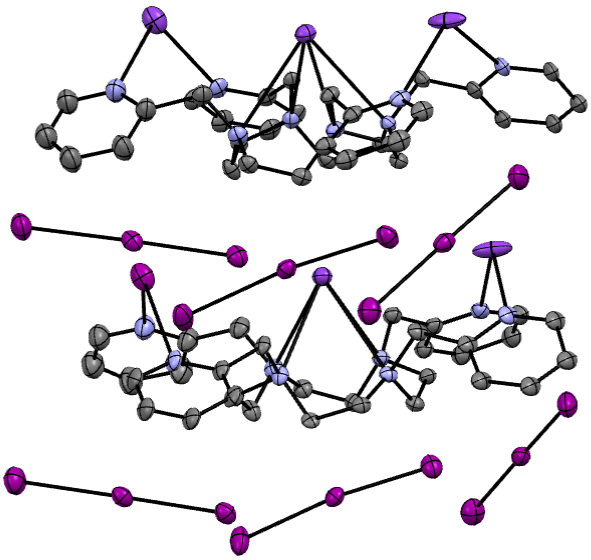

Figure 8.5: Crystal structure of K(I)3-12N4Py4 triiodide complex (WTS06). Hydrogen atoms not displayed, probability level at 50%.

The structure was obtained from crystals that formed at the interface of an aqueous and a toluene phase, suggesting that this salt is highly insoluble in both solvents. This is of significant consequence for minor actinide separation, as precipitation of ligand species decrease availability of the extractant for actinide and lanthanide binding, but also cause mechanical and phase separation problems.

The potassium complex forms at low pH, meaning that the insolubility of the triiodide salt enables potassium to effectively compete with protonation. Another precipitation of a potential potassium salt is discussed in chapter 9.

From the original sample that produced the first triiodide salt of 12N4Py4 to be measured (WTS05), a second type of colourless crystals was obtained upon prolonged standing. The structure was determined to be an iodide salt of protonated 12N4Py4 (Figure 8.6, measured, solved and refined by Dr. L. Pfeifer and Dr. A. Thompson). As no further material was added to the sample, evaporation of HCl would have caused a drift in pH and less triiodide and iodine remained, only allowing 12N4Py4 to crystallise with unreacted iodide. It can be deduced that the composition of 12N4Py4 salts containing iodine can vary strongly depending on available reactants and conditions.

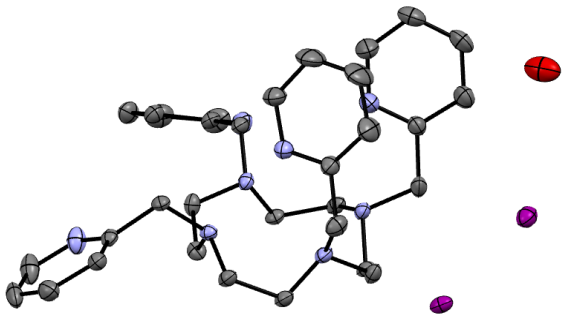

Figure 8.6: Crystal structure of 12N4Py4H2 iodide (WTS07). Hydrogen atoms not displayed, probability level at 50%.

8.3.3 Protonation of 12N4Py4 in iodide crystals

The structures of the triiodide salt shown in Figure 8.3 and the iodide salt in Figure 8.6 both contain protonated 12N4Py4 and thereby allowed further insight into the sites of protonation.

In the diprotonated structure of the iodide salt, the hydrogen atoms were found to be most likely positioned on two aza-nitrogens on opposite sides of the ring (Figure 8.7). This is consistent with the first pK_a being of similar strength (K_1 = 10.3) as other tertiary amines (triethylamine 10.6).

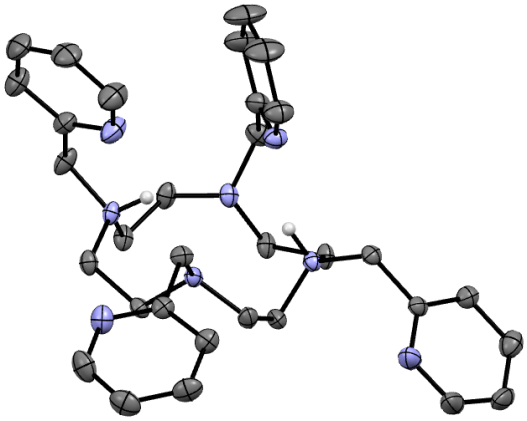

Figure 8.7: Crystal structure of 12N4Py4H2 iodide. Only nitrogen bound hydrogens displayed, probability level at 50%.

The second pK_a is somewhat lower (K_2 = 7.7), but still relatively high for a second protonation step. It was suggested that these protons can transfer rapidly between neighbouring nitrogen atoms and are essentially shared between them. It was however observed that two neighboring pyridyl arms are positioned directly above the macrocycle and might be involved with the stabilisation of these protons. The reason why two neighbouring pyridyl arms take these positions and not two on opposite sides of the molecule might simply be the spacial demands to form a stable crystal packing or direct sterical hindrance of the pyridyl moieties.

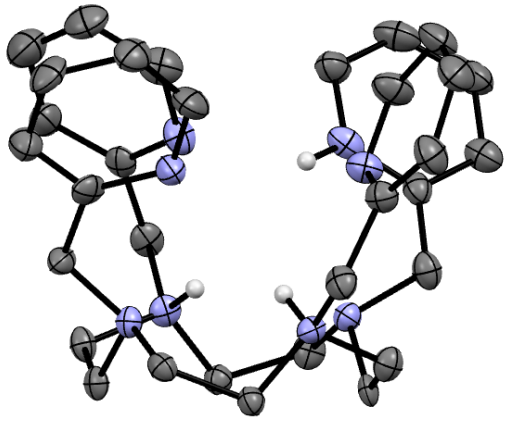

Figure 8.8: Crystal structure of 12N4Py4H3 tri triiodide. Only nitrogen bound hydrogens displayed, probability level at 50%.

In the triprotonated 12N4Py4 (Figure 8.8) it

was expected to find an additional proton located on a pyridyl arm. This was found to be the case for the triiodide salt. All four pyridyl arms are located above the macrocycle, two possibly being involved with the stabilisation of the protons on the macrocyclic nitrogens, while the other two form a pair sharing the third proton. Positions of the protons within the molecules are not trivial to determine for crystal structures and aren't necessarily static in the solid state, given another binding site is within short distance and the correct orientation. For both structures the pyridyl arms tend to wrap around the molecule's centre, allowing an extended hydrogen bonding network to estabish.

8.3.4 Iodide trapping

Iodide is one of the troublesome fission products in the nuclear fuel cycle, as volatile I_2 of highly radioactive iodine isotopes is produced in the acidic solution used to dissolve the fuel rods. It is necessary to trap iodine to avoid its escape to the environment. If iodine could be trapped in the form of triiodide salts, this might be of considerable interest for the nuclear industry. Experiments were performed to investigate the functionalities in 12N4Py4 capable of stabilising the triiodide ion in the solid state.

Aqueous solutions of pyridine and cyclen were combined with KI and acidified by addition of HCl. A layer of toluene was added to follow the formation of iodine and inhibit it from escaping the solution in gaseous form. The results were compared to the observation of 12N4Py4 under the same conditions.

In the sample containing cyclen a colourless precipitate was observed immediately following the addition of HCl and the toluene phase indicated the formation of

triiodide as expected. Analysis of the precipitate however indicated the precipitate to be merely an HCl salt of cyclen which is insoluble in HCl at high concentrations.

The toluene phase of the pyridine sample indicated the presence of iodine as well. Crystallisation of the aqueous phase produced dark red needles. Single crystal X-ray diffraction (measured by Dr. L. Pfeifer) of one of the formed crystals gave a unit cell that is consistent with the previously published dipyridiunium decaiodide (Figure 8.9).[25] In the structure, the two pyridinium cations are present with a total of 10 iodine atoms, that form a linear triiodide and a T-shaped heptaiodide molecules. Both are however interconnected and form what the authors described as an infinite chain structure.[25] Whereas I_3^- is the most stable ionic chain structure of iodine, longer chains can form under certain conditions.[21]

Both pyridine and 12N4Py4 seem to be very effective in forming triiodide salts of low solubility and were investigated and compared further to evaluate their potential to be employed as iodine trapping agents.

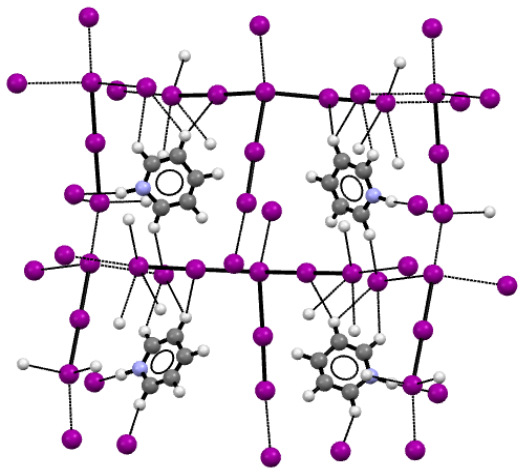

Figure 8.9: Packing of pyridinium decaiodide, reproduced from published structure.[25]

In industrial environments, the iodine molecule formed from oxidative conditions has to be extracted from the gas phase. An experiment was set up to test the potential of pyridine and 12N4Py4 to extract gaseous iodine.

A solution of KI was layered with toluene and stirred. Elemental iodine was heated to sublimation in a continuous stream of nitrogen as carrier gas and bubbled into the iodide solution. In the presence of 12N4Py4, the toluene phase took on a yellow colour that intensified to a dark orange

until a brown oily precipitate started to separate. When the addition of I_2 was stopped after 2 equivalents, there was a significant amount of precipitate visible at the interface between toluene and water. The aqueous phase showed a weak yellow colour, while the toluene phase showed a light shade of pink. Upon prolonged standing the oily precipitate solidified and was identified to be a triiodide salt of 12N4Py4 as previously observed. It is poorly soluble in water, toluene and methanol, but shows good solubility in acetone.

The experiment was repeated using pyridine instead, where both the toluene phase and the aqueous also quickly displayed a yellow colour. No precipitation was observed.

As a baseline another experiment was set up without any amine bases. Here the first indication of reaction was a yellow colour observed in the aqueous phase, followed by the development of a pink colour in the toluene phase.

All three samples were measured by UV-Vis spectrometry. Figure 8.10 shows the absorptions of the baseline experiment. The pink colour of the toluene phase associated with elemental iodine presents itself with an absorption maximum at around 500 nm. In the aqueous phase an absorption at around 350 nm was observed, which is attributed to the presence of the triiodide ion.

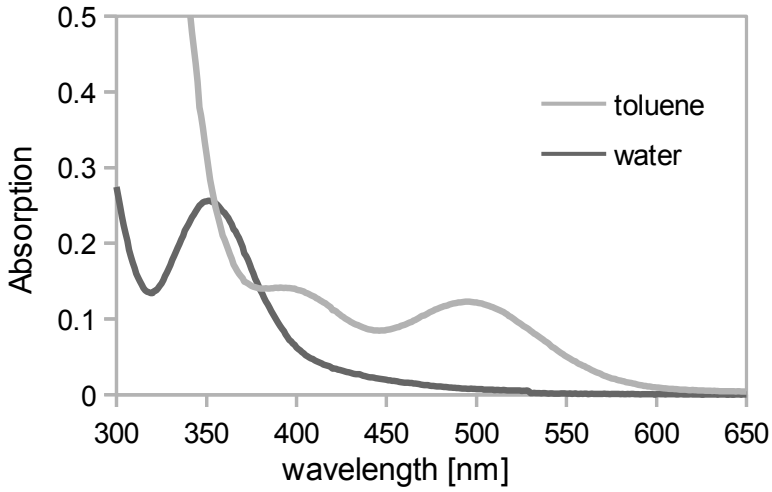

Figure 8.10: UV absorption of toluene and water phase of iodine trapping without amine bases

Measurement of the pyridine experiment indicated triiodide in both phases, suggesting that the pyridinium triiodide is soluble in the toluene phase. For 12N4Py4 very similar results as for the baseline were observed, however the concentrations of both iodine and triiodide were considerably lower than for the other experiments, as most of the iodine precipitated from solution.

Both pyridine and 12N4Py4 have the potential to act as effective trapping agents of iodine by stabilising them as a triiodide anion. They differ in their solubility in apolar solvents, causing 12N4Py4 salts to precipitate rapidly. This might be an advantage and the same reaction mixture could potentially be used to trap iodine as long as iodide and 12N4Py4 are continuously supplied. Immediate precipitation might also lead to problems, depending on the equipment design. Here pyridine offers the possibilty to stabilise the triiodide salt in solution and to continuously remove the organic phase. The triiodide could then be further reacted to other compounds or the pyridinium salt isolated by evaporation of the solvent. As the two compounds are very similar in their functionalities there is a potential for further fine tuning of the properties of the produced salt.

8.4 Other anions

The strong association of protonated forms of 12N4Py4 and its metal complexes with pertechnetate, perrhenate and triiodide ions further suggest that other anions might have a similar influence on these compounds.

Neutral and acidic solutions of 12N4Py4 were mixed with various salt such as potassium bromide, potassium hydrogen sulfate, potassium hydrogen phosphate or potassium carbonate. However no precipitate or crystal growth was observed in any

of them.

It was decided to investigate the influence of anion on 12N4Py4 species further as part of the extraction study presented in chapter 9. This was expected to give a sufficient understanding on how anions would influence the reprocessing of nuclear fuel. In depth studies of anion binding to metal complexes, such as the fluoride binding capability of Ln(III)-12N4Py4 complexes presented by Blackburn[26], go beyond the scope of this project.

8.5 Conclusion

In this chapter it was established that 12N4Py4 can form highly insoluble salts with large anions. Perrhenate combines with sodium complexes of the ligand and precipitates from basic solution. Similar structures could be expected for pertechnetate, there is however also the possibility that reduction to [$TcOCl_4^-$] leads to the formation of alternative compounds. Meanwhile reduction of iodide allows the accumulation of triiodide and crystallisation of both protonated 12N4Py4 and potassium complex salts.

Whereas the precipitation of triiodide salts is unlikely to be a cause of concern in minor actinide separations and might even offer novel pathways of trapping iodine earlier in the processing of spent nuclear fuel, interactions of 12N4Py4 with pertechnetate and their effects on extractions need to be investigated further.

References

[1] P. D. Wilson, Ed. , *The Nuclear Fuel Cycle: From Ore to Waste*, Oxford University Press, Oxford; New York, **1996**.
[2] G. H. John, I. May, M. J. Sarsfield, H. M. Steele, D. Collison, M. Helliwell, J. D. McKinney, *Dalton Trans.* **2004**, 734–740.
[3] P. Moeyaert, T. Dumas, D. Guillaumont, K. Kvashnina, C. Sorel, M. Miguirditchian, P. Moisy, J.-F. Dufrêche, *Inorg. Chem.* **2016**, *55*, 6511–6519.
[4] M. J. Sarsfield, A. D. Sutton, I. May, G. H. John, C. Sharrad, M. Helliwell, *Chem. Commun.* **2004**, 2320.
[5] S. K. Shukla, *J. Chromatogr. A* **1978**, *151*, 51–57.
[6] W. Preetz, G. Peters, *Z Naturforsch* **1980**, *35 b*, 1355–1358.
[7] K. V. Katti, C. L. Barnes, *Inorg. Chem.* **1992**, *31*, 4231–4235.
[8] N. Long, W.-T. Wong, Eds. , *The Chemistry of Molecular Imaging: Long/The Chemistry of Molecular Imaging*, John Wiley & Sons, Inc, Hoboken, NJ, **2014**.
[9] P. D. Beer, P. K. Hopkins, J. D. McKinney, *Chem. Commun.* **1999**, 1253–1254.
[10] C. E. Housecroft, A. G. Sharpe, H. Bera, A. Rompel, *Anorganische Chemie*, Pearson Studium, München, **2008**.
[11] C. F. Baes, B. A. Moyer, *J. Phys. Chem. B* **1997**, *101*, 6566–6574.
[12] R. Herbert, W. Kulke, R. T. Shepherd, *Postgrad. Med. J.* **1965**, *41*, 656.
[13] C. Xavier, A. Paulo, A. Domingos, I. Santos, *Eur. J. Inorg. Chem.* **2004**, *2004*, 243–249.
[14] C. Pomp, K. Wieghardt, *Polyhedron* **1988**, *7*, 2537–2542.
[15] R. M. Pearlstein, A. Davison, *Polyhedron* **1988**, *7*, 1981–1989.
[16] N. Saini, R. Varshney, A. K. Tiwari, A. Kaul, M. Allard, M. P. S. Ishar, A. K. Mishra, *Dalton Trans.* **2013**, *42*, 4994.
[17] H. P. Vanbilloen, K. Eraets, N. Evens, C. Terwinghe, D. Rattat, G. Bormans, L. Mortelmans, A. M. Verbruggen, *J. Label. Compd. Radiopharm.* **2005**, *48*, 1003–1011.
[18] H. Braband, S. Imstepf, M. Benz, B. Spingler, R. Alberto, *Inorg. Chem.* **2012**, *51*, 4051–4057.
[19] M. A. Wuillemin, W. T. Stuber, T. Fox, M. J. Reber, D. Brühwiler, R. Alberto, H. Braband, *Dalton Trans* **2014**, *43*, 4260–4263.
[20] R. Schibli, R. Alberto, U. Abram, S. Abram, A. Egli, P. A. Schubiger, T. A. Kaden, *Inorg. Chem.* **1998**, *37*, 3509–3516.
[21] D. F. Shriver, P. W. Atkins, *Inorganic Chemistry*, Oxford Univ. Press, Oxford, **2002**.
[22] J. C. Thresh, *J Chem Soc Trans* **1890**, *57*, 185–195.
[23] L. I. Katzin, E. Gebert, *J. Am. Chem. Soc.* **1955**, *77*, 5814–5819.
[24] R. D. Shannon, *Acta Crystallogr. Sect. A* **1976**, *32*, 751–767.
[25] T. L. Hendrixson, M. A. ter Horst, R. A. Jacobson, *Acta Crystallogr. C* **1991**, *47*, 2141–2144.
[26] O. A. Blackburn, A. M. Kenwright, A. R. Jupp, J. M. Goicoechea, P. D. Beer, S. Faulkner, *Chem. – Eur. J.* **2016**, *22*, 8929–8936.

Chapter 9: Extraction

9.1 Introduction

In nuclear reprocessing, the method of choice for species separation is liquid-liquid extraction, as it can be operated continuously. So far, investigations in this project have concentrated on behaviour of species in aqueous solution. To understand processes that aid or inhibit efficient separation through extraction it is necessary to also consider the organic phase and transit across the interface. In this chapter, extraction of ligands and complexes are discussed, as well as the influence of the presence of different anions.

To investigate the extraction behaviour of 12N4Py4 and its metal complexes a measurement technique had to be chosen that could follow the distribution between solvents. Whereas many techniques require standards for quantification or address a specific property on one species that might not be present in the next, the chromophores on 12N4Py4 and 9N3Py3 allows their identification in solution quantitatively by UV-absorption and luminescence spectroscopy.

9.2 Choice of organic phase

While the use of water as the polar phase in extraction processes for reprocessing nuclear waste is likely to remain firmly in place, the organic phase can be varied according to the needs of extractants and complexes, as well as their physical properties.

For next generation extractants one requirement is that they do not contain any

element apart from carbon, hydrogen, oxygen and nitrogen (CHON extractants) to ensure complete incineratability and minimise radiolysis.[2] The same requirement has to apply to any solvent used, which eliminates chlorinated solvents as candidates.

Other solvents can not be used due to their reactivity towards acids and/or bases, such as carboxylic acids, esters, ketones, aldehydes, amides or amines.

For any study of extraction using UV-absorption and luminescence it is also important to choose solvents that do not absorb in the region of the ligand chromophores, in the presented case at around 260nm. Aromatic solvents can therefore not be used with this technique. In order to be able to study the ligand effectively, the solvent should only act as a medium and not participate in metal complexation or specific interactions with other species. Therefore solvents containing functionalities that would enable such interactions also cannot be considered for ligand investigations.

In the current PUREX process, the liquid extractant TBP (tri-n-butyl-phosphate) is mixed with a hydrocarbon diluent, often kerosene. Kerosene is also frequently used to assess the extraction properties of novel extractant candidates within the field of nuclear reprocessing.[3–6] To stay as close as possible to extraction conditions in industrial applications, kerosene was chosen as the first solvent to be studied.

As kerosene is a mixture of varying composition, its chemical and physical properties can differ greatly, even though standardised kerosene is available for industrial applications. Its major components are alkanes and cycloalkanes with chain lengths of 6-16 carbons and should therefore have a similar extraction behaviour as pure alkanes. Hexane, which is easily accessible in most chemistry research laboratories,

was chosen as a second solvent of interest.

The assessment of the polarity of substances and their distribution between hydrophilic and lipophilic phases in chemistry is traditionally performed in a water-octanol system.[7–9] 1-Octanol is also a popular additive in nuclear reprocessing to increase the polarity of the organic phase.[10,11]

With octanol and hexane as organic phases, a wide spectrum of solvent polarity was covered, while kerosene should serve as a reference for the comparison with established extractants.

These three solvents were tested on their potential as a medium for the extraction study. UV-spectra and emission spectra were recorded after contacting them with water for 7 days. Hexane starts absorbing UV light between 220 and 210 nm (Figure 9.1a), octanol does so between 240 and 230 nm (Figure 9.1b), while kerosene completely covers the area of interest for the ligands with an absorption starting at 340 nm (Figure 9.1c). Emission spectra suggest that there are some aromatic

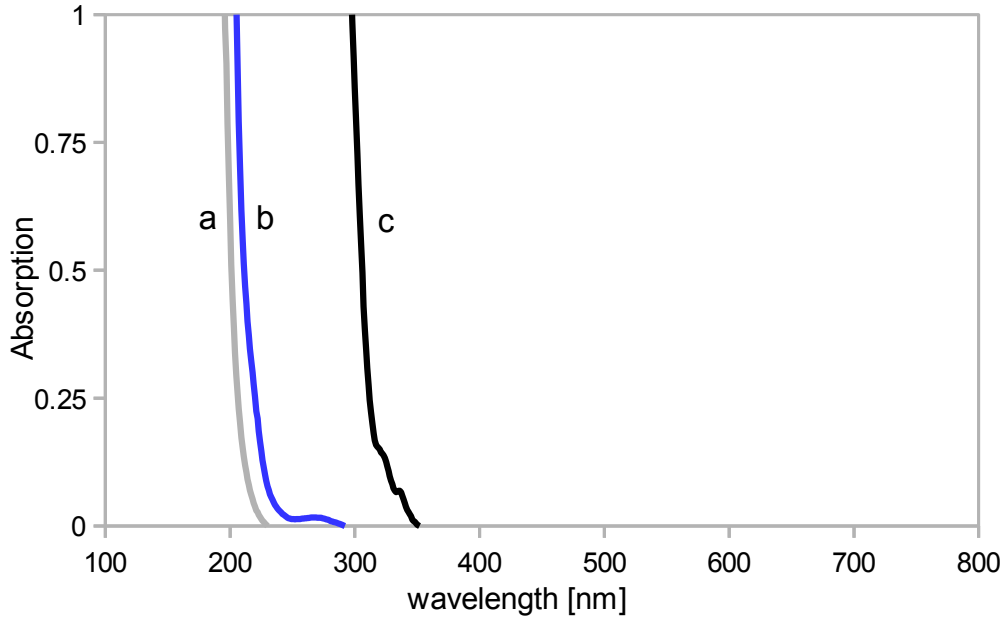

Figure 9.1: Absorption of the solvents: hexane (a), octanol (b) and kerosene (c)

components present in kerosene. Kerosene is therefore not suitable for the investigation of pyridyl chromophores. The study of 12N4Py4 and 9N3Py3 was continued with only octanol and hexane.

9.3 Choice of buffer system

The protonation states of the ligands and the degree of complexation to metal ions are dependent on the pH of the aqueous phase, so it is vital to control the pH of the solution. A buffer system had to be found to control the species even when one or several species are removed from the aqueous equilibrium system.

A wide array of buffer mixtures has been developed for biological systems. However, for pH values at the far ends of the spectrum fewer have been established. To be used in the extraction study, the buffering agents do not only need to keep the pH constant at a certain value but also need to have negligible absorption in the UV-region around 260 nm while interacting with ligands and complexes as minimally as possible. Some buffer systems, like citric acid[12] or N-(2-acetamido)iminodiacetic acid (ADA), can potentially act as ligands for calcium and lanthanides.

Ideally, one buffer system is identified that covers all pH values at which measurement results should be compared to each other. In the present study the pH range of 2 to 12 covers all possible protonated and complexed states of 12N4Py4 and 9N3Py3. Buffer system that buffer over such a large range of pH are referred to as universal buffers.[13] One popular buffer invented by Britton and Robinson consists of boric acid, phosphoric acid and acetic acid, and the pH is adjusted by addition of sodium hydroxide.[14]

From the pK_a and metal binding determinations already discussed it is known that

12N4Py4 and 9N3Py3 tend to bind sodium, so the Britton-Robinson buffer was modified to contain potassium hydroxide instead of sodium hydroxide.

These buffer solutions were left in contact with octanol and hexane for one week and measured to ensure none of the components would interfere with the measurement of the ligands and complexes. While the UV-spectrum was not affected by the addition of the buffer, a weak emission was seen in the luminescence spectrum. This is very likely to have originated from a minor impurity in one of the compounds used for the preparation of the buffer solution. Even when the greatest care was taken, the emission persisted. Luminescence measurements could therefore only be used as a supplementary and qualitative indicator of extraction, while UV absorption was used as the main measurement technique.

Many of the equilibrium constants discussed previously have been determined under several different conditions. Due to long equilibration times, the volatility of hexane and instrument limitations, extractions were carried out at room temperature (approximately 20°C) and in a 1M solution of KCl to keep the ionic strength effectively constant.

9.4 12N4Py4 ligand measurements

In chapter 2 the absorption and luminescence of the free base of 12N4Py4 in methanolic solution was discussed. Any measurement in an aqueous system has to consider which protonated form is the dominant species at a certain pH. Buffer solutions were prepared for the pH values where most of the ligand should be present in one protonated form: 2.0 ($[LH_4]$), 3.5 ($[LH_3]$), 6.2 ($[LH_2]$), 9.4 ([LH]) and 12.0 ([L]). The pH regions where the ligand occurs as $[LH_3]$ and [LH] are very narrow, so

other species are invariably present in solution as well. Figure 9.10 shows the simulation for the species of 12N4Py4 in the conditions relevant to the extraction experiment.

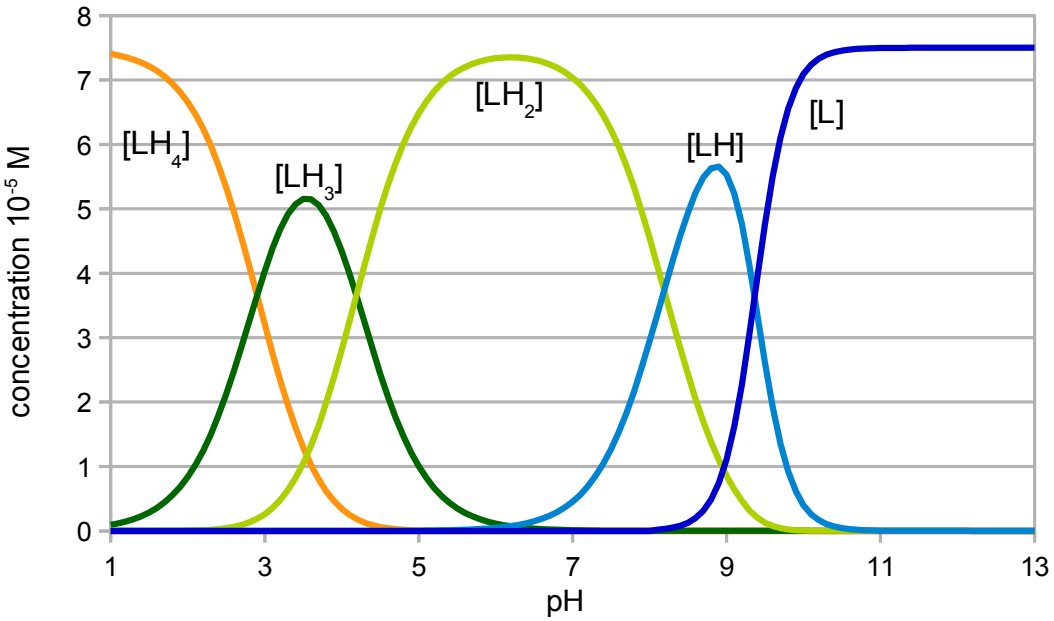

Figure 9.2: Simulation of species distribution in conditions for UV-absorption measurement

The dilution required for reproducible UV-measurement ($7.5*10^{-5}$ M) ensures that all species are sufficiently soluble and do not precipitate, including the neutral free base [L].

Figure 9.3 shows the relevant region of their UV-absorption spectra. The absorption of the free base [L] at pH 12 (dark blue) aligned with the absorption in methanol. With protonation of the macrocycle-nitrogen donors ([LH] and [LH_2]) the absorption maximum intensity slightly decreased, shifted slightly from 263 nm to 260 nm and the fine structure became more clearly defined. The minute hypsochromic effect might be caused by the local increase of polarity caused by protonation on the substituent of the chromophore (Py-CH_2-NR_2 → Py-CH_2-NR_2H^+).[15]

Upon protonation of pyridyl chromophores ([LH_3] and [LH_4]), a hyperchromic effect

was observed. Even though the n → π* transition is no longer possible for the affected pyridyl groups, the proton increases the dipole moment in the π-system of the aromatic ring, making the π→ π* transition more accessible.[16]

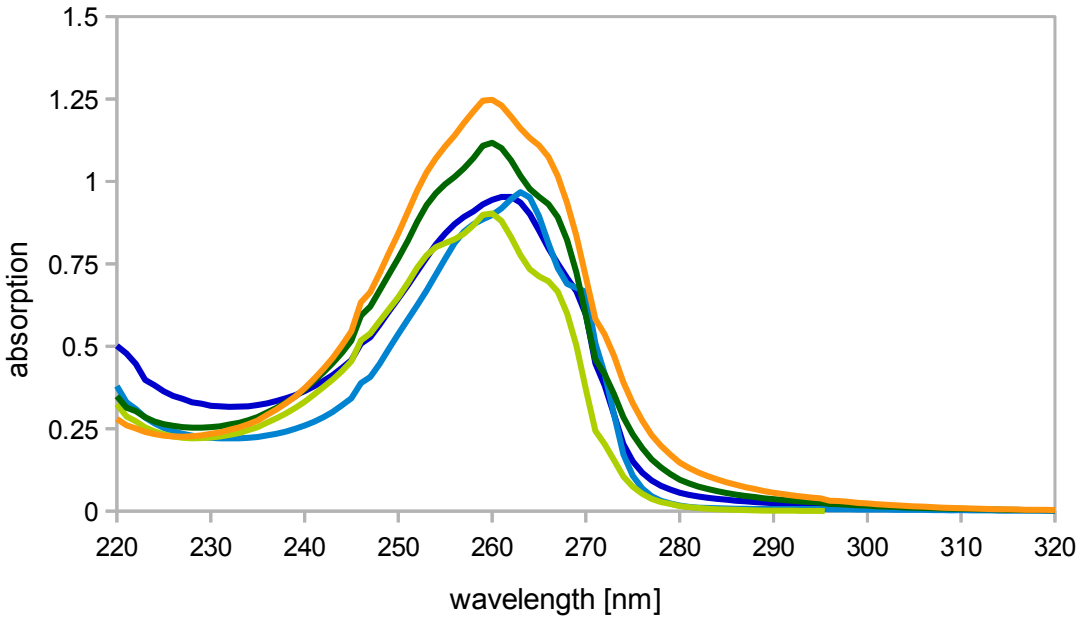

Figure 9.3: UV-absorption of 12N4Py4 in buffer. [L] dark blue, [LH] light blue, [LH_2] light green, [LH_3] dark green, [LH_4] orange.

The luminescence spectra obtained for 12N4Py4 at different protonated stages were weak and strongly influenced by any impurities present in the buffer solution. No additional information could be deduced from them. While lifetimes were expected to be slightly longer for protonated species[17], the emission was found to be too short lived to be defined using the available instrumentation.

Measurements in pure octanol and hexane (Figure 9.4) showed a hypochromic effect due to the decrease in solvent polarity. The effect was observed to be stronger for the long wavelength part of the absorption peak, causing different relative heights of the fine structure signals, which lead to an apparent shift of the maximum in hexane towards shorter wavelengths.

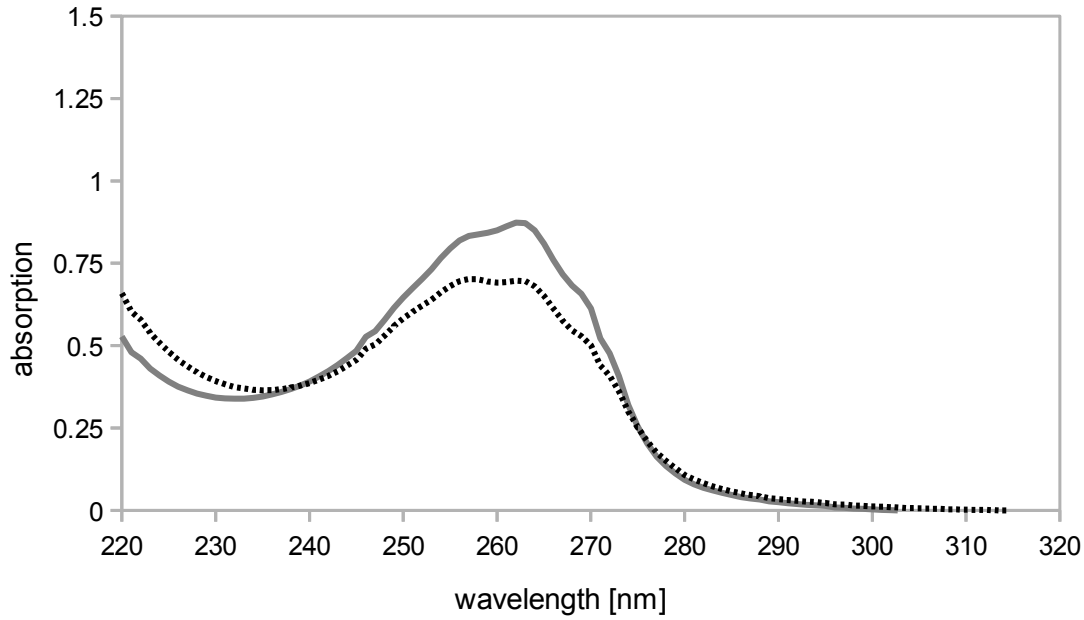

Figure 9.4: UV-absorption of 12N4Py4 in octanol (grey) and hexane (black dashed)

Solutions of 12N4Py4 at the five different pH values were contacted with octanol and hexane for 7 days and measured by UV. At several wavelengths, the concentration of each phase was determined using the respective extinction coefficient determined from the previous experiment. The relative content in each phase as an average over 5 wavelengths (250, 255, 260, 265 and 270 nm) is given in Table 9.1.

Table 9.1: Percentage of 12N4Py4 observed in the organic phase (rounded to 1%)

	pH 2.0	pH 3.5	pH 6.2	pH 9.4	pH 12.0
octanol	0 % ± 0.07	2 % ± 0.23	9 % ± 0.49	19 % ± 0.50	56 % ± 3.68
hexane	2 % ± 0.24	0 % ± 0.07	0 % ± 0.08	1 % ± 0.16	27 % ± 0.86

As expected, the protonated species of 12N4Py4 did not extract well into organic solvents due to their charge. Octanol, being a protic solvent, can form hydrogen bonds to partially protonated polyamines and is able to accommodate some 12N4Py4 in the lower protonated states. In order to maintain charge balance they also necessarily extract some anion. This could be either chloride or one of the pH

dependent buffering anions. Table 9.2 shows the predominant species for the studied pH conditions.

Table 9.2: Anions of buffer reagents present at different pH values

pH 2.0	pH 3.5	pH 6.2	pH 9.4	pH 12.0
CH_3COOH	CH_3COOH	CH_3COO^-	CH_3COO^-	CH_3COO^-
H_3PO_4 / $H_2PO_4^-$	$H_2PO_4^-$	$H_2PO_4^-$	HPO_4^{2-}	HPO_4^{2-} / PO_4^{3-}
$B(OH)_3$	$B(OH)_3$	$B(OH)_3$	$BO(OH)_2^-$	$BO(OH)_2^-$ / $BO_2(OH)^{2-}$

The free base 12N4Py4 was extracted relatively well at 12.0, but obviously preferred the more polar solvents octanol and water over the highly apolar hexane due to their hydrogen bonding capabilities. In the previous measurement in buffer it was observed that at pH 12 the shoulders of the 260 nm absorption were poorly defined. Upon the addition of octanol however the definition became clearer and showed a slight shift of the maximum from 261 nm to 263 nm. The spectrum then had a strong similarity to the one recorded at pH 9.4. Such an effect was not observed for the hexane extraction. A shift in pH does not seem plausible. It is however known that octanol does have some solubility in water (7.5×10^{-3} mol %).[7] Amines and alcohols can form hydrogen bond complexes[18] which could be stronger than hydrogen bonding to water molecules in a basic solution and might account for the observed changes in absorption. A more defined signal structure of the absorption was also found for 12N4Py4 in pure octanol. Results from later experiments also make a change in solvent structure a plausible explanation for the observed change in absorption at pH 12.0.

9.4.1 Influence of buffer

In order to guarantee consistent conditions buffering agents and salts are indispensable, they are however not inert to interactions with other components of the sample. To estimate their effect on the extraction, two series were prepared. One of them contained neither buffer nor potassium chloride, while the other one contained only potassium chloride. pH values were adjusted by addition of potassium hydroxide or hydrogen chloride. After contacting the samples with either hexane or octanol, the percentage of 12N4Py4 in the organic phase was determined using the same technique as described before. Figure 9.5 shows the results for the hexane extractions in comparison to the buffered solutions. It is clear that protonated species remain in the aqueous phase where they are stabilised by hydrogen bonds, which is in alignment with findings for the buffered samples.

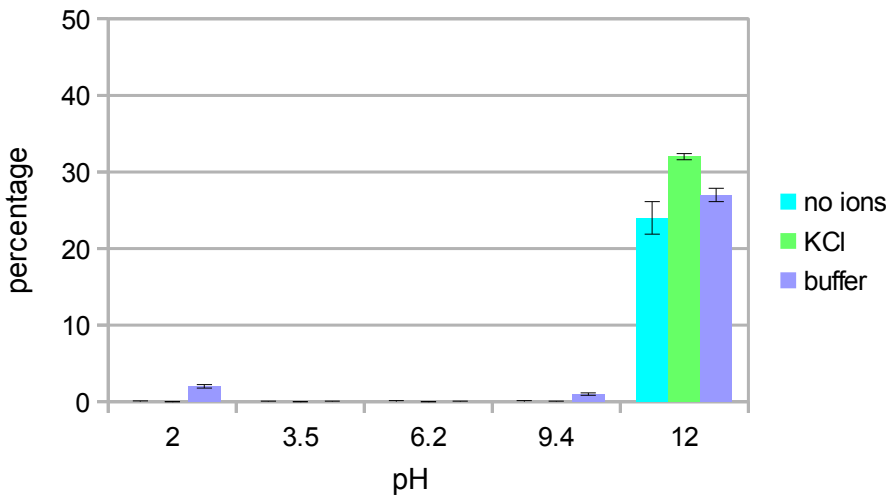

Figure 9.5: Percentage of 12N4Py4 observed in the hexane phase for different ion compositions

The free base extracted slightly more efficiently from the KCl solution. It appears that one of the buffering agents retained 12N4Py4 in the aqueous phase. A likely candidate for this is the boric acid and borates as a consequence of borate complexation with amines. Their solubility is estimated to be greater in water than in organic solvents.

In the absence of KCl extraction slightly decreased. This could be attributed to the known effect of "salting out", where an increase of ionic strength decreases the solubility of neutral compounds in the aqueous phase.[19]

Protonated species were also found not to extract into octanol (Figure 9.6) in the absence of buffer. It appears that chloride does not form extractable ion pairs with protonated 12N4Py4 and one of the buffer anions is the preferred counter ion. At pH 12.0 the absence of buffer agents caused an increase of extraction comparable to the effect seen in hexane. In the absence of KCl a further increase was observed, in sharp contrast to extraction into hexane. The spectra give no clues as to the species involved. It may simply be down to solubilities in the presence of potassium chloride. Varied responses to ionic composition in octanol-water extractions have been reported,[20] investigations into the mechanisms and molecular interactions however are rare. It also should be remarked that the proper adjustment of pH in unbuffered systems as well as measurements at such low concentrations is challenging and open to small concentration deviations. The interactions between KCl, the buffer agents and 12N4Py4 are however not specific enough to mask other processes that will be discussed in this chapter.

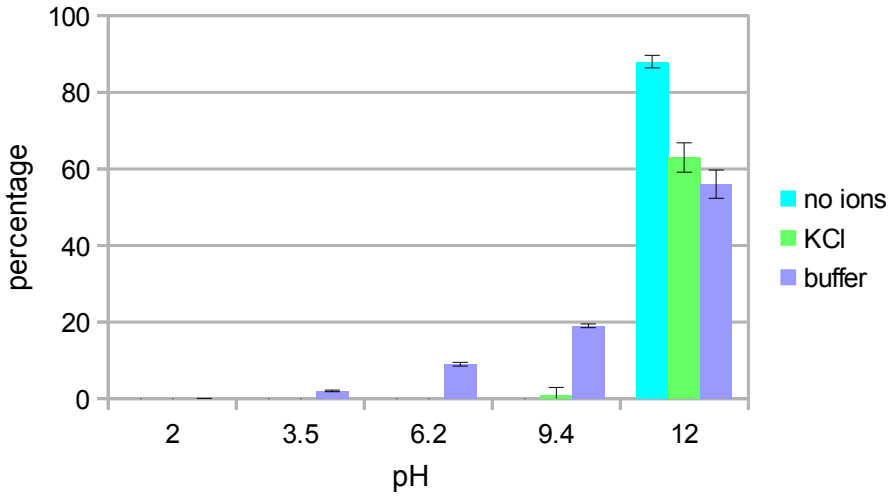

Figure 9.6: Percentage of 12N4Py4 observed in the octanol phase for different ion compositions

9.5 12N4Py4 and anions

In cases where protonated 12N4Py4 extracts into an organic phase, it is highly likely to coextract as an ion pair with an anion to maintain charge neutrality in the phases. For 12N4Py species, it can be assumed that the interaction between the cation and the anion is more or less unspecific. More lipophilic ion pairs that extract more efficiently will, however, form with larger and softer anions. The extraction of protonated 12N4Py4 however decreases the ligand available for complexation of the target metals, the minor actinides. Furthermore, the coextracted anions might interfere with further processing and be viewed as an unwanted contaminant.

It is therefore essential to identify ion pairings with unexpected behaviour and quantify the effect more lipophilic anions have on the extraction of 12N4Py4 in general.

Extraction experiments in buffer were repeated in the presence of one or ten equivalents of an anion of interest, a high affinity to a certain anion could be expected to give a linear response to the anion concentration.

This part of the study will also give more insight into insoluble salts of 12N4Py4 as were discussed in chapter 8.

9.5.1 Choice of anions

An anion of special interest in nuclear reprocessing is pertechnetate, which is already known to coextract in the PUREX process. As a entirely radioactive element, its use is strictly regulated. A collaboration allowed the use of the long lived isotope ^{99}Tc in the radio laboratory of the University of Zürich. Some of the experimental procedure had to be adjusted to comply with the restrictions set by the laboratory.

For the extraction experiments this meant that samples were equilibrated in Eppendorf vials instead of the otherwise used air tight mass spectrometry vials, that unfortunately are not capable of keeping hexane from evaporating. Hexane was added after 7 days of equilibration and 2-3 hours prior to measurements. The UV samples were prepared by dilution of the slightly more concentrated equilibration samples to reach the same concentration for the absorption spectra as for the non-radioactive samples. The series containing 10 equivalents of pertechnetate was not included in the following analysis, because the strong absorption of the anion overlapped with the signal of 12N4Py4 and made the determination of ligand concentration highly inaccurate. An advantage of the radioactivity is however that the radiation itself can be used to quantify concentration easily. Liquid scintillation counting was performed on both phases of the extractions, which allows to analyse the extraction of pertechnetate independently.

As perrhenate and iodide were previously used as models for pertechnetate and had shown interesting behaviour of their own, they were also included in the extraction study. Both perrhenate and pertechnetate were available as ammonium salts and used as such, instead of the desired potassium salt. To get an estimate of the possible interference of the ammonium ion on the extraction, a separate series of extractions of 12N4Py4 with ammonium chloride was prepared.

While chloride had been established not to interact with 12N4Py4 significantly in a pK_a titration, the larger bromide might show a behaviour more like iodide. Its inclusion in the study alongside iodide and chloride might also highlight the effect of anion size.

Most reprocessing procedures start with the dissolution of the material to be reprocessed in nitric acid, meaning that nitrate anions are omnipresent in subsequent

separation steps. It is therefore essential to analyse its effect on the extraction of 12N4Py4.

Unless reprocessing progresses under inert atmosphere there is the potential for carbon dioxide to dissolve in solutions and influence processes as carbonate anions. It is also very interesting as it can carry one or two negative charges.

Sulfate was also added to the series of anions. It is not an anion of special concern in nuclear reprocessing, but might offer valuable insight into molecular processes of coextraction of divalent anions.

This gives a total of seven anions and one non-metallic cation that were chosen to be investigated in 12N4Py4 extractions.

9.5.2 Extraction of protonated 12N4Py4 in the presence of anions

In the investigation of 12N4Py4 described above it was found that protonated species did not extract into hexane. None of the investigated anions were able to form an ion pair with protonated 12N4Py4 of sufficient lipophilicity to extract under these conditions.

The situation however was very different in octanol, which is significantly more polar. In many of the samples, absorption at around 260 nm was detected in the organic phase, indicating extraction of species of 12N4Py4.

At pH 2.0 (Figure 9.7) the ligand is four fold protonated ([LH_4]) and as such is the most unlikely candidate to form extractable ion pairs, especially as no tetravalent anions were provided. In the baseline measurement in buffer (labelled "none") no extraction was observed at this pH. Addition of iodide, pertechnetate or perrhenate

gave rise to spectra that suggest the extraction of some 12N4Py4. From earlier experiments (chapter 8) it is already known that these three ions have a high affinity for protonated species of 12N4Py4.

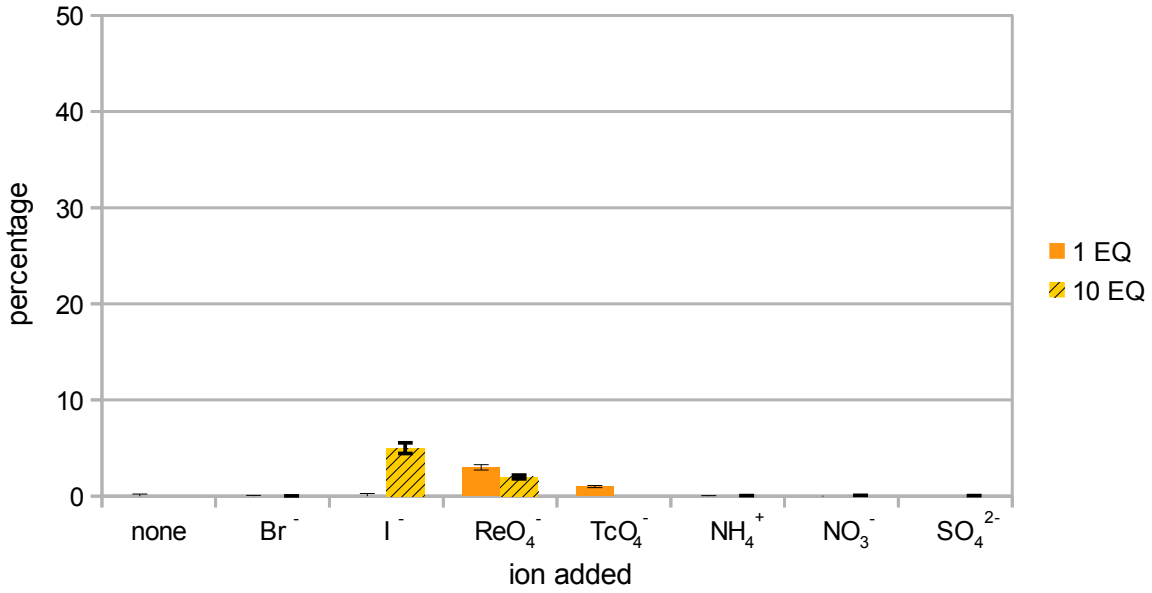

Figure 9.7: Percentage of total 12N4Py4 observed in the octanol phase at pH 2.0.

All three anions however are absorptive in the same wavelength region as 12N4Py4. Even though baseline measurements of the corresponding anion salts were performed in extraction conditions to allow correction for their absorption, the presence of [LH_4] in the aqueous phase might cause their concentration in octanol to increas Absorption levels in the organic phase are too low to distinguish the distinctive shape of 12N4Py4 absorption from the baseline. From liquid scintillation counting of the technetium concentration a slight increase of the anion content of the organic phase can be seen. It is therefore possible that no or little 12N4Py4 was extracted and an increase of anion absorption was observed instead.

[LH_3] at pH 3.5 does extract into octanol in very small quantities. Addition of anions tends to decrease extraction (Figure 9.8), differences however are extremely small.

The threefold charge of [LH_3] is difficult to counterbalance with mono- and divalent anions in order to form a charge neutral compound. The effects caused by the absorption of the counter ions as discussed for pH 2.0 also have to be considered similarly for pH 3.5. In general, extraction of threefold protonated 12N4Py4 can be considered to be insignificant.

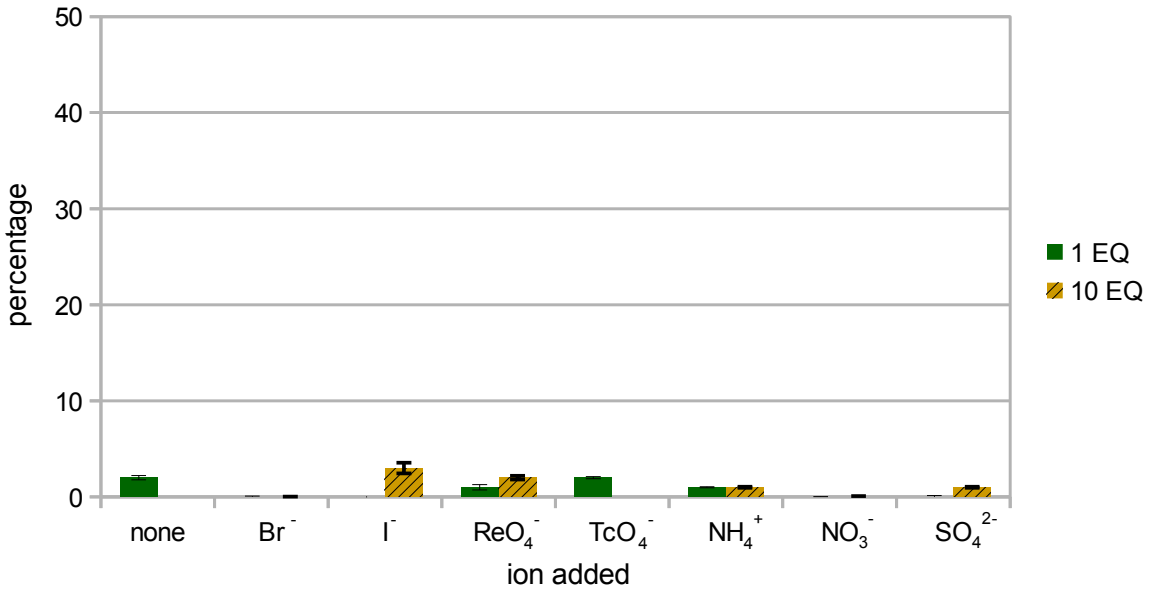

Figure 9.8: Percentage of total 12N4Py4 observed in the octanol phase at pH 3.5

At pH 6.2 [LH_2] is now predominant; it was shown to extract into the octanol phase, however at just below 10% there still is a strong preference for the aqueous phase. The addition of most anions has no significant impact on extraction of [LH_2] (Figure 9.9).

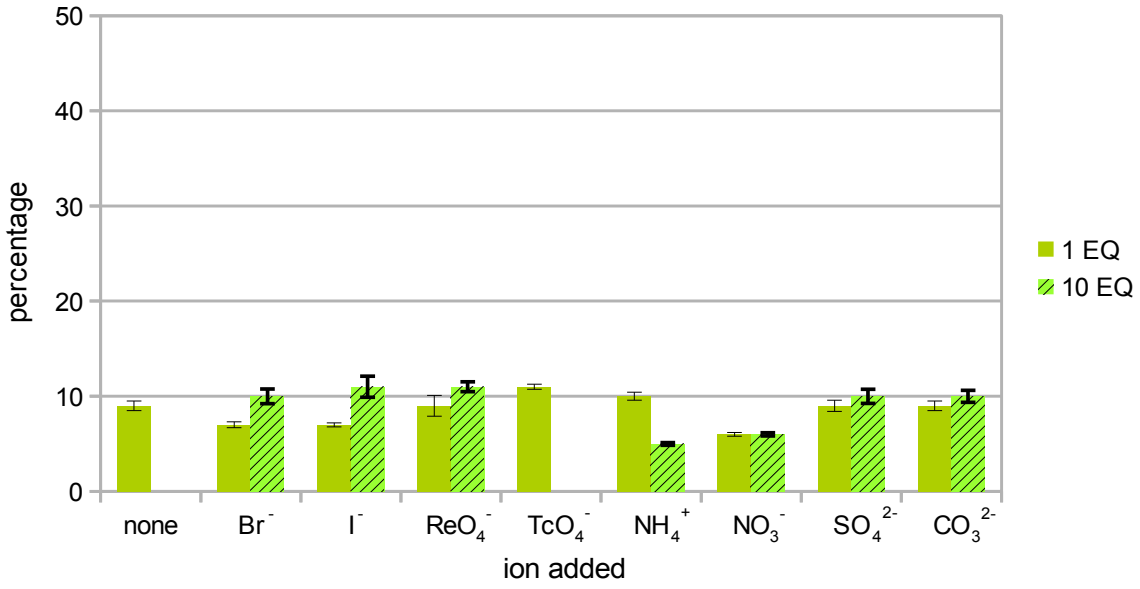

Figure 9.9: Percentage of total 12N4Py4 observed in the octanol phase at pH 6.2.

Results of the measurement in the presence of 1 equivalent of bromide, iodide, 10 equivalents of ammonium and both amounts of nitrate indicate a decrease in extraction. If specific and directed interactions between 12N4Py4 and the anions can be dismissed, the effect could be caused by two phenomena. Conceivably the anion is extracted into octanol as part as a different ion pair and competes with protonated 12N4Py4 for hydrogen bonding opportunities, decreasing its solubility in octanol. Alternatively the anion increases the stability of 12N4Py4 in the aqueous phase by allowing the formation of favourable hydrogen bonding structures. It remains unknown what exactly causes the observed decrease.

Extraction becomes significantly more favourable for the monovalent [LH] at pH 9.4. Nearly 20% of 12N4Py4 extracts into octanol in the absence of additional anions. It is also the condition for which the most drastic changes were observed with the addtion of anions.

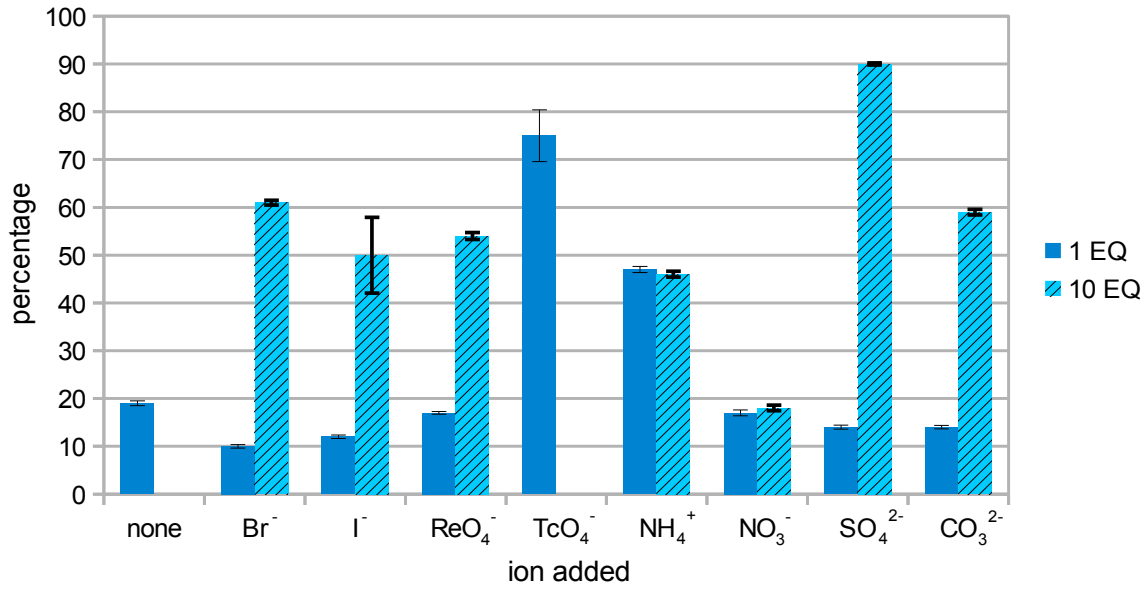

Figure 9.10: Percentage of total 12N4Py4 observed in the octanol phase at pH 9.4

At pH 6.2 it was observed that one equivalent of many anions caused a decrease in extraction. Very likely the low total concentrations of the components do not allow very specific interactions to have a visible effect. It is possible that the changes observed are caused by the change of the solvent structures, causing an indirect effect on the extraction of 12N4Py4. Larger amounts (10 equivalents) of most anions however increase extraction, their size and charge distribution being suitable to form lipophilic ion pairs with [LH].

No significant changes were observed for nitrate. Even though it only carries an overall charge of 1-, its structure in solution is somewhere between the three possible resonance structures (Figure 9.11), causing it to appear much more charge dense than other anions of similar size. As such, it does not form an extractable ion pair with 12N4Py4.

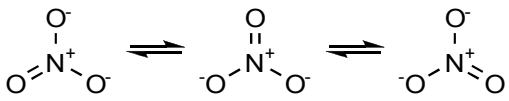

Figure 9.11: Structure of nitrate ion

Interestingly ammonium increases the extraction nearly 1.5 times, and independently of the amount of ammonium chloride that was added. With a pK_a of 9.24[21] it would be partially deprotonated in the aqueous phase. It is however suggested that a complex of ammonium and protonated 12N4Py4 could be formed that shares a proton between several nitrogens and stabilises 12N4Py4 in the organic layer.

Extraction in the presence of 1 equivalent of pertechnate was found to be much stronger than with any other additive. Liquid scintillation counting showed that indeed the technetium content in the organic phase increased from 0 to 12.9 % of the total amount. To account for the much larger increase of 12N4Py4 determined several other factors have to be considered. The counter ion of the pertechnetate, ammonium, also increases the 12N4Py4 content of the organic phase as was discussed for ammonium chloride. Extraction of both ammonium and pertechnetate alongside 12N4Py4 increases the polarity of the organic phase, which might further allow more 12N4Py4 to extract with less lipophilic counter ions. And finally this was the only measurement where the pertechnetate ion was present in octanol in such high concentrations, allowing no effective correction for the overlapping absorption of TcO_4^- and 12N4Py4. This means that 12N4Py4 is likely to extract less efficiently than indicated, but significantly stronger than with other anions at the same content level. As pertechnetate contamination is already a problem in nuclear reprocessing, finding that it shows an affinitiy to amine based extractants is a significant discovery and might have consequences for several other potential extractants as well. It also aligns well with the observation of precipitate formation of 12N4Py4, 9N3Py3 and $CyMe_4$-BTPhen in the presence of pertechnetate upon acidification.

In the presence of ammonium perrhenate measurements are more comparable to

the potassium salts, suggesting a less suitable pairing for extraction. Also iodide, deemed a good model for the size and charge density did not show a response as strong as pertechnetate, which could however be attributed to the absence of ammonium/ammonia.

9.5.3 Extraction of free base 12N4Py4 with anions

The free base at pH 12.0 is lipophilic enough to extract readily into both organic solvents. Without any charge that needs counter balancing the process should in theory be independent of the presence of anions.

Figure 9.12 shows the percentage of extracted 12N4Py4 with octanol.

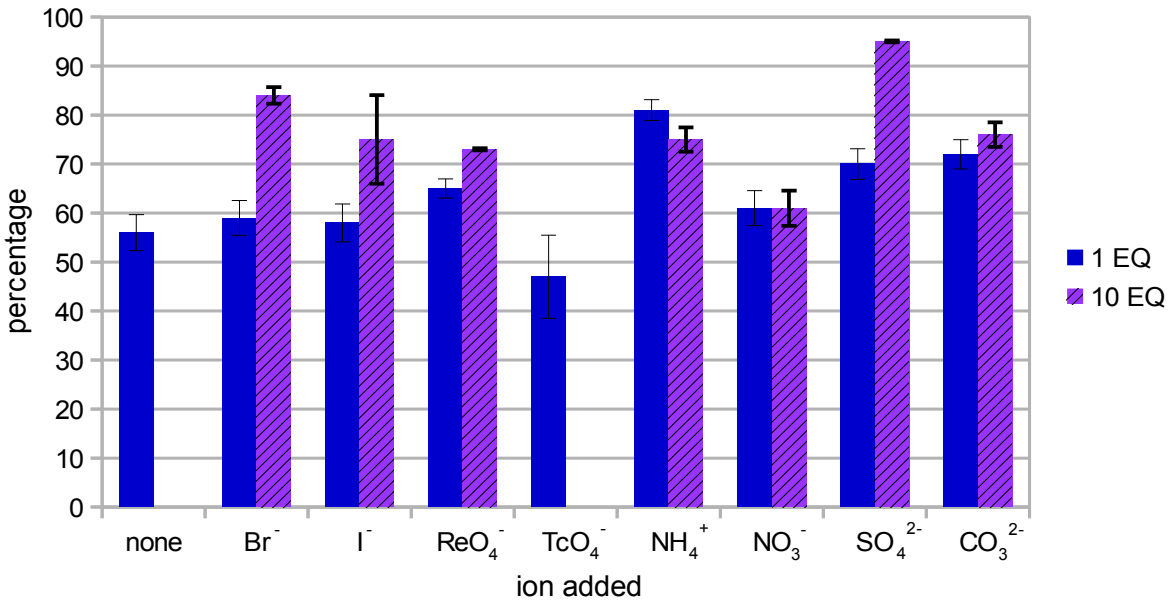

Figure 9.12: Percentage of total 12N4Py4 observed in the octanol phase at pH 12.0

In all samples the concentration of the ligand in the organic phase was found to be increased from the baseline measurement. The only exception is the pertechnetate sample, which could however be attributed to the conditions used, such as the higher

concentrations during equilibration. Some compounds might have reached their solubility limit in either phase. It can generally be assumed that none of the anions form defined species with 12N4Py4 in significant concentrations, as this would add negative charge and decrease the likelihood of extraction. Instead the anions influence extraction by modifying the properties of the solvent. An increase in ionic strength in the aqueous phase might decrease the solubility of a neutral species in this medium (salting out)[19], in the organic phase however extraction of the anion might bring its polarity to a more favourable level for 12N4Py4 solvation. Changes in extraction of 12N4Py4 are therefore dependent on size and charge density of the anions as well as their solubility in the organic phase as a potassium or ammonium salt, a parameter which could not be measured for most anions. For pertechnetate a slight increase to 2.4 % of total technetium content was measured in octanol. Unfortunately, since not many studies have been conducted on the octanol-water partition of inorganic salts, reference values are rare.

Ammonium is expected to have almost completely deprotonated at pH 12.0 and would extract into the organic phase as ammonia. There it would also change the structure of the bulk solvent and its interaction with 12N4Py4. In this specific combination it appears to increase the extraction of the ligand.

Neutral 12N4Py4 also extracted into hexane, the corresponding results are shown in Figure 9.13. The degree of extraction was less affected by the presence of anions than observed in the octanol series.

In the pertechnetate sample no extraction was observed. This could however attributed to the volatility of hexane and the circumstance that the organic layer could

only be added shortly before measurements. This then of course does not allow an equilibrium to establish and slows the accumulation of 12N4Py4 in the organic phase.

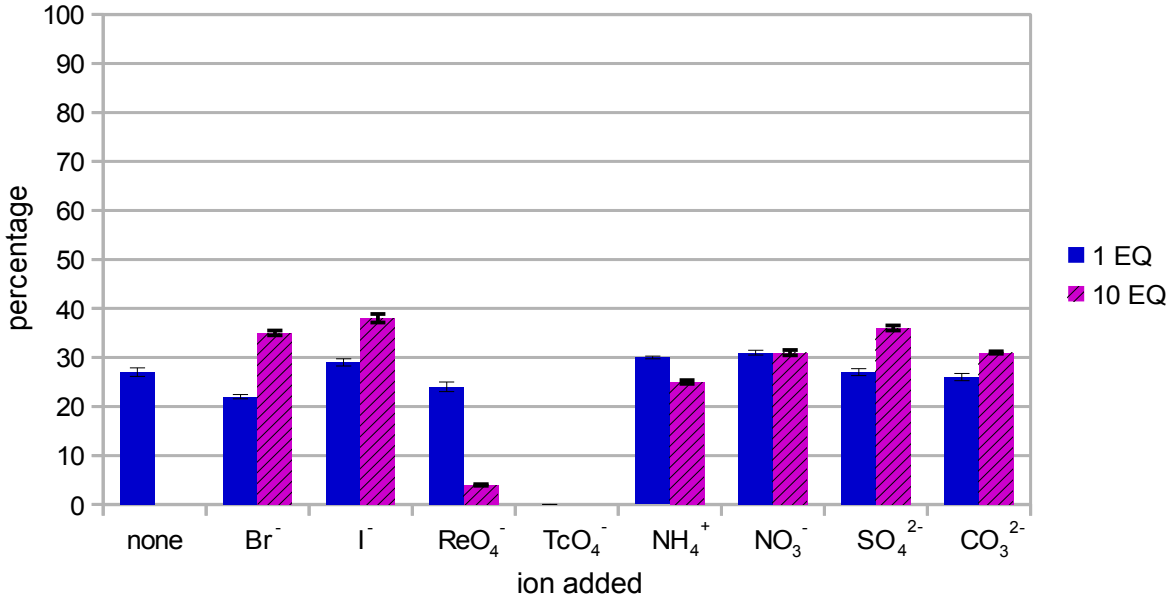

Figure 9.13: Percentage of total 12N4Py4 observed in the hexane phase at pH 12.0

While one equivalent of perrhenate slightly decreases extraction efficiency, the absorption measured sharply drops for 10 equivalents. Upon closer inspection it was observed that the concentration had also decreased in the aqueous phase and a colourless precipitate had formed at the interface between the solvents. It has been discussed in chapters 4 and 8 that the sodium complex of 12NP4y4 does crystallise with perrhenate as the counter ion under similar circumstances.

In the absence of sodium, the only viable cation in these conditions is potassium. Its binding constant to 12N4Py4 in equilibrium was found to be negligible (chapter 3). However, low solubility of the perrhenate salt would act as a thermodynamic sink and drive complex formation according to the principle of Le Chatelier. In an attempt to confirm this hypothesis, 12N4Py4 was mixed with ammonium perrhenate in a slightly

acidic aqueous solution, followed by an increase of pH by addition of KOH, causing an immediate formation of a colourless precipitate. Even though no crystals could be obtained and analysed from this experiment, the existence of a structure of a potassium complex (WTS06, chapter 8) as the triiodide salt further supports this theory. In the solid state, species can be stabilised that are not expected to be kinetically stable in solution.

Ion pairs of potassium complexes and perrhenate might be sufficiently soluble in octanol, explaining why no such precipitation was observed in those experiments.

9.6 Ca(II)-12N4Py4 and Nd(III)-12N4Py4

The primary focus of this study was, of course, to establish the potential of 12N4Py4 to extract f-elements, with a potential preference for the minor actinides. 12N4Py4 wraps around spherical cations, creating a lipophilic surface that might enable efficient extraction. Counter ions will still be necessary to balance charge, and would coextract. Coordination possibilities for anions to the complex are however small due to the bulky nature of the ligand, which was hoped to limit specific anion-complex interactions to axial coordination along the C_4 axis of the complex. In the ideal case, metal complexes of 12N4Py4 would extract into an organic phase with minimal preference for any specific anion.

Lanthanides can be considered to behave very similarly under extraction conditions, so studies were limited to only one of them. Nd(III) was chosen as a representative for the lanthanides, also due to it being the closest match in ionic radius to Am(III), the available representative of the minor actinides. In theory the ionic radius of Pm(III) would be even closer to that of Am(III), but promethium does not have any

stable isotopes and is rarely studied owing to its high specific activities.[22]

While lanthanides can show some intricate behaviour in aqueous conditions by forming hydroxide species, calcium shows a similar binding behaviour but no significant hydroxide formation, making it a good simplified model for f-element complexes. In case Nd(III) showed unexpected side reactions in extraction conditions, the Ca(II) complex was included in the study to have a model that is more likely to follow expected extraction behaviour.

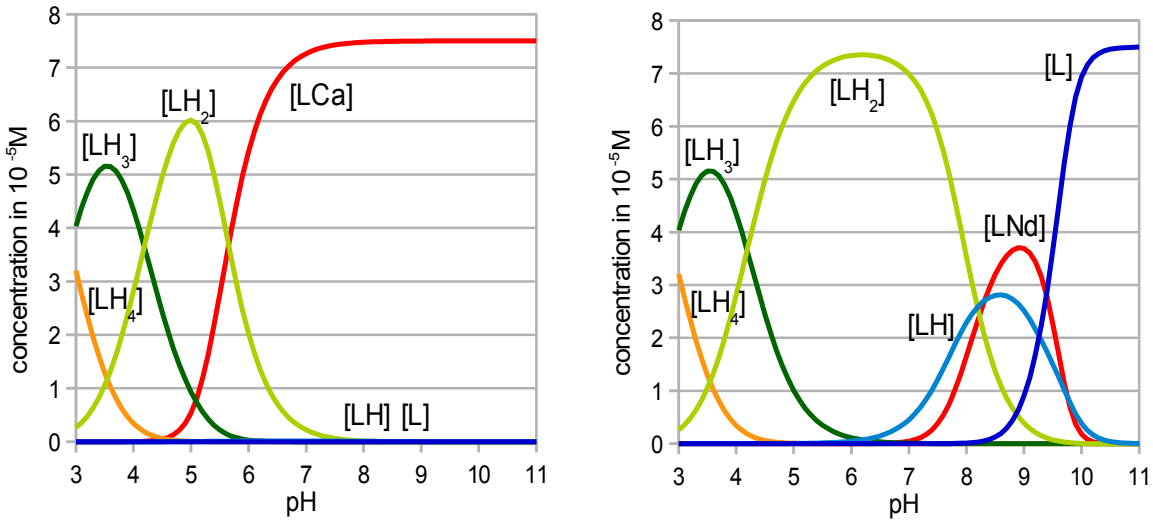

Figure 9.14: Simulation of speciation for Ca(II)-12N4Py4 (left) and Nd(III)-12N4Py4 (right) for conditions of extraction study.

As established in chapters 3 and 5, the stability of metal complexes is pH dependent. Using simulations of aqueous equilibria it was determined which buffer solutions would ensure sufficiently high concentrations of complex. Figure 9.14 shows these simulations using previously determined equilibrium constants for the relevant conditions (22°C, 1 M KCl). For the calcium complex, a large pH range is available where [LCa] dominates. For the study two pH values were chosen, 6.2 and 9.4. At pH 9.4 complete complexation can be expected, while at 6.2 there is the possibility that some protonated ligand is present. Neodymium is expected not to be fully complexed

at any pH due to the low concentration of metal and ligand compared to protons and hydroxides. The same pH values were chosen as for Ca(II)-12N4Py4, in expectation that significant amounts of Nd(III)-12N4Py4 should be detectable in the higher pH range, but less so at pH 6.2.

9.6.1 Ca(II)-12N4Py4

As the complexation of metal cations by 12N4Py4 changes the absorption spectrum of the ligand, a new set of baseline measurements in buffers and pure organic solvents was recorded. Figure 9.15 shows the spectra obtained for the calcium complex. In both buffer systems (top graph) the absorption shape and position is identical with each other and measurements previously conducted in methanolic solution (A_{max} = 263 nm). Even though simulation predicted the complexation to be incomplete at pH 6.2, the spectra suggest no significant diference in complexation degree. Absorptions of the complex and the free ligand are however very similar and incomplete complexation might

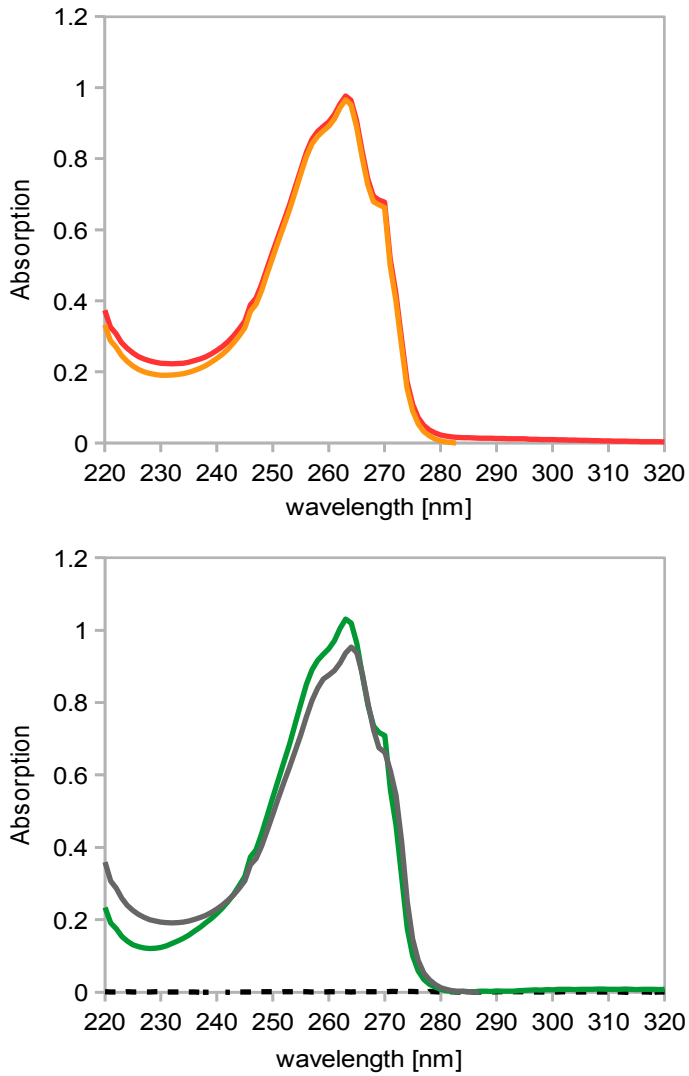

Figure 9.15: UV Absorption of Ca(II)-12N4Py4 in pure solvents:buffer (pH 6.2 orange, pH 9.4 red) and organic solvents (octanol grey, hexane black dashed, methanol green).

not be detectable. In octanol the absorption also closely resembles the methanol measurement, a slight decrease in intensity is observed due to the less polar character of the solvent. For the hexane solution no absorption was observed, suggesting that Ca(II)-12N4Py4 is not soluble in this medium. Extraction into hexane is therefore highly unlikely. This was confirmed in extraction experiments.

Even though the complex is soluble in pure octanol, in extraction conditions absorption in the organic phase indicated a content of only 1% of the total 12N4Py4 concentration. It appears that the divalent complexes are still considerably more stabilised in the aqueous phase.

As discussed previously for the free ligand, samples were prepared to estimate the effect of KCl and the buffer system. In order to eliminate issues arising from having to adjust the pH in such a narrow range, the complexes were simply dissolved in decarbonised water (pH ~ 7) with and without additional KCl. Extraction remained undetectable for samples with a hexane organic phase. For octanol extractions, a weak absorption was measured in the organic phase, indicating extraction of around 6 % of the total 12N4Py4 concentration. It is likely that triflate anions are lipophilic enough to form an extractable ion pair if competition with buffer anions is removed.

Triflate ions are not a component of spent nuclear fuel and their addition is not viable, as the fluorine atoms would cause problems in the incineration of the extraction agents at the end of their life cycle (CHON principle). However, this observation suggests that other lipophilic anions might be able to increase extraction efficiencies.

9.6.2 Nd(III)-12N4Py4

For the neodymium complex, a new set of baseline measurements were also recorded. Figure 9.16 shows the absorption spectra recorded for Nd(III)-12N4Py4 in buffer at pH 6.2 and 9.4 (top graph) and in pure organic solvents hexane and octanol (bottom graph). Based on the equilibrium constants determined in chapter 5, Nd(III) should not be complexed by 12N4Py4 at pH 6.2, the absorption however is very similar to the Nd(III)-12N4Py4 absorption in methanol and differs significantly from the spectrum of the free ligand under the same conditions. At pH 9.4, where some of the complex was expected to be present a spectrum was measured with a shape different from all previous measurements. It could be interpreted as the combination of the spectra of both the complex and the ligand at pH 9.4. By adding their respective spectra in different proportions to fit the measured combination, approximate complexation of 75% of 12N4Py4 was found. It is however unclear how complexation could be incomplete at pH 9.4 but apparently complete at pH 6.2 if

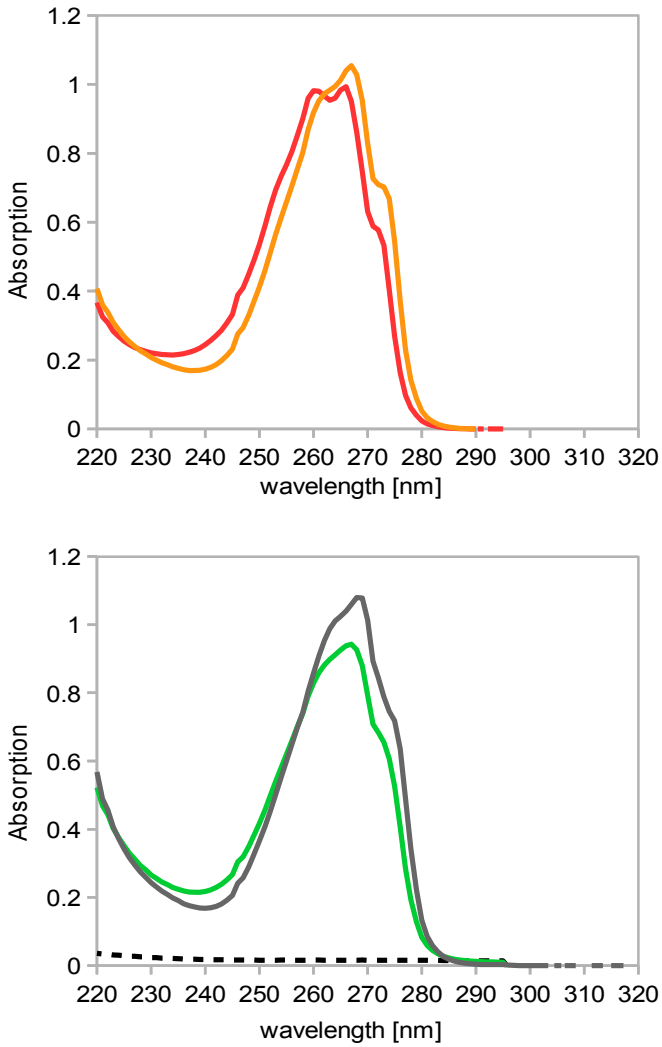

Figure 9.16: UV Absorption of Nd(III)-12N4Py4 in buffer (pH 6.2 orange, pH 9.4 red) and organic solvents (octanol grey, hexane black dashed, methanol green).

equilibrium is being achieved.

Initially it was suspected that one of the anions, most likely a pH dependent one, could coordinate to the complex and increase its stability. In measurements at pH 7 in the absence of buffer and the absence of any ions except triflate the same absorption as at pH 6.2 was obtained.

The octanol spectrum is in close agreement with the methanol spectrum, but hexane again showed insufficient solubility of the complex.

Extraction experiments were conducted with hexane and octanol, but neither showed any absorption in the organic phase that could be attributed to either complex or dissociated ligand. As the protonated ligand would show some extraction at the chosen pH values, this suggests that complexation dominates the equilibrium.

It could be argued that in fact the complex is kinetically stable on the timescale of these measurements and does not dissociate to the degree that was predicted by simulations in the given equilibration time. The high concentration of anions that might facilitate dissociation however should allow a thermodynamic equilibrium to be reached. It remains unknown why the apparent behaviour of Nd(III)-12N4Py4 differs so significantly from binding strength titration experiment findings (chapter 5), though it might be linked to formation of hydroxide formation, causing the system to operate outside of equilibrium.

Control experiments in pure water and 1M KCl at pH 7 showed some extraction into octanol. This is consistent with experiments for Ca(II)-12N4Py4 extractions. Triflate is likely to be the coextracted counter ion also for the trivalent neodymium complex, its higher charge reduces extraction efficiencies slightly to 5 %, which is however within experimental error.

9.7 Ca(II)- and Nd(III)-12N4Py4 extractions in the presence of anions

Based on extraction experiments of the two metal complexes in buffer, KCl and pure water it was proposed that extraction into octanol is possible with triflate as a counter ion. Other anions might similarly be capable of forming extractable ion pairs.

A series of samples were prepared to measure the response of the two metal complexes to the presence of the anions that were previously used in the study of interactions between anions and the ligand.

For most samples no extraction was observed for either complex.

There were two exceptions; the Ca(II)-12N4Py4 / pertechnetate ion pair resulted in 5% (1 equivalent) and a 10% (10 equivalents) of 12N4Py4 species to be detected in the organic phase, while for Nd(III)-12N4Py4 some extraction was observed after addition of 10 equivalents of KI (only for pH 6.2) and 10 equivalents of pertechnetate. For all these measurements however absorptions are too weak to give relative extraction efficiencies.

The UV spectra of the aqueous phases were compared to check for any changes that could be attributed to interactions with anions. No significant shifts in maxima or relative intensities of the vibrational substructure signals were found. It was however observed that for all

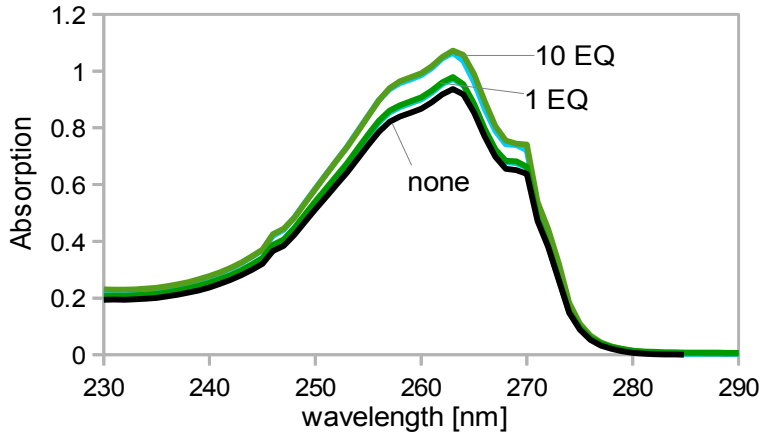

Figure 9.17: Absorption spectra of Ca(II)-12N4Py4 at pH 6.2 in presence of no additional ions (none, black), bromide (blue) and carbonate (green).

conditions the total absorption varied considerably in the presence of different anions. It may be argued that errors in concentration lead to the effect, however there seems to be a correlation between the amount of added anion and absorption intensity. Figure 9.17 shows one of these spectra sets for Ca(II)-12N4Py4 at pH 6.2.

To cause such a change by simply increasing the ionic strength is highly unlikely, otherwise a much stronger effect would have been seen in the study of the influence of buffer and KCl. More likely there is an association of the anions to the complex directly changing the local environment around the pyridine chromophores.

From this it can be deduced that there is some direct interaction between complex and anions. No ion pair is formed however with sufficient solubility in the organic phases. To efficiently extract these complexes it might be necessary to use lipophilic, organic anions as additives. It is also very likely that 12N4Py4 would have to be derivatised to be more hydrophobic to achieve effective extraction.

9.8 Am(III)-12N4Py4 extraction

In chapter 7 the attempts to identify Am(III)-12N4Py4 by americium luminescence failed due to quenching of Am(III) in buffered solutions and the absence of significant changes in emission in 1M KCl. Due to the restrictions applying to the work with ^{243}Am meant that no further luminescence experiments could be conducted. UV-Vis absorption of 12N4Py4 however require considerably lower concentrations than those used to follow the partially parity forbidden f-f transitions of Am(III). One of the buffered solutions containing Am(III) and 12N4Py4 in equal amounts was used to prepare extraction experiments at pH 3, 5 and 7 with both hexane and americium, in a final attempt to gain insight into potential interactions between the ligand and the

actinide.

No extraction was measured for most samples, and only at pH 7 a weak absoprtion was recorded in the organic phase of the octanol extraction. Unfortunately the instrumental restrictions causes the spectra to be of too low quality to determine percentages. Gamma spectroscopy was measured for all phases and revealed that no condition provided enabled any Am(III) to extract into an organic phase. The absorption increase observed at pH 7 might therefore be caused by the extraction of protonated ligand, further suggesting that at best, only partial complexation of Am(III) had occurred.

The hydroxide formation constants (see chapter 7) only allow for a very narrow pH range for Am(III) to bind to 12N4Py4. It appears that none of the investigated conditions met the requirements for 12N4Py4 binding. To investigate it further, different techniques would have to become available at Sellafield for the monitoring of speciation.

9.9 Influence of other metal cations

In the investigation of the effects of anions on the extraction of 12N4Py4 it has already been mentioned that some of these compounds might be viewed as undesirable contaminants in industrial application. Another source for problems with the extraction systems is the presence of metal cations that might compete for ligands more effectively than both lanthanide and actinide ions. Two cations that might interfere with minor actinide separations are uranyl (UO_2^{2+}) and Na^+. It is therefore important to evaluate their potential to interact with 12N4Py4 in extraction conditions.

9.9.1 Na(I)-12N4Py4 extraction

In equilibrium measurements it was found that the binding of sodium with 12N4Py4 is considerably weaker than for lanthanides and calcium. The high solubility and low formation constant of sodium hydroxide however allows the complexation to take place at high pH. Even so, at 1 to 1 ligand to metal ratio, full complexation will not be reached (Figure 9.18). Therefore a solution of 12N4Py4 was treated with one and with ten equivalents of sodium chloride and extracted. At ten equivalents simulation suggest the complexation would be able to reach completion.

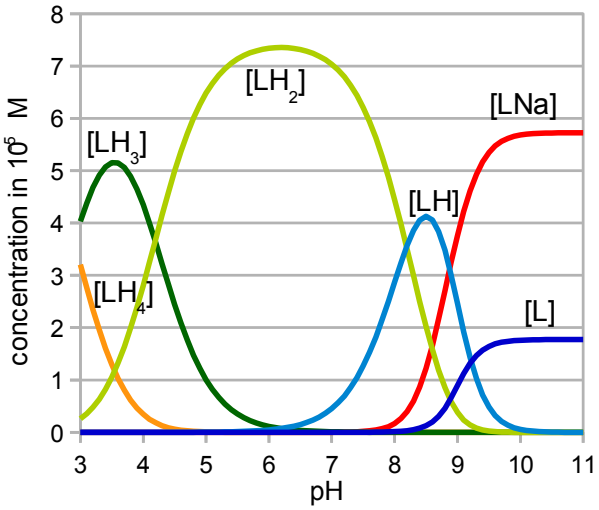

Figure 9.18: Simulation of equilibrium system of 12N4Py4 in presence of one equivalent of sodium chloride at conditions relevant for extraction experiments.

In hexane (Figure 9.19) extraction did not occur at low pH. At pH 12, where full complexation could be expected, no significant change is observed upon the addition of one equivalent of sodium chloride, at ten equivalents however extraction

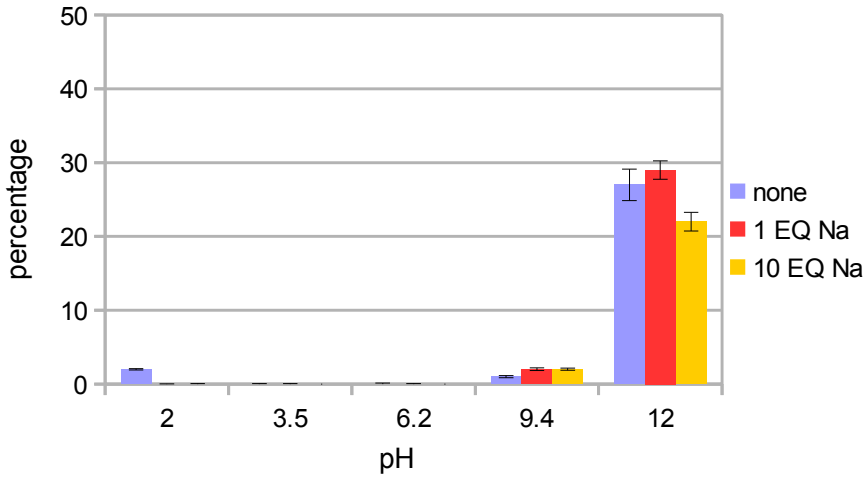

Figure 9.19: Percentage of 12N4Py4 in hexane phase dependent on sodium content

decreases. With the excess of metal complexation appears to effectively compete with extraction and the charged sodium complex does not seem to extract into hexane as was observed for all charged 12N4Py4 species so far.

In octanol (Figure 9.20) extraction was already observed for protonated ligand. No significant changes to extraction efficiencies were observed at pH 2.0, 3.5 and 6.2, where simulation predicts no complex to be present. At pH 9.4 and 12.0 an increase in extraction was found, independent however of sodium concentration. It appears that the sodium complex forms quantitatively and that the low charge of the sodium complex allows extraction into octanol, even in the absence of lipophilic triflate anions. The shift of the absorption maximum from 260 nm towards 263 nm further supports the formation of the sodium complex. Studies of the interaction between the sodium complex and anions were not pursued as they are of little interest to the industrial application. It can however be assumed that the presence of more lipophilic anions will only further increase extraction into the organic phase. Sodium was found to be extracted considerably more efficiently than Ca(II) and f-element complexes. Unless sodium free conditions are provided, this competition will significantly interfere with minor actinide separations.

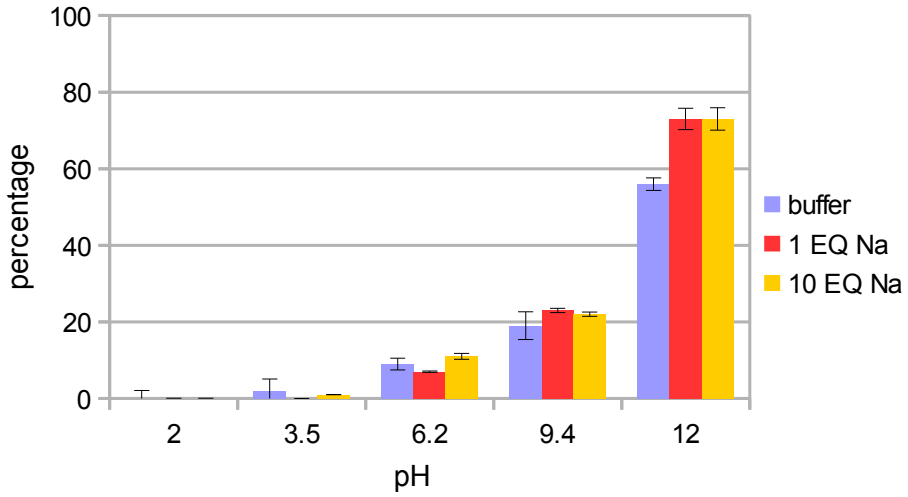

Figure 9.20: Percentage of total 12N4Py4 in octanol phase dependent on sodium content

9.9.2 Influence of Uranium

During the attempt to synthesise U(IV) complexes (chapter 7) it was suspected that the oxidation to U(VI) was at least partially responsible for the absence of any paramagnetic complex. The same oxidation would be expected under the conditions used throughout the extraction study and formation of U(IV) complexes would be impossible. It can however not be excluded that the uranyl ion might have its own way to influence extraction of the ligand. A sample series of buffered 12N4Py4 solutions was prepared with 1 equivalent of UCl_4 and extracted with octanol and hexane.

At very low pH, as encountered in traditional PUREX procedures, uranium is in an equilibrium with U(IV) and uranyl(VI) as the main species. In the pH range between 2.0 and 12.00 the U(VI) core dominates, forms however a complex system of hydrolysis species (see Figure 9.21) and combinatory species with various anions.[23]

The figure originally presented here cannot be made freely available via ORA because of copyright. The figure was sourced from "Hydrolysis of Metal Ions" by P. L. Brown and C. Ekberg (Wiley)[23]

Figure 9.21: Predominance diagram for U(VI)O_2 speciation.

Speciation is highly dependent on concentrations and counter ions, as can be seen from Figure 9.21. In the presence of buffer it is therefore highly likely that speciation will be different to literature values.

Without the consideration of interaction with buffer anions and the ligand, it could be assumed that at pH 2.0 and 3.5 the unhydrolysed UO_2^{2+} is predominant. At pH 6.2 the diagram suggests the formation of a precipitate of $UO_3 \bullet 2H_2O$. No precipitate would be expected for pH 9.4 and 12.0, instead $UO_2(OH)_3^-$ would be found, along with some $UO_2(OH)_4^{2-}$ at pH 12.0.

In hexane extractions (Figure 9.22) it was found that the presence of uranium slightly decreases the extraction of the free ligand at pH 12.0.

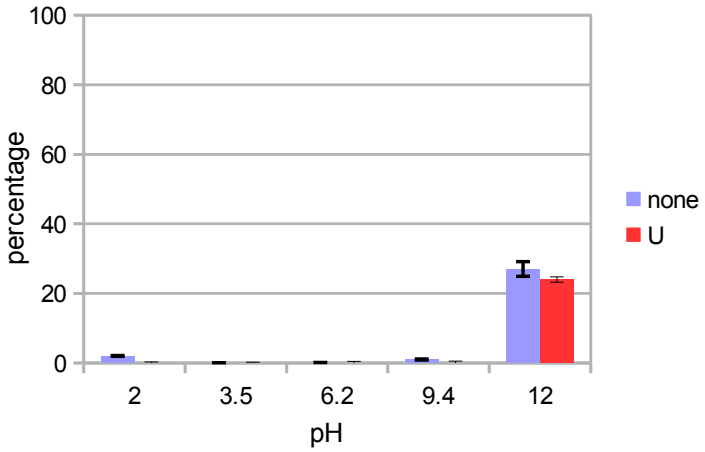

Figure 9.22: Percentage of total 12N4Py4 in hexane phase with and without uranium added content

Meanwhile in the octanol extraction series (Figure 9.23), very little influence of the uranyl ions is observed on the extraction at lower pH values (2.0 - 6.2). At pH 9.4 the 12N4Py4 concentration decreases and then increases at pH 12.0. The samples were further analysed by fluorescence emission. In hexane emission was observed to be very weak, which is also the case in the absence for baseline measurements of the ligand. The very apolar solvent allows for little or no hydrogen bonds to establish that would involve the ligands lone pair of the pyridylic nitrogens, making it more likely that excited electrons return to the ground state via non-radiative routes. In octanol emissions were recorded that correspond to protonated and deprotonated ligands, no changes or additional emissions were

found.

In the aqueous phase the ligand emission had been established as being very weak and heavily influenced by the presence of impurities that very commonly absorb and emit at very similar wavelengths. A weak emission was observed in the region where 12N4Py4 was established to emit (400-475 nm). Additionally, a pattern of sharp signals was found at longer wavelengths (Figure 9.24). The signal maxima at 502, 548 and 574 nm show great similarity to reported spectra of uranyl species in aqueous media.[24] At higher pH the peaks broaden and the pattern becomes less obvious, in agreement with the literature.[24] It can therefore be deduced that U(IV) is in fact oxidised in solution to the uranyl ion. The absence of the fluorescence signals in the organic phase further suggest that it does not coextract with 12N4Py4.

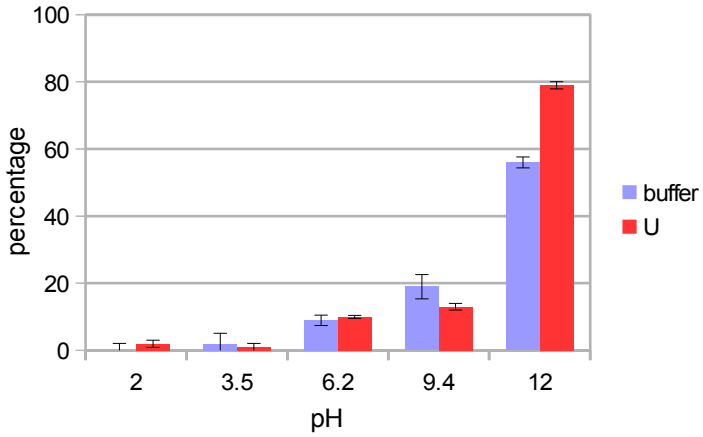

Figure 9.23: Percentage of total 12N4Py4 in octanol phase with and without uranium added content

While 12N4Py4 is not thought to complex uranyl ions for steric reasons, other components of the solution, such as buffer anions, might

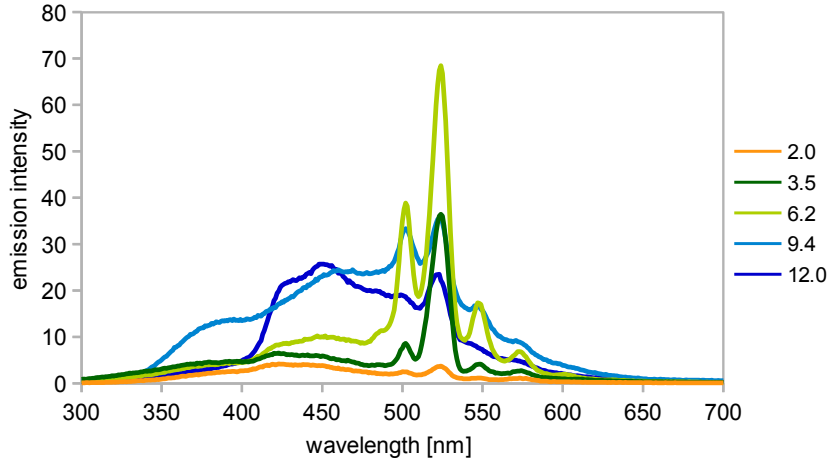

Figure 9.24: Emission from aqueous phase in hexane extraction in presence of uranyl ion (λ_{ex} = 260 nm).

coordinate to the metal ion. This might reduce their respective interactions with 12N4Py4, causing the observed changes in extraction.

In general, it can be deduced that uranyl will not compete with minor actinides and lanthanides for 12N4Py4. It should however be considered how uranyl might change conditions in solvents that indirectly affect extraction of ligand and complexes.

9.10 Discussion of the method

Extraction is most commonly described with partition ratio, also often named partition coefficients, the ratio of concentrations of a species between two extraction phases.[19] Best known is probably the octanol-water partitioning coefficient P_{ow} (or K_{ow}).[7] In order to measure P_{ow} data accurately it is essential to be able to measure concentrations of individual species. This was not always possible for this study, as different species of 12N4Py4 tend to give highly similar UV absorptions. An alternative measure is the D_{ow} (or more generally D), a distribution coefficient that defines the ratio between solvents of several species that are derived from one compound.[25]

Both P_{ow} and D_{ow} constants range very widely and are often expressed on a logarithmic scale. To ensure a high accuracy when performing their determination it is essential to also measure concentrations when the partition coefficient is very large or very small. With UV-absorption as the chosen method this would require to repeat the measurement at different total concentrations. Additionally in this study it was not always possible to determine the exact composition of species observed. The main purpose of this study was to establish compounds and combinations that have a drastic influence on extraction, but the exact quantification would require a different

approach. Therefore it was decided not to use a partition coefficient when extraction was discussed.

The experimental methods also deviate somewhat from standardised procedures for partitioning studies. Often extraction samples are agitated to facilitate phase transfer. In order to ensure equilibration of metal complexation reactions, samples had to be prepared 7 days prior to measurement. It was assumed that the extraction process is considerably faster and the partition would therefore equilibrate in this time frame without stirring or shaking.[26] Air tight vials were chosen for the experiment to ensure stable conditions.

Alternative methods to study lipophilicity and partitioning such as chromatography[27] or solvent specific determination of solubilities[26] were not used, as they were not expected to be able to reflect extraction conditions and weak interactions between components adequately.

Extraction of minor actinides and other metal species are often followed by isotope or element specific measurements such as gamma spectroscopy, liquid scintillation counting or atomic absorption spectroscopy. For this study the former two methods were able to give insight into some unexpected effects.

Instead, structure dependent properties have to be used for the monitoring of all species. NMR would be most specific and would allow more accurate distinction between species, but requires high concentrations where solubility limits become an issue. This leaves electronic transition spectroscopy. Luminescence was less useful as previously anticipated, and could only be used as supplementary source of information. UV-Vis measurement is one of the more established methods for detection of organic species in partitioning experiments.[26] It is relatively accurate, the

absorption is however not perfectly linear to the concentration and does change for different species. For this system however the changes are also not strong enough to clearly distinguish species from each other, like protonated ligand and metal complexes. Nevertheless it proved to be a useful tool in determining relative extraction efficiencies for different conditions and gave some insight into interactions of species.

It has to be mentioned that this study is not and does not attempt to provide quantitative data concerning the partitioning of species, but aims to provide a qualitative understanding of how compounds might respond to different conditions and to point out interactions that would need to be understood in depth for the development of an applicable extraction procedure.

9.11 Summary of findings

In this study it was established that the free base of 12N4Py4 ([L]) extracts well into both investigated solvents, hexane and octanol. At lower pH extraction becomes less likely with increasing protonation degree and ceases to be of significance for [LH_3] and [LH_4].

For the metal complexes with di- and trivalent metals (Ca(II) and Nd(III)) extraction was found to be very limited due to their charge density. For both protonated ligand and complexes, extraction was highly dependent on the available anions. Modifications of the ligand or addition of more lipophilic counter ions might be able to increase the solubility of M(III)-12N4Py4 complexes to make extraction in minor actinide separations more effective.

Many ions, including uranyl, change extraction efficiencies indirectly by modifying the

solvent structure of the phases.

Sodium was found to bind strongly to the ligand at high pH values and is expected to effectively compete with f-elements for ligands. Depending on pH and sodium content of the raffinate this could significantly decrease extraction in minor actinide separations.

Problematic ion pairs were found in K(I)-12N4Py4 perrhenate, which had low solubility in both water and apolar solvents, and [LH] pertechnetate, which showed an extraction into octanol exceeding any other ion pair at a 1:1 ratio.

In order to develop appropriate extractants for procedures in nuclear reprocessing, the system could be adjusted at several points. The ligand does so far not contain any functionalities to specifically increase lipophilicity. Addition of aliphatic substituents is expected to considerably change extraction behaviour. Anionic phase transfer reagents and solvent modifiers could be used to adjust solvent properties and cationic complex solubilities to achieve effective extraction and separation. The ligand could also be modified to allow one or two anions to coordinate directly to the metal ion, which would decrease overall charge and increase lipophilicity. Most effectively this would remove donor sites of the ligand from the metal and would be specific for certain anions that do not interfere with further processing.

Modifications of the system are however also highly dependent on the sequence of separations that determine conditions and contaminant that need to be considered.

References

[1] P. D. Wilson, Ed. , *The Nuclear Fuel Cycle: From Ore to Waste*, Oxford University Press, Oxford; New York, **1996**.
[2] C. Madic, O. Courson, R. Malmbeck, K. Römer, G. Pagliosa, B. Sätmark, J.-P. Glatz, P. Baron, **1998**.
[3] G. Sun, X. Cai, J. Han, Y. Li, Y. Zhang, T. Yang, Y. Cui, *J. Radioanal. Nucl. Chem.* **2016**, *308*, 753–757.
[4] S. Trumm, A. Geist, P. J. Panak, T. Fanghänel, *Solvent Extr. Ion Exch.* **2011**, *29*, 213–229.
[5] M. Carrott, A. Geist, X. Hères, S. Lange, R. Malmbeck, M. Miguirditchian, G. Modolo, A. Wilden, R. Taylor, *Hydrometallurgy* **2015**, *152*, 139–148.
[6] K. Bell, A. Geist, F. McLachlan, G. Modolo, R. Taylor, A. Wilden, *Procedia Chem.* **2012**, *7*, 152–159.
[7] J. Sangster, *J. Phys. Chem. Ref. Data* **1989**, *18*, 1111–1229.
[8] N. K. Pandit, *Introduction to the Pharmaceutical Sciences*, Lippincott Williams & Wilkins, Baltimore, MD, **2007**.
[9] R. P. Schwarzenbach, P. M. Gschwend, D. M. Imboden, *Environmental Organic Chemistry*, Wiley, Hoboken, N.J, **2003**.
[10] J. Chen, S. Wang, *J. Radioanal. Nucl. Chem.* **2007**, *273*, 59–63.
[11] A. Geist, *Solvent Extr. Ion Exch.* **2010**, *28*, 596–607.
[12] T. B. Field, J. Coburn, J. L. McCourt, W. A. E. McBryde, *Anal. Chim. Acta* **1975**, *74*, 101–106.
[13] D. D. Van Slyke, *J. Biol. Chem.* **1922**, *52*, 525–570.
[14] H. T. S. Britton, R. A. Robinson, *J. Chem. Soc.* **1931**, 1456–1462.
[15] M. Hesse, H. Meier, B. Zeeh, *Spektroskopische Methoden in der organischen Chemie: 102 Tabellen*, Thieme, Stuttgart, **2005**.
[16] L. D. S. Yadav, *Organic Spectroscopy*, Kluwer; Anamaya Publishers, Dordrecht [Netherlands]; Boston: New Delhi, **2005**.
[17] A. G. Motten, A. L. Kwiram, *Chem. Phys. Lett.* **1977**, *45*, 217–220.
[18] F. Toda, S. Hyoda, K. Okada, K. Hirotsu, *J. Chem. Soc. Chem. Commun.* **1995**, 1531.
[19] N. M. Rice, H. M. N. H. Irving, M. A. Leonard, *Pure Appl. Chem.* **1993**, *65*, 2373.
[20] L. A. Ferreira, A. Chervenak, S. Placko, A. Kestranek, P. P. Madeira, B. Y. Zaslavsky, *RSC Adv* **2015**, *5*, 20574–20582.
[21] D. H. Ripin, D. A. Evans, "Evans pKa table," can be found under http://evans.rc.fas.harvard.edu/pdf/evans_pKa_table.pdf, accessed 16.6.2017, accessed 16.6.2017.
[22] D. Delacroix, *Radionuclide and Radiation Protection Data Handbook 2002*, Nuclear Technology Publishing, Ashford, Kent, **2002**.
[23] P. L. Brown, C. Ekberg, *Hydrolysis of Metal Ions*, Wiley-VCH Verlag GmbH & Co. KGaA, Weinheim, **2016**.
[24] K. Müller, V. Brendler, H. Foerstendorf, *Inorg. Chem.* **2008**, *47*, 10127–10134.
[25] R. A. Scherrer, S. M. Howard, *J. Med. Chem.* **1977**, *20*, 53–58.
[26] J. C. Dearden, G. M. Bresnen, *Quant. Struct.-Act. Relatsh.* **1988**, *7*, 133–144.
[27] K. Valkó, *J. Chromatogr. A* **2004**, *1037*, 299–310.

Chapter 10: Comparison & Conclusion

10.1 12N4Py4 in aqueous and extraction systems

In this project a variety of aspects of the behaviour of 12N4Py4 in solution have been analysed and discussed, many of which have consequences for potential industrial application and importance that extends beyond this system. In this section the different equilibria are brought together to paint a more complete picture of the system under conditions relevant for extraction. Scheme 10.1 shows the complete system as it was established in this project.

Chapter 2 of this thesis concentrated on establishing the synthesis and properties of 2 ligands, 12N4Py4 and 9N3Py3. The latter soon proved to be of limited interest, as it is not capable of binding lanthanides effectively. 12N4Py4 ([L]) was therefore the main focal point of further research. Its amine donor set was expected to show affinity towards trivalent actinides, they do however also act as bases in an aqueous solution. The basicity of 4 of the 8 amine functionalities was measured in **chapter 3**, employing back titrations and a fitting procedure[1] that allows determination of incompletely measured and overlapping pK_as (light blue frame). As the ligand is expected to bind actinides in extraction conditions, it was further studied how the free base and protonated species distribute between the aqueous and organic phases (light/dark blue dashed frames, **chapter 9**) and found that the free base is well extractable into solvents of different polarity. In the absence of an organic phase its aqueous solubility is low (dark blue frame). Protonated species of lower charge do extract into polar organic solvents as well, an equilibrium that will reduce the extraction efficiency of f-elements.

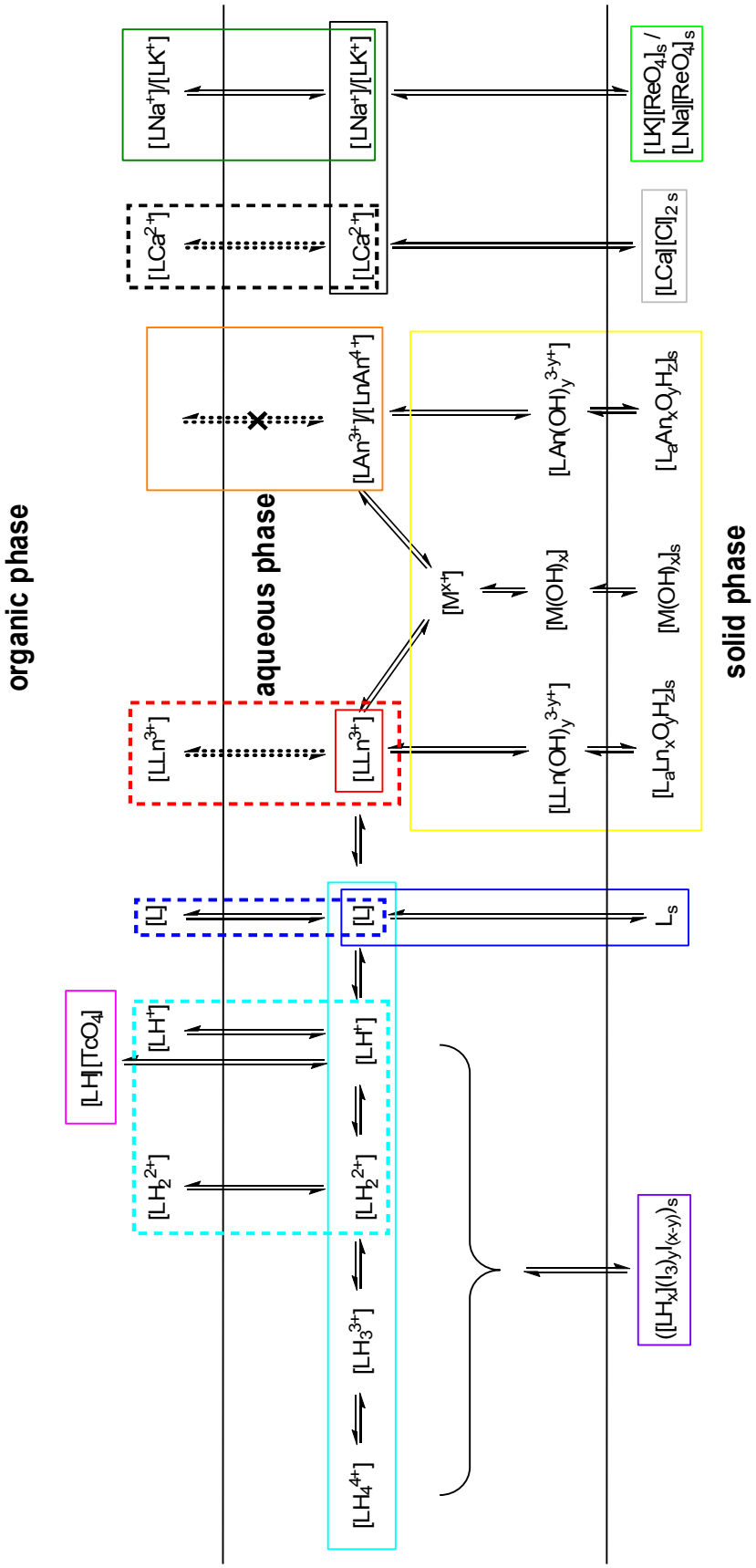

Scheme 10.1: Equilibria of 12N4Py4 investigated in this project

Pertechnetate, an anion that is known to contaminate extracts of PUREX processes, was found to show a strong affinity towards protonated amine species and form precipitates (**chapter 8**) or highly lipophilic ion pairs (pink frame, **chapter 9**). Iodide, which was studied as a model of pertechnetate due to its similar size, and charge density, does not show the same strong response in solution. It was, however, found that triiodide salts of protonated 12N4Py4 are highly insoluble (purple frame, **chapter 8**). Triiodide is formed from iodide and iodine, which in is produced from iodide by oxidation. This interaction is not of particular concern for minor actinide separation, might however offer novel ways to trap radioactive iodine in earlier steps of nuclear reprocessing.

During the synthesis and characterisation of lanthanide complexes of 12N4Py4[2] (**chapter 4**) it became apparent that the Ce(III) complex has properties that differs from the other lanthanides due to d orbital involvement. The closeness in energy of the d and f orbitals, which is exploited in redox chemistry[3], allows emissive d-f transitions sensitised by the pyridyl chromophores of 12N4Py4 and influences the paramagnetic behaviour in NMR spectroscopy. Binding constants of three Ln(III) ions, Pr(III), Nd(III) and Yb(III) were determined using various methods (red frame, **chapter 5**, approximately $\log K_c$ = 6 - 8) and found to be large enough to compete with other extractants as described in section 10.1. Reaction kinetics were established to be very slow, which would be a significant problem in industrial applications due prolonged procedures and associated radiolysis.

Extraction into organic solvents of the neodymium complex (dashed red frame, **chapter 9**) was found to be very low due to it being a highly charged species and only detectable when lipophilic anions (triflate) were available without the competition

of more hydrophilic anions (buffer agents).

Uranium complexes of 12N4Py4 could not be synthesised under ambient conditions, as the non-spherical uranyl ion (UO_2^{2+}) faces sterical hindrance and U(IV) was found to hydrolyse in the provided conditions (**chapter 7**).

Am(III) was studied in a collaboration with *NNL* in Sellafield. Limited means of detection however meant that the existence of Am(III)-12N4Py4 could not be verified. In extraction experiments (orange frame, **chapter 9**), no uptake of the metal into organic solvents was measured at ambient to slightly acidic pH.

Both lanthanide and actinide ions are prone to hydrolysis even in the presence of small amounts of hydroxide, provoking precipitation (yellow frame, **chapters 4, 5** and **7**). This significantly limits the conditions where complexation to 12N4Py4 may take place and is proposed to be part of the reason no Am(III) complexation was observed. Beside simple lanthanide hydroxide species, it is also feasible that 12N4Py4 capped hydroxides form, the insolubility of the compounds however severely limits means for structure determination (solid state ^{13}C-NMR, **chapter 4**) and precise structures could not be elucidated.

Other metal cations are known to bind to 12N4Py4[4,5], two of which, Ca(II) and Na(I) were compared to the lanthanide complexes. Their non-paramagnetic character allowed a better understanding of lanthanide behaviour (**chapter 4**). Binding strengths were determined for both (black frame, **chapter 5**), showing that Ca(II) forms complexes of higher stability ($\log K_c$ = 10 - 12) than the lanthanides , whereas the larger Na(I) ion competes less effectively with protonation ($\log K_c$ = 2 - 5) and only forms at high pH. Ca(II)-12N4Py4 was shown to behave similar to lanthanide complexes in solid state (crystal structure WTS02), aqueous equilibrium (**chapter 4**)

and extraction (black dashed frame, **chapter 9**), where uptake into organic solvents was only observed with triflate in absence of competition of other anions. The calcium complex was also found to have reduced solubility in aqueous solutions at ambient temperature (grey frame).

Even though the sodium ion binds less strongly to 12N4Py4, its low charge allows efficient extraction into polar solvents (dark green frame, **chapter 9**). Crystal structure WTS03 also showed that perrhenate forms Na(I)-12N4Py4 salts of low solubility (light green frame, **chapter 8**). Potassium had been assumed to show insignificantly small binding constants to 12N4Py4, addition of perrhenate however similarly provoked precipitation in the absence of polar non-aqueous solvents. Both calcium and sodium are neither fission nor decay products in nuclear fuel, but are likely to be introduced into processing from various sources, commonly water. Their effective competition with f-elements for ligands in aqueous solution (Ca(II)) and extraction environments (Na(I)) significantly lowers extraction yields of the f-elements. Precipitation would also be a major issue as they interfere with the function of the separation equipment and phase separation.[6] Perrhenate content in raffinates used for minor actinide separations would however depend on the sequence of separation and extractants used in previous steps.

Extraction of any charged species across a phase boundary requires the coextraction of counter ions. The effect of various anions on the presented cationic species was investigated. Beside the highly specific pairings discussed above, most anions were found to indirectly affect extraction by modification of solvent structure and polarity.

9N3Py3 was found not to form Ln(III) complexes (**chapter 6**), a Ca(II) complex was however isolated and characterised. It was the first example of a TACN based

calcium complex of which a crystal structure was obtained. Binding in aqueous solutions was found only to be significant in the presence of large excesses of the metal. Low acid stability and low solubility of the free base required the development of a fitting procedure tailored to the system, that produced both pK_a and metal binding constant K_c of high quality.

Over the course of this project several phenomena were observed that require more detailed understanding, such as the structures of lanthanide hydroxide precipitates with ligand and the unidentified blue technetium compound. Also the full potential of iodine trapping with pyridine compounds was not evaluated. Binding mechanisms of anions and their effect on the complex geometry and electronic structure for lanthanide and other metal complexes would also be of interest for other fields.[7]

12N4Py4 proved to be a valuable model for lanthanide and actinide binding and extraction that revealed several side reactions of consequence for industrial application. Its properties could further be derivatised to better meet the requirements of conditions in future nuclear reprocessing.

10.2 12N4Py4 in comparison to other extractants

In the field of extractants for actinide-lanthanide separtions 12N4Py4 stands in competition with a multitude of other compounds and compound classes that have been developed and improved upon in the past decades. Several examples of these compounds are presented in this section and compared to 12N4Py4 in order to gain an estimate of its potential to be a next generation extractant.

Both 12N4Py4 and 9N3Py3 (Figure 10.1) have previously been studied in metal extractions, however with a focus on the binding of sodium.[5,8] Amongst several other functionalities it was found that macrocycles substituted with pyridyl groups were unexpectedly effective in binding and extracting the hard cation Na^+ across a dichloromethane liquid membrane.[5] Especially 9N3Py3 was found to show a strong selectivity for sodium over lithium and potassium. In comparison to several transition metal complexes of the ligand, Na(I)-9N3Py3 also showed a significantly higher extraction rate.

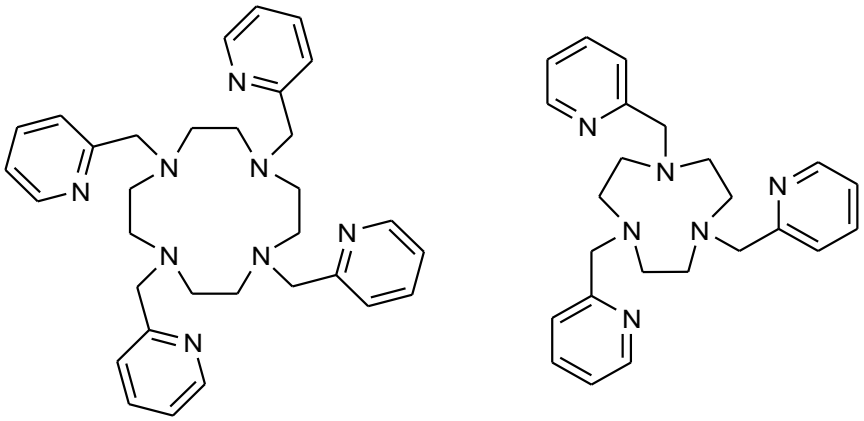

12N4Py4 **9N3Py3**

Figure 10.1: Structures of ligands 12N4Py4 and 9N3Py3.

Tsukube et al. also tested the larger macrocycles 12N4Py4, 14N4Py4 and 15N4Py4 (Figure 10.2) for their potential of transporting sodium ions across a dichloromethane liquid membrane.[5]

They found that these systems, as might be expected, became progressively less effective at extracting sodium as the ring size was increased. For actinide extractions it might be interesting to explore macrocycles of varying sizes to find an optimal fit for increased selectivity.

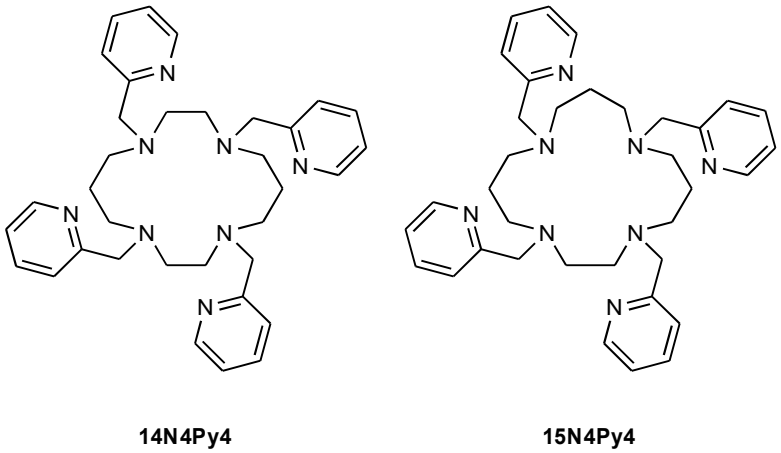

Figure 10.2: Structures of ligands 14N4Py4 and 15N4Py4

The increased stability provided by macrocyclic ligands compared to open chain ligands is widly explored in synthetic inorganic chemistry. But in the field of minor actinide separation macrocycles are not so well represented, which is linked to higher prices for macrocyclic compounds and precursors. 12N4Py4 offered a unique insight into a potential new class of macrocyclic extractants with higher binding strength.

Two open chain ligands with a close similarity to 12N4Py4 are TPA (tris(2-pyridylmethyl)amine) and TPEN (N,N,N',N'-tetrakis(2-pyridylmethyl)ethylenediamine) (Figure 10.3). Both have been intensly explored for their potential in minor actinide separations.[9–13]

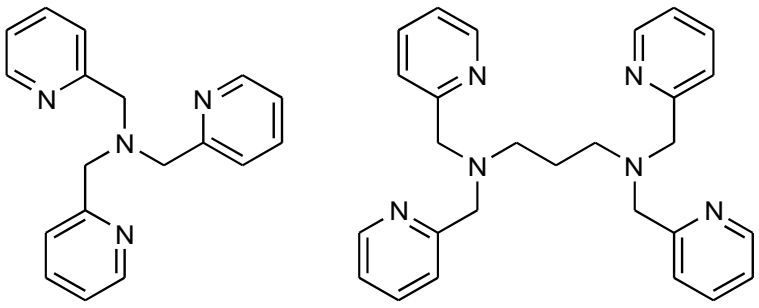

Figure 10.3: Structures of ligands TPA and TPEN

The pK_a values of the larger TPEN have been determined to be approx. 7.2, 4.9, 3.3

and 3.0.[11] They are generally somewhat smaller than the ones determined for 12N4Py4, highlighting the possibility of cyclen to stabilise a proton between two nitrogens, increasing the pK_a. TPEN offers only 6 binding sites, decreasing binding strength to around logK = 3.5 for the lanthanides. Actinides bind with equilibrium constants of around logK = 6.7, showing the expected increase in stability due to covalent contributions of the actinide elements.12N4Py4 with a binding strength of 6-8 for the lanthanides is a significantly stronger chelator, which might however be an effect of a larger number of binding sites.

The thermodynamic factors measured for TPEN are also of interest for the comparison to the ligands discussed in this thesis. Enthalpy values (around 10 kJ/mol) are lower than was found for the equally hexadentate 9N3Py3 (51.9 kJ/mol for Ca(II)), which is attributed to the absence of the macroyclic effect and the lower hydration enthalpy of the earth alkali metals.[14] Entropy contribution is lower (51-55 J/molK vs 226 J/molK for Ca(II)-9N3Py3) but still a low positive value. In chapter 6 it was discussed if the hydration of the metals might be used to control complexation of metals. Jensen et al.[11] also suspected the hydration sphere of the metal to play an important role in the overall entropically controlled complexation reaction. They have found however very similar entropy contribution for both actinides and lanthanides. A more significant contribution to the absolute value of the entropy appears to be the hydration of the ligand, that significantly changes upon complexation. Differences in hydration between actinides and lanthanides only come into play within a set of very similar ligands. It suggests that entropy might not be useful to control selectivity of one metal over another, but could still be exploited to control complexation strength through temperature.

TPEN was found to transport sodium across liquid membranes, however it showed no selectivity between different alkali and transition metals.[5] Its open structure does not allow selectivity for metals based on small size differences, which is a clear advantage of the macrocyclic 12N4Py4 and 9N3Py3.

The smaller TPA ligand only offers 4 binding sites, is however small enough to form 2:1 complexes,[10,12,15] increasing the total amount of binding sites to 8. Binding strengths determined in acetonitrile of individual steps of ligand association were of intermediate strength ($\log K_c$ approx. 7.5 and 5.2), in combination the 2:1 complex however shows a very high binding strength (12.7).[10] The 1:1 complex with U(III) was synthesised and it was found that no reduction of the ligand occured and the complex was stable over time in strictly anhydrous conditions.[12]

Measurements of binding strength are dependent on the solvent, making it important to know binding strengths in solvents relevant for the application. Values from different solvents can not be compared directly, it is however likely that for the hydrophilic lanthanides binding strength in water will be weaker than in non-aqueous solvents. 12N4Py4 therefore can be expected to show stronger complexation compared to the TPA 1:1 complex and maybe even the 1:2 complex.

Indeed, in aqueous conditions TPA was found to only form the 1:1 complex at a reduced binding strength (logK approx. 2).[16] Excess of ligand did cause hydrolysis of the comples to form dinuclear hydroxo species of the lanthandides, the second equivalent of TPA aiding hydrolysis by binding the formed proton.[9] A crystal structure determination confirmed the formation of $(EuTPA(\mu\text{-}OH)(OTf)_2)_2$ With trivalent uranium oxidation and hydrolysis was observed to give $(U(IV)TPA(\mu\text{-}O)I)_3$. This observation of course makes TPA a significantly less valuable extractant in nuclear

reprocessing. Hydrolysis of lanthanides was also observed for 12N4Py4, was however found to be pH dependent.

Intense studies of TPA nevertheless gave a lot of insight into the effects of small structural changes. Insertion of methyl groups on the pendant arms to increase sterics generally lead to a reduction of binding strength.[10] This is essential to know if ligands are to be fine tuned to extraction applications by addition of lipophilic functionalities and will have to be considered if 12N4Py4 was to be modified to achieve better partition coefficients in extractions.

It was also found that NMR signals of the TPA complexes show no splitting pattern for CH_2 groups,[12] indicating a certain flexibility of the ligand not observed in the rigid macrocyclic ligands.

The motif to use smaller ligands to form 2:1 complexes has also been explored with other ligands. ADPTZ (2-amino-4,6-di-(pyridin-2-yl)-1,3,5-triazine, Figure 10.4) uses three heteroaromatic nitrogens to coordinate to metals.[17] The amine functionality is the most likely first point of protonation, as it is not part of the coordination set this is not in direct competition with complexation and further decreases basicity of the remaining nitrogens. Binding strength of the tridentate ligand and its derivatives are relatively low ($\log K_c$ 3.6 to 4.6) for lanthanides but do show selectivity towards actinides. Enthalpy of the complexation is negative but very low, entropy contributions are very similar to previously discussed systems. 1:3 complexes are formed to achieve the high coordination numbers prefered by f-element ions, ligands with higher coordination numbers like 12N4Py4 however have the advantage of a

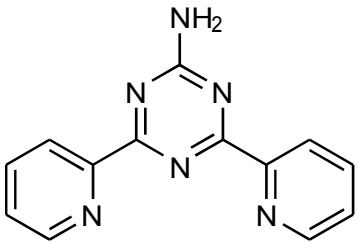

ADPTZ

Figure 10.4: Structure of ADPTZ

stronger chelate effect (stronger binding of polydentate ligands).

An alternative ligand, TPTZ (2,4,6-tripyridyl-s-triazine) (Figure 10.5) offers the same number of binding sites, but has three equivalent ways to coordinate.[18] In extraction studies it showed very good separation factors for Americium over Europium. Distribution ratios however were very low. Lipophilicity was increased by the addition of aliphatic substituents. It was found that one long carbon chain produces preferable extraction properties compared to multiple shorter ones.

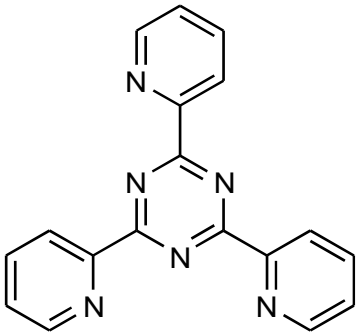

TPTZ

Figure 10.5: Structure of TPTZ

Another class of pyridyl based extractants are BTBP ligands (bis-triazine-bipyridines, Figure 10.6). They have four binding sites, two of which are either the 2 or the 4 position of the triazine. In crystal structures it was found that lanthanides prefer the 4 position.[19] In comparison to tridentate ligands such as TPTZ the BTBPs show a significantly higher stability towards radiolysis and hydrolysis.[20] Binding strengths in 1:1 complexes are lower that for the octadentate 12N4Py4 (log K_c 4 - 6) but for the 1:2 complex higher binding strengths were observed (logK_c 8-12).[20] BTBP ligands have been found to show good separation factors but very low solubility in organic solvents.[21] These were however improved upon addition of lipophilic substituents. Reaction kinetics were slow, but could be greatly increased with the use of phase transfer agents.[22]

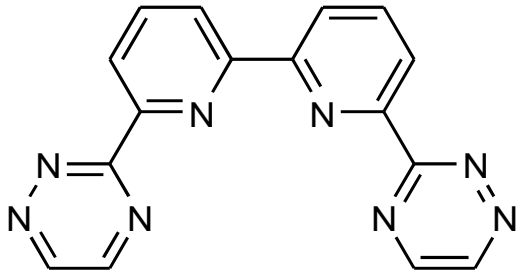

BTBP

Figure 10.6: Structural motif of BTBP ligands

Preorganisation is one major factor known to increase binding strength and complexation kinetics. BTBP in solution rotates freely around the central bipy bond. In order to preorganise the ligand in favour of the complexation conformation, this bond was fixed in place by addition of a phenyl group, giving rise to BTPhen ligands (Figure 10.7) with the hope to increases overall binding strength in the lanthanide complexes as well as extraction kinetics.[22] BTPhens (logK 4 - 8 for 1:1, 11 - 16 for 1:2) and BTBPs (logK 6 - 11 for 1:1, 12 - 19 for 1:2) show higher binding strengths to lanthanides than 12N4Py4, measurements however are based on methanolic solutions.[23] The decrease of binding strength from BTBP to BTPhens were attributed to a mismatch in size for the lanthanide ions, which can be counter acted by the flexibility of the BTBP back bone. Both ligands have been extensively tested in various conditions and are among the most promising candiates for future industrial applications.

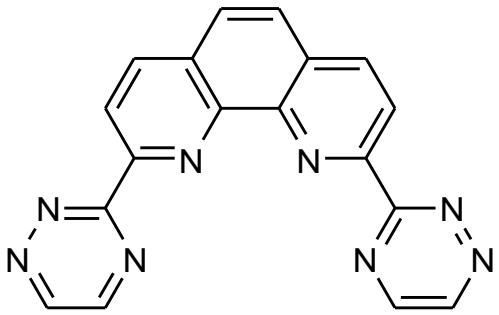

BTPhen

Figure 10.7: Structural motif of BTPhen ligands

BTPhens have even been modified and attached to nanoparticles[24], allowing novel ways of removing actinide ions from solution, which might be interesting in smaller scale applications.

Whereas the properties of BTBP and BTPhen ligands meet the requirements for effective minor actinide separtion, their synthesis is often elaborate and requires multiple reaction steps, making the end product very expensive. Even though cyclen is not considered a particularly cheap starting material, it can be produced in bulk and the synthesis of 12N4Py4 is quick and high yielding. Increase in demand might

be able to further lower the cost of production.

Overall it was shown that 12N4Py4 shows lanthanide binding constants comparable to that of other extractant classes and is expected to show the same affinity towards trivalent minor actinide ions.

Binding strength of extractants are frequently determined in non-aqueous solvents, it was however found that they cannot be directly translated to aqueous systems. The use of alternative solvents offers the advantage that hydroxide formation and protonation largely does not need to be considered, which might be a preferable method to further investigate Am(III) binding. It was however also established in this project that fitting procedures developed specifically for the system at hand enable the simultaneous determination of several equilibria in aqueous systems.

The presence of tertiary amines in 12N4Py4 besides nitrogen heteroaromatic binding sites increases basicity of the ligand, requiring higher pH for quantitative complexation. Precipitation of hydroxides become an issue for both lanthanides and actinides at high pH. For extraction application however it might be viable to operate at lower pH and allow competition with protonated ligand in order to achieve effective separation of the minor actinides.

With its macrocyclic nature and the pronounced size selectivity, 12N4Py4 is not only a good model for the study of metal binding and extraction in conditions relevant for industrial application, but it has also proven to be a strong competitor in the field of extractants for minor actinide separations.

References

[1] A. Kraft, *J Chem Educ* **2003**, *80*, 554.
[2] L. S. Natrajan, N. M. Khoabane, B. L. Dadds, C. A. Muryn, R. G. Pritchard, S. L. Heath, A. M. Kenwright, I. Kuprov, S. Faulkner, *Inorg. Chem.* **2010**, *49*, 7700–7709.
[3] P. Jacob, P. S. Callery, A. T. Shulgin, N. Castagnoli, *J. Org. Chem.* **1976**, *41*, 3627–3629.
[4] H. Ito, H. Tsukube, S. Shinoda, *Chem. - Eur. J.* **2013**, *19*, 3330–3339.
[5] H. Tsukube, K. Yamashita, T. Iwachido, M. Zenki, *J. Chem. Soc. [Perkin 1]* **1991**, 1661.
[6] P. D. Wilson, Ed. , *The Nuclear Fuel Cycle: From Ore to Waste*, Oxford University Press, Oxford; New York, **1996**.
[7] O. A. Blackburn, A. M. Kenwright, A. R. Jupp, J. M. Goicoechea, P. D. Beer, S. Faulkner, *Chem. – Eur. J.* **2016**, *22*, 8929–8936.
[8] H. Tsukube, Y. Mizutani, S. Shinoda, T. Okazaki, M. Tadokoro, K. Hori, *Inorg. Chem.* **1999**, *38*, 3506–3512.
[9] L. Natrajan, J. Pécaut, M. Mazzanti, C. LeBrun, *Inorg. Chem.* **2005**, *44*, 4756–4765.
[10] T. Yamada, S. Shinoda, H. Sugimoto, J. Uenishi, H. Tsukube, *Inorg. Chem.* **2003**, *42*, 7932–7937.
[11] M. P. Jensen, L. R. Morss, J. V. Beitz, D. D. Ensor, *J. Alloys Compd.* **2000**, *303–304*, 137–141.
[12] R. Wietzke, M. Mazzanti, J.-M. Latour, J. Pécaut, *J. Chem. Soc. Dalton Trans.* **2000**, 4167–4173.
[13] L. . Morss, R. D. Rogers, *Inorganica Chim. Acta* **1997**, *255*, 193–197.
[14] D. W. Smith, *J Chem Educ* **1977**, *54*, 540.
[15] L. S. Natrajan, *Dalton Trans.* **2012**, *41*, 13167.
[16] F. Bravard, Y. Bretonnière, R. Wietzke, C. Gateau, M. Mazzanti, P. Delangle, J. Pécaut, *Inorg. Chem.* **2003**, *42*, 7978–7989.
[17] M. Miguirditchian, D. Guillaneux, D. Guillaumont, P. Moisy, C. Madic, M. P. Jensen, K. L. Nash, *Inorg. Chem.* **2005**, *44*, 1404–1412.
[18] Z. Kolarik, *Chem. Rev.* **2008**, *108*, 4208–4252.
[19] F. W. Lewis, L. M. Harwood, M. J. Hudson, M. G. B. Drew, J. F. Desreux, G. Vidick, N. Bouslimani, G. Modolo, A. Wilden, M. Sypula, et al., *J. Am. Chem. Soc.* **2011**, *133*, 13093–13102.
[20] V. Hubscher-Bruder, J. Haddaoui, S. Bouhroum, F. Arnaud-Neu, *Inorg. Chem.* **2010**, *49*, 1363–1371.
[21] P. J. Panak, A. Geist, *Chem. Rev.* **2013**, *113*, 1199–1236.
[22] F. W. Lewis, L. M. Harwood, M. J. Hudson, M. G. B. Drew, V. Hubscher-Bruder, V. Videva, F. Arnaud-Neu, K. Stamberg, S. Vyas, *Inorg. Chem.* **2013**, *52*, 4993–5005.
[23] D. M. Whittaker, T. L. Griffiths, M. Helliwell, A. N. Swinburne, L. S. Natrajan, F. W. Lewis, L. M. Harwood, S. A. Parry, C. A. Sharrad, *Inorg. Chem.* **2013**, *52*, 3429–3444.
[24] A. Afsar, L. M. Harwood, M. J. Hudson, P. Distler, J. John, *Chem Commun* **2014**, *50*, 15082–15085.

Experimental Part

General

Chemicals were purchased from various suppliers including *Sigma-Aldrich*, *Fisher Scientific*, *Acros Organics* and *Alfa Aesar* and used without further purification unless stated otherwise. Unless indicated, solvents were not dried before use. Water was purified with a *Millipore Elix Essential* system. Room temperature was between 18-22°C. Column chromatography was performed on silica (*Merck* Geduran® Si 60 (40-63 µm)) or basic alumina (*Sigma-Aldrich*, Brockmann I, standard grade, ~150 mesh, 58Å). pH was determined with pH indicator sticks (*Fisherbrand pH-Fix 0-14*). pH values were determined with a *Hannah instruments PH 211* microporcessor pH meter and a *Hannah instrument* NMR glass pH electrode.

NMR spectra were recorded on a *Bruker AVIII 400 nanobay* or a *Bruker AVIIIHD 500* instrument. Samples were prepared in deuterated solvents. Solid state spectra were recorded by Dr. Nick Rees on a *Bruker Avance III HD Solid state NMR* with a 9.4T magnet. Spectrum analysis was performed using *Topspin 3.2*. Chemical shifts (δ) are reported as ppm (parts per million), coupling constants (*J*) are reported in Hz (hertz). ^{1}H-NMR was referenced to the solvent signal using literature values.[1] ^{13}C-NMR was referenced to the solvent signal or left as processed by internal referencing procedure of the instrument for D_2O measurements. Multiplicities were determined using DEPT spectra. Full assignment of signals are based upon COSY, HSQC and HMBC spectra. Signals of paramagnetic compounds given as far as observed. Electron spray mass spectrometry (ESI-MS) was recorded using an *Agilent 6120* mass spectrometer equipped with *Agilent 1260 LC* pump and *CTC* autosampler.

Instrument control and data processing were performed using *Agilent Chemstation* software. A mixture of 10 % water, 89.9% methanol and 0.1% formic acid was used to transport samples to the mass spectrometer at a flow rate of 0.2 ml/min. Unit resolution was used throughout.

Accurate mass (HR-MS) service was provided by the Department of Chemistry. Analyses were performed on a Thermo Exactive mass spectrometer (*Waters LCT Premier XE* equipped with electrospray interface), equipped with *Waters Accquity* liquid chromatography system. Instrument control and data processing were performed using *Thermo Xcalibur* software. The instrument was operated using a heated electrospray (HESI-II) probe and resolution was set to 50'000 FWHM. A mixture of 10% water, 89.9% methanol and 0.1 % formic acid was used to transport samples to the mass spectrometer at a flow rate of 0.2 ml/min, injection volume was 5µl. Separation was achieved on a *Merck Chromolith* C18 2 x 5 mm guard column with a gradient of 95 % aqueous formic acid (0.1%)/5 % acetonitrile to 100% acetonitrile. Instrument control was perfomed with *Masslynx 4.1*. ICP-MS were analysed by the University of Manchester.

IR spectra were recorded on a *Bruker Tensor 27 FT-IR* spectrometer as neat samples and analysed using *Bruker OPUS Data Collection and Analysis* software or *Openoffice Calc 4.1.1*. Elemental analyses on carbon, hydrogen and nitrogen (CHN) were performed by Stephen Boyer at the London Metropolitan University. UV-Vis spectra were recorded on a *PG instruments T60U* baselined against the pure solvent or an empty cuvette. Luminescence spectra were recorded on a *Horiba Fluorolog-3 steady state Spectrafluorometer* at a slit width of 5 nm.

Low temperature[2] (150° K) single crystal X-ray diffraction was measured by Dr.

Lukas Pfeifer on a (Rigaku) Oxford Diffraction Supernova system using Cu radiation ((λ=1.54180) or a Nonius KappaCCD using Mo radiation (λ=0.71073), both of which were graphite-monochromated. Suitable crystals were chosen and mounted using the oil-drop method on a standard MiTeGen mount. The program suite *CrysAlis*^{Pro} or HKLCollect/DenzoSMN[3] was used for data collection, cell refinement and data reduction. Structures were solved using *Superflip*[4] and refined with CRYSTALS[5,6]. Where twinning was supsected, ROTAX[7] was used within CRYSTALS to investigate and apply a twin law as approppriate. Where disorder was identified it was treated in the usual fashion.[8] Hydrogen atoms were generally visible in the difference Fourier map towards the end of the refinement and treated in the usual manner[6] or as per details in the CIF file, Structures were solved and refined by Dr. Lukas Pfeifer and Dr. Amber Thompson. ORTEP representations were created with Mercury[9].

Structure illustrations and Schemes were made using *ChemDraw Professional*.

Experiments conducted at the National Nuclear Laboratory in Sellafield

^{243}Am is a radionuclide with a high specific activity. All experiments were performed in specifically designated laboratories, complying with British radiation safety regulations, within the *National Nuclear Laboratory (NNL)* in Sellafield, Cumbria. Stock solutions of ^{243}Am were obtained as aqueous hydrochloric acid solutions. Gamma spectroscopy was recorded with a *DSG HPGe* photon detector, *Model GC10*, connected to an *Ortec DSPEC jr.* digital gamma ray spectrometer operated using *Ortec GammaVision-32* software Version 6. Detectors were calibrated for energy, fwhm (resolution) and efficiency using mixed gamma nuclide reference standards (*QCY48* supplied by *HTSL*, traceable to national standards).

Luminescence spectroscopy: *Quantel Brilliant B* Nd:YAG laser (output of 1064 nm) was used to optically pump a tunable dye laser (*Quantel TDL-90*) after passing a second harmonic generator (532 nm output) and a third harmonic generator (355 nm output). The dye laser using a *Coumarin 500* dye was tuned to produce an output at around 510 nm. Fiber optics were used to connect the laser to the sample chamber. The spectrum was recorded using a *Acton SpectraPro 2500i* spectrograph combined with *Princeton instruments*, *ST-133 controller* and *Pi-Max Charged Coupled Device* (CCD) camera (0.500 m Imaging Triple Grating Monochromator). Data were collected within a gate width of 60 to 90 ns, with a 1.58 ns delay width. The instrument was controlled remotely using *Winspec* software. Daily mercury/argon (HgAR) wavelength calibration were performed prior to measurements. UV-Vis was recorded on a *Perkin Elmer Lambda 1050* connected to an external sample chamber with fiber optics. The instrument was controlled by *Perkin Elmer UV WinLab* software. All manipulations of radioactive compounds were performed by Dr. Tamara Griffiths and Dr. Sean D. Woodall under supervision of the presenting student.

Experiments conducted at the University of Zürich

^{99}Tc is a weak β-emitter. All experiments were performed in laboratories approved for working with low-level radioactive materials, complying with Swiss radiation safety regulations, in the radiochemistry facilities of the Chemistry Department of the University of Zürich. $[NH_4][^{99}TcO_4]$ was purchased from *Oak Ridge National Laboratory*. ^{1}H-NMR spectra were recorded on a *Bruker AV-400* spectrometer, δ in ppm rel. to solvent peak. Liquid scintillation counting was performed with a *Hidex 300 SL liquid scintillation counter* with a *Packard Ultimate Gold XR* scintillation cocktail.

UV-Vis spectrophotometry was performed with a *Analytik Jena Specord 250 Plus*. HPLC analyses were performed on a *Merck Hitachi LaChrom L 7100* pump coupled to a *Merck Hitachi LaChrom L7200* UV detector and a radio detector. UV-Vis detection was performed at 250 nm. The detection of radioactive ^{99}Tc compounds was performed with a Berthold LB513 radio detector equipped with a YG cell. Separations were achieved on a Macherey-Nagel C18 reversed-phase column (Nucleosil 10 lm, 250 4 mm) with a gradient of MeOH/0.1% CF_3COOH eluent and a flow rate of 0.5 ml/min. Gradient: 0% MeOH (t = 0 - 3 min); 0-25% MeOH (t = 3 - 3.1 min); 25% MeOH (t = 3.1 - 9 min); 25-34% MeOH (t = 9 - 9.1 min); 34-100% MeOH (t = 9.1 -18 min); 100% MeOH (t = 18 - 25 min); 100-0% MeOH (t = 25 - 25.1 min); 0% MeOH (25.1 - 30 min).

Synthesis and Characterisation

Ligands

(1,4,7,9-tetrapicolyl)-1,4,7,9-tetraazadocecane (12N4Py4)

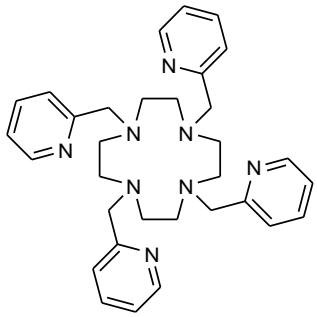

12N4Py4 was synthesised according to a literature procedure[10]: Cyclen (1 g, 5.8 mmol) was mixed with $CsCO_3$ (38 g, 116.6 mmol) and suspended in MeCN (30 ml). 2-picolylchloride hydrochloride (3.7 g, 22.6 mmol) was dissolved in MeCN (70 ml) and added dropwise to the cyclen mixture under nitrogen atmosphere. After complete addition, the mixture was heated to reflux. After 24h the mixture was filtered while hot to remove the inorganic salts. Evaporation of the red-brown solution gave a crude product that was purified by recrystallisation from hot MeCN. The product was obtained as slightly orange crystals (2.42 g, 4.5 mmol, 80 %).

Alternative procedure:

Cyclen (34 mg, 0.20 mmol) was dissolved in H_2O (0.5 ml) by addition of HCl (conc. 2 drops). 2-picolyl chloride hydrochloride (125 mg, 0.77 mmol) was dissolved in H_2O (1.5 ml) and added to the cyclen solution. A KOH solution (conc.) was added dropwise to adjust the pH to 11. After 4 hours, the formed precipitate was washed

with H_2O, dissolved in $CHCl_3$, dried over K_2CO_3 and evaporated to give 12N4Py4 (83.3 mg, 0.16 mmol, 83%) as a colourless powder.

^{1}H-NMR (400 MHz, $CDCl_3$): 8.47 (*dq*, *J*=4.9, 0.9, 4H, arom. CH); 7.69 (*d*, *J*=7.84, 4H, arom. CH); 7.42 (*t*, *J*=7.65, 4H, arom CH); 7.08 (*t*, *J*=4.13, 1.10, 4H, arom. CH); 3.63 (*s*, 8H, arm CH_2); 2.77 (*s*, 16H, ring CH_2).

^{1}H-NMR (400 MHz, MeOD): 8.39 (*dq*, *J*=5.0, 0.8, 4H, arom. CH); 7.74 (*d*, *J*=7.8, 4H, arom. CH); 7.60 (*td*, *J*=11.5, 1.6, 4H, arom. CH); 7.23 (*m*, 4H, arom. CH); 3.59 (*s*, 8H, arm CH_2); 2.76 (*s*, 16H, ring CH_2).

^{13}C-NMR (126 MHz, $CDCl_3$): 160.43 (*s*, arom. C); 149.01 (*d*, arom. CH); 136.31 (*d*, arom. CH); 123.01 (*d*, arom. CH); 121.79 (*d*, arom. CH); 61.81 (*t*, arm CH_2); 53.61 (*t*, ring CH_2).

^{13}C-NMR (126 MHz, MeOD): 161.2 (*s*, 4C, arom C); 149.3 (*d*, 4C, arom. CH); 138.4 (*d*, 4C, arom CH); 124.9 (*d*, 4C, arom. CH); 123.5 (*d*, 4C, arom. CH); 62.2 (*t*, 4C, arm CH_2); 54.4 (*t*, 8C, ring CH_2).

ESI-MS: 269.3 (100, $[M+2H]^{2+}$); 537.3 (35, $[M+H]^+$); 559 (18, $[M+Na]^+$).

Elemental analysis: calc. for $C_{32}H_{40}N_8$: C, 71.61; H, 7.51; N, 20.88. Found: C, 71.78; H, 7.64; N, 20.84.

IR (neat): 2948 (*w*), 2929 (*w*), 2912 (*w*), 2823 (*m*), 2795 (*m*), 2361 (*m*), 2338 (*m*), 1588 (*s*), 1567 (*m*), 1473 (*m*), 1433 (*s*), 1363 (*m*), 1308 (*m*), 1288 (*w*), 1245 (*w*), 1154 (*w*), 1134 (*w*), 1097 (*m*), 1075 (*s*), 1047 (*s*), 1014 (*w*), 986(*s*), 930(*m*), 830(*w*), 808(*m*), 773(*m*), 755(*s*), 731(*w*).

UV (MeOH): 260 nm (11568 L $mol^{-1}cm^{-1}$).

Luminescence: Emission 450 nm (λ_{ex} = 260 nm, MeOH).

1,4,7-tritosyl-1,4,7-triazacyclononane (tosyl-TACN)

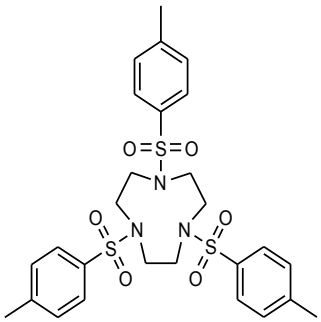

tosyl-TACN was synthesised according to a literature procedure[11]: N,N',N''-tritosyldiethylene triamine disodium salt (25.26 g, 41.4 mmol) was dissolved in dry DMF (130 ml) under nitrogen atmosphere and heated under stirring to 110°C. In a separate nitrogen flushed container, ethylene glycol ditosylate (15.13 g, 40.8 mmol) was also dissolved in dry DMF (85 ml) and then dropwise added to the triamine solution. The mixture was stirred at 110°C for one hour, then water (80 ml) was added while the solution was allowed to cool to RT. Precipitation of a colourless solid occured, which was allowed to complete overnight. The solid was filtered off and washed with EtOH until it was completely colourless. After drying the title compound was obtained as a colourless powder (18.56 g, 31.4 mmol, 77%).

^{1}H-NMR (400 MHz, $CDCl_3$): 7.70 (*m*, 6H, arom. tosyl-H); 7.30 (*m*, 6H, arom. tosyl-H); 3.42 (*s*, 12H, cyclen-H); 2.43 (*s*, 9H, tosyl-CH3).

^{13}C-NMR (126 MHz, $CDCl_3$): 143.9 (*s*, 3C, tosyl-C); 134.6 (*s*, 3C, tosyl-C); 129.9 (*d*, 6C, tosyl-CH); 127.5 (*d*, 6C, tosyl-CH); 51.9 (*t*, 6C, cyclen-CH_2); 21.5 (*q*, 3C, tosyl-CH_3).

ESI-MS: 614 (100, $[M+H]^+$), 592 (41, $[M+Na]^+$), 331 (27, $[M+Ca+MeOH]^{2+}$).

1,4,7-triazacyclononane (TACN) hydrochloride

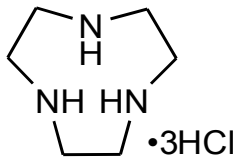

TACN was synthesised according to a modified version of a literature procedure[11]: 1,4,7-tritosyl-1,4,7-triazacyclononane (16.31 g, 27.6 mmol) was stirred in conc. H_2SO_4 (60 ml) at 100°C for 3 days. The solution was cooled to 0°C and Et_2O (100 ml) and EtOH (80ml) were added carefully. A precipitate separated overnight which was collected by filtration and washed with EtOH and Et_2O (approx 1:1). The gray to black solid was suspended in conc. HCl (65 ml) and stirred at RT for 2h. It was collected by filtration and washed with conc. HCl until colourless. Remaining HCl was removed by washing with EtOH and Et_2O. Drying on the filter yielded TACN•HCl (5.14 g, 21.7 mmol, 79%) as a colourless powder.

^{1}H-NMR (400 MHz, D_2O): 3.50 (*s*, 12H).

^{13}C-NMR (126 MHz, D_2O): 41.9 (*t*, 6C, ring-CH_2).

ESI-MS: 130 (100, $[M-3Cl-2H]^+$).

1,4,7-tripicolyl-1,4,7-triazacyclononane (9N3Py3)

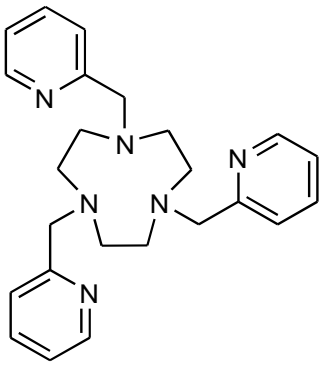

9N3Py3 was synthesised according to a literature procedure.[12]

1,4,7-triazacyclononane hydrochloride (1.03 g, 4.3 mmol) was dissolved in water (15 ml). 2-picolylchloride hydrochloride (2.1 g, 12.8 mmol) was added under stirring. The pH was raised by slow addition of NaOH (pellets) until it remained stable at 11. A red oil started to slowly separate from the solution. The water phase was decanted and the oil washed several times with cold water. It was dissolved in $CHCl_3$ (30 ml), dryed over Na_2CO_3 and filtered. Evaporation of the solvent yielded the product as a dark red or brownish oil (1.43 g, 3.5 mmol, 82%).

It can decompose over time so storage at low temperatures is suggested. Impure product was purified by column chromatography (alumina, chloroform: hexane 4:1).

^{1}H-NMR (400 MHz, $CDCl_3$): 8.50 (*dq*, *J*=4.9, 0.8, 3H, arom. CH); 7.63 (*td*, *J*=11.5, 1.8, 3H, arom. CH); 7.51 (*d*, *J*=7.8, 3H, arom CH); 7.14 (*ddd*, *J*=7.3, 5.0, 0.9, 3H, arom. CH); 3.83 (*s*, 6H, arm CH_2); 2.89 (*s*, 12H, ring CH_2).

^{1}H-NMR (400 MHz, MeOD): 8.84 (*dd*, *J* = 5.5, 0.8, 3H, arom. CH); 8.40 (*td*, *J* = 7.9, 1.5, 3H, arom. CH); 8.05 (*d*, *J* = 8.0, 3H, arom. CH); 7.86 (*m*, 3H, arom. CH); 4.46 (*s*, 6H, arm CH_2); 3.20 (*s*, 12H, ring CH_2).

^{13}C-NMR (126 MHz, $CDCl_3$): 160.3 (*s*, 3C, arom. C); 148.9 (*d*, 3C, arom CH); 136.3

(*d*, 3C, arom. CH); 123.3 (*d*, 3C, arom. CH); 121.9 (*d*, 3C, arom. CH); 64.7 (*t*, 3C, arm CH_2); 55.8 (*t*, 6C, ring CH_2).

ESI-MS: 202.2 ($[M+2H]^{2+}$, 22); 403.3 ($[M+H]^{+}$, 100); 425.3 ($[M+Na]^{+}$, 49).

UV(MeOH): 260 nm (8819 L mol^{-1} cm^{-1}).

Luminescence: Emission 421 nm (λ_{ex} = 260 nm, MeOH).

Metal complexes

Ce(III)-12N4Py4 triflate

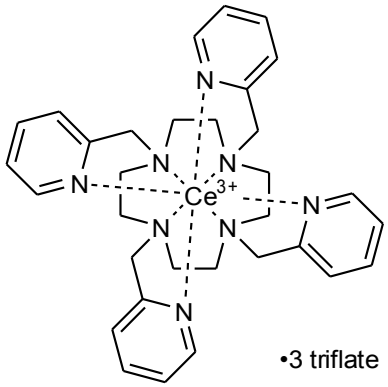

The Ce(III) complex of 12N4Py4 was synthesised following a literature procedure[10] Cerium(III) triflate (112.3 mg, 0.19 mmol) was dissolved in MeOH (5 ml) and stirred under nitrogen atmosphere. 12N4Py4 (102.5 mg, 0.19 mmol) was dissolved in MeOH (5 ml) and added dropwise to the metal solution. After complete addition the mixture was heated to 40°C for 24h. The solvent was removed to give an off-white powder which was recrystallised from MeCN/Et_2O by slow diffusion to give 12N4Py4-Ce(III) (177.3 g 0.16 mmol, 83%) as colourless, brittle needles.

^{1}H-NMR (400 MHz, D_2O): 10.49 (*bs*, 4H, ring CH_2); 10.14 (*bs*, 4H, arom. CH); 7.94 (*bt*, *J*=7.3, 4H, arom. CH); 7.74 (*bd*, *J*=6.6, 4H, arom. CH); 6.44 (*bm*, 4H, arom. CH); 5.71 (*bm*, 8H, ring CH_2); 1.51 (*bm*, 4H, arm CH_2); 0.91 (*bs*, 4H, ring CH_2); -2.66 (*bs*, 4H, arm CH_2).

^{1}H-NMR (400 MHz, MeOD): 9.07 (*bs*, 4H, arom. CH); 8.32 (*bs*, 4H, arom. CH); 7.73 (*bs*, 4H, arom. CH); 7.49 (*bs*, 4H, arom. CH); 5.34 (*bs*, 4H, ring CH_2); 4.80 (*bs*, 4H, ring CH_2); 4.60 (*bs*, 4H, ring CH_2); 2.93 (*bs*, 4H, arm CH_2); 2.63 (*bs*, 4H, ring CH_2); 1.22 (*bs*, 4H, arm CH_2).

^{13}C-NMR (126 MHz, D_2O): 144.4 (*s*, 4C, arom. C); 142.5 (*d*, 4C, arom. CH); 139.5 (*d*, 4C, arom. CH); 127.6 (*d*, 4C, arom. CH); 127.2 (*d*, 4C, arom. CH); 48.4 (*t*, 4C, ring CH_2); 46.9 (*t*, 4C, ring CH_2); 43.1 (*t*, 4C, arm CH_2).

^{13}C-NMR (126 MHz, MeOD): 150.0 (*s*, 4C, arom. C); 145.7 (*d*, 4C, arom. CH); 141.3 (*d*, 4C, arom. CH); 130.0 (*d*, 4C, arom. CH); 128.7 (*d*, 4C, arom. CH); 48.6 (*t*, 4C, arm CH_2); 46.9 (*t*, 4C, ring CH_2); 45.7 (*t*, 4C, ring CH_2).

UV-Vis (MeOH): 265 nm (12513 $Lmol^{-1}$ cm^{-1}).

Luminescence: Emission 489 nm (λ_{ex} = 265 nm, MeOH).

Elemental analysis: calc. for $C_{35}H_{48}CeF_9N_8O_{13}S_3$: C, 35.15; H, 4.05; N, 9.37. Found: C, 35.66; H, 4.04; N, 9.38.

ESI-MS: 974 (2, $[M\text{-}OTf]^{2+}$).

ICP-MS: 37% cerium content

Crystals obtained from synthesis were analysed by single crystal X-ray diffraction (structure WTS01).

Pr(III)-12N4Py4 triflate

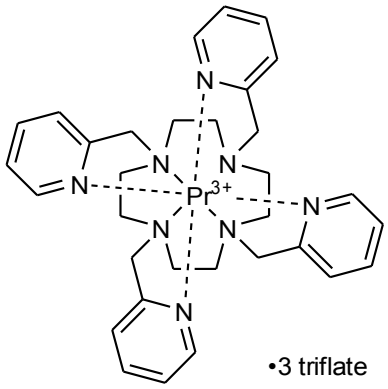

The Pr(III) complex of 12N4Py4 was synthesised following a literature procedure[1] 12N4Py4 (50 mg, 0.09 mmol) and praseodymium(III) triflate (61 mg, 0.10 mmol) were dissolved in MeOH (3 ml) and stirred at 40°C for 24h. Removal of the solvent gave an off-white powder. It was recrystallised from MeCN/Et_2O by slow diffusion to afford a beige powder and colourless crystals of Pr-12N4Py4 triflate (98 mg, 0.087 mmol, 97%).

^{1}H-NMR (400 MHz, D_2O): 11.12 (*bs*, 4H, arom. CH); 10.19 (*b s*, 8H, ring CH_2); 9.32 (*b s*, 4H, ring CH_2); 8.27 (*m*, 4H, arom. CH); 8.16 (*m*, 4H, arom. CH); 6.96 (*m*, 4H, arom. CH); 2.93 (*b s*, 4H, arm CH_2); 1.21 (*b s*, 4H, ring CH_2); -3.45 (*b s*, 4H, arm CH_2).

^{13}C-NMR (126 MHz, D_2O): 138.8 (*s*, 4C, arom. C); 138.0 (*d*, 4C, arom. CH); 136.8 (*d*, 4C, arom. CH); 134.5 (*d*, 4C, arom. CH); 132.2 (*d*, 4C, arom. CH); 36.9 (*t*, 4C, ring CH_2); 36.6 (*t*, 4C, ring CH_2); 30.6 (t, 4C, arm CH_2).

ESI-MS: 975 (12, $[M\text{-}OTf]^+$); 1125 (1, $[M+H]^+$).

UV-Vis (MeOH): 265 nm (14073 $Lmol^{-1}$ cm^{-1}).

Nd(III)-12N4Py4 triflate

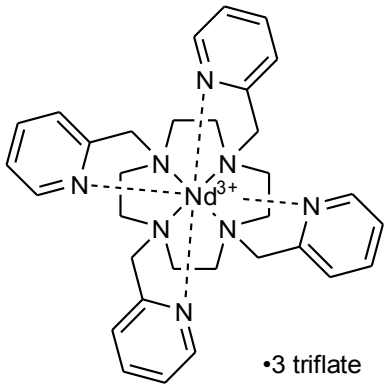

The neodymium complex of 12N4Py4 was synthesised following literature[10]:

12N4Py4 (50 mg, 0.09 mmol) and neodymium(III) triflate (56 mg, 0.09 mmol) were dissolved in MeOH (3 ml) and stirred at 40°C for 24h. Removal of the solvent gave an off-white powder. Recrystallisation from MeCN/Et_2O by slow diffusion afforded a white powder and colourless crystals of Nd(III)-12N4Py4 triflate (68 mg, 0.06 mmol, 64 %).

^{1}H-NMR (400 MHz, D_2O): 12.44 (*b s*, 4H); 11.00 (*b s*, 8H); 8.60 (*b s*, 4H); 8.48 (*b s*, 4H); 8.14 (*b s*, 4H, arom. CH); 6.16 (*b s*, 4H, ring CH_2); 5.44 (*b s*, 4H, arm CH_2); 2.63 (*b s*, 4H, ring CH_2); 0.06 (*b s*, 4H, arm CH_2).

^{13}C-NMR (126 MHz, D_2O): 139.5 (*d*, 4C, arom. CH); 138.0 (*d*, 4C, arom. CH); 136.9 (*d*, 4C, arom. CH); 136.1 (*d*, 4C, arom. CH). remaining signals not observed.

ESI-MS: 977.1 (5, $[M\text{-}OTf]^+$)

UV-Vis: 267 nm (12576 $Lmol^{-1}$ cm^{-1}).

Yb(III)-12N4Py4 triflate

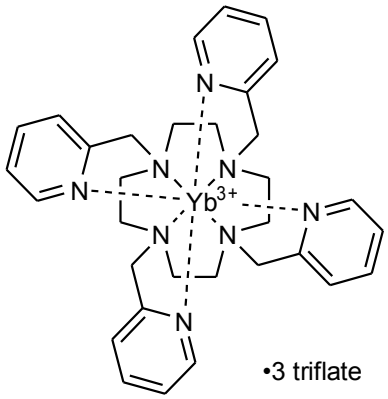

The ytterbium complex of 12N4Py4 was synthesised following literature[13]:

12N4Py4 (50 mg, 0.09 mmol) and ytterbium(III) triflate (61 mg, 0.10 mmol) were dissolved in MeOH (3 ml) and stirred at 55°C for 11 days under N_2 atmosphere. The solvent was removed to give an off-white powder that was recrystallised from MeCN/Et_2O by slow diffusion to give some colourless crystals and white precipitate. After washing with ether and drying, 12N4Py4-Yb(III) triflate (57 mg, 0.05 mmol, 55%) was obtained.

^{1}H-NMR (400 MHz, MeOD): 71.53 (*bs*, 4H, ring CH_2); 49.55 (*bs*, 4H, arom. CH); 14.26 (*bs*, 4H, arom. CH), 13.80 (*bs*, 4H, ring CH_2); 8.12 (*bs*, 4H, ring CH_2); 5.43 (*bs*, 4H, arom. CH); -4.47 (*bs*, 4H, arom. CH); -14.22 (*bs*, 4H, arm CH_2); -25.76 (*bs*, 4H, ring CH_2); -42.05 (*bs*, 4H, arm CH_2).

ESI-MS: 559 (100; $[M\text{-}Yb\text{-}3OTf+Na]^+$); 1008 (1; $[M\text{-}OTf]^+$).

Elemental analysis: calc. for $C_{34}H_{44}F_9N_8O_{11}S_3Yb$: C, 35.24; H, 3.72; N, 9.39. Found: C, 34.38; H, 3.33; N, 8.58.

UV: 265 nm (13656 $Lmol^{-1}$ cm^{-1}).

Ca(II)-12N4Py4 triflate

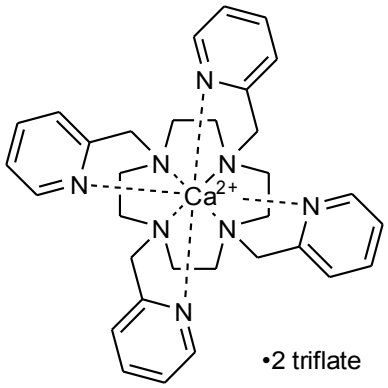

12N4Py4 (100 mg, 0.19 mmol) and calcium(II) triflate (65 mg, 0.19 mmol) were dissolved in MeOH (5 ml) and stirred at 40°C for 24h. Removal of the solvent gave an off-white powder. Recrystallisation from MeCN/Et_2O by slow diffusion yielded a white precipitate or colourless crystals of Ca-12N4Py4 triflate (151 mg, 0.17 mmol, 93 %).

Spectral data in accordance with published data.[14]

^{1}H-NMR (400 MHz, D_2O): 7.89 (*td*, *J*=7.7, 1.6, 4H, arom. CH); 7.41 (*d*, *J*=7.88, 4H, arom. CH); 7.28 (*d*, *J*=4.6, 4H, arom. CH); 7.19 (*b m*, 4H, arom. CH); 4.03 (*d*, *J*=15.9, 4H, arm CH_2)); 3.67 (*td*, *J*=13.9, 2.8, 4H, ring CH_2); 3.5 (*d*, *J*= 15.9, 4H, arm CH_2); 3.07 (*td*, *J*=13.8, 2.7, 4H, ring CH_2); 2.46 (*t*, *J*=13.8, 8H, ring CH_2).

^{13}C-NMR (126 MHz, D_2O): 158.1(*s*, 4C, arom. C); 148.2 (*d*, 4C, arom. CH); 139.4 (*d*, 4C, arom. CH); 125.1(*d*, 4C, arom. CH); 123.9 (*d*, 4C, arom. CH); 58.3 (*t*, 4C, arm CH_2); 51.1 (*t*, 4C, ring CH_2); 49.5 (*t*, 4C, ring CH_2).

ESI-MS: 288 (7; $[M\text{-}2OTf]^{2+}$); 537 (3; $[M\text{-}Ca\text{-}2OTf+H]^+$); 687 (40; $[M\text{-}Ca\text{-}OTf+2H]^+$); 725 (100; $[M\text{-}OTf]^+$).

HR-MS (ESI): 725.2517, $[M\text{-triflate}]^+$.

Elemental analysis: calc. for $C_{34}H_4CaF_6N_8O_6S_2$: C, 46.67; H, 4.61; N, 12.81. Found:

C, 46.75; H, 5.40; N, 12.70.

UV-Vis: 263 nm (13724 $Lmol^{-1}$ cm^{-1}).

Crystals obtained from synthesis were analysed by single crystal X-ray diffraction (structure WTS02).

Na(I)-12N4Py4 triflate

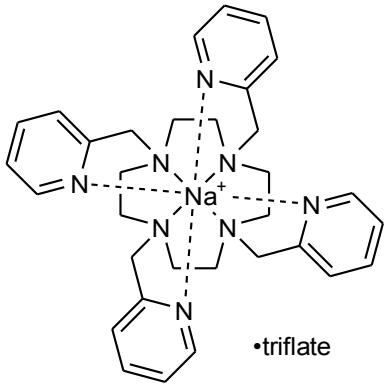

12N4Py4 (100 mg, 0.186 mmol) and sodium triflate (32 mg, 0.186 mmol) were suspended in MeCN (3 ml) and stirred at room temperature for 26 h, during which all solids dissolved. The solvent was removed and the residue recrystallised from DCM layered with hexane to give the triflate salt of Na(I)-12N4Py4 (127 mg, 0.178 mmol, 96%) as colourless crystals.

Spectral data in accordance with published data.[10]

^{1}H-NMR (400 MHz, MeOD): 7.67 (*t*, *J* = 7.6 Hz, 4H, arom. CH); 7.60 (*d*, *J* = 4.8 Hz, 4H, arom. CH); 7.21 (*d*, *J* = 7.8, 4H, arom. CH); 7.02 (*dd*, *J* = 7.0, 5.3, 4H, arom. CH); 4.05-1.61 (*bm*, 24H, arm & ring CH_2).

^{13}C-NMR (126 MHz, MeOD): 160.5 (*s*, 4C, arom. C); 150.1 (*d*, 4C, arom. CH); 138.1 (*d*, 4C, arom. CH); 125.0 (*d*, 4C, arom. CH); 123.4 (*d*, 4C, arom. CH); 60.2 (*t*, 4C,

arm CH_2); 51.7 (*t*, 8C, ring CH_2).

ESI-MS: 135 (39; $[M\text{-}Na\text{-}OTf+4H]^{4+}$); 269 (64; $[M\text{-}Na\text{-}OTf+2H]^{2+}$); 403 (25; $[M+2H+3MeOH]^{2+}$); 537 (100; $M\text{-}Na\text{-}OTf+H]^{+}$); 559 (68; $[M\text{-}OTf]^{+}$); 645 (49; $[M\text{-}OTf+DCM]^{+}$).

UV-Vis: 262 nm (19712 $Lmol^{-1}$ cm^{-1}).

Elemental analysis: calc. for $C_{33}H_{42}F_3N_8NaO_4S$: C, 54.62; H, ; N, 11.35. Found: C, 54.62; H, 5.50; N, 15.00.

Ca(II)-9N3Py3 triflate

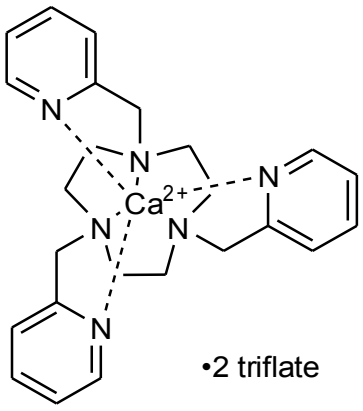

9N3Py3 (454 mg, 1.23 mmol) was dissolved in MeOH (6.7 ml) and Ca(II) triflate (383 mg, 1.13 mg) was added. The mixture was stirred unter N_2 atmosphere for 24h at 40°C. The methanolic solution was concentrated and layered with Et_2O to yield the triflate salt of Ca(II)-9N3Py3 (453.5 mg, 0.61 mmol, 54 %) as beige crystals.

^{1}H-NMR (400 MHz, MeOD): 8.61 (*d*, *J* = 4.6, 4H, arom. CH); 7.94 (*t*, *J* = 7.66, 4H, arom. CH); 7.47 (*m*, 8H, arom. CH); 4.07 (*s*, 8H, arm CH_2); 2.95 (*m*, 8H, ring CH_2); 2.57 (*m*, 8H, ring CH_2).

^{13}C-NMR (126 MHz, MeOD): 159.5 (*s*, arom. C), 150.6 (*d*, arom. CH), 140.7 (*d*, arom.

CH), 125.4 (*d*, arom. CH), 125.2 (*d*, arom. CH), 65.9 (*t*, arm. CH_2), 54.8 (*t*, ring CH_2).

ESI-MS: 202.2 ([M-Ca-2triflate+2H]$^{2+}$, 9.1); 221.2 ([M-2triflate]$^{2+}$, 7.3); 403.2 ([M-Ca-2triflate+H]$^{+}$, 100.0); 425.2 ([M-Ca-2triflate+Na]$^{+}$, 19.8).

HR-MS (ESI): 221.1073, [M-2OTf^{2+}].

UV-Vis: 260 nm (8985 Lmol^{-1} cm^{-1}).

Elemental analysis: calc. for $C_{26}H_{30}CaF_6N_6O_6S_2$: C, 42.16; H, 4.08; N, 11.35. Found: C, 41.33; H, 3.55; N, 11.03.

Crystals obtained from synthesis were analysed by single crystal X-ray diffraction (structure WTS04).

Attempted synthesis of U(IV)-12N4Py4

Under nitrogen atmosphere, a methanolic solution of 12N4Py4 (52.0 mg, 0.097 mmol, 5.1 ml) was added to UCl_4 (36.5 mg, 0.096 mmol) to give a dark green solution. The mixture was heated at 40° C for 24h, during which the solution turned yellow. A beige solid was obtained upon removal of the solvent at reduced pressure.

NMR in MeOD did not show indication of complexation.

Attempted synthesis of U(IV)-9N3Py3

Under nitrogen atmosphere, 9N3Py3 (21.1 mg, 0.052 mmol) and UCl_4 (20 mg, 0.053 mmol) were dissolved in deuterated methanol (1.6 ml) and stirred at 40°C for 24h. The mixture was analysed without work up.

NMR in MeOD did not show indication of complexation.

Attempted synthesis of U(IV)-CyMe$_4$-BTPhen

Under nitrogen atmosphere, CyMe$_4$-BTPhen (27.5 mg, 0.049 mmol) and UCl_4 (46 mg, 0.121 mmol) were dissolved in deuterated methanol (2 ml) and stirred at 40°C for 24h. The mixture was analysed without work up. ^{1}H-NMR (400 MHz) showed indication of a paramagnetic compound among other signals. The solvent was removed and the residue dissolved with acetonitrile. Addition of diethyl ether gave a precipitate. Both the precipitate and the solution were dried and analysed by NMR, where no indication of a paramagnetic compound could be detected anymore in either sample.

Solubility and precipitation measurements

Perrhenate experiments

12N4Py4 (10 mg, 0.02 mmol) and NH_4ReO_4 (22 mg, 0.08 mmol) were dissolved in a MeOH/H_2O mixture (1:1, 1 ml) and left to stand overnight without stirring. Evaporation and addition of D_2O still left some undissolved solid. Deuterated DCl was added, which lead to complete dissolution. NMR analysis showed no unexpected proton signals. The pH of the solution was increased by addition of NaOH which lead to immediate precipitation. This solid was redissolved in H_2O and left to crystallise. The crystals were analysed by single crystal X-ray diffraction to give structure WTS03.

Several attempts to react NH_4ReO_4 with 12N4Py4 in strongly acidic solutions (HCl) did only produce ammonium perrhenate crystals.

Iodide experiments

An acidic solution of 12N4Py4 (2 ml, 0.005 M, 4 equivalents HCl) was treated with KI (spatula tip). After several days dark reddish crystals were observed and analysed by single crystal X-ray diffraction (structure WTS05). Two months later, colourless crystals started to appear, that were also analysed by single crystal X-ray diffraction (structure WTS07).

Comparison of triiodide formation with toluene phase

KI (62 mg, 0.37 mmol) was dissolved in 0.5 ml H_2O and mixed with either no ligand, 12N4Py4 (14.3 mg, 0.027 mmol), pyridine (0.1 ml, 97.8 mg, 1.23 mmol) or cyclen (29 mg, 0.17 mmol). The aqueous solution was layered with toluene (1 ml). Dropwise addition of HCl (aq., conc.) produced a yellowish colour in the aqueous phase and a pink colour in the toluene phase, indicating formation of iodine. Only the cyclen sample showed a difference in behaviour, beside the described colour changes, a colourless precipitate formed in the aqueous phase. Upon prolonged standing crystals were obtained from the pyridine and 12N4Py4 samples that were analysed by X-ray crystallography. The cyclen sample was measured by NMR and determined to be protonated cyclen.

Iodide trapping experiments

A Schlenk flask was charged with solid I_2 (60 mg, 0.24 mmol) and connected to a nitrogen inlet (carrier gas) and a second Schlenk flask. In the second flask a KI solution (20 ml, 0.25 M) and toluene (25 ml) were stirred, the carrier gas was bubbled through from the bottom of the Schenk flask. The outlet from the second flask was

connected to a splash trap in an acetone ice bath and the carrier gas (nitrogen) was finally bubbled through toluene. The aqueous solution of KI was either left unchanged or charged with 12N4Py4 (100 mg, 0.19 mmol) or pyridine (0.5 ml, 6.2 mmol). Carrier gas was set to produce a steady bubble formation in the trapping solution. With a heat gun the solid iodine was evaporated to be carried into the trapping solution. Some of the iodine was retained in the tubing between the first and second flask.

In the presence of 12N4Py4, the toluene phase turned yellow, then orange. When addition was complete, a dark oil had separated at the interphase of water and toluene. A faint yellow colour was observed in the aqueous phase and a faint pink colour in the toluene phase.

In the presence of pyridine the toluene phase was intensly yellow, the aqueous phase had a similar but fainter colour.

Without any trapping agent, the aqueous phase turned yellow, then the toluene phase turned pink.

All phases were measured by UV to confirm the presence of iodine and triiodide as discussed in chapter 8.

pK_a titration 12N4Py4

Water used for stock solution and sample preparation was decarbonised by heating to 100° C and cooling down in a covered vessel. Volumes larger than 2 ml were measured with graduated and volumetric pipettes, smaller volumes were measured with *Eppendorf* pipettes. To avoid the accumulation in the solutions, titrations were conducted on the same day as the solutions were prepared. Stock solutions of HCl and KOH could be stored in air tight flasks. Reassessment of their concentration after 3 months confirmed that pH changes were minimal.

Preparation of stock solutions

The pK_a measurements of 12N4Py4 were conducted as follows:

KOH pellets were dissolved in water and decarbonised by stirring overnight with suspended CaO. The solution was decanted and diluted to a concentration of approximately 1 M. aq. HCl was diluted to approximately 0.1 M. Exact concentrations were determined by titration of an aqueous solution of a primary standard (potassium hydrogen phthalate, dried at 150°C for 2h) with phenolphthalein as the indicator using the KOH solution, followed by titration of the HCl stock solution with KOH.

Sample preparation

KCl was dried overnight (150°C), amounts of 12N4Py4 were corrected for solvent content, estimated by ^{1}H-NMR.

A solution was prepared containing 12N4Py4 (0.01 M), KCl (0.0, 0.5, 1.0 or 2.0 M), and HCl (0.04 - 0.06 M) with a pH of 1-2.

Measurement

Titrations were conducted at 0°C, 22°C, 30°C and 38°C.The temperature was controlled using a waterbath and a *IKA® ETS-D5* temperature control.

The prepared solution (4 or 5 ml) was titrated with KOH stock solution in steps of 1 to 5 µl while stirring. pH was continuously measured and values were recorded manually.

Data processing

Concentrations of components, concentrations of bound protons [H_b] and average bound protons per molecule nH_b were calculated using *Openoffice Calc 4.1.1*. Fitting procedures were performed in *OriginPro® 9.1* using the technique published by Arno Kraft.[15] Sets of titration data obtained for the same conditions were fitted using a global fitting procedure.

The water autoprotolysis constant K_w was determined for each condition using a method described by Sweeton et al.[16], the vapor pressure was determined using the Antoine equation[17]. Ionic strength was not strictly constant due to formation of protonated ligand species. The determined autoprotolysis constant K_w is dependent on ionic strength. An initial fitting was performed, ionic strength recalculated from obtained species concentration and fitting repeated with the corrected K_w. Thermodynamic constants were determined by linear fit in *OriginPro® 9.1*.

Results

Table E1 gives the results obtained for the pK_a titration of 12N4Py4 including the standard error as well as the adjusted R^2 and reduced chi square values obtained for

the fitting procedure.

Table E1: pK_a values of 12N4Py4 for different conditions							
Temp.	**[KCl] in M**	**pK_a 1**	**pK_a 2**	**pK_a 3**	**pK_a 4**	**adj. R^2**	**red. chi^2**
0°C	0	10.77 ±0.02	8.26 ±0.02	3.67 ±0.02	1.85 ±0.07	0.99642	0.00283
0°C	0.5	10.71 ±0.02	8.59 ±0.01	4.24 ±0.02	2.86 ±0.02	0.99812	0.00209
0°C	1	10.87 ±0.01	8.70 ±0.01	4.39 ±0.01	3.07 ±0.02	0.99866	0.00143
0°C	2	10.86 ±0.02	8.79 ±0.02	4.50 ±0.02	3.20 ±0.02	0.9969	0.0025
22°C	0	10.31 ±0.04	7.72 ±0.02	3.57 ±0.02	2.22 ±0.03	0.99304	0.00456
22°C	0.5	10.32 ±0.01	7.98 ±0.01	3.96 ±0.01	2.69 ±0.01	0.99905	6.55 E-4
22°C	1	10.57 ±0.02	8.19 ±0.01	4.19 ±0.01	2.90 ±0.01	0.99843	0.00115
22°C	2	10.19 ±0.03	8.21 ±0.02	4.30 ±0.02	3.09 ±0.02	0.99577	0.00301
30°C	0	10.53 ±0.05	7.60 ±0.01	3.48 ±0.01	1.88 ±0.04	0.9975	0.00106
30°C	0.5	10.50 ±0.02	7.93 ±0.01	3.97 ±0.01	2.65 ±0.01	0.99952	3.21 E-4
30°C	1	10.92 ±0.10	8.20 ±0.01	4.14 ±0.01	2.83 ±0.01	0.99754	0.00157
30°C	2	12.16 ±3.00	8.40 ±0.01	4.44 ±0.01	3.04 ±0.01	0.99849	9.05 E-4
38°C	0	9.89 ±0.05	7.34 ±0.02	3.36 ±0.02	2.03 ±0.04	0.99318	0.00363
38°C	0.5	9.88 ±0.02	7.53 ±0.01	3.74 ±0.01	2.45 ±0.02	0.99834	9.89 E-4
38°C	1	10.42 ±0.07	7.88 ±0.01	4.00 ±0.01	2.67 ±0.02	0.99722	0.00159
38°C	2	9.90 ±0.03	7.98 ±0.01	4.27 ±0.01	3.05 ±0.01	0.99865	8.68 E-4

General remark: reduced chi^2 values in Origin deviate from standard interpretation, values approaching 0 are associated with good fits.

Metal titrations 12N4Py4

Water used for stock solution and sample preparation was decarbonised by heating to 100° C and cooling down in a covered vessel. Volumes larger than 2 ml were measured with graduated and volumetric pipettes, smaller volumes were measured with *Eppendorf* pipettes. All metal salts were dried in an oven (150°C) overnight prior to use. KOH and HCl stock solutions were prepared as described for pK_a titrations.

Sample preparation and measurement

For each titration step, an individual sample was prepared containing 12N4Py4 (0.01 mmol, 0.005 M), metal triflate (Ce(III), Pr(III), Nd(III), Yb(III), Ca(II) or Na(I), 0.01 mmol, 0.005 M), HCl (0.04 mmol, 0.02 M) and varying amounts of KOH (0-0.05 mmol, 0-0.025 M) as an aqueous solution of 2ml volume. Per titration between 10 and 20 samples were prepared. The samples were equilibrated in closed sample vials using a waterbath and a *IKA® ETS-D5* temperature control at 22°C for 6 - 7 days. After measurement, the same samples were reequilibrated at 30°C and 38°C for a further 6 -7 days each. pH was recorded manually

Data processing

Concentrations of components, concentrations of bound protons [H_b] and average bound protons per molecule nH_b were calculated using *Openoffice Calc 4.1.1*. The water autoprotolysis constant K_w was determined for each condition using the method described by Sweeton et al.[16] and the vapor pressure was determined using the Antoine equation[17].

From [H_b] the concentration of [L] was calculated using the equation

$$[H_b] = [L]\left(\frac{[H]}{K_1} + 2\frac{[H]^2}{K_1 K_2} + 3\frac{[H]^3}{K_1 K_2 K_3} + 4\frac{[H]^4}{K_1 K_2 K_3 K_4}\right) \quad \text{E1}$$

Subsequently [LH], [LH_2], [LH_3] and [LH_4] were calculated using the proton dissociation constants determined in the pK_a titrations earlier. [LM] was calculated as the residual of the total ligand concentration minus all free and protonated ligand concentrations and following [M] from the total metal concentrations minus [LM].

A binding constant was calculated for each titration point by inserting the corresponding concentration into the equilibrium equation

$$K_c = \frac{[LM]}{[L][M]} \quad \text{E2}$$

The final estimated binding constant was produced by averaging all determined binding constants over the range where [LM] was between 20 and 80% of the toal ligand concentration. All these calculation were perfomed in *Openoffice Calc 4.1.1*.

Table E2 gives the results obtained using this method.

For the fitting procedures, the same titration data were used. The fitting function as developed in chapter 5 and the appendix was entered into *OriginPro® 9.1* and applied with non-linear fitting to data sets of [H_b] against [H] as previously determined for the estimated binding constants. K_1, K_2, K_3 and K_4 were taken from the pK_a fitting described earlier, kept constant in the constrained fitting and allowed to vary in turn in the unconstrained fitting. Tables E3 and E4 give the corresponding results obtained.

Finally, the estimation technique including the formation of hydroxide species was applied to the data in *Openoffice 4.1.1*, the results are summaried in Table E5.

Table E2: binding constants logK$_c$ obtained by estimation method				
metal	**ionic str.**	**T= 22°C**	**T= 30°C**	**T= 38°C**
Cerium	0.5	10.67 [a]	11.30 [a]	10.88 [a]
	1	10.97 [a]	11.92 [a]	11.73 [a]
	2	9.95 [a]	13.26 [a]	11.26 [a]
Praseodymium	0.5	6.23	7.64	8.15
	1	6.74	8.74	8.82
	2	6.32	9.38	8.11
Neodymium	0.5	6.08 [a]	8.38 [a]	7.81
	1	6.73 [a]	8.49	8.97
	2	6.69	9.20	7.54 [a]
Ytterbium	0.5	7.58	8.28	7.92
	1	8.08	9.08	8.99
	2	7.52	10.11	8.26
Calcium	0.5	11.56	11.91	11.99
	1	11.87	12.63	11.94
	2	11.56	14.52	11.70
Sodium	1	5.26	7.72	5.04

[a] *determined from data where precipitation interfered*

Table E3: binding constants logK$_c$ obtained by constrained fitting procedure				
ionic str.	**Temp.**	**logKc**	**adj. R^2**	**red. chi^2**
Cerium				
0.5	22	*11.36 ±0.17*	0.95704	2.73241E-7
0.5	30	*11.77 ±0.17*	0.94162	3.66684E-7
0.5	38	*11.18 ±0.28*	0.76349	1.00019E-6
1.0	22	*10.70 ±0.25*	0.96137	2.633E-7
1.0	30	*11.30 ±0.24*	0.95618	2.87066E-7
1.0	38	*11.11 ±0.42*	0.70818	1.36926E-6
2.0	22	*8.34 ±0.36*	0.90372	4.30207E-7
2.0	30	*11.38 ±0.20*	0.98169	6.0263E-8
2.0	38	*9.97 ±0.68*	0.97297	6.00331E-8
Praseodymium				
0.5	22	*6.08 ±0.13*	0.91933	8.86556E-7
0.5	30	*7.64 ±0.07*	0.97718	2.5061E-7
0.5	38	*8.02 ±0.09*	0.94877	5.62379E-7
1.0	22	*6.52 ±0.16*	0.85753	1.5659E-6
1.0	30	*8.82 ±0.10*	0.9563	4.80157E-7
1.0	38	*8.78 ±0.10*	0.94141	6.43577E-7
2.0	22	*6.39 ±0.14*	0.82446	1.77913E-6
2.0	30	*9.41 ±0.08*	0.947	5.37163E-7
2.0	38	*8.13 ±0.05*	0.98224	1.79905E-7
Neodymium				
0.5	22	6.37 *±0.08*	0.99849	1.13011E-8
0.5	30	*7.53 ±0.05*	0.9994	4.77059E-9
0.5	38	*7.79 ±0.04*	0.99525	7.04494E-8
1.0	22	*6.71 ±0.09*	0.98227	3.03964E-7
1.0	30	*8.52 ±0.04*	0.99637	6.33453E-8
1.0	38	*8.82 ±0.06*	0.98391	2.56954E-7
2.0	22	*6.68 ±0.07*	0.97574	2.66125E-7
2.0	30	*8.95 ±0.09*	0.92434	8.30458E-7
2.0	38	*7.51 ±0.05*	0.97956	2.24078E-7

ionic str.	Temp.	logKc	adj. R^2	red. chi^2
Ytterbium				
0.5	22	6.96 *±0.16*	0.80364	2.15861E-6
0.5	30	*7.59 ±0.19*	0.71777	3.1024E-6
0.5	38	*7.20 ±0.21*	0.65505	3.79161E-6
1.0	22	*7.34 ±0.15*	0.79455	2.2586E-6
1.0	30	*8.30 ±0.14*	0.78774	2.3334E-6
1.0	38	*8.25 ±0.19*	0.77427	2.48125E-6
2.0	22	*7.22 ±0.14*	0.69443	3.35937E-6
2.0	30	*9.86 ±0.11*	0.82154	1.96191E-6
2.0	38	*8.06 ±0.13*	0.74645	2.78714E-6
Calcium				
0.5	22	*11.51 ±0.05*	0.98163	2.31161E-7
0.5	30	*11.92 ±0.05*	0.97895	2.63887E-7
0.5	38	*11.00 ±0.02*	0.99467	6.63325E-8
1.0	22	*11.88 ±0.05*	0.98083	2.43966E-7
1.0	30	*12.69 ±0.05*	0.97452	3.21935E-7
1.0	38	*11.97 ±0.04*	0.98631	1.72083E-7
2.0	22	*11.91 ±0.09*	0.88687	1.45188E-6
2.0	30	*14.53 ±0.05*	0.9684	4.03035E-7
2.0	38	*12.24 ±0.06*	0.96327	4.65876E-7
Sodium				
1.0	22	*5.16 ±0.06*	0.98778	2.62067E-7
1.0	30	*7.63 ±0.07*	0.98462	3.63331E-7
1.0	38	*5.10 ±0.09*	0.97883	4.47728E-7

Table E4: binding constants logK$_c$ obtained by unconstrained fitting procedure					
ionic str.	**Temp.**	**logKc**	**pK$_4$**	**adj. R2**	**red. chi^2**
Cerium					
0.5	22	*11.36 ±0.13*	2.68	0.99028	6.18033E-8
0.5	30	*11.77 ±0.12*	2.63	0.98844	7.25818E-8
0.5	38	*11.18 ±0.13*	2.01	0.97579	1.02398E-7
1.0	22	*10.70 ±0.13*	2.84	0.99664	2.29289E-8
1.0	30	*11.30 ±0.11*	2.75	0.99688	2.04622E-8
1.0	38	*11.12 ±0.17*	2.23	0.98523	6.93126E-8
2.0	22	*8.34 ±0.11*	3.39	0.9884	5.18433E-8
2.0	30	*11.38 ±0.10*	3.08	0.99183	2.68825E-8
2.0	38	*8.96 ±0.49*	2.87	0.98997	2.22703E-8
Praseodymium					
0.5	22	*6.08 ±0.13*	6.99	0.92044	8.74322E-7
0.5	30	*7.64 ±0.07*	6.25	0.97887	2.32045E-7
0.5	38	*8.01 ±0.05*	6.57	0.98098	2.08777E-7
1.0	22	*6.52 ±0.16*	7.42	0.85993	1.53956E-6
1.0	30	*8.82 ±0.09*	6.15	0.95948	4.4518E-7
1.0	38	*8.78 ±0.08*	6.36	0.96123	4.2592E-7
2.0	22	*6.39 ±0.12*	8.86	0.86291	1.3895E-6
2.0	30	*9.41 ±0.07*	7.38	0.95664	4.39463E-7
2.0	38	*8.13 ±0.05*	-12.04	0.98279	1.74385E-7
Neodymium					
0.5	22	6.37 *±0.08*	2.58	0.99849	1.13011E-8
0.5	30	*7.53 ±0.05*	2.70	0.9994	4.77059E-9
0.5	38	*7.79 ±0.04*	2.30	0.99525	7.04494E-8
1.0	22	*6.71 ±0.09*	2.76	0.98227	3.03964E-7
1.0	30	*8.52 ±0.04*	2.84	0.99637	6.33453E-8
1.0	38	*8.82 ±0.06*	2.52	0.98391	2.56954E-7
2.0	22	*6.68 ±0.07*	4.23	0.97574	2.66125E-7
2.0	30	*8.95 ±0.09*	4.16	0.92434	8.30458E-7
2.0	38	*7.51 ±0.05*	3.14	0.97956	2.24078E-7

ionic str.	Temp.	logKc	pK_4	adj. R2	red. chi^2
Ytterbium					
0.5	22	6.96 *±0.16*	8.68	0.80364	2.15861E-6
0.5	30	*7.59 ±0.19*	6.93	0.71777	3.1024E-6
0.5	38	*7.20 ±0.21*	7.10	0.65505	3.79161E-6
1.0	22	*7.34 ±0.15*	8.78	0.79455	2.2586E-6
1.0	30	*8.30 ±0.14*	8.45	0.78774	2.3334E-6
1.0	38	*8.25 ±0.16*	7.28	0.77427	2.48125E-6
2.0	22	*7.22 ±0.14*	8.42	0.69443	3.35937E-6
2.0	30	*9.86 ±0.11*	7.81	0.82154	1.96191E-6
2.0	38	*8.06 ±0.13*	7.15	0.74645	2.78714E-6
Calcium					
0.5	22	*11.41 ±0.01*	2.40	0.99871	1.62198E-8
0.5	30	*11.81 ±0.02*	-12.35	0.99743	3.2214E-8
0.5	38	*10.95 ±0.01*	2.04	0.99943	7.10139E-9
1.0	22	*11.77 ±0.02*	2.28	0.9959	5.22079E-8
1.0	30	*12.53 ±0.01*	-11.42	0.99911	1.12272E-8
1.0	38	*11.87 ±0.01*	-16.19	0.99919	1.02002E-8
2.0	22	*11.96 ±0.09*	3.13	0.88993	1.41262E-6
2.0	30	*14.49 ±0.04*	-20.08	0.97612	3.04573E-7
2.0	38	*12.07 ±0.02*	-13.42	0.99503	6.30965E-8
Sodium					
1.0	22	*5.16 ±0.05*	2.76	0.99198	1.72106E-7
1.0	30	*7.63 ±0.05*	-8.96	0.99057	2.22883E-7
1.0	38	*5.10 ±0.06*	-5.47	0.98906	2.31373E-7

Table E5: binding constants logK$_c$ obtained by estimation method including metal hydroxide formation				
metal	**ionic str.**	**T= 22°C**	**T= 30°C**	**T= 38°C**
Cerium	0.5	10.68 [a]	11.30 [a]	10.87 [a]
	1	10.97 [a]	11.92 [a]	11.73 [a]
	2	9.96 [a]	13.25 [a]	11.25 [a]
Praseodymium	0.5	5.99	7.67	8.10
	1	6.45	8.89	8.88
	2	6.53	9.37	8.15
Neodymium	0.5	6.07	8.38	7.80
	1	6.68	8.48	8.97
	2	6.65	9.18	7.54
Ytterbium	0.5	7.05	7.49	7.15
	1	7.31	8.32	8.20
	2	7.48	10.09	8.24
Calcium	0.5	11.49	11.91	10.99
	1	11.87	12.64	11.94
	2	11.56	14.52	11.70
Sodium	1	5.26	7.73	5.09

[a] *determined from data where precipitation interfered*

From Calcium titrations crystal structure WTS02 was obtained.

Titrations 9N3Py3

Water used for stock solution and sample preparation was decarbonised by heating to 100° C and cooling down in a covered vessel. Volumes larger than 2 ml were measured with graduated and volumetric pipettes, smaller volumes were measured with *Eppendorf* pipettes. All metal salts were dried in an oven (150°C) overnight prior to use. KOH and HCl stock solutions were prepared as described for pK_a titrations.

Sample preparation and measurement

For each titration point, an individual sample was prepared containing Ca(II)-9N3Py3 (0.008 mmol, 0.004 M), KCl (1 mmol, 0.5 M) and HCl (0 - 0.024 mmol) or KOH (0 - 0.008 mmol) as an aqueous solution of 2 ml volume.

The solutions were equilibrated at 22°C using a waterbath and a *IKA® ETS-D5* temperature control for 7 days and then their pH was measured individually, values were recorded manually.

Following the first measurement, $CaCl_2$ (150 µl, 0.795 mmol, 5.3 M) solution were added to each sample, increasing the metal concentration to 104 equivalents of that of the ligand. The samples were re-equilibrated at 22°C for 7 days before they were remeasured using the same technique, and the procedure was repeated for equilibration temperatures 30°C and 38°C.

Data processing and results

The obtained data were entered into *OriginPro® 9.1* and fitted with the equation developed in the appendix. All constants were being fitted simultaneously. Dissociation and metal binding constants obtained for the four series are summarised

in Table E6.

Table E6: pK_a and $logK_c$ values obtained for Ca(II)-9N3Py3						
condition	**pK_1**	**pK_2**	**pK_3**	**$logK_c$**	**adj. R2**	**red. chi^2**
T = 22°C, 1 eq metal	9.98 ±0.09	5.45 ±0.05	4.03 ±0.04	0.03 ±0.22	0.99261	5.865E-8
T = 22°C, 100 eq metal	9.95 ±1684	5.59 ±0.17	4.35 ±0.16	2.55 ±1696	0.95531	8.00395E-7
T = 30°C, 100 eq metal	10.02 ±3214	5.48 ±0.19	4.3 ±0.17	3.02 ±3221	0.94891	9.30675E-7
T = 38°C, 100 eq metal	9.97 ±8884	5.35 ±0.20	4.13 ±0.18	3.03 ±8905	0.94385	1.0223E-6

Thermodynamic data (Table E7) was calculated from these binding constants using *Openoffice Calc 4.1.1*.

Table E7: Thermodynamic constants of 9N3Py3		
constant	**ΔH in kJ/mol**	**ΔS in J/molK**
K_1	-1.5	-195.9
K_2	26.2	-18.3
K_3	24.9	0.6
K_c	51.9	226.3

Extraction experiments

Water used for stock solution and sample preparation was decarbonised by heating to 100° C and cooling down in a covered vessel. Volumes were measured with *Eppendorf* pipettes.

Preparation of buffer solutions

KOH was dissolved in water (approx. 5g in 10 ml) and stirred overnight with CaO and charcoal to remove luminescent impurities. The near concentrated solution was filtered over cotton wool and stored in mass spectrometry vials with a PTFE cap.

Stock solutions of boric acid (2.4731 g in 100 ml H_2O), acetic acid (from anhyd., 2.4277 g in 100 ml H_2O) and phosphoric acid (from anhyd., 3.9552 g in 100 ml H_2O).

To make the 0.04 M Britton-Robinson[18] buffer solutions, 10 ml of each stock solution (boric acid, acetic acid and phosphoric acid) were mixed with dried KCl (6.56g, 0.088 mol) and diluted to approx. 90 ml with decarbonised water. pH was adjusted by addition of KOH as prepared above and conc. HCl to pH 2.0, 3.5, 6.2, 9.4 or 12.0 before diluting the solution to 100 ml. Buffer solutions were stored in air tight containers. All buffers were measured by UV-Vis and luminescence spectroscopy to ensure they were free of impurities which would interfere with measurements.

Solvent measurements

Kerosene, Octanol and Hexane were stored in air tight mass spectrometry vials on their own and with water (1:1, total of 4 ml) for a week before they were analysed by UV-Vis and luminescence spectroscopy. Absorption and luminescence was observed from kerosene samples and it was no further considered for measurements. Octanol

and Hexane samples were approved to be used for extraction experiments.

Octanol and Hexane extractions were repeated with all buffer solutions to ensure no interference from interactions of the buffer agents and the organic phase was observed. These measurements were also used as baselines for the extraction experiments.

Extraction of 12N4Py4

12N4Py4 (32.3 mg, 0.06 mmol) was dissolved in 2 ml of 0.04 M Britton-Robinson buffer (pH 6.2) to give a ligand stock solution

For ligand measurements, 12N4Py4 stock solution (5 µl) was diluted to 2 ml with Britton-Robinson buffer of the required pH (2.0, 3.5, 6.2, 9.4 or 12.0). This gave a concentration of $7.5*10^{-5}$ M. Hexane or Octanol (2ml) was added for extraction measurements. The mixture was equilibrated for 7 days at room temperature prior to measurement by UV-Vis and luminescence spectroscopy.

Extraction of 12N4Py4 with anions

Fresh extraction samples were prepared as described for 12N4Py4 and 5 µl of a 0.03 mM solution (1 equivalent) or a 0.3 mM solution (10 equivalents) of one of the anions was added. The salts for the anions were: potassium bromide, potassium iodide, ammonium perrhenate, ammonium chloride, potassium carbonate, potassium hydrogen sulfate, potassium nitrate. Carbonate samples were only prepared for pH 6.2, 9.4 and 12.0. Samples were equilibrated for 7 days and measured by UV-Vis and luminescence spectroscopy.

The same procedure also applies for the measurement with sodium chloride.

Extraction of calcium and neodymium complexes.

Stock solutions of Ca(II)-12N4Py4 (21.8 mg, 0.0245 mmol in 5 ml MeOH) and Nd(III)-12N4Py4 (28.0 mg, 0.0248 mmol in 5 ml MeOH) were prepared. For each extraction sample, 30 µl of one of these solutions were evaporated to dryness in a vial before adding the other components. Buffer solutions (either pH 6.2 or 9.4, 2 ml) and organic phases (octanol or hexane, 2 ml) were added and if required 5 µl of the corresponding anion solution (0.03 M for 1 equivalent, 0.3 M for 10 equivalent, as prepared for anion extractions of 12N4Py4). After equilibration of 7 days the samples were measured by UV-Vis and luminescence spectroscopy.

Extraction with uranium

2 µl of a uranium chloride stock solution in methanol (0.075 M) was added to individual vials and left to evaporate for a few hours. Then extraction experiments with 12N4Py4 were prepared as previously described. Measurements were performed using a screw cap luminescence cuvette with septum.

Treatment of data

UV-spectra were processed as follows: The original spectrum was recorded using an empty cuvette as blank, as over a measurement period different solvents were measured. Raw data was then baseline corrected with a spectrum of the respective solvent/buffer in the respective extraction conditions. Samples containing iodide, perrhenate or uranium were further corrected with a spectrum of the salt in the respective conditions that was previously treated as all the other spectra. For 10 equivalents of perrhenate the absorption of the anion was too strong to be corrected

for, and only three wavelenghts outside the overlap were used (260, 265 and 270 nm). The instrument introduced a random vertical shift of the spectrum, which was corrected for by substracting the average of absorptions in the wavelenght range 330-340 m from all values.

Molar extinction coefficients of the ligand and the Ca(II)/Nd(III) complexes were determined for each solvent at 5 wavelengths (250, 255, 260, 265, 270 nm). Concentrations in each phase of the extraction samples were determined with the respective molar extinction coefficient. The relative concentration for each phase was determined by dividing the concentration by the sum of concentration of both phases. An average was calculated over all 5 wavelenghts and the standard deviation determined using *Openoffice Calc. 4.1.1*. As the standard deviation is drawn from the five wavelengths from one measurement, it does not include systematic and random error between samples.

Pertechnetate samples were only analysed after the visit at the University of Zürich had ended, when it became obvious that the absorption of pertechnetate significantly influenced the spectra. No correction spectrum for pertechnetate was available. For these spectra the concentration was determined from the organic phase alone and the relative content determined from the expected total concentration.

Tables E8 to E11 show the numerical results obtained in the extraction experiments.

For the complexes of Ca(II) and Nd(III) no spectrum was observed in pure hexane due to their low solubilities in the solvent, so no adequate baseline spectrum was available. Instead the molar extinction coefficient or 12N4Py4 in hexane was used for used for the determination of 12N4Py4 concentration in the organic phase.

Table E8: extraction of 12N4Py4 into hexane, results in % conc.					
condition	**pH 2.0**	**pH 3.5**	**pH 6.2**	**pH 9.4**	**pH 12.0**
buffer	2 ± 0.24	0 ± 0.07	0 ± 0.08	1 ± 0.16	27 ± 0.86
KCl only	0 ± 0.00	0 ± 0.00	0 ± 0.00	0 ± 0.05	32 ± 0.41
no ions	-0 ± 0.09	-0 ± 0.07	-0 ± 0.13	-0 ± 0.15	24 ± 2.13
1 eq KBr	0 ± 0.09	-1 ± 0.19	-1 ± 0.25	1 ± 0.07	22 ± 0.43
10 eq KBr	0 ± 0.08	0 ± 0.05	-1 ± 0.18	2 ± 0.32	35 ± 0.51
1 eq KI	-0 ± 0.13	-0 ± 0.08	-0 ± 0.15	-0 ± 0.12	29 ± 0.71
10 eq KI	-3 ± 0.77	-3 ± 0.54	1 ± 1.06	-2 ± 1.85	38 ± 0.88
1 eq NH_4ReO_4	2 ± 0.29	2 ± 0.28	1 ± 0.20	2 ± 0.31	24 ± 0.97
10 eq NH_4ReO_4	-0 ± 0.08	-0 ± 0.05	-0 ± 0.02	2 ± 0.29	4 ± 0.15
1 eq NH_4TcO_4	0 ± 0.00	0 ± 0.00	0 ± 0.00	0 ± 0.00	0 ± 0.00
1 eq NH_4Cl	0 ± 0.09	0 ± 0.03	0 ± 0.11	1 ± 0.14	30 ± 0.29
10 eq NH_4Cl	0 ± 0.11	0 ± 0.08	1 ± 0.15	1 ± 0.14	25 ± 0.40
1 eq KNO_3	0 ± 0.14	-1 ± 0.18	0 ± 0.17	0 ± 0.06	31 ± 0.50
10 eq KNO_3	0 ± 0.07	1 ± 0.04	0 ± 0.21	0 ± 0.10	31 ± 0.54
1 eq $KHSO_4$	0 ± 0.07	-1 ± 0.12	-1 ± 0.24	0 ± 0.03	27 ± 0.71
10 eq $KHSO_4$	-1 ± 0.20	0 ± 0.07	0 ± 0.16	2 ± 0.45	36 ± 0.51
1 eq K_2CO_3	-	-	0 ± 0.22	0 ± 0.05	26 ± 0.73
10 eq K_2CO_3	-	-	1 ± 0.14	2 ± 0.20	31 ± 0.24

condition	pH 2.0	pH 3.5	pH 6.2	pH 9.4	pH 12.0
1 eq NaCl	0 ± 0.04	0 ± 0.06	0 ± 0.05	2 ± 0.18	29 ± 1.24
10 eq NaCl	0 ± 0.07	-1 ± 0.13	-1 ± 0.29	2 ± 0.14	22 ± 1.27
1 eq UCl_4	0 ± 0.29	0 ± 0.23	-1 ± 1.40	0 ± 0.48	24 ± 0.77

Table E9: extraction of 12N4Py4 into octanol, results in % conc.

condition	pH 2.0	pH 3.5	pH 6.2	pH 9.4	pH 12.0
buffer	0 ± 0.07	2 ± 0.23	9 ± 0.49	19 ± 0.50	56 ± 3.68
KCl only	-5 ± 1.23	-6 ± 1.82	-2 ± 1.58	1 ± 1.90	63 ± 3.82
no ions	-7 ± 2.09	-7 ± 3.08	-5 ± 1.55	-4 ± 3.61	88 ± 1.63
1 eq KBr	0 ± 0.05	0 ± 0.09	7 ± 0.30	10 ± 0.38	59 ± 3.56
10 eq KBr	0 ± 0.16	0 ± 0.03	10 ± 0.76	61 ± 0.51	84 ± 1.68
1 eq KI	0 ± 0.07	-1 ± 0.27	7 ± 0.21	12 ± 0.34	58 ± 3.85
10 eq KI	5 ± 0.59	3 ± 0.55	11 ± 1.11	50 ± 7.93	75 ± 9.03
1 eq NH_4ReO_4	0 ± 0.20	1 ± 0.27	9 ± 1.09	17 ± 0.27	65 ± 1.96
10 eq NH_4ReO_4	2 ± 0.33	2 ± 0.19	11 ± 0.52	54 ± 0.75	73 ± 0.22
1 eq NH_4TcO_4	3 ± 0.55	2 ± 0.12	11 ± 0.26	75 ± 5.40	47 ± 8.49
1 eq NH_4Cl	1 ± 0.33	1 ± 0.04	10 ± 0.41	47 ± 0.68	81 ± 2.11
10 eq NH_4Cl	0 ± 0.12	1 ± 0.07	5 ± 0.14	46 ± 0.62	75 ± 2.50
1 eq KNO_3	0 ± 0.09	0 ± 0.04	6 ± 0.20	17 ± 0.61	61 ± 3.57
10 eq KNO_3	0 ± 0.09	0 ± 0.10	6 ± 0.16	18 ± 0.58	61 ± 3.59

condition	pH 2.0	pH 3.5	pH 6.2	pH 9.4	pH 12.0
1 eq $KHSO_4$	-1 ± 0.15	0 ± 0.12	9 ± 0.59	14 ± 0.43	70 ± 3.13
10 eq $KHSO_4$	0 ± 0.10	1 ± 0.07	10 ± 0.75	90 ± 0.20	95 ± 0.19
1 eq K_2CO_3	-	-	9 ± 0.51	14 ± 0.35	72 ± 2.99
10 eq K_2CO_3	-	-	10 ± 0.63	59 ± 0.58	76 ± 2.50
1 eq NaCl	0 ± 0.07	0 ± 0.03	7 ± 0.17	23 ± 0.57	73 ± 2.79
10 eq NaCl	0 ± 0.09	1 ± 0.04	11 ± 0.79	22 ± 0.56	73 ± 2.91
1 eq UCl_4	2 ± 1.08	1 ± 1.09	10 ± 0.41	13 ± 0.98	79 ± 1.08

Table E10: extraction of Ca(II)-12N4Py4, results in % conc.				
solvent	**octanol**		**hexane**	
condition	**pH 6.2**	**pH 9.4**	**pH 6.2**	**pH 9.4**
buffer	1 ± 0.17	1 ± 0.23	0 ± 0.10	0 ± 0.15
1 eq KBr	0 ± 0.18	1 ± 0.46	0 ± 0.00	1 ± 0.11
10 eq KBr	0 ± 0.02	0 ± 0.04	1 ± 0.09	1 ± 0.04
1 eq KI	1 ± 0.19	1 ± 0.28	0 ± 0.00	1 ± 0.05
10 eq KI	3 ± 2.27	1 ± 0.22	1 ± 1.07	-5 ± 2.43
1 eq NH_4ReO_4	0 ± 0.04	1 ± 0.12	0 ± 0.00	0 ± 0.09
10 eq NH_4ReO_4	1 ± 0.46	1 ± 0.53	-1 ± 0.16	0 ± 0.09
1 eq NH_4TcO_4	-	5 ± 1.00	-	0 ± 0.00
10 eq NH_4TcO_4	-	10 ± 3.4	-	4 ± 3.35
1 eq KNO_3	0 ± 0.20	1 ± 0.24	0 ± 0.00	1 ± 0.13
10 eq KNO_3	0 ± 0.09	1 ± 0.05	0 ± 0.02	0 ± 0.03
1 eq $KHSO_4$	0 ± 0.15	1 ± 0.39	0 ± 0.00	1 ± 0.11
10 eq $KHSO_4$	2 ± 0.14	1 ± 0.17	0 ± 0.08	0 ± 0.07
1 eq K_2CO_3	0 ± 0.16	1 ± 0.27	0 ± 0.00	1 ± 0.14
10 eq K_2CO_3	1 ± 0.08	1 ± 0.14	0 ± 0.05	0 ± 0.04
	pH 7 octanol		**pH 7 hexane**	
only KCl	6 ± 0.99		0 ± 0.08	
no ions	6 ± 0.99		0 ± 0.06	

Table E11: extraction of Nd(III)-12N4Py4, results in % conc.				
solvent	**octanol**		**hexane**	
condition	**pH 6.2**	**pH 9.4**	**pH 6.2**	**pH 9.4**
buffer	0 ± 0.03	0 ± 0.19	0 ± 0.05	1 ± 0.13
1 eq KBr	1 ± 0.50	1 ± 0.37	0 ± 0.00	0 ± 0.04
10 eq KBr	0 ± 0.12	1 ± 0.34	1 ± 0.65	0 ± 0.04
1 eq KI	2 ± 0.99	1 ± 0.26	0 ± 0.00	0 ± 0.07
10 eq KI	9 ± 5.13	0 ± 0.19	0 ± 1.14	-5 ± 2.57
1 eq NH_4ReO_4	1 ± 0.38	1 ± 0.33	0 ± 0.00	0 ± 0.03
10 eq NH_4ReO_4	0 ± 0.44	2 ± 0.86	1 ± 0.33	0 ± 0.05
1 eq NH_4TcO_4	-	0 ± 0.53	-	0 ± 0.00
10 eq NH_4TcO_4	-	4 ± 0.69	-	2 ± 1.75
1 eq KNO_3	0 ± 0.02	0 ± 0.03	0 ± 0.00	0 ± 0.08
10 eq KNO_3	0 ± 0.13	1 ± 0.16	1 ± 0.67	0 ± 0.03
1 eq $KHSO_4$	0 ± 0.18	0 ± 0.18	0 ± 0.00	0 ± 0.08
10 eq $KHSO_4$	0 ± 0.11	1 ± 0.32	1 ± 0.67	0 ± 0.03
1 eq K_2CO_3	1 ± 0.59	2 ± 0.59	0 ± 0.00	0 ± 0.05
10 eq K_2CO_3	0 ± 0.24	1 ± 0.20	1 ± 0.93	0 ± 0.05
	pH 7 octanol		**pH 7 hexane**	
only KCl	5 ± 2.25		0 ± 0.13	
no ions	4 ± 1.80		0 ± 0.07	

Americium Experiments

Stock solution 0.83 ml of a 3.6 MBq/ml (0.487 mg/ml, 0.002 mmol/ml) stock solution of ^{243}Am in aqueous HCl was evaporated to dryness under a heat lamp. The residue were repeadedly disolved in water and reevaporated to remove traces of HCl. It was then disolved in an aqueous KCl solution (3 ml, 1M) .

Experiment A) A methanolic solution of 12N4Py4 (29 µl, $5.77*10^{-4}$ mmol, 0.0199 M) was left in a fluorescence cuvette to evaporate overnight. It was redissolved in Britton Robinson buffer (as described for extractions, 1 ml, pH 9.04) and mixed with ^{243}Am stock solution (1 ml, $5.53*10^{-4}$ mmol). Luminescence at several wavelenghts (497, 510 and 515 nm) was measured over time, but no emission was recorded. After an excess of 24 h it was observed that a colourless precipitate had formed in the cuvette. The pH was adjusted to 4-5 by addition of HCl (ca 6 M) and by means of pH paper. Luminescence was measured over time, no emission was observed after 9 days and the experiment was aborted. The solution was used to set up extraction experiment D.

Experiment B) A methanolic solution of 12N4Py4 (29 µl, $5.77*10^{-4}$ mmol, 0.0199 M) was left in a fluorescence cuvette to evaporate overnight. The residue was redissolved in Britton-Robinson buffer (as described for extractions, 1ml, pH 5.5) and mixed with ^{243}Am stock solution (1 ml, $5.53*10^{-4}$ mmol). Precipitation was observed again and no luminescence was measured. The experiment was aborted. The solution was used to set up extraction experiments E and F.

Experiment C) A third experiment was set up. 1 ml of the americium stock solution ($5.53*10^{-4}$ mmol) was diluted with aqueous KCl (1 ml, 1 M). 12N4Py4 solution (0.015 M) was added in steps of 10 µl, briefly heated to 40°C to encourage complexation and the luminescence recorded. After a total addition of 100 µl, another 100 µl were added to bring the total addition of 12N4Py4 to 5.4 equivalents of the americium concentration. No significant change to the emission was observed.

Extraction with Americium

Experiment D: Two samples were prepared with 130 µl of the first luminescence titration with americium, that were diluted with 685 µl of buffer pH 5.5 and 685 µl of a 1 M KCl solution. 1.5 ml of either hexane or octanol were added.

Experiment E: The solution obtained in luminescence experiment 2 was acidified with HCl to pH 3 and checked by pH paper. This completely redissolved the observed precipitate. Two samples were prepared by diluting 130 µl of this solution with 685 µl of buffer pH 3.5 and 685 µl of a 1M KCl solution. 1.5 ml of either hexane or octanol were added.

Experiment F: The two solutions used for the extraction experiment E were basified with KOH to approximately pH 7 and remeasured after a further 7 days equilibration time.

After 7 days of equilibration both phases of each sample were analysed by UV-Vis spectroscopy and gamma spectroscopy. UV-Vis spectra were deemed not accurate enough and not further processed. Table E12 shows the results of the gamma

spectroscopy for ^{243}Am.

Table E12: ^{243}Am γ-spectroscopy results, relative content (%) in organic phase		
condition	**octanol**	**hexane**
pH 3	0	0
pH 5	0	1
pH 7	0	0

Technetium experiments

Protonation studies

12N4Py4 (27.3 mg, 0.05 mmol) was dissolved in MeOH (1 ml) and added to a solution of NH_4TcO_4 (0.05 mmol in 1 ml H_2O). The mixture was stirred for 24 h and analysed by HPLC. A peak observed in the radio trace at 4.08 min is congruent with the known retention for pertechnetate. The solution was evaporated under a stream of nitrogen and dissolved in D_2O for NMR analysis. Both ^{1}H-NMR and ^{99}Tc-NMR showed spectra consistent with the starting materials.

Deuterated hydrochloric acid (DCl in D_2O) was added to the sample. After 3 days a blueish solution with blue-green crystals was obtained. The sample was remeasured to give a ^{1}H-NMR consistent with protonated 12N4Py4 and a ^{99}Tc-NMR consistent with pertechnetate. HPLC did not show any new species. The material was completely dissolved in acidic water to give a blueish solution and left standing to crystallise. No crystals were obtained appropriate for single crystal X-ray diffraction and the material decomposed over time to a brownish substance.

Similar experiments were conducted with 9N3Py3 and $CyMe_4$-BTPhen. A solution of NH_4TcO_4 (0.05 mmol, 1 ml H_2O) and a solution of the respective ligand (0.05 mmol, 1 ml MeOH) were mixed and stirred for 24h. A HPLC analysis showed the presence of pertechnetate. NMR were consistent with the starting materials. Upon acidification with deuterated HCl a precipitate slowly formed. Spectra were consistent with protonated ligand and free pertechnetate. Attempts to recrystallise the precipitates were unsuccessful.

Extraction with technetium

NH_4TcO_4 (150.2 mg) was dissolved in H_2O (0.5 ml), treated with 4 drops of H_2O_2 and stirred overnight. The solvent was removed under a stream of nitrogen and the residue redissolved in H_2O (2 ml) and filtered. The concentration of pertechnetate was determined by liquid scintillation counting to be 0.178 mmol/ml (stock A). This stock solution was used to produce a tenfold dilution (stock B).

In Eppendorf vials, 12N4Py4 (20 µl of a 0.0094 M solution), Ca(II)-12N4Py4 (37.5 µl, same stock solution as described above) and Nd(II)-12N4Py4 (37.5 µl, same stock solution as described above) were evaporated under a stream of nitrogen and redissolved with 0.5 ml buffer and 0.5 ml of octanol or hexane. The vials were transfered to the radio-chemistry laboratory and 10.5 µl of either stock A (10 equivalents) or stock B (1 equivalent) of pertechnetate was added. After an equilibration time of 7 days the hexane phases had completely evaporated. Hexane was re-added and left to equilibrate for 2-3 hours. While measuring the 1 equivalent batch it quickly became obvious that this time was not sufficient for extraction to equilibrate and the 10 equivalent samples were not measured for the ligand.

Due to limited time available for the study, the metal complexes Ca(II)-12N4Py4 and Nd(III)-12N4Py4 were only measured at pH 9.4.

UV-Vis spectra were measured after 0.3 ml of the respective phase were diluted to 2 ml in water (aqueous phase), hexane (hexane phase) or methanol (octanol phase). UV-measurements were processed as described in the extraction section of non-radioactive species and the results are given in the corresponding Tables.

Each original phase was also analysed by liquid scintillaition counting, using 30 µl of sample in 7 ml of the scintillation solution.

Table E13 gives the results of the liquid scintillation counting (LSC) for ^{99}Tc.

Table E13: ^{99}Tc LSC results, relative content (%) in organic phase				
	octanol		**hexane**	
condition	**1 eq ^{99}Tc**	**10 eq ^{99}Tc**	**1 eq ^{99}Tc**	**10 eq ^{99}Tc**
pertechnetate blank pH 2.0	0.6	-	0.1	-
pertechnetate blank pH 3.5	0.2	-	0	-
pertechnetate blank pH 6.2	0.1	-	0.2	-
pertechnetate blank pH 9.4	0.0	-	0.3	-
pertechnetate blank pH 12.0	0.9	-	0.0	-
12N4Py4 pH 2.0	1.1	1.4	0.2	-
12N4Py4 pH 3.5	0.8	1.2	0.0	-
12N4Py4 pH 6.2	2.4	1.3	0.0	-
12N4Py4 pH 9.4	12.9	1.0	0.0	-
12N4Py4 pH 12.0	2.4	1.0	0.0	-
Ca(II)-12N4Py4 pH 9.4	0.9	1.4	0.0	0.1
Nd(III)-12N4Py4 pH 9.4	0.8	0.8	0.1	0.0

Crystallography

Crystals were measured at 150°K. Absorption correction was performed using semi-empirical methods from equivalents. Refinement was performed using full-matrix least-squares methods on F^2.

All structures were measured, solved and refined by Dr. Lukas Pfeifer and Dr. Amber Thompson.

Cif files as obtained from Dr. Amber Thomspon were included on the CD attached to this thesis.

compound	**Ce(III)-12N4Py4 triflate**	**Ca(II)-12N4Py4 chloride**
identification code	WTS01	WTS02
empirical formula	C40.78 H50.66 Ce1 F9 N10 O9.55 S3	C32 H70 Ca1 Cl2 N8 O15
formula weight	1241.06	917.94
diffractometer	Oxford Diffraction SuperNova	Oxford Diffraction SuperNova
crystal system	orthorhombic	tetragonal
space group	P b c n	P 4/n
unit cell a [Å]	34.1500(2)	14.3034(1)
unit cell b [Å]	13.4023(1)	14.3034(1)
unit cell c [Å]	22.0154(1)	11.2073(1)
unit cell α [°]	90	90
unit cell β [°]	90	90
unit cell γ [°]	90	90
Volume [$Å^3$]	10076.20(11)	2292.87(4)
Z	8	2
Density (calculated)	1.636 Mg/m^3	1.329 Mg/m^3
Absorption coefficient	9.005 mm^{-1}	2.848 mm^{-1}
F(000)	5030.057	984.000
crystal size	0.21 x 0.20 x 0.19 mm^3	0.20 x 0.10 x 0.05 mm^3
Theta range for data collection	3.543 to 76.224°	4.371 to 76.158°
index ranges	-40<=h<=42, -16<=k<=16, -27<=l<=24	-17<=h<=17, -17<=k<=12, -14<=l<=12
Reflections collected	198326	23131
Independent reflections	10531 [R(int) = 0.052]	2395 [R(int) = 0.019]
completeness to theta=76.158°	99.8 %	99.7 %
max and min transmission	0.18 and 0.08	0.87 and 0.63
data/ restraints/ parameters	10530/1493/724	2392/0/133
Goodness-of-fit on F^2	1.0221	1.0257
Final R indices [I>2sigma(I)]	R1 = 0.0423, wR2 = 0.0998	R1 = 0.0315, wR2=0.0811
R indices (all data)	R1 = 0.0452, wR2 = 0.1020	R1=0.0321, wR2=0.0817
Largest diff. peak and hole	1.40 and -1.22 $e.Å^{-3}$	0.26 and -0.29 $e.Å^{-3}$

compound	**Na(I)-12N4Py4 ReO_4**	**Ca(II)-9N3Py3 triflate**
identification code	WTS03	WTS04
empirical formula	C32 H40 N8 Na1 O4 Re1	C26 H30 Ca1 F6 N6 O6 S2
formula weight	809.91	740.76
diffractometer	Nonius KappaCCD	Oxford Diffraction SuperNova
crystal system	monoclinic	monoclinic
space group	P 21/c	P 21/n
unit cell a [Å]	9.1578(1)	10.1338(1)
unit cell b [Å]	14.2594(1)	16.6704
unit cell c [Å]	24.8352(2)	18.6438(2)
unit cell α [°]	90	90
unit cell β [°]	97.5846(3)	93.2943(8)
unit cell γ [°]	90	90
Volume [$Å^3$]	3214.72(5)	3144.38(6)
Z	4	4
Density (calculated)	1.673 Mg/m^3	1.565 Mg/m^3
Absorption coefficient	3.844 mm^{-1}	3.746 mm^{-1}
F(000)	1624	1528
crystal size	0.25 x 0.20 x 0.07 mm^3	0.20 x 0.12 x 0.08 mm^3
Theta range for data collection	5.115 to 27.484°	3.559 to 76.152°
index ranges	-11<=h<=11, -18<=k<=18, -32<=l<=32	-12<=h<=8, -20<=k<=20, -23<=l<=23
Reflections collected	92584	33871
Independent reflections	7310 [R(int) = 0.040]	6549 [R(int) = 0.024]
completeness to theta=76.158°	99.3 %	99.9%
max and min transmission	0.76 and 0.62	0.74 and 0.56
data/ restraints/ parameters	7310/0/415	6547/0/424
Goodness-of-fit on F^2	0.9983	0.9965
Final R indices [I>2sigma(I)]	R1 = 0.0397, wR2 = 0.0748	R1 = 0.0311, wR2 = 0.0763
R indices (all data)	R1 = 0.0645, wR2 = 0.0965	R1 = 0.0342, wR2 = 0.0789
Largest diff. peak and hole	4.33 and -2.02 e.$Å^{-3}$	0.48 and -0.54 e.$Å^{-3}$

compound	**12N4Py4*3H*3I3**	**12N4Py4*3K*3I3**
identification code	WTS05	WTS06
empirical formula	C32 H43 I9 N8	C32 H40.38 I9.19 K2.81 N8
formula weight	1681.89	1813.48
diffractometer	Oxford Diffraction SuperNova	Nonius KappaCCD
crystal system	orthorhombic	monoclinic
space group	P 21 21 21	P 1 21/c 1
unit cell a [Å]	15.3147(4)	26.0257(4)
unit cell b [Å]	18.0068(4)	15.2653(2)
unit cell c [Å]	33.8400(9)	13.0057(2)
unit cell α [°]	90	90
unit cell β [°]	90	94.0974(5)
unit cell γ [°]	90	90
Volume [Å3]	9332.0(4)	5153.83(13)
Z	8	4
Density (calculated)	2.394 Mg/m3	2.337 Mg/m3
Absorption coefficient	6.011 mm-1	5.787 mm-1
F(000)	6144	3315.754
crystal size	0.18 x 0.10 x 0.02 mm3	0.20 x 0.04 x 0.02 mm3
Theta range for data collection	3.409 to 30.680°	5.118 to 27.544°
index ranges	-21<=h<=21, -24<=k<=24, -43<=l<=47	-16<=h<=16, -19<=k<=19, -33<=l<=33
Reflections collected	111722	68743
Independent reflections	26164 [R(int) = 0.050]	11654 [R(int) = 0.075]
completeness to theta=76.158°	99.5 %	98.8 %
max and min transmission	0.89 and 0.52	0.89 and 0.78
data/ restraints/ parameters	26163/142/939	8822/773/471
Goodness-of-fit on F2	0.9324	0.9999
Final R indices [I>2sigma(I)]	R1 = 0.0411, wR2 = 0.0727	R1 = 0.1740, wR2 = 0.5083
R indices (all data)	R1 = 0.0598, wR2 = 0.0878	R1 = 0.1894, wR2 = 0.5157
Largest diff. peak and hole	2.02 and -1.88 e.Å-3	5.42 and -6.09 e.Å-3

compound	**12N4Py4*2H*2I**
identification code	WTS07
empirical formula	C32 H43.45 I2 N8 O0.72
formula weight	805.58
diffractometer	Oxford Diffraction SuperNova
crystal system	monoclinic
space group	P 21/c
unit cell a [Å]	13.3423(2)
unit cell b [Å]	13.8933(1)
unit cell c [Å]	18.8826(2)
unit cell α [°]	90
unit cell β [°]	95.6801(10)
unit cell γ [°]	90
Volume [$Å^3$]	3483.05(7)
Z	4
Density (calculated)	1.536 Mg/m^3
Absorption coefficient	14.460 mm^{-1}
F(000)	1612.929
crystal size	0.22 x 0.10 x 0.06 mm^3
Theta range for data collection	3.329 to 76.297°
index ranges	-16<=h<=15, -17<=k<=14, -23<=l<=23
Reflections collected	79672
Independent reflections	7279 [R(int) = 0.058]
completeness to theta=76.158°	99.7%
max and min transmission	0.42 and 0.08
data/ restraints/ parameters	7279/0/389
Goodness-of-fit on F^2	1.0032
Final R indices [I>2sigma(I)]	R1 = 0.0340, wR2 = 0.0888
R indices (all data)	R1 = 0.0357, wR2 = 0.0921
Largest diff. peak and hole	1.47 and -1.22 e.$Å^{-3}$

References

[1] H. E. Gottlieb, V. Kotlyar, A. Nudelman, *J. Org. Chem.* **1997**, *62*, 7512–7515.
[2] J. Cosier, A. M. Glazer, *J. Appl. Crystallogr.* **1986**, *19*, 105–107.
[3] Z. Otwinowski, W. Minor, in *Methods Enzymol.*, Elsevier, **1997**, pp. 307–326.
[4] L. Palatinus, G. Chapuis, *J. Appl. Crystallogr.* **2007**, *40*, 786–790.
[5] P. W. Betteridge, J. R. Carruthers, R. I. Cooper, K. Prout, D. J. Watkin, *J. Appl. Crystallogr.* **2003**, *36*, 1487–1487.
[6] R. I. Cooper, A. L. Thompson, D. J. Watkin, *J. Appl. Crystallogr.* **2010**, *43*, 1100–1107.
[7] R. I. Cooper, R. O. Gould, S. Parsons, D. J. Watkin, *J. Appl. Crystallogr.* **2002**, *35*, 168–174.
[8] P. Parois, R. I. Cooper, A. L. Thompson, *Chem. Cent. J.* **2015**, *9*, DOI 10.1186/s13065-015-0105-4.
[9] C. F. Macrae, I. J. Bruno, J. A. Chisholm, P. R. Edgington, P. McCabe, E. Pidcock, L. Rodriguez-Monge, R. Taylor, J. van de Streek, P. A. Wood, *J. Appl. Crystallogr.* **2008**, *41*, 466–470.
[10] L. S. Natrajan, N. M. Khoabane, B. L. Dadds, C. A. Muryn, R. G. Pritchard, S. L. Heath, A. M. Kenwright, I. Kuprov, S. Faulkner, *Inorg. Chem.* **2010**, *49*, 7700–7709.
[11] S. H. Eitel, M. Bauer, D. Schweinfurth, N. Deibel, B. Sarkar, H. Kelm, H.-J. Krüger, W. Frey, R. Peters, *J. Am. Chem. Soc.* **2012**, *134*, 4683–4693.
[12] K. Wieghardt, E. Schoeffmann, B. Nuber, J. Weiss, *Inorg. Chem.* **1986**, *25*, 4877–4883.
[13] O. A. Blackburn, A. M. Kenwright, A. R. Jupp, J. M. Goicoechea, P. D. Beer, S. Faulkner, *Chem. – Eur. J.* **2016**, *22*, 8929–8936.
[14] H. Ito, H. Tsukube, S. Shinoda, *Chem. - Eur. J.* **2013**, *19*, 3330–3339.
[15] A. Kraft, *J Chem Educ* **2003**, *80*, 554.
[16] F. H. Sweeton, R. E. Mesmer, C. F. Baes Jr, *J. Solut. Chem.* **1974**, *3*, 191–214.
[17] L. C. Antoine, *Comptes Rendus* **1888**, *107*, 681–684.
[18] H. T. S. Britton, R. A. Robinson, *J. Chem. Soc.* **1931**, 1456–1462.

Appendix

In chapters 5 and 6 equations were used to fit dissociation constants and metal binding constants to pH data obtained in pH titrations of metal complexes. The development of these equations is shown in this section.

Fitting equation

The starting point is to find equations that completely describe the system with relations between species. All quantities, in this case concentrations of species, that cannot be directly be measured, have to be substituted with expressions of measurable quantities and/or constants. To eliminate all unknown and unmeasurable concentrations at least as many equations have to be found to start with.

In a system of a ligand with four protonated species, a 1:1 metal complex, free metal and no alternative species there are seven unknown concentrations: [L], [LH], [LH_2], [LH_3], [LH_4], [LM] and [M]. The quantity [H_b] is deduced from the measured data. They are described by the following eight equations (correspond to equations 5.6 - 5.13 in chapter 5).

The equilibria between different protonated ligand species are defined by

$$K_1 = \frac{[L][H]}{[LH]} \qquad \text{A1}$$

$$K_2 = \frac{[LH][H]}{[LH_2]} \qquad \text{A2}$$

$$K_3 = \frac{[LH_2][H]}{[LH_3]} \qquad \text{A3}$$

and

$$K_4 = \frac{[L_3][H]}{[LH_4]} \quad \text{A4}$$

The equilibrium of metal complex formation is

$$K_c = \frac{[LM]}{[L][M]} \quad \text{A5}$$

From chapter 3 it is known that the concentration of protons bound by ligand [H_b] can be determined from the experimental set up and the measured pH values, being dependent on the concentrations of the protonated ligand species.

$$[H_b] = [LH] + 2[LH_2] + 3[LH_3] + 4[LH_4] \quad \text{A6}$$

Finally, two equations can be formed from the total added metal and ligand quantities and the unknown species that derive from them.

$$M_{tot} = [LM] + [M] \quad \text{A7}$$

$$L_{tot} = [L] + [LH] + [LH_2] + [LH_3] + [LH_4] + [LM] \quad \text{A8}$$

In order to derive a function capable to fit the equilibrium constants K_1, K_2, K_3, K_4 and K_c to experimental data, an equation has to be found that consists entirely of known quantities and the constants to be fitted.

First, equations A1, A2, A3 and A4 are rearranged to express [LH], [LH_2], [LH_3] and [LH_4] as a function of [L] and the dissociation constants K_1 to K_4 to be able to eliminate them from the other equations.

$$K_1 = \frac{[L][H]}{[LH]} \rightarrow [LH] = [L]\frac{[H]}{K_1} \quad \text{A9}$$

$$K_2 = \frac{[LH][H]}{[LH_2]} \rightarrow [LH_2] = [LH]\frac{[H]}{K_2} \rightarrow [LH_2] = [L]\frac{[H]^2}{K_1 K_2} \quad \text{A10}$$

$$K_3 = \frac{[LH_2][H]}{[LH_3]} \rightarrow [LH_3] = [LH_2]\frac{[H]}{K_3} \rightarrow [LH_3] = [L]\frac{[H]^3}{K_1 K_2 K_3} \quad \text{A11}$$

$$K_4 = \frac{[LH_3][H]}{[LH_4]} \rightarrow [LH_4] = [LH_3]\frac{[H]}{K_4} \rightarrow [LH_4] = [L]\frac{[H]^4}{K_1 K_2 K_3 K_4} \quad \text{A12}$$

Equation A7 is rearranged to give an expression for [LM].

$$M_{tot} = [LM] + [M] \rightarrow [LM] = M_{tot} - [M] \quad \text{A13}$$

Then [LM] is substituted in equation 5 and rearranged to give an expression for [L].

$$K_c = \frac{[LM]}{[L][M]} \rightarrow [L] = \frac{[LM]}{[M]K_c} = \frac{M_{tot} - [M]}{[M]K_c} \quad \text{A14}$$

$[H_b]$ (equation A6) can now be described using the expressions A9-A14.

$$[H_b] = [LH] + 2[LH_2] + 3[LH_3] + 4[LH_4]$$

$$= [L]\frac{[H]}{K_1} + 2[L]\frac{[H]^2}{K_1 K_2} + 3[L]\frac{[H]^3}{K_1 K_2 K_3} + 4[L]\frac{[H]^4}{K_1 K_2 K_3 K_4}$$

$$= \frac{M_{tot} - [M]}{[M]K_c}\underbrace{\left(\frac{[H]}{K_1} + 2\frac{[H]^2}{K_1 K_2} + 3\frac{[H]^3}{K_1 K_2 K_3} + 4\frac{[H]^4}{K_1 K_2 K_3 K_4}\right)}_{A}$$

$$[H_b] = \frac{M_{tot} - [M]}{[M]K_c}A \quad \text{A15}$$

The equation is then rearranged to receive an expression for [M].

$$[H_b][M]K_c = (M_{tot} - [M])A$$

$$[H_b][M]K_c = M_{tot}A - [M]A$$

$$[M]([H_b]K_c + A) = M_{tot}$$

$$[M] = \frac{M_{tot}}{[H_b]K_c + A} \quad \text{A16}$$

Similarly the equation for L_{tot} (equation A8) is rewritten with the established

expressions.

$$
\begin{aligned}
L_{tot} &= [L] + [LH] + [LH_2] + [LH_3] + [LH_4] + [LM] \\
&= [L]\underbrace{\left(1 + \frac{[H]}{K_1} + \frac{[H]^2}{K_1 K_2} + \frac{[H]^3}{K_1 K_2 K_3} + \frac{[H]^4}{K_1 K_2 K_3 K_4}\right)}_{B} + M_{tot} - [M] \\
&= [L]B + M_{tot} - [M] \\
&= \frac{M_{tot} - [M]}{[M] K_c} B + M_{tot} - [M] \\
&= \frac{M_{tot} - \dfrac{M_{tot} A}{K_c [H_b] + A}}{\dfrac{M_{tot} A}{K_c [H_b] + A} K_c} B + M_{tot} - \frac{M_{tot} A}{K_c [H_b] + A}
\end{aligned}
\qquad \text{A17}
$$

M_{tot} in the first term is expanded by multiplication with $\frac{K_c[H_b] + A}{K_c[H_b] + A}$, allowing several variables to be cancelled.

$$
\begin{aligned}
L_{tot} &= \frac{\dfrac{M_{tot}\left(K_c[H_b] + A\right)}{K_c[H_b] + A} - \dfrac{M_{tot} A}{K_c[H_b] + A}}{\dfrac{M_{tot} A K_c}{K_c[H_b] + A}} B + M_{tot} - \frac{M_{tot} A}{K_c[H_b] + A} \\
&= \frac{M_{tot}\left(K_c[H_b] + A\right) - M_{tot} A}{M_{tot} A K_c} B + M_{tot} - \frac{M_{tot} A}{K_c[H_b] + A} \\
&= \frac{K_c[H_b] + A - A}{A K_c} B + M_{tot} - \frac{M_{tot} A}{K_c[H_b] + A} \\
&= \frac{K_c[H_b] B}{A K_c} + M_{tot} - \frac{M_{tot} A}{K_c[H_b] + A} \\
&= \frac{[H_b] B}{A} + M_{tot} - \frac{M_{tot} A}{K_c[H_b] + A}
\end{aligned}
\qquad \text{A18}
$$

In order to rearrange the equation to obtain a function for [Hb], M_{tot} is subtracted from

both sides and (L_{tot} - M_{tot}) substituted by Δ_{tot}, which allows it to be cancelled from the solution in cases where L_{tot} and M_{tot} are equal, such as in the case for 9N3Py3.

$$L_{tot} - M_{tot} = \frac{[H_b]B}{A} - \frac{M_{tot}A}{K_c[H_b] + A} \qquad \text{A19}$$

The equation is multiplied by ($K_C[H_b]$ + A).

$$\Delta_{tot} K_c[H_b] + \Delta_{tot} A = \frac{[H_b]B(K_c[H_b]+A)}{A} - M_{tot}A$$

$$\Delta_{tot} K_c[H_b] + \Delta_{tot} A = \frac{[H_b]^2 B K_c}{A} + \frac{A[H_b]B}{A} - M_{tot}A$$

$$[H_b]K_c\Delta_{tot} + A\Delta_{tot} = \frac{[H_b]^2 B K_c}{A} + [H_b]B - M_{tot}A \qquad \text{A20}$$

by rearrangement the typical form of a quadratic equation is obtained.

$$0 = [H_b]^2\frac{B K_c}{A} + [H_b](B - K_c\Delta_{tot}) - A(M_{tot} + \Delta_{tot})$$

$$0 = [H_b]^2\frac{B K_c}{A} + [H_b](B - K_c\Delta_{tot}) - A(M_{tot} + L_{tot} - M_{tot})$$

$$0 = [H_b]^2\frac{B K_c}{A} + [H_b](B - K_c\Delta_{tot}) - AL_{tot} \qquad \text{A21}$$

A function for $[H_b]$ can be obtained using the quadratic formula.

$$[H_b] = \frac{-(B - K_c\Delta_{tot}) \pm \sqrt{(B - K_c\Delta_{tot})^2 + 4BK_cL_{tot}}}{\frac{2BK_c}{A}} \qquad \text{A22}$$

This equation corresponds to equation 5.14.

For titrations of 9N3Py3 the metal complex was used as a component for the preparation of each sample instead of ligand and metal salt separately, in this case Δ_{tot} is equal zero and the equation can be simplified. This equation was also used in

chapter 6 (equation 6.1).

$$[H_b] = \frac{-B \pm \sqrt{B^2 + 4 B K_c M_{tot}}}{\frac{2 B K_c}{A}} \qquad \text{A23}$$

For systems with more or less protonated species, only the expressions A and B have to be adjusted accordingly.

For each value of $[H_b]$ two solutions with different values for K_c are obtained that are both mathematically correct. For chemical systems, however, certain constraints apply that determine which of the two solutions is valid.

Generally concentrations of chemicals and therefore also binding constants can never be negative, which includes $[H_b]$. Only the solution that adds the term under the square root yields a valid solution for this system.

Comment on $[H_b]$

In chapter 3 the basis of the fitting function was defined through the sum of anions and cations in solution being equal. With the addition of metal salts in principle more anions and cations are added. On the cation side there is [M] and [LM], both being trivalent, so 3[M] and 3[LM] would have to be added to the cation side of the equation. The counter ion of the metal salt employed is added to the anion side, here named [X].

$$[Cl] + [OH] + 3[X] = [LH] + 2[LH_2] + 3[LH_3] + 4[LH_4] + 3[LM] + 3[M] \qquad \text{A24}$$

The anion is not considered to participate in any reaction and is equal to three times the initial metal salt concentration M_{tot} (for M(III)). Also the sum of [LM] and [M] is equal to M_{tot}, allowing to cancel [X], [LM] and [M] from the equation.

$$[Cl] + [OH] + M_{tot} = [H] + [K] + [LH] + 2[LH_2] + 3[LH_3] + 4[LH_4] + 3M_{tot} \quad \text{A25}$$

For this system H_b can still be calculated directly from experimentally known concentrations and equation A6 is valid.

Including hydroxide formation

When it is assumed that metal hydroxide plays a role in the titration, the very basic assumption that negative and positive charges balance themselves in solution has to be adjusted.

$$[Cl]+[OH] + 3M_{tot} = [H] + [K] + [LH] + 2[LH_2] + 3[LH_3] + 4[LH_4] + 3[LM] + 3[M] + 2[MOH] + [MOH_2] \quad \text{A26}$$

As discussed in the previous section, the counter ion of the original metal salt can be substituted by M_{tot}. On the cation side M_{tot} is now distributed onto [M], [LM], [MOH], [MOH_2] and [MOH_3], the hydroxides however carry a lower charge or are even neutral. This does no longer allow their substitution with $M_{tot.}$

[Cl], [OH], [H] and [K] were previously combined to give [H_b], the concentration of protons bound to ligand molecules. Here this is no longer true as it also contains metal concentrations. It is however still a valuable quantity and for this example it is renamed [H_b']. The more familiar form of equation A26 is obtained by taking all unknown quantities to one side. All concentrations of protonated 12N4Py4 can be substituted by the expression [L]A that has been previously established.

$$[H_b'] = [L]A + 3[LM] + 3[M] + 2[MOH] + [MOH_2] - 3M_{tot} \quad \text{A27}$$

It is mathematically possible to transform equation A27 to give a fitting equation equivalent to equations A22 and A23, but because there are now three more species

present and the terms get increasingly more complicated. This is mostly due to the form of the metal complex equilibration equation that requires quadratic equations to be solved. Instead, all but one unknown species in [H_b'] are substituted with expressions obtained from other equations describing the system, to allow all of them to be calculated for each experimental data point. K_c is then derived from these concentrations. In principle any concentration could be chosen to remain in the equation and to be calculated first. Here, [L] is chosen because several expressions using [L] have already been established.

The metal hydroxide concentrations can be substituted using their formation constants.

$$K_{OHx} = \frac{[M(OH)_x][H]^x}{[M]}$$

$$[H_b] = [L]A + 3[LM] + 3[M] + 2[M]\frac{K_{OH}}{[H]} + [M]\frac{K_{OH2}}{[H]^2} - M_{tot}$$

$$[H_b] = [L]A + 3[LM] + [M]\underbrace{\left(3 + 2\frac{K_{OH}}{H} + \frac{K_{OH2}}{H^2}\right)}_{C} - M_{tot}$$

$$[H_b] = [L]A + 3[LM] + [M]C - M_{tot} \qquad \text{A28}$$

Similarly, the total metal concentration M_{tot} now also has to include the hydroxides. They are also substituted by using their formation constants.

$$M_{tot} = [LM] + [M] + [MOH] + [MOH_2] + [MOH_3]$$

$$M_{tot} = [LM] + [M] + [M]\frac{K_{OH}}{[H]} + [M]\frac{K_{OH2}}{[H]^2} + [M]\frac{K_{OH3}}{[H]^3}$$

$$M_{tot} = [LM] + [M]\underbrace{\left(1 + \frac{K_{OH}}{[H]} + \frac{K_{OH2}}{[H]^2} + \frac{K_{OH3}}{[H]^3}\right)}_{D}$$

$$M_{tot} = [LM] + [M]D \qquad \text{A29}$$

No new ligand species are introduced, the equation for L_{tot} does not contain any new components and is shortened with the previously established expression [L]B for all protonated and free ligand species.

$$L_{tot} = [L] + [LH] + [LH_2] + [LH_3] + [LH_4] + [LM]$$

$$L_{tot} = [L]B + [LM] \qquad \text{A30}$$

Equation A30 is used to find an expression for [LM] that is inserted into equations A28 and A29.

$$L_{tot} - [L]B = [LM] \qquad \text{A31}$$

$$[H_b] = [L]A + 3L_{tot} - 3[L]B + [M]C - 3M_{tot} \qquad \text{A32}$$

$$M_{tot} = L_{tot} - [L]B + [M]D \qquad \text{A33}$$

The last species to be substituted is [M], and equation A33 is used to develop the expression.

$$M_{tot} - L_{tot} + [L]B = [M]D$$

$$\frac{M_{tot} - L_{tot} + [L]B}{D} = [M] \qquad \text{A34}$$

This is inserted into equation A32 and the equation rearranged to provide an

expression of [L]

$$[H_b] = [L]A + 3L_{tot} - 3[L]B + C\frac{M_{tot} - L_{tot} + [L]B}{D} - 3M_{tot}$$

$$[H_b] + 3M_{tot} - 3L_{tot} = [L]A - 3[L]B + C\frac{M_{tot} - L_{tot}}{D} + [L]\frac{CB}{D}$$

$$[H_b] + 3M_{tot} - 3L_{tot} - C\frac{M_{tot} - L_{tot}}{D} = [L]\left(A - 3B + \frac{CB}{D}\right)$$

$$[L] = \frac{[H_b] + 3M_{tot} - 3L_{tot} - C\frac{M_{tot} - L_{tot}}{D}}{A - 3\mathrm{B} + \frac{CB}{D}} \qquad \text{A35}$$

This equation corresponds to equation 5.16

Metals other than Ln(III)

For metal ions with different charges the equation needs to be adjusted. The development is very similar and will not be shown in detail again. In the case of M(II), such as Ca(II), equation A35 becomes

$$[L] = \frac{[H_b] + 2M_{tot} - 2L_{tot} - C\frac{M_{tot} - L_{tot}}{D}}{A - 2\mathrm{B} + \frac{CB}{D}} \qquad \text{A36}$$

with

$$C = 2 + \frac{K_{OH}}{[H]}$$

$$D = 1 + \frac{K_{OH}}{[H]} + \frac{K_{OH2}}{[H]^2}$$

For M(I) like Na(I) the equation becomes

$$[L] = \frac{[H_b] + M_{tot} - L_{tot} - C\frac{M_{tot} - L_{tot}}{D}}{A - B + \frac{CB}{D}} \qquad \text{A37}$$

with

$$C = 1$$

$$D = 1 + \frac{K_{OH}}{[H]}$$

Comment on the choice of hydroxide formation constants

Even though the formation constants of lanthanide hydroxide species have already been studied in the 1970s[1,2], values given in the literature vary. The low solubility of lanthanide hydroxides make determination of their formation constants extremely challenging.

In the fitting procedure values taken from "Hydrolysis of metal ions"[3] published in 2016 where used. The second and third hydroxide formation constants tend to be less reliable, which is why said publication does not give values for many of the lanthanide ions under investigation in this project. For cerium, praseodymium and ytterbium values for neodymium were used instead. Wherever possible, the constants were calculated based on the temperature dependent equation given in literature.[3] For Ca(II) the second constant was never accurately measured experimentally. It was decided to use pK_{OH2}= 25, which is somewhat lower than pK_{OH3}= 26.5 for Neodymium and seemed reasonable for $Ca(OH)_2$, being a very strong base.

When varying this value in the numerical determination of the binding constant it was discovered that the exact value chosen for K_{OH2} does not have an influence on the

outcome of the calculation, so for this system it is not necessary to obtain a more accurate value.

Simulation of equilibria

To simulate concentrations of species in solution, expressions have to be formed that describe one single species in dependence of total amounts added, pH and the predetermined binding constants. The most straight forward technique is to develop one such equation for one concentration and to calculate the remaining species from the first species concentration. In the previous discussions expressions for [L] have been used frequently, so it was also chosen as the starting concentration in the simulations. The protonated ligand species are substituted with the expression [L]B as previously established, for the metal hydroxide the expression D can be used accordingly. [LM] and [M] are isolated from equations for K_c and M_{tot} and inserted into the sum of ligand species. This is then converted to an equation for [L].

$$K_c = \frac{[LM]}{[L][M]} \rightarrow K_c[L][M] = [LM]$$

$$M_{tot} = [LM] + [M]D \rightarrow [M] = \frac{M_{tot}}{[L]K_c + D}$$

$$L_{tot} = [L]B + [LM] \rightarrow L_{tot} = [L]B + K_c[L]\frac{M_{tot}}{[L]K_c + D}$$

$$0 = [L]^2 BK_c + [L](BD + K_c M_{tot} - K_c L_{tot}) - L_{tot} D$$

$$[L] = \frac{-(BD + K_c M_{tot} - K_c L_{tot}) + \sqrt{((BD + K_c M_{tot} - K_c L_{tot})^2 + 4\mathrm{BDK}_c L_{tot})}}{2\mathrm{BK}_c} \quad \text{A38}$$

The remaining species can be calculated using [L] with the following equations

$$[M] = \frac{M_{tot}}{[L]K_c + D} \quad \text{A39}$$

$$[LM] = K_c[L][M] \quad \text{A40}$$

$$[LH] = \frac{[L][H]}{K_1} \quad \text{A41}$$

$$[LH_2] = \frac{[LH][H]}{K_2} \quad \text{A42}$$

$$[LH_3] = \frac{[LH_2][H]}{K_3} \quad \text{A43}$$

$$[LH_4] = \frac{[LH_3][H]}{K_4} \quad \text{A44}$$

$$[M(OH)] = \frac{K_{OH1}[M]}{[H]} \quad \text{A45}$$

$$[M(OH)_2] = \frac{K_{OH2}[M]}{[H]^2} \quad \text{A46}$$

$$[M(OH)_3] = \frac{K_{OH3}[M]}{[H]^3} \quad \text{A47}$$

For a better overview in the graphs shown in chapter 5, all protonated ligand species were combined to one quantity, as were the metal hydroxide species.

$$[LH_x] = L_{tot} - [LM] - [L] \quad \text{A49}$$

$$[M(OH)_x] = M_{tot} - [LM] - [M] \quad \text{A50}$$

References

[1] J. Kragten, *Atlas of Metal-Ligand Equilibria in Aqueous Solution*, E. Horwood; Halsted Press, Chichester, Eng.: New York, **1978**.
[2] R. M. Smith, A. E. Martell, R. M. Smith, *Critical Stability Constants Volume 4: Inorganic Complexes*, Plenum Press, New York, **1976**.
[3] P. L. Brown, C. Ekberg, *Hydrolysis of Metal Ions*, Wiley-VCH Verlag GmbH & Co. KGaA, Weinheim, **2016**.